Holm, Robert J. (2013) ***Magmatic arcs of Papua New Guinea: insights into the late Cenozoic tectonic evolution of the northern Australian plate boundary.*** **PhD Thesis, James Cook University.**

Magmatic arcs of Papua New Guinea: Insights into the Late Cenozoic tectonic evolution of the northern Australian plate boundary

Thesis submitted by

Robert J. Holm

July 2013

For the Degree of Doctor of Philosophy in the
School of Earth and Environmental Sciences of
James Cook University

Statement of Access

I, the undersigned author of this thesis, understand that James Cook University will make this thesis available for use within the university library and allow access in other approved libraries after its submission. All users consulting this thesis will have to sign the following statement:

> *In consulting this thesis I agree not to copy or closely paraphrase it in whole or in part without the written consent of the author; and to make proper public written acknowledgement for any assisstance which I have obtained from it.*

Beyond this, I do not wish to place any restrictions on access to this thesis.

Robert J. Holm
July 2013

Declaration

I declare that this thesis is my own work and has not been submitted in any form for another degree or diploma at any university or other institute or tertiary education. Information derived from the published or unpublished work of others has been acknowledged in the text and a list of references is given.

Robert J. Holm
July 2013

Statement of Contribution by Others

Nature of Assistance	Contribution	Names, Titles and Affiliations of Co-Contributors
Intellectual Support	Proposal writing	Simon Richards (JCU)
	Data analysis	Simon Richards (JCU) Carl Spandler (JCU) Mark Schmitz (Boise State)
	Editorial assistance	Carl Spandler (JCU) Simon Richards (JCU) Gideon Rosenbaum (UQ)
Financial Support	Field research	Barrick Australia (In-kind contribution)
	Stipend	Australian Postgraduate Award
	Research funding	SEES ($15,580) Research account of Simon Richards ($5,000)
Data Collection	Research assistance	Richard Wormald (JCU) Yi Hu (JCU)

Statement of Contribution by Others

Title of thesis: Magmatic arcs of Papua New Guinea: Insights into the Late Cenozoic tectonic evolution of the northern Auatralian plate boundary
Name of candidate: Robert J. Holm

Chapter #	Details of publication(s) on which chapter is based	Nature and extent of the intellectual input of each author
3	Holm, R.J., Spandler, C., Richards, S.W., 2013. Melanesian arc far-field response to collision of the Ontong Java Plateau: Geochronology and pertrogenesis of the Simuku Igneous Complex, New Britain, Papua New Guinea. Tectonophysics, In Press.	I contributed to the writing and development of concepts

I confirm the candidate's contribution to this paper and consent to the inclusion of the paper in this thesis.

Name: Carl Spandler

Signature:

Date: 31-07-2013

Statement of Contribution by Others

Title of thesis: Magmatic arcs of Papua New Guinea: Insights into the Late Cenozoic tectonic evolution of the northern Auatralian plate boundary
Name of candidate: Robert J. Holm

Chapter #	Details of publication(s) on which chapter is based	Nature and extent of the intellectual input of each author
3	Holm, R.J., Spandler, C., Richards, S.W., 2013. Melanesian arc far-field response to collision of the Ontong Java Plateau: Geochronology and pertrogenesis of the Simuku Igneous Complex, New Britain, Papua New Guinea. Tectonophysics, In Press.	I contributed to the development of concepts
7	Holm, R.J., Richards, S.W., 2013. A re-evaluation of arc-continent collision and along-arc variation in the Bismarck Sea region, Papua New Guinea. Australian Journal of Earth Sciences, Accepted.	I contributed to the writing and development of concepts

I confirm the candidate's contribution to this paper and consent to the inclusion of the paper in this thesis.

Name: Simon Richards

Signature:

Date: 31.07.2013

Acknowledgments

There are many people who were involved or contributed in some way to my thesis work over the last three and a half years. Although they cannot all be thanked here individually, their help is greatly appreciated.

I owe the greatest debt of thanks to my supervisors, Simon Richards, Carl Spandler and Gideon Rosenbaum. Firstly, a huge thanks Simon for the opportunity to study in such a region and his enthusiasm for the project and willingness to explore weird and wonderful ideas. An enormous thanks to Carl for reigning back some of the ideas and whose time and wide range of knowledge got me over the line. And lastly, great thanks to Gideon for all your time and effort, and input into the project. Simon, Carl, and Gideon, I look forward to working with you in the future.

I would also like to thank Richard Wormald and Yi Hu for their time an effort for the zircon and LA-ICP-MS work, one of the most enjoyable and key aspects of my research.

Thanks to all the staff at SEES for the last three and a half years who made this an enjoyable and worthwhile experience, and for all your time and help.

And thanks to my fellow PhD and honours students over the years, particularly Johannes, Mark, Babo, Ryan, Grace and Jainrich (and those to come). As mates and colleagues you all provided plenty of advice and many fruitful discussions, as well as the many that were not so useful but entertaining nonetheless.

I would like to thank Barrick Australia for making this project possible and particularly those in PNG for providing samples and assistance in the field.

Also thanks to the AAC staff for assistance with analytical work, and Mark Schmitz for help with the TIMS analyses and dating.

And finally, my parents for their support and always being interested in my work despite not understanding the details, and for putting up with two perennial students for sons.

Abstract

Papua New Guinea, as part of the southwest Pacific, lies in a complex tectonic setting of oblique convergence between the Pacific and Australian plate, and trapped between the converging Ontong Java Plateau of the Pacific plate and the Australian continent. Through studying the tectonic evolution of Papua New Guinea we can gain insight into how the region formed through time and explore the relationships between the driving forces of tectonics and the responses or feedbacks reflected in the geology. At present we lack the evidence to fully constrain the evolution of Papua New Guinea, however, through the study of arc magmatism I illustrate how we might approach defining a geodynamic framework for the region and unraveling the complex tectonic history.

In general, the deformation history of Papua New Guinea is well constrained but the same robust records do not exist for magmatism. To progress with unravelling the tectonic evolution of the region we require a time and cost effective means of robust age dating in young rocks. Investigation into the timing of two Quaternary magmatic occurrences by LA-ICP-MS U-Pb zircon dating compared with CA-TIMS and SHRIMP dating methods reveal good correlation and age agreement between dating methods. This is one of only few studies utilizing LA-ICP-MS U-Pb zircon dating for Quaternary ages. Uncertainty in such young rocks is relatively large due to potential matrix effects related to differential alpha dose accumulation and limitations on instrumental precision with an associated error threshold of 5% for a determined age. This makes LA-ICP-MS U-Pb dating a useful tool in regional studies of this nature.

The Late Cenozoic tectonic evolution of Papua New Guinea is set in motion with initial convergence at the Australia-Pacific plate boundary from 45 Ma. Combined U-Pb zircon geochronology and geochemical investigation into the evolution of the Melanesian arc from the Simuku Igneous Complex of West New Britain, Papua New Guinea reveals development of the embryonic island arc from at least 43 Ma. Progressive arc growth was punctuated by distant collision of the Ontong Java Plateau and subduction cessation from 26 Ma. This change in subduction dynamics is represented by emplacement of the adakitic Simuku Porphyry Complex between 24 and 20 Ma. Petrological and geochemical affinities highlight genetic differences between contemporaneous "normal" arc volcanics and adakite-like signatures of Cu-Mo mineralized porphyritic intrusives. Not only is this one of few studies into the geology of the Melanesian arc, it is also among the first to address the distant tectono-magmatic effects of major arc/forearc collision events and subduction cessation on magmatic arcs.

Understanding of the tectonic evolution of mainland Papua New Guinea throughout the Miocene is hampered by a lack of robust geological evidence. The Maramuni arc of Papua New Guinea represents the only continuous tectonic element throughout this dynamic period. I present the first detailed U-Pb geochronology and geochemical investigation of the Maramuni arc from intrusive rocks of the Kainantu region of the eastern Papuan Highlands. Arc magmatism related to north-dipping subduction at the Pocklington trough is punctuated by arrival of the Australian continent at approximately 12 Ma and growth of the New Guinea Orogen. Arc geochemistry from 12 Ma highlights a changing tectonic setting, marked by anomalous enrichments in high-field strength elements at 9 Ma. Crustal delamination from approximately 7 Ma is coincident with porphyry intrusion bearing similarities to adakitic rocks and renewed uplift of the New Guinea Orogen from 6 Ma. Although the fundamental controls on arc evolution are yet to be conclusively determined, this study contributes understanding of subduction dynamics in Papua New Guinea during the Miocene.

Papua New Guinea is a unique part of the planet in that Cenozoic orogenesis is superimposed on an earlier basement structure that has, in turn, influenced how the New Guinea Orogen has grown over time. Specifically, the underlying/underthrust Australian continental basement is characterized by a major accretionary boundary referred to as the Tasman Line separating a younger Paleozoic-Mesozoic Tasmanide orogenic belt from Precambrian cratonic rocks to the west. Using precise age dating of inherited zircon from Quaternary magmatic rocks in the overriding Cenozoic fold belt coupled with an evaluation of orogen-scale deformation and magmatic morphology, I show where the Tasman Line extends to the north beneath younger crust. This result is significant as it demonstrates that with the use of a well established technique combined with detailed structural and tectonic assessment, deep crustal boundaries can be traced in relatively young terrains.

The Bismarck Sea region of Papua New Guinea is marked by recent arc-continent collision giving rise to a highly dynamic tectonic environment. We present a new crustal and upper mantle architecture model for northeastern Papua New Guinea and western New Britain that reveals overprinting slab subduction and partial continental subduction. Earthquake hypocentre databases are combined with detailed topography and seafloor structure together with geology and regional-scale gravity in conjunction with an updated 3-D slab map to unravel this sub-surface structure. Subducting continental crust has resulted in a complex pattern of arc-related geochemical signatures from east to west along the Bismarck arc. In the east where the Solomon Sea plate is subducting beneath New Britain, the sedimentary component is low whereas in the west the arc volcanics exhibit a greater sedimentary component, consistent with subduction of Australian crustal sediments. As a result, a new plate reconstruction is provided for the region together with forward-looking reconstructions.

Overall the studies presented here reflect a region controlled by compounding major collision events resulting in increasing levels of tectonic complexity acting on decreasing spatial-scales. This thesis presents an insight into the tectonics of Papua New Guinea and significantly contributes to our understanding of the dynamic Australia-Pacific plate boundary zone, while also providing new tools that we can use to unravel complex tectonic scenarios at both the present day and at ancient plate boundary settings.

Table of Contents

Contents of Digital Appendices

List of Tables

List of Figures

Chapter 1

Introduction

Structure of this thesis

It is intended that the entire contents of this thesis will be published in internationally recognized Earth Science journals. This thesis has been written as a series of five independent papers (Chapters 2–6) and each section is cross-referenced as a separate paper accordingly. At the time of submission, Chapter 3 is already published in *Tectonophysics*, and Chapter 6 is published in the *Australian Journal of Earth Sciences*. As most of the chapters of this thesis have undergone, or are soon to be submitted for peer review as part of the publication process, I have decided against major reformatting of these papers during thesis preparation. The sections are all presented in the same written style with consistent use of specialist terms and geological unit names. However, each chapter represents an independent body of work that is presented in a format similar to a published manuscript. Structuring the thesis in this manner has inevitably led to repetition of some descriptive text, such as geological setting and analytical techniques. However, this in minimal due to the nature of the individual studies addressing different tectonic settings and different periods in the evolution of Papua New Guinea.

A single reference list for the entire thesis follows Chapter 7. Presenting the cited references in this manner allows the reader to locate individual reference details with relative ease and saves considerable space as many publications are cited in two or more chapters.

Subject of this thesis

The southwest Pacific comprises some of the youngest and most dynamic tectonic elements on Earth (Figure 1-1). As such, the tectonics in the southwest Pacific is often used as an analogue to illustrate how complex tectonic regions may have formed, and in particular, accretionary orogens (e.g. northern Appalachians and British Caledonides [Van Staal et al., 1998]; Central Asian Orogenic Belt and Arabian-Nubian shield [Kröner et al., 2007]; the Lachlan Fold Belt [Collins and Richards, 2008] and Tasmanides of Australia [Glen and Meffre, 2009]; Western European Alps [Malusà and Garzanti, 2012]). Although much of the southwest Pacific is either tectonically active or geologically very young, the geodynamic framework of the southwest Pacific itself is not yet fully understood. Much of the apparent tectonic complexity in the southwest Pacific arises from major collision events along the Australia-Pacific plate boundary zone that trigger episodes of large-scale tectonic reorganization. Most notable are the collision of the Ontong Java Plateau with the Melanesian arc (Petterson et al., 1999; Hall, 2002; Mann and Taira, 2004; Knesel et al., 2008; Holm et al., 2013; Chapter 3), and collision of the Australian continent with a proto-New Guinea (Hill and Hall, 2003; Cloos et al., 2005; Schellart et al., 2005; Chapter 4). The nature and timing of these events, however, is the subject of much dispute in the geological

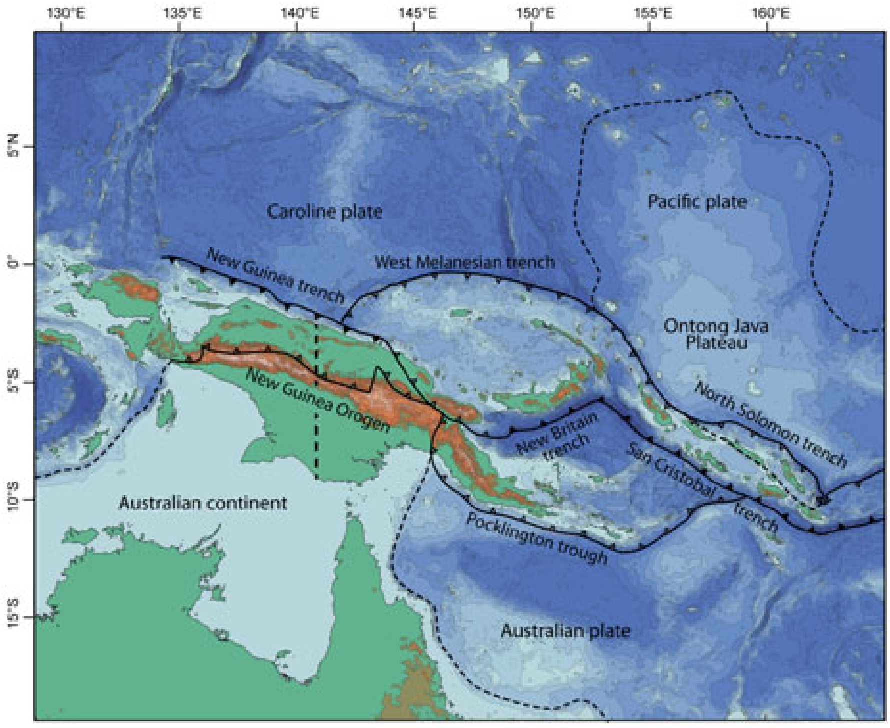

Figure 1-1. Regional tectonic setting of Papua New Guinea within the southwest Pacific. Papua New Guinea lies between the converging Australian continent and Ontong Java Plateau. During the Cenozoic Australia-Pacific convergence has been accommodated at three different plate boundaries at distinct times, together forming the wider Australia-Pacific plate boundary zone. Currently the New Guinea trench, New Britain trench and San Cristobal trench form the active plate boundary.

community, leading to uncertainty around the tectonic drivers and mechanisms that shaped the southwest Pacific. Furthermore, the region also hosts some of the world's largest subduction-related porphyry deposits including Lihir, Bougainville, Ok Tedi and Grasberg, therefore, this region presents an ideal location to examine the tectonic and geodynamic processes associated with subduction, orogenesis, basin formation and mineralization.

Papua New Guinea is critical to our understanding of southwest Pacific tectonics, as it lies within a zone of oblique convergence between the Ontong Java Plateau of the Pacific plate, and the Australian continent (Figure 1-1). This unique tectonic configuration results in a complex arrangement of tectonic feedbacks between terrane collision and orogenesis, microplate development, and varying subduction dynamics (Figure 1-2). Unraveling the tectonic history of Papua New Guinea requires a multidisciplinary approach encompassing an equally diverse array of geological evidence. At present, a well-established regional structural framework exists for Papua New Guinea recording the timing and characteristics of deformations episodes (Hill and Gleadow, 1989; Abbott, 1995; Hill and Raza, 1999). However, structural deformation histories are inherently non-unique and require a robust tectonic framework to provide spatial context for observations. Determining the history of collision and subduction dynamics of the region can provide this tectonic framework, but additionally, this must be constrained in both time and space. Studies into the nature of arc magmatism through time and during periods of tectonic change can provide us with insight into subduction dynamics and crustal processes that may be difficult to resolve through other means. However, at present, robust and extensive records for the magmatic history of Papua New Guinea simply do not exist.

This work seeks to unravel the complex tectonic history of Papua New Guinea and present a clear and innovative case as to the nature and development of arc magmatism to provide insight into the recent tectonic development of the northern Australian plate boundary. I primarily utilize U-Pb zircon geochronology combined with major and trace element geochemistry to investigate the magmatic arcs of Papua New Guinea (Figure 1-2), but supplemented by a compilation and reinterpretation of an extensive catalogue of previous data including geophysical and earthquake data, mineralization, sedimentology, structural and metamorphic geology, and geomorphology. From this I re-evaluate and address gaps in our knowledge of the present day tectonic setting of Papua New Guinea and interpret the tectonic history of the region. Throughout the study I emphasize the complexity of interpreting tectonic history in a region lacking in abundant geological evidence and demonstrate that this complexity and variability must be considered when examining the tectonic, geochemical and mineralogical characteristics of ancient arcs. At the global-scale the results will provide a potential explanation and an additional tool to help unravel the complexity of accretionary orogens that exhibit markedly different structural, magmatic and even metamorphic characteristics in what appears to be a single arc or accretionary event.

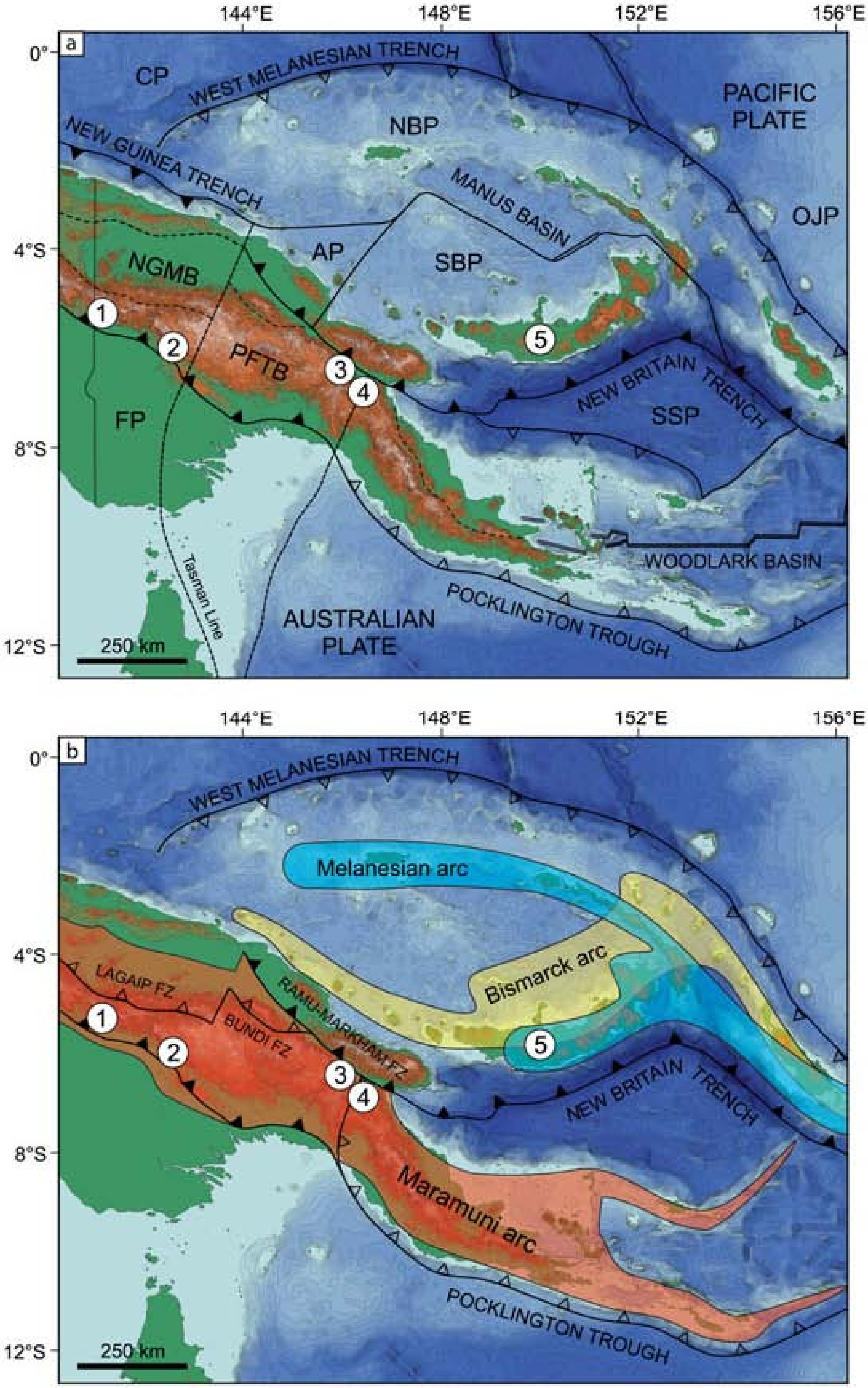
144°E
148°E
152°E
156°E
0°
4°S
8°S
12°S
a
CP
WEST MELANESIAN TRENCH
PACIFIC PLATE
NBP
NEW GUINEA TRENCH
MANUS BASIN
OJP
NGMB
AP
SBP
1
2
PFTB
3
4
5
NEW BRITAIN TRENCH
SSP
FP
WOODLARK BASIN
Tasman Line
AUSTRALIAN PLATE
POCKLINGTON TROUGH
250 km
b
Melanesian arc
Bismarck arc
LAGAIP FZ
BUNDI FZ
RAMU-MARKHAM FZ
Maramuni arc

Figure 1-2. Tectonic and magmatic setting of Papua New Guinea. a) Papua New Guinea is marked by complex tectonics, the mainland is comprised of multiple terranes accreted to the northern Australian continental margin (suture zones marked as dashed lines) and development of the New Guinea Orogen comprising the Papuan Fold and Thrust Belt and New Guinea Mobile Belt, and overlying the inherited crustal architecture of the Australian plate. To the east a microplate complex accommodates Australia-Pacific plate convergence through subduction, microplate rotation and associated spreading systems. CP, Caroline plate; NBP, North Bismarck plate; AP, Adelbert plate; SBP, South Bismarck plate; SSP, Solomon Sea plate; OJP, Ontong Java Plateau; NGMB, New Guinea Mobile Belt; PFTB, Papuan Fold and Thrust Belt; FP, Fly Platform (stable Australian continental crust). b) Magmatic arcs of Papua New Guinea studied within this thesis and their correlative subduction zones; FZ, fault zone. Sample localities for the thesis are as indicated: 1) Ok Tedi; 2) Baia; 3) Kokofimpa, Kainantu; 4) Wamum; 5) Simuku, West New Britain.

Furthermore, these results can be used to gain a better understanding of ancient orogenic belts where ongoing deformation and magmatism may have masked some of the evidence for ancient fold belt subduction.

The studies investigate different aspects of the magmatic arcs of Papua New Guinea (Figure 1-2) in both space and time and provide insight into the plate tectonic evolution of the northern Australian plate boundary throughout the Late Cenozoic. The different chapters are arranged with an initial study addressing the methodology of geochronology and young terrains, and thereafter are in geochronological order of the study areas from oldest to the present day. Outlines for the five papers are below:

The objective of Chapter 2 is to develop the methodology and explore the limitations associated with laser ablation ICP-MS U-Pb zircon geochronology through an applied study of Quaternary magmatism in Papua New Guinea. Samples from the Sydney Monzodiorite of Ok Tedi and andesitic volcanics from the Baia Prospect, both from the Plio-Pleistocene magmatic belt of the Papuan Fold and Thrust Belt in western Papua New Guinea were analyzed to investigate the application of LA-ICP-MS U-Pb zircon dating in young magmatic terrains. In addition, I compare and validate results from this method against CA-TIMS and SHRIMP dating methods as traditionally more reliable methods.

Addressing first the earliest Cenozoic magmatism of Papua New Guinea in terms of the regional tectonic history, Chapter 3 examines the little known magmatic history of the Melanesian arc. The Melanesian arc is exposed in Papua New Guinea on the outboard islands of New Britain and New Ireland. The Simuku Igneous Compex of New Britain provides a record of arc activity through U-Pb zircon geochronology from arc inception at 43 Ma through to termination of the Melanesian arc at approximately 20 Ma. This period of arc activity spans the timing for collision of the Ontong Java Plateau with the Solomon Islands providing an ideal opportunity to examine the geochemical relationships between arc activity and subduction dynamics in response to a major collision event and cessation of Pacific plate subduction.

Chapter 4 examines the Upper Oligocene and Miocene tectonics of the Papua New Guinea mainland to address the development of the New Guinea Orogen and evolution of the Maramuni arc. Much of the mineral endowment and porphyry mineralisation of Papua New Guinea is attributed to the Maramuni arc, however, the subduction system that gave rise to arc magmatism is disputed. I apply a similar approach to Section B whereby I utilize U-Pb zircon geochronology combined with detailed geochemistry from the Wamum and Kainantu regions of the eastern Papuan Highlands to investigate evolution of the Maramuni arc and the relationship between arc magmatism and major collision coupled with complex subduction dynamics. Further, I review the available geological data for the mainland of Papua New Guinea from the Oligocene through to the present and develop a geodynamic model for collision of the Australian continent with an outboard proto-New Guinea terrane and emplacement of the Maramuni arc.

Chapter 5 utilizes the same Quaternary magmatic sample set as Section A but takes a contrasting and innovative approach to arc magmatism. In addition to Quaternary zircon crystals within the rock material, there are also extensive populations of inherited zircon grains. Zircon inheritance patterns are often used as a tectono-magmatic fingerprint of a region where age patterns can be used to help match terranes or infer the source or magmatic pathway for intrusive rocks. Comparing contrasting age populations from the Papuan Fold and Thrust Belt to orogen-scale variation in structural and magmatic morphology, I interpret the underlying crustal controls on orogen development reflecting a crustal architecture inherited from the Australian continent.

Lastly, in Chapter 6 I assess the present day tectonic setting of Papua New Guinea, and more specifically the Bismarck Sea region and northeastern Papua New Guinea mainland. This is the site of recent and ongoing arc-continent collision and active offshore arc magmatism. Although previous work provides a good understanding of the timing and implications of the collision event at the surface, the sub-surface and mantle crustal geometries are not yet appreciated. Chapter 6 addresses the crustal architecture underlying the site of collision by utilizing existing gravity and seismic datasets. Furthermore, the findings from the sub-surface model are related back to the present day setting with consequences for arc genesis in the Bismarck Sea and our understanding of the relationship between complex collision events, subduction dynamics and arc magmatism around the world.

Subsequently, I will discuss the Late-Cenozoic plate tectonic evolution of Papua New Guinea in Chapter 7, drawing from the five studies, and the implications of these results for the southwest Pacific.

Publications by the author of relevance to this thesis are also included in the appendix, these are: "When slabs collide: A tectonic assessment of deep earthquakes in the Tonga-Vanuatu region" published in *Geology*; "Melanesian arc far-field response to collision of the Ontong Java Plateau: Geochronology and pertrogenesis of the Simuku Igneous Complex, New Britain, Papua New Guinea" published in *Tectonophysics* (Chapter 3); and "A re-evaluation of arc-continent collision and along-arc variation in the Bismarck Sea region, Papua New Guinea" published in *Australian Journal of Earth Sciences* (Chapter 6).

Chapter 2

Pushing the limits of LA-ICP-MS U-Pb geochronology: Applied multi-method U-Pb zircon dating of Quaternary magmatism in Papua New Guinea

Abstract

Papua New Guinea is the site of late Cenozoic arc development and orogenesis at the northern Australian plate boundary. The age and characteristics of orogenesis are well understood but the same robust records do not exist for magmatism; as a relative "blank-slate", immediate progress requires time and cost effective means of radiogenic dating in young rocks. I investigated the timing of two Quaternary magmatic occurrences using LA-ICP-MS U-Pb zircon dating, and compared these to results from new CA-TIMS and previous SHRIMP dating methods. Results showed good internal correlation and age agreement between dating methods. This is one of only few studies to date utilizing LA-ICP-MS U-Pb zircon dating for Quaternary ages. I also consider the additional uncertainty that arises in young U-Pb dating. In addition to procedural analytical corrections for elemental fractionation and mass bias, I find that potential matrix effects related to differential alpha dose accumulation and limitations on instrumental precision are likely the greatest contributors to uncertainty and a realistic 2σ error threshold is 5% of the determined age. This makes LA-ICP-MS U-Pb dating a useful tool in regional studies of, for example, Quaternary volcanism and related timing in hominid evolution or climate change.

Introduction

A well-established regional tectonic framework exists for Papua New Guinea recording the timing and characteristics of deformation episodes (Hill and Gleadow, 1989; Abbott, 1995; Hill and Raza, 1999); however, the same robust records do not exist for the magmatic history of Papua New Guinea. A comprehensive suite of Late Cenozoic age dating over mainland Papua New Guinea was completed by various workers (e.g. Page, 1976; Rogerson and Williamson, 1985; Richards and McDougall, 1990), primarily generated by the K-Ar dating method. With advances in geochronology, U-Pb or Ar-Ar are now the preferred age dating methods in tectonically and thermally active regions. However, to date van Dongen et al. (2010) is the only published study concerning Cenozoic U-Pb magmatic ages from mainland Papua New Guinea, and this work is restricted to the Ok Tedi intrusive complex. To progress with unraveling the complex tectono-magmatic history of Papua New Guinea we must begin to compile a robust dataset of radiogenic age dating. Furthermore, the increasing demand for Quaternary science in general and associated geochronological controls open new avenues for the application of time and cost effective U-Pb dating methods.

Here I take an applied approach to advances in LA-ICP-MS U-Pb zircon dating and present new U-Pb ages for two Quaternary magmatic occurrences in the Papuan Fold and Thrust Belt (Figure 2-1). These ages were generated by the LA-ICP-MS zircon dating method and evaluated against new CA-TIMS and previous SHRIMP dating (van Dongen et al., 2010). Quaternary ages obtained in this study are some of the youngest zircon ever measured by LA-ICP-MS, furthermore, this is one of few studies to conduct targeted age dating utilizing both LA-ICP-MS and CA-TIMS on the same rocks, let alone the same zircon crystals (see also: Black et al., 2004; Rioux et al., 2007; von Quadt et al., 2011). Moreover, I review and discuss sources of uncertainty in LA-ICP-MS U-Pb dating, particularly with regard to young rocks.

Geological Setting and Samples

Papua New Guinea represents the tectonically active northern margin of the Australian plate in the wider southwest Pacific zone of oblique convergence between the Australian and Pacific plates. The island of New Guinea, incorporating both Papua New Guinea and West Papua is geologically composed of multiple terranes accreted to the northern Australian continental margin during Cenozoic northward drift (e.g. Hill & Hall 2003; Crowhurst et al., 2004; Davies, 2012), and forming an accretionary orogen of sedimentary cover rocks developed on Australian continental crust (Papuan Fold and Thrust Belt; Hill and Gleadow, 1989; Craig and Warvakai, 2009) buttressed against variably deformed sedimentary, metamorphic and crystalline rocks of the New Guinea Mobile Belt (Figure 2-1; Hill and Raza, 1999; Davies, 2012). The Late Cenozoic

Maramuni arc intrudes and overprints the New Guinea Orogen. Early Maramuni arc activity intruded the New Guinea Mobile Belt during the Upper Oligocene (Hill and Raza, 1999; Cloos et al., 2005), and migrated south into the Papuan Fold and Thrust Belt by the Upper Miocene (Page, 1976; Rogerson and Williamson, 1985). More recent Pliocene and Quaternary magmatism is almost exclusively hosted within the Papuan Fold and Thrust Belt and stable Australian continental crust of the Fly Platform (Figure 2-1). Quaternary magmatism is expressed as widespread large shoshonitic and andesitic stratovolcanoes and intrusive bodies (Page, 1976; Johnson et al., 1978), often controlled by regional-scale structural lineaments (Davies, 1990). Maramuni arc activity has been previously attributed to north-dipping subduction beneath New Guinea, however, this subduction ceased due to collision between the Australian continent and New Guinea at approximately 12 Ma (Cloos et al., 2005) leaving little evidence as to the petrogenesis of more recent magmatism. Several workers still pertain to a subduction-related origin for the recent magmatism (Jakeš and White, 1969; Johnson et al., 1978; Davies, 1990) while others attribute emplacement of the mantle-derived magmas to Upper Miocene-Pliocene crustal shortening with associated melting of the underlying mantle (Johnson et al., 1978; Hill et al., 2002). More recently Cloos et al. (2005) suggested collisional delamination following trench collision ultimately led to magma generation due to asthenospheric upwelling and decompression of stretched lithospheric mantle.

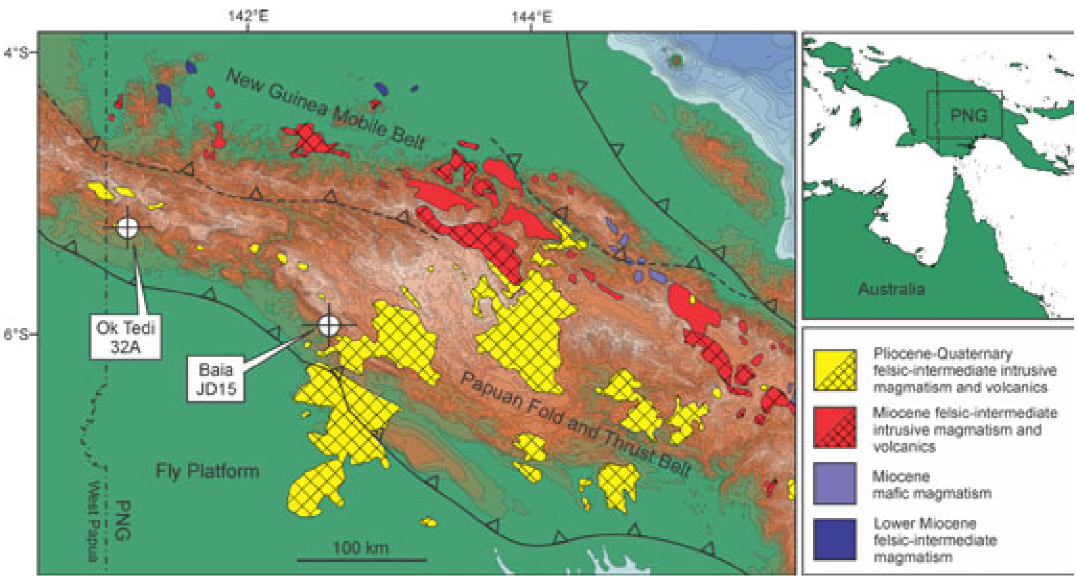

Figure 2-1. Topography, major tectonic elements and magmatic occurrence map of mainland Papua New Guinea. Samples 32A, Ok Tedi and JD15, Baia (668956 9341950 AGD66 zone 54) lie within a belt of Quaternary magmatism intruded into the Papuan Fold and Thrust Belt. Distribution of magmatism is from Australian Bureau of Mineral Resources (1972, 1986).

I sampled two Quaternary magmatic occurrences within the Papuan Fold and Thrust Belt in western Papua New Guinea. Both sample localities occupy a similar tectonic context within the foreland Papuan Fold and Thrust Belt (Figure 2-1). Sample 32A, from Ok Tedi, is a porphyritic phase of the Sydney Monzodiorite (Southern Porphyry Area) that comprises phenocrysts of plagioclase and mafic minerals, especially hornblende. Sample JD15 (Baia) is an andesitic volcanic, crystal-rich lapilli tuff with complexly zoned plagioclase and minor hornblende in a fine-grained fragmental matrix.

Methods

Samples selected for U-Pb dating of zircon were taken from the Ok Tedi Sydney Monzodiorite (sample 32A) and Baia prospect (sample JD15). Mineral separation was carried out at James Cook University (JCU) in a standard four-step process. Samples were crushed and milled to 500 µm, washed to remove the clay fraction, and separated by a combination of heavy liquid density separation and magnetic separation. All zircons within the separates were hand picked and mounted in epoxy with GJ1, Temora 2 and Fish Canyon Tuff zircon standards; a total of 128 grains from sample 32A, and 247 crystals from JD15 were mounted by this method. Epoxy mounts were polished and carbon-coated. Cathodoluminescence (CL) images of all zircon crystals were obtained using a Jeol JSM5410LV scanning electron microscope equipped with a Robinson CL detector, housed at JCU.

LA-ICP-MS U-Pb Dating

All work was done at the Advanced Analytical Centre of James Cook University. U-Pb dating of zircon was conducted using the laser ablation ICP-MS setup, full details are given in Tucker et al. (2013). The ICP-MS was tuned to ensure approximately equal senestivity of U, Th and Pb to minimize isotope fractionation due to matrix effects. Analyses collected were ^{29}Si, ^{90}Zr, ^{202}Hg, ^{204}Pb, ^{206}Pb, ^{207}Pb, ^{208}Pb, ^{232}Th, ^{235}U, and ^{238}U. In order to obtain a higher sensitivity for the low Pb signal intensity expected for young zircon, the High Sensitivity mode of 820-MS was used with the sensitivity for ^{238}U of about 10,000 cps/ppm at 44 µm laser beam diameter using laser conditions of 5 Hz, 6 J/cm energy density. The zircon to be dated were potentially very young, hence Pb concentration could be extremely low which demands a very high sensitivity of the ICP-MS, while on the other hand, concentration of U and Th could be very high in zircon samples and their high signal intensity would overload the detector of the ICP-MS. To overcome this problem, freshly calibrated attenuation factors were applied to ^{232}Th and ^{238}U so that the linear dynamic range of the ICP-MS was extended to accommodate the requirement of this young zircon dating. Remaining fractionation and mass bias was corrected by using standard bracketing techniques with every ten zircon sample measurements bracketed by measurements of GJ1 (primary calibration standard; Jackson et al., 2004), Temora 2 (Black et al., 2004) and Fish

Canyon Tuff (secondary checking standards; Schmitz and Bowring, 2001; Renne et al., 2010). For quantification of U and Th concentration in zircon samples, analysis of the NIST SRM 612 reference glass was conducted at the beginning, middle and end of every analytical session, with ^{29}Si used as the internal standard assuming perfect zircon stoichiometry.

Zircon analyses were carried out with a beam diameter of 60 μm, with the exception of JD15-2 age determination for subsequent CA-TIMS analyses where a 24 μm spot size was used. Selection of analytical sample spots was guided by CL images and targeted both cores and rims. All data reduction was carried out by Glitter software (Van Achterbergh et al., 2001). All time-resolved single isotope signals from standards and samples were filtered for signal spikes or perturbations related to inclusions and fractures. Subsequently, the most stable and representative isotopic ratios were selected taking into account possible mixing of different age domains and zoning. Analyses of Temora 2 and Fish Canyon Tuff zircon were used for verification of GJ1 following drift correction (Figure 2-2). Background corrected analytical count rates, calculated isotopic ratios and 1σ uncertainties were exported for further processing and data reduction.

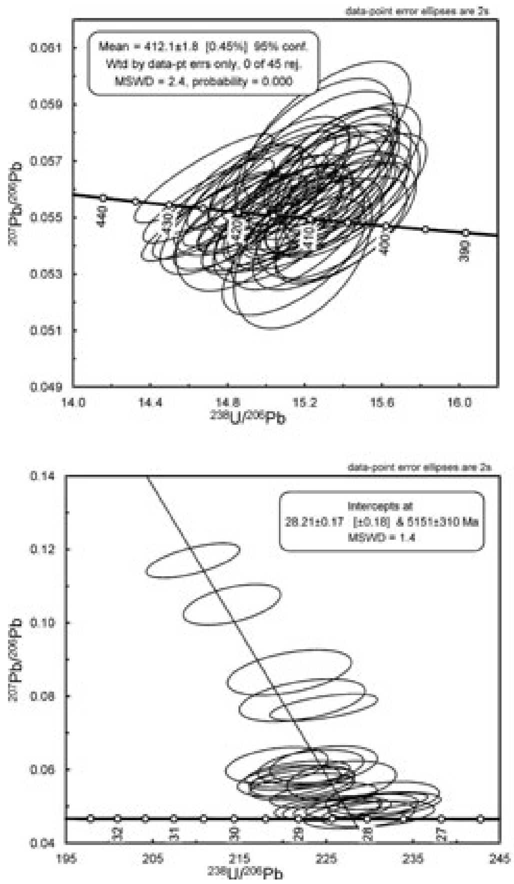

Figure 2-2. Tera-Wasserburg plots and weighted average (Temora 2) for U-Pb zircon geochronology standards. All data-point error ellipses and calculated errors are ± 2σ, and 95% confidence for associated weighted average.

Initial Th/U disequilibrium in zircon caused by an exclusion of ^{230}Th results in a ^{206}Pb deficit (Schärer, 1984; Parrish, 1990). Young zircon ages (<10 Ma) are particularly susceptible to this disequilibrium with an upward age correction in the order of 100 k.y. (Crowley et al., 2007), typically comparable or greater than the measured analytical error. Correction of $^{206}Pb/^{238}U$ dates for the deficit requires estimates of Th/U concentration in the zircon and Th/U concentration of the magma as the source of zircon. LA-ICP-MS zircon analysis routinely measures both Th and U elemental concentrations in addition to isotopic ratios for individual zircon. These were standardized to NIST SRM 612 reference glass for each analytical session using Glitter software and exported with the respective 1σ errors. The initial Th/U concentration of the magma is more difficult to estimate and has a larger effect on the age correction (Crowley et al., 2007). I substituted measured trace element measurements from bulk rock data determined with conventional ICP-MS following the procedures of Harris et al. (2004). Bulk rock Th/U ratios were 3.37 ± 0.52 and 3.05 ± 0.61 (2σ) respectively for samples 32A and JD15. Uncertainties associated with the correction were propagated into errors on the corrected ages according to Crowley et al. (2007).

The effect of common Pb is often taken into account by the use of Tera-Wasserburg Concordia plots (Tera and Wasserburg, 1972; Jackson et al., 2004), however, given that in young zircon errors in both measured $^{207}Pb/^{206}Pb$ and $^{207}Pb/^{235}U$ are proportionally much larger than the correlative error of $^{206}Pb/^{238}U$ measured isotope ratios, a concordia age may be of questionable statistical significance. Instead I employ weighted average plots within Isoplot/Ex version 4.15 (Ludwig, 2009) as the primary means of age resolution. Weighted mean $^{206}Pb/^{238}U$ age calculations were corrected for common Pb by utilizing the Age7Corr and AgeEr7Corr algorithms in Isoplot. The composition of common-Pb was taken to be that of the modern day composition modeled from Stacey and Kramers (1975), that is a $^{207}Pb/^{206}Pb$ common-Pb composition of 0.83, and incorporating a conservative corresponding 2σ error of 0.3. Although this is a relatively large error given the common-Pb composition in the AgeEr7Corr algorithm, it serves to emphasize analytical data points with poor error correlation between $^{207}Pb/^{206}Pb$ and $^{206}Pb/^{238}U$ isotopic ratios while not exaggerating the associated errors of 'normal' analyses. The dataset was then filtered for obvious aberrations, this included any data points with unrealistically small or large errors, and any points which did not belong to the zircon population, assuming concordance. All errors were propagated at 2σ level and reported at 95% confidence for weighted averages.

CA-TIMS U-Pb Dating

Zircon crystals for CA-TIMS analysis were selected on the basis of LA-ICP-MS spot analyses where young ages were achieved prior to processing of analytical data and corrections, indicative of low common Pb contributions. Selected zircon (zircon CL images are shown in Figure 2-3) were subjected to a modified version of the chemical abrasion method of Mattinson (2005), reflecting a preference to prepare and analyze the carefully selected single crystals. Zircon crystals were plucked from the epoxy mount and annealed in quartz beakers in a muffle furnace at 900°C for 60 hours. Individual grains were then transferred to 3 ml Teflon PFA beakers, rinsed twice with 3.5 M HNO_3, and loaded into 300 ml Teflon PFA microcapsules. The microcapsules were placed in a large-capacity Parr vessel, and the crystals partially dissolved in 120 ml of 29 M HF with a trace of 3.5 M HNO_3 for 10-12 hours at 180°C. The contents of each microcapsule were returned to 3 ml Teflon PFA beakers, the HF removed and the residual grains rinsed in ultrapure H_2O, immersed in 3.5 M HNO_3, ultrasonically cleaned for an hour, and fluxed on a hotplate at 80°C for an hour. The HNO_3 was removed and the grains were again rinsed in ultrapure H_2O or 3.5M HNO_3, before being reloaded into the same 300 ml Teflon PFA microcapsules (rinsed and fluxed in 6 M HCl during crystal sonication and washing) and spiked with the Boise State University mixed ^{233}U-^{235}U-^{205}Pb tracer solution (BSU1B), which has been calibrated against the EARTHTIME gravimetric standards. These chemically abraded grains were dissolved in Parr vessels in 120 ml of 29 M HF with a trace of 3.5 M HNO_3 at 220°C for 48 hours, dried to fluorides, and then re-dissolved in 6 M HCl at 180°C overnight. U and Pb were separated from the zircon matrix using an HCl-based anion-exchange chromatographic procedure (Krogh, 1973), eluted together and dried with 2 µl of 0.05 N H_3PO_4.

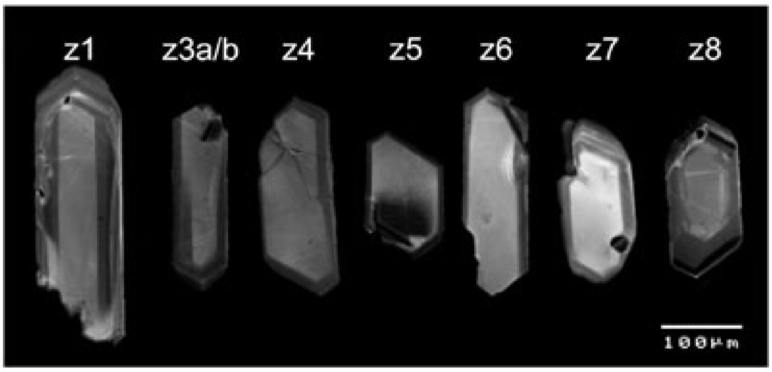

Figure 2-3. Cathodoluminescence images of zircon from sample JD15 selected for CA-TIMS dating.

Pb and U were loaded on a single outgassed Re filament in 2 μl of a silica-gel/phosphoric acid mixture (Gerstenberger and Haase, 1997), and U and Pb isotopic measurements made on a GV Isoprobe-T multicollector thermal ionization mass spectrometer equipped with an ion-counting Daly detector. Pb isotopes were measured by peak-jumping all isotopes on the Daly detector for 100 to 150 cycles, and corrected for 0.18 ± 0.04%/a.m.u. mass fractionation. Transitory isobaric interferences due to high-molecular weight organics, particularly on ^{204}Pb and ^{207}Pb, disappeared within approximately 30 cycles, while ionization efficiency averaged 104 cps/pg of each Pb isotope. Linearity (to ≥1.4 x 106 cps) and the associated deadtime correction of the Daly detector were monitored by repeated analyses of NBS982, and have been constant since installation. Uranium was analyzed as UO^{2+} ions in static Faraday mode on 1011 ohm resistors for 150 to 200 cycles, and corrected for isobaric interference of $^{233}U^{18}O^{16}O$ on $^{235}U^{16}O^{16}O$ with an $^{18}O/^{16}O$ of 0.00205. Ionization efficiency averaged 20 mV/ng of each U isotope. U mass fractionation was corrected using the known $^{233}U/^{235}U$ ratio of the BSU1B tracer solution.

U-Pb dates and uncertainties were calculated using the algorithms of Schmitz and Schoene (2007), and the U decay constants of Jaffey et al. (1971). Ratios of $^{206}Pb/^{238}U$ and dates were corrected for initial ^{230}Th disequilibrium using a $Th/U_{[magma]}$ of 3 ± 10%. All common Pb in analyses was attributed to laboratory blank and subtracted based on the measured laboratory Pb isotopic composition and associated uncertainty. U blanks were <0.1 pg.

The weighted mean age error includes analytical uncertainties based on counting statistics, mass fractionation correction, spike and blank subtraction, and ^{230}Th disequilibrium correction, and is appropriate when comparing to other $^{206}Pb/^{238}U$ ages obtained with spikes cross-calibrated with the EARTHTIME gravimetic standards. If used in comparison with ages derived from other U-Pb methods or decay schemes (e.g. Ar/Ar, ^{187}Re-^{187}Os) then the uncertainty in the spike U-Pb ratio and the ^{238}U decay constant can be added in quadrature, respectively. Quoted errors for individual analyses are of the form ±X(Y)[Z], where X is solely analytical uncertainty, Y is the combined analytical and tracer uncertainty, and Z is the combined analytical, tracer and ^{238}U decay constant uncertainty.

Treatment of Data From Previous SHRIMP U-Pb Dating

Previous U-Pb SHRIMP dating of the Sydney Monzodiorite, Ok Tedi from van Dongen et al. (2010) have been used in this study to complement new LA-ICP-MS zircon dating. Isotopic ratios and modeled Th/U zircon content for samples 508-366 and 809-116 from van Dongen et al. (2010) have been re-evaluated within the context of this study. This data has been freshly corrected for both initial Th disequilibrium and common Pb according to the same processes described above for LA-ICP-MS dating. All errors were propagated at 2σ level and reported at 95% confidence for weighted averages.

Results

Zircon Imaging and Characteristics

Inherited zircons are present in both samples but will not be a part of this study (Chapter 5). Zircons from Ok Tedi, sample 32A, are all pink in color. Young crystals are between 125 μm and 500 μm in length. Aspect ratios range between 1:3.5 and 1:1.25 with an average of approximately 1:2. These crystals typically exhibit dull to moderate luminescence in CL images (Figure 2-4), and are characterized by uniform cores with minor oscillatory zoning in the rim. There are, however, exceptions to this, more complex zoning is not uncommon with distinct variations between core and rim zonation patterns. In general crystals are euhedral. Some inherited cores with young magmatic rims are present.

Zircon crystals from Baia, sample JD15, are predominantly pink with subsidiary populations of both yellow and colorless crystals. Primary magmatic crystals are between 100 μm and 400 μm in length with average aspect ratios of 1:2.5, however, these vary between 1:3.3 and 1:1.75. These generally exhibit euhedral crystal shapes and appear dull in CL images (Figure 2-4) with featureless cores and minor oscillatory zoning in the rim typically in the order of 10 μm in width; no young crystals contain inherited cores. Some young crystals do conversely show signs of corrosion.

Primary zircons in both samples hold CL textures consistent with a magmatic origin. These are typically euhedral crystal shapes and exhibiting oscillatory zoning (Figure 2-4; Corfu et al., 2003;

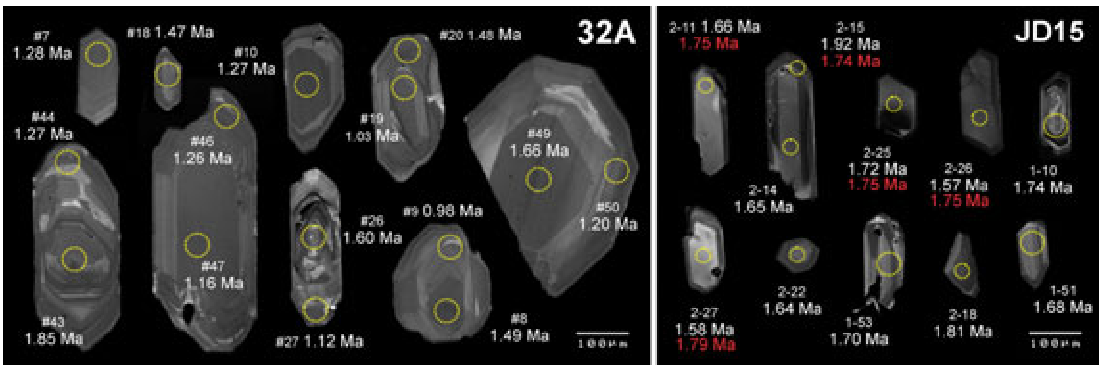

Figure 2-4. Cathodoluminescence images of zircon from sample 32A and JD15. Analytical spots are indicated with the associated age calculated from LA-ICP-MS U-Pb isotope ratio analyses; corresponding CA-TIMS ages for zircon are shown in red.

Hoskin and Schaltegger, 2003). A magmatic origin for these zircons is supported by low Th/U ratios (e.g. Heaman et al., 1990). JD15 zircon analyses returned average Th and U concentrations of 323 and 269 respectively and associated ranges of 57 to 958 and 94 to 625. Overall these gave an average Th/U ratio of 1.04. Thorium and U concentrations in 32A zircon were much lower compared with sample JD15 with average values of 131 and 152 respectively, and ranging from 28 to 618, and 44 to 632. Sample 32A returned an average Th/U ratio of 0.84.

LA-ICP-MS U-Pb Dating

Sample 32A utilized 50 analytical spots over 36 crystals, 34 out of the 50 spots yielded robust young ages and 26 of these made up the final age regression. Sample 32A returned a weighted average age of 1.308 ± 0.067 Ma (MSWD = 1.19; prob. = 0.23). In total 89 spot analyses were carried out on 75 zircon crystals from JD15, this entailed 60 spots over 51 crystals from an initial sample mount and a further 29 spots over 24 crystals in an additional sample mount with the purpose of targeting young crystals for CA-TIMS analysis. Of these, a total of 24 out of 89 spots yielded robust young ages, 21 of which were carried forward for age regression. Sample JD15 yielded a weighted average age of 1.735 ± 0.048 Ma (MSWD = 1.60; prob. = 0.04). Figure 2-5 presents the final age regressions for samples 32A and JD15; ages for each sample are in Table 2-1; zircon U-Pb analytical data are given in the digital appendix.

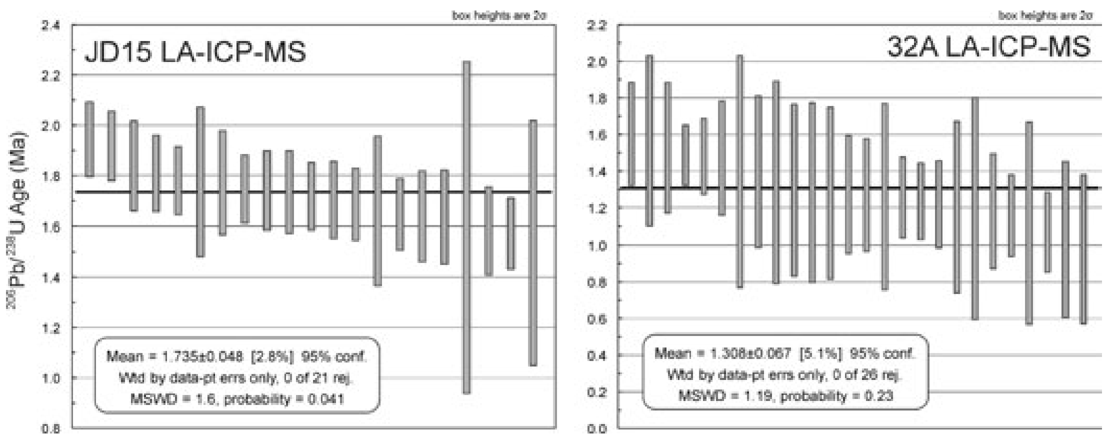

Figure 2-5. LA-ICP-MS weighted average plots for samples JD15 and 32A. Error bars represent ± 2σ precision.

Table 2-1. Compilation of U-Pb zircon ages

	Ok Tedi			Baia	
	32A	508-366*	809-116*	JD15	JD15
	LA-ICP-MS	SHRIMP	SHRIMP	LA-ICP-MS	CATIMS
Weighted Mean Age	1.308	1.237	1.287	1.735	1.746
95% Confidence	0.067	0.057	0.045	0.048	0.005
% Uncertainty	5.1	4.6	3.5	2.8	0.3
MSWD	1.19	1.4	0.51	1.6	1.15
Probability of Fit	0.23	0.16	0.90	0.041	0.33
Number	26/34	14/16	12/12	21/24	5/8

* Data re-evaluated from van Dongen et al. (2010)

CA-TIMS U-Pb Dating

Eight zircon crystals from sample JD15 were selected for analysis on the basis of LA-ICP-MS spot analysis (Figure 2-3); one of these crystals (z3) was broken into two fragments each for separate analysis. Of these nine analyses, three crystals yielded resolvable older ages, including both fragments of crystal z3; these analyses are interpreted as having a contribution from cores of significantly older, xenocrystic zircon (z2) or only slightly older antecrystic zircon (z3, z7). Equivalent $^{206}Pb/^{238}U$ dates were obtained from the remaining five crystals. Analytical data is shown in Table 2-2. The age of igneous crystallization may be interpreted from the weighted mean $^{206}Pb/^{238}U$ date of 1.746 ± 0.005(0.005)[0.006] Ma (n = 5; MSWD = 1.15; Figure 2-6); a more conservative error may be derived from the nominal ± 12-13 ka uncertainty of individual analyses. Ages are included in Table 2-1.

Re-evaluation of Previous SHRIMP Dating

Previous SHRIMP U-Pb analytical data from van Dongen et al. (2010) for the Sydney Monzodiorite was incorporated into this study with fresh correction factors. Of the two samples previously dated, sample 508-366 returned a weighted average age of 1.247 ± 0.060 Ma (MSWD = 1.60; prob. = 0.36) and sample 809-116 yielded a weighted average age of 1.287 ± 0.045 Ma (MSWD = 0.51; prob. = 0.90). Figure 2-7 presents the final age regressions for samples 508-366 and 809-116; final ages corrected for initial Th disequilibrium and common Pb are in Table 2-1.

Table 2-2. CA-TIMS U-Pb isotopic data for zircon, sample JD15

	Compositional Parameters						Radiogenic Isotope Ratios								Isotopic Ages					
Sample	$\frac{Th}{U}$	$^{206}Pb^*$ x10^{-13} mol	mol % $^{206}Pb^*$	$\frac{Pb^*}{Pb_c}$	Pb_c (pg)	$\frac{^{206}Pb}{^{204}Pb}$	$\frac{^{208}Pb}{^{206}Pb}$	$\frac{^{207}Pb}{^{206}Pb}$	% err	$\frac{^{207}Pb}{^{235}U}$	% err	$\frac{^{206}Pb}{^{238}U}$	% err	corr. coef.	$\frac{^{207}Pb}{^{206}Pb}$	±	$\frac{^{207}Pb}{^{235}U}$	±	$\frac{^{206}Pb}{^{238}U}$	±
(a)	(b)	(c)	(c)	(c)	(c)	(d)	(e)	(e)	(f)	(e)	(f)	(e)	(f)		(g)	(f)	(g)	(f)	(g)	(f)
JD15																				
z2	0.088	4.4333	99.88%	230	0.43	15499	0.028	0.050599	0.07	0.135991	0.14	0.019492	0.071	0.946	223	2	129.47	0.17	124.45	0.09
z7	0.952	0.0079	62.19%	0.6	0.40	48	0.319	0.059688	152	0.002284	152	0.000277	1.171	0.102	592	3240	2.32	3.51	1.789	0.021
z3b	0.930	0.0069	58.60%	0.5	0.40	44	0.312	0.048345	232	0.001844	232	0.000277	1.328	0.093	116	5380	1.87	4.35	1.783	0.024
z3a	0.891	0.0065	58.96%	0.5	0.38	44	0.299	0.052148	240	0.001974	240	0.000275	1.285	0.082	292	5384	2.00	4.80	1.769	0.023
z6	0.962	0.0141	75.57%	1.1	0.38	74	0.323	0.047116	47.68	0.001767	47.8	0.000272	0.692	0.217	55	1116	1.79	0.86	**1.754**	**0.012**
z8	1.622	0.0471	86.62%	2.6	0.60	135	0.536	0.052552	4.87	0.001969	5.08	0.000272	0.738	0.697	309	110	2.00	0.10	**1.751**	**0.013**
z4	1.369	0.0253	84.65%	2.1	0.38	118	0.455	0.049115	16.85	0.001835	17.0	0.000271	0.655	0.305	153	389	1.86	0.32	**1.747**	**0.011**
z5	2.265	0.0291	83.77%	2.3	0.47	111	0.739	0.049502	15.21	0.001849	15.3	0.000271	1.016	0.371	172	353	1.88	0.29	**1.746**	**0.018**
z1	1.015	0.0532	92.52%	4.3	0.36	241	0.340	0.047127	3.87	0.001754	3.97	0.000270	0.458	0.560	56	91	1.78	0.07	**1.740**	**0.008**

(a) z1, z2 etc. are labels for single zircon grains or fragments annealed and chemically abraded after Mattinson (2005).
(b) Model Th/U ratio calculated iteratively from radiogenic 208Pb/206Pb ratio and 230Th disequilibrium-corrected 206Pb/238U age.
(c) Pb* and Pbc represent radiogenic and common Pb, respectively; mol % $^{206}Pb^*$ with respect to radiogenic, blank and initial common Pb.
(d) Measured ratio corrected for spike and fractionation only. Fractionation estimated at 0.18 +/- 0.04 %/a.m.u. for Daly analyses, based on analysis of NBS-981 and NBS-982.
(e) Corrected for fractionation, spike, and common Pb; all common Pb was assumed to be procedural blank: 206Pb/204Pb = 18.042 ± 0.61%; 207Pb/204Pb = 15.537 ± 0.52%; 208Pb/204Pb = 37.686 ± 0.63% (all uncertainties 1-sigma).
(f) Errors are 2-sigma, propagated using the algorithms of Schmitz and Schoene (2007).
(g) Calculations are based on the decay constants of Jaffey et al. (1971). 206Pb/238U and 207Pb/206Pb ages corrected for initial disequilibrium in 230Th/238U using Th/U [magma] = 3 ± 10%.

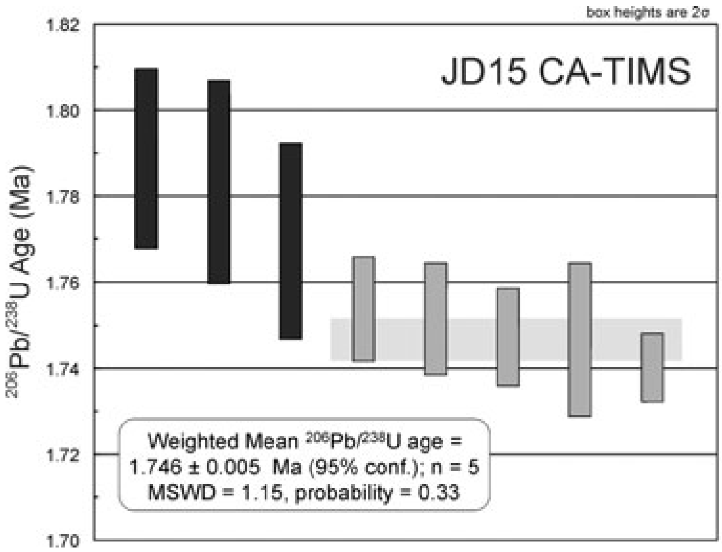

Figure 2-6. CA-TIMS Weighted average plot for sample JD15. Black bars indicate ages rejected from the age calculation; all error represent ± 2σ precision.

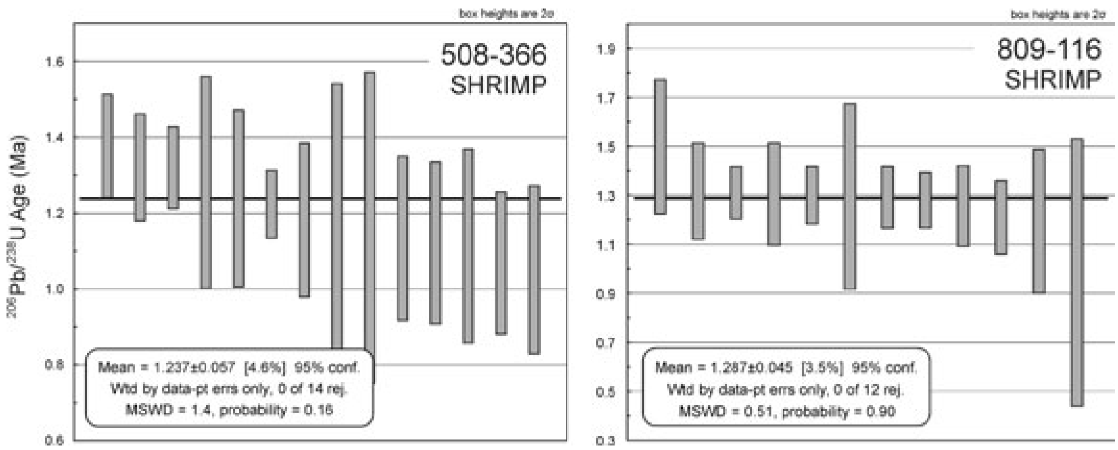

Figure 2-7. SHRIMP weighted average plots for Ok Tedi samples 508-366 and 809-116. Error bars represent ± 2σ precision. Data is re-evaluated from van Dongen et al. (2010).

Discussion

U-Pb zircon dating for all samples by the different dating methods yielded Quaternary crystallization ages consistent with their geological setting and previous work (van Dongen et al., 2010). In addition to adding knowledge to the rapidly growing geological database for Papua New Guinea, this work compares common methods of obtaining zircon age data applied to very young rocks. Zircons from sample 32A, the Sydney Monzodiorite intrusive of the Ok Tedi porphyry complex were measured by LA-ICP-MS and SHRIMP (van Dongen et al., 2010), whereas targeted LA-ICP-MS and CA-TIMS dating methods were utilized for sample JD15, andesitic volcanics of the Baia prospect, in some cases on the same zircon crystals. Figure 2-8 presents a correlation between the calculated weighted averages for both sample suites given the different U-Pb dating methods. These ages are all corrected for initial Th disequilibrium and common Pb. Weighted average ages for both samples show good internal correlation between the different U-Pb dating methods. Sample JD15 shows very close correlation between both LA-ICP-MS and CA-TIMS analyses while correlation between sample 32A and the associated SHRIMP ages does show some scatter, however, all 2σ errors are shown to overlap (Figure 2-8). Although there is good correlation between the different dating methods in this instance, it is useful to understand the potential sources of uncertainty in LA-ICP-MS analyses that contribute to the resultant ages, while also drawing from findings of alternative methods such as SHRIMP. Furthermore, given the particularly young ages of these samples and the propensity of such samples to exacerbate uncertainties, it is important to assess the appropriateness of the statistical errors.

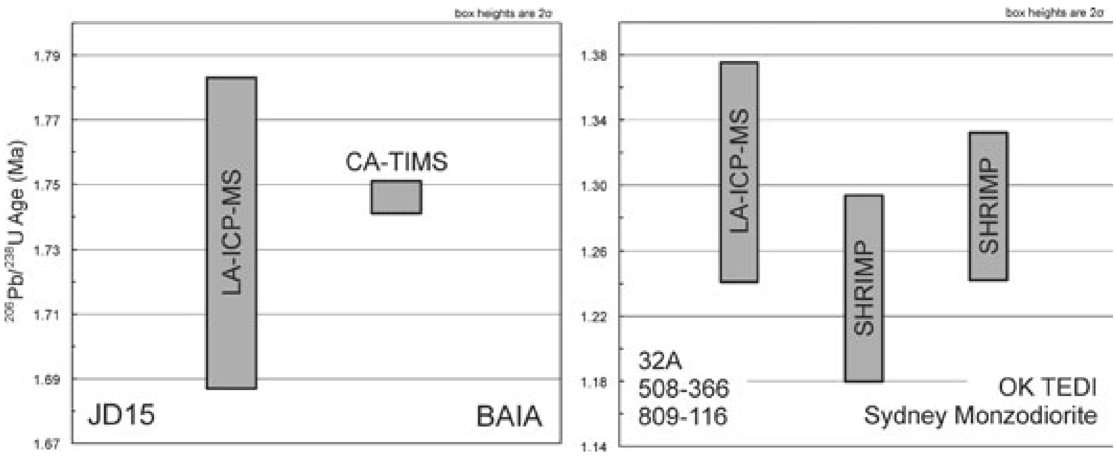

Figure 2-8. Multi-method U-Pb dating comparison diagrams for sample JD15, Baia and Sydney Monzodiorite, Ok Tedi samples. Weighted average ages are shown for LA-ICP-MS, CA-TIMS and SHRIMP U-Pb dating with corresponding boxes for ± 2σ errors; samples 508-366 and 809-116 are re-evaluated from van Dongen et al. (2010).

The application of LA-ICP-MS in U-Pb geochronological studies is a relatively recent advance (Horn et al., 2000) and as such the intricacies and sources of uncertainty are still susceptible to revision and corrections. There are however, a number of well-established procedures for calibrating U-Pb analyses by LA-ICP-MS to correct for elemental fractionation associated with laser ablation, and the sample transport and ionisation processes, together with the inherent mass bias of the ICP-MS (Jackson et al., 2004). These factors contributing to correction rely on the stability, reproducibility and standardisation (e.g. spot size, laser fluence, integration time) of analyses to allow for empirical correction of ablation-related elemental fractionation (Horn et al., 2000). In the first instance an accepted external standard is used to correct for sources of fractionation, ideally this will be a very good matrix-matched standard where ablation conditions for both unknown and standard are essentially identical (Tiepolo et al., 2003; Tiepolo, 2003; Jackson et al., 2004). For correction of instrumental mass bias an on-line spike (Tl/^{233}U or ^{235}U) is often introduced into the carrier gas stream (Horn et al., 2000; Košler et al., 2002), or alternatively a solution-based spike is used. The latter, however, can result in high background Pb compromising data for young and/or low-U zircon (Košler et al., 2002; Jackson et al., 2004). In general, common Pb contributions at a high level can typically result in exclusion of a few analyses per analytical session without serious concerns; however, a variety of strategies can be adopted to adequately address conventional common Pb contributions and may include selective integration of signals or graphical evaluation (Jackson et al., 2004). Additionally, Williams and Hergt (2000) note the U-content of zircon can produce a systematic offset in zircon ages. Above a threshold of ~2500 ppm U an increase in ^{206}Pb/^{238}U ages can be expected at a rate of between 1.5% and 2.0% for every additional 1000 ppm of U. This is not often a concern with U content in zircon rarely achieving these concentrations.

The above corrections are typically regarded as routine protocols minimizing error and uncertainty in the instrumental set-up and empirical corrections. A topic of more conjecture, however, is the contribution of uncertainties in the behavior of the ablation process to the overall analytical uncertainty and at the present day, our failure to fully quantify these uncertainties. Initially there are several factors that can contribute to uncertainty and should be considered, but in general can be easily accommodated for. Firstly the layout of the zircon-mount has significant potential to contribute to analytical uncertainty if not correctly accounted for. The effect of crystallographic orientation can result in variation of ^{206}Pb/^{238}U emission with crystal orientation for baddeleyite (another Zr-rich mineral) as demonstrated by Wingate and Compston (2000); however, the same orientation-related effect has not previously been detected in zircon studies. Secondly and more importantly, Stern and Amelin (2003) identified considerable variation in ^{206}Pb/^{238}U ionization in the plane the primary beam impacts the target, particularly approaching the edges of the mount. The impact of this effect is typically limited by sample arrangement within a relatively small central area of the mount.

The precision of the mechanical ablation process must also be considered. Jackson et al. (2004) highlighted that while the external precisions of the $^{206}Pb/^{238}U$ and $^{207}Pb/^{235}U$ ratios are very similar, even given a magnitude difference in count rate, they are significantly poorer than the $^{207}Pb/^{206}Pb$ ratios for the same analyses. The authors attribute these variations in precision to small differences in Pb/U fractionation behavior from analysis to analysis associated with drift in laser operating conditions, for example variation in laser focus (Jackson et al., 2004); although these sources of analytical uncertainty cannot realistically be accounted for at every analytical stage, routine standard bracketing techniques limit the analytical session-scale implications of instrumental drift. Disparities in isotopic ratios can also potentially arise from heterogeneity of ablated material, either from the zircon itself or systematic variation in ablated particle size distribution with implications for plasma conditions and mass bias effects (Guillong et al. 2003; Klötzli et al., 2009). Similarly, the ablation product or ejecta around holes must be considered in fractionation and mass bias. Experimental work from Košler et al. (2005) found that ejecta around holes drilled in zircon is dominated by zircon, baddeleyite and silica in various forms. Furthermore, the deposition of zircon and baddelyite will fractionate Pb from U as U is compatible in zircon and baddelyite while Pb is not. It follows that the deposition of zircon and baddeleyite in or near the ablation hole is responsible for downhole fractionation of Pb from U in zircon (Košler et al., 2005; Allen et al., 2012).

All the above sources of uncertainty can be observed and accounted for to some degree, however, more subtle expressions of $^{206}Pb/^{238}U$ heterogeneity reflect the dispersion and interactions of ablated particles, termed matrix effects. Findings from Black et al. (2004) suggest bias or offsets in measured ages can often be related to the abundance and combination of trace elements that is likely a function of REE + Y and P substitution into the Si-site within zircon. This substitution, also termed the 'xenotime' substitution may induce a lattice strain in ablated material affecting the secondary ion formation and mass bias, particularly in near stoichiometric $Zr(Hf)SiO_4$ zircon crystals (Finch et al., 2001; Black et al., 2004). While this matrix effect process has yet to be fully documented, Black et al. (2004) identified a correlation with the abundance of a variety of elements, where P, Nd and Sm, while present in too low concentrations to be primarily responsible for the matrix effect, are promising element proxy indicators. Klötzli et al. (2009), however, also observed shifts in Pb isotopic ratios in addition to $^{206}Pb/^{238}U$, suggesting the matrix effect proposed by Black et al. (2004) alone is not sufficient to quantify isotopic variation and uncertainty. Furthermore, additional bias in bias-corrected Pb isotope ratios has been related to matrix components such as Ca, Al, Fe and Mg, and demonstrated to cause non-spectral matrix effects (Barling and Weis, 2008). Moreover, an associated enhancement in both Pb and Tl signal has been attributed to a matrix-induced decrease in Ar charge density, subsequently leading to an over representation of measured Pb^+ and Tl^+ ions. Klötzli et al. (2009) went on to suggest shifts in both U-Pb and Pb isotopic ratios are potentially a response to fractionation effects combined with ^{233}U-^{205}Tl-^{203}Tl normalization.

In a different approach to matrix effects, Allen et al. (2012) interpreted the alpha dose accumulated in zircon as a major limitation on the accuracy of LA-ICP-MS $^{206}Pb/^{238}U$ dating. This matrix effect is a key contributor to uncertainty in dating young zircon because the alpha dose accumulated by the unknown can be appreciably less than that received by the zircon standard, and this difference can lead to an inaccuracy of up to −5% (Allen et al., 2012). Although not conclusive as to the reasons, a strong correlation exists between the alpha dose received by the zircon and the difference between $^{206}Pb/^{238}U$ measured by TIMS versus LA–ICP–MS. Allen et al. (2012) suggested the degree of radiation damage may be related to an increase in the measured $^{206}Pb/^{238}U$ in response to comparatively higher rates of Pb escape over U around the ablation hole due to variations in particle size distribution. Quantitative assessment of the alpha dose and associated degree of radiation damage in the zircon can potentially yield a relationship to correct for matrix effects in existing LA-ICP-MS $^{206}Pb/^{238}U$ dates, however, at present this in hindered by poor constraint of the accumulated alpha dose received by zircon.

An inherent trade-off will always be present between precision and homogeneity of the standard zircon and appropriateness of the standard to a particular study, that is, how well the zircon standard and unknown is matrix-matched. The GJ1 standard used in this study is typically the primary procedural zircon standard of choice in various U-Pb dating methods including LA-ICP-MS. However, as a much older zircon than the unknowns in this study, GJ1 likely holds an elevated alpha dose (Allen et al., 2012) and is not an ideal matrix-match. Matching the matrix, and more particularly for young zircon, the alpha dose accumulated by the zircon standard as closely as possible to the unknown can substantially reduce matrix-related uncertainty (Allen et al., 2012). However, our ability to measure the retained alpha dose at present and likewise the associated uncertainty makes this approach problematic. The Fish Canyon Tuff as a much younger zircon standard, but still with greater than a magnitude difference in relative ages to the unknown zircon presented here, is shown to have a significantly lower alpha dose than GJ1 (Allen et al., 2012) and may be considered a more appropriate standard. However, the Fish Canyon Tuff standard itself has shown to be heterogeneous, and often suffers from common Pb effects, significantly limiting the precision of analyses. In the absence of a reliable, high-precision young standard that is homogeneous, we propose GJ1 still be retained as a primary standard zircon. This lack of an age appropriate standard can make correction for matrix effects difficult but in the first instance will provide more precise isotopic ratios by minimizing uncertainty related to fractionation.

In this instance where I have extremely young zircon and associated low radiogenic Pb count rates and $^{206}Pb/^{238}U$ ratios, I must also take into consideration uncertainty generated in post-data acquisition signal processing and data treatment. Zircon with low count rates are more susceptible to signal spikes and zircon heterogeneity, and exhibit greater count rate fluctuation compared with older zircon with comparatively greater radiogenic Pb accumulation. In addition, such low $^{206}Pb/^{238}U$ ratios and corresponding errors (see supplementary material) are nearing the detection limit of the laser ablation ICP-MS set-up; as a result analyses begin to lose resolution and precision of the measured isotope ratios. Although these factors cannot be fully accounted for given the state-of-the-art laser ablation ICP-MS methods, erratic signals can largely be visually filtered to exclude aberrations that may arise from ablating zircon affected by, for example, Pb-loss or inclusions. Conversely, with such low $^{206}Pb/^{238}U$ ratios as presented here, it is counter productive to select only small signal windows for processing as these will be more susceptible to minor signal fluctuations in downhole fractionation, and therefore may not reflect the overall zircon isotopic composition. Considering these factors, we must acknowledge the analytical uncertainties in the data related to signal processing, where small changes in a selected signal processing window will lead to changes in resultant isotopic ratios. In older zircon these affects will largely be insignificant and taken into account by any associated error margin, however, a minute change in isotopic ratios given the young ages represents a comparatively large shift with the potential to shift a determined age by up to tens of thousands of years, often comparable to given error margins. Signal processing must therefore be considered as major contributor to uncertainty of any young age determination.

Previous studies by Klötzli et al. (2009) suggested that the precision of current laser ablation methods for obtaining U-Pb ages from zircon are limited by our understanding of uncertainties and can be no better than 3% of the determined age at a 2σ level. I take a more conservative approach to uncertainties in this study given the very young Quaternary ages obtained. I suggest a realistic but conservative uncertainty in the analytical error in this instance is 5% of the determined age at a 2σ level. Although the error (95% uncertainty) associated with sample 32A at 5.1% is already in excess of 5%, the resultant analytical error attributed to sample JD15 is quoted at just 2.8%. Uncertainties in signal processing mentioned above are typically in the order of 0.5% but can equate to up to 1% additional error. Furthermore, beyond normal protocols for correction of fractionation and mass bias, the greatest source of uncertainty in such young zircon is likely to be matrix affects related to the relative alpha dose between standard and unknown highlighted by Allen et al. (2012). Although this is more difficult to quantify, taking into account the potential for a -5% age determination for LA-ICP-MS compared with CA-TIMS analyses, a 5% uncertainty will fully account for this potential disparity given the results for sample JD15. Such an assessment of errors will quantitatively adjust the JD15 weighted average from 1.735 ± 0.048 Ma (2.8%) to 1.735 ± 0.087 (5%), while 32A retains the calculated weighted average of

1.308 ± 0.67 Ma (5.1%).

The results of this study demonstrate that while CA-TIMS will be the benchmark for U-Pb dating for the foreseeable future, the LA-ICP-MS U-Pb dating method is more than capable of resolving zircon crystallization ages to within 5% error (2σ) of a determined age with confidence, and is comparable in precision to SHRIMP U-Pb dating. This has implications for advances in Quaternary science and geochronology, where LA-ICP-MS dating provides an avenue for rapid and cost effective acquisition of large datasets. Where detailed locality-scale investigations or dense age resolution is required it remains necessary to obtain TIMS ages. However, given the results here, LA-ICP-MS dating is without doubt appropriate for application in studies of a regional nature where less temporal resolution is required. Such applications of this method may have implications for studies that may include recent volcanism and associated natural hazard analysis, hominid evolution and even climate change through dating of tuffs, sediment horizons or cave-fill for example.

Conclusions

I sampled two Quaternary magmatic occurrences from Ok Tedi and Baia within the Pliocene–Quaternary magmatic belt of the Maramuni arc hosted by the Papuan Fold and Thrust Belt of Papua New Guinea. Zircon from both samples were subjected to LA-ICP-MS U-Pb dating and subsequently compared with CA-TIMS and previous SHRIMP U-Pb dating. All U-Pb dating was determined by weighted average and corrected for common Pb contributions and initial Th disequilibrium. Sample JD15 yielded an analytical LA-ICP-MS age of 1.735 ± 0.048 Ma and a corresponding CA-TIMS age of 1.746 ± 0.005 Ma. The Sydney Monzodiorite of Ok Tedi returned a LA-ICP-MS age of 1.308 ± 0.067 Ma in comparison to two previous samples (van Dongen et al., 2010) dated via SHRIMP analysis and re-evaluated in this study at 1.237 ± 0.057 Ma (508-366) and 1.287 ± 0.045 Ma (809-116). These are some of the youngest LA-ICP-MS U-Pb zircon ages obtained to date and among the few Quaternary ages. Both sample suites show good correlation of ages through the different dating methods. Moreover, the particularly young zircon ages found in this study demanded an assessment with regard to contributions to uncertainty and errors relevant to very young LA-ICP-MS U-Pb dating. The largest contributors to uncertainty in addition to conventional protocols are the current lack of age-appropriate zircon standards. This principally recognizes the limitation of our ability to reliably matrix-match the accumulated alpha dose in young zircon; and secondly the analytical limitations of the LA-ICP-MS apparatus set-up. Young zircon and the associated low radiogenic lead content result in $^{206}Pb/^{238}U$ close to the lower limit of detection making measurement susceptible to heterogeneity in the zircon and laser ablation fractionation processes. I propose a uncertainty of 5% is appropriate for Quaternary U-Pb ages obtained by LA-ICP-MS dating methods.

Chapter 3

Melanesian arc far-field response to collision of the Ontong Java Plateau: Geochronology and petrogenesis of the Simuku Igneous Complex, New Britain, Papua New Guinea

Published in *Tectonophysics*

Abstract

Understanding the evolution of the mid-Cenozoic Melanesian arc is critical for our knowledge of the regional tectonic development of the Australian-Pacific plate margin, yet there have been no recent studies to constrain the nature and timing of magmatic activity in this arc segment. In particular, there are currently no robust absolute age constraints at the plate margin related to either the initiation or cessation of subduction and arc magmatism. I present the first combined U-Pb zircon geochronology and geochemical investigation into the evolution of the Melanesian arc utilizing a comprehensive sample suite from the Simuku Igneous Complex of West New Britain, Papua New Guinea. Development of the embryonic island arc from at least 40 Ma and progressive arc growth was punctuated by distant collision of the Ontong Java Plateau and subduction cessation from 26 Ma. This change in subduction dynamics is represented in the Melanesian arc magmatic record by emplacement of the Simuku Porphyry Complex between 24 and 20 Ma. Petrological and geochemical affinities highlight genetic differences between "normal" arc volcanics and adakite-like signatures of Cu-Mo mineralized porphyritic intrusives. The contemporaneous emplacement of both "normal" arc volcanics and adakite-like porphyry intrusives may provide avenues for future research into the origin of diverse styles of arc volcanism. Not only is this one of few studies into the geology of the Melanesian arc, it is also among the first to address the distant tectono-magmatic effects of major arc/forearc collision events and subduction cessation on magmatic arcs, and also offers insight into the tectonic context of porphyry formation in island arc settings.

Introduction

The study of subduction-related magmatic arcs is well established for both continental and oceanic island arcs. Likewise the spectrum of arc related magmatism is relatively well understood in terms of melt fractionation and magma evolution in response to arc development and associated crustal thickening (e.g. Jakes and Gill, 1970; Hamilton, 1981; Hildreth and Moorbath, 1988; DeBari and Sleep, 1991; de Boer et al., 1995; Woodhead et al., 1998). The magmatic response of arcs to plate scale tectonic changes is comparatively poorly understood; continental arcs (e.g. Andean arc) and collision zones (e.g., Himalaya) have been, and currently are, the focus of collision-related magmatic studies (Bignold and Treloar, 2003; Searle et al., 2003; Chung et al., 2005; Hou et al., 2006; Kay et al., 2005; Rosenbaum et al., 2005; Harris et al., 2008; Sillitoe, 2010; Rosenbaum and Mo, 2011). These studies, however, focus on regions where collision events have direct implications for the area in the immediate vicinity of collision. In contrast, the response of magmatic arcs to collision and subduction cessation is currently not well understood. Our lack of knowledge in this field reflects our lack of constraint on pre-collision tectonics, collision dynamics and precise geochronological controls on collision timing.

There are very few regions on Earth where we have a well-documented framework of plateau arrival at a trench and collision at a magmatic arc that has not been adversely complicated by the collision itself or later overprinting. New Britain, Papua New Guinea is an exceptional natural laboratory in these terms (Figure 3-1). The island initially formed as part of the Melanesian arc from at least c. 45 Ma, at which time the Pacific plate subducted to the southwest beneath the Australian plate (Figure 3-2; e.g. Petterson et al., 1999; Hall, 2002; Schellart et al., 2006). This subduction and arc development is one of the most poorly understood elements of the southwest Pacific. The Melanesian arc comprised New Britain, New Ireland and Bougainville of Papua New Guinea, much of the Solomon Islands, Vanuatu and Fiji (e.g. Kroenke, 1984; Musgrave, 1990; Abbott, 1995; Petterson et al., 1999). Since the time of arc formation, however, these terranes have undergone complex tectonic reorganizations within the southwest Pacific region by multiple episodes of arc/forearc collision, subduction cessation and subsequent subduction polarity reversal to displace and reorientate the fragments of arc-basement (Petterson et al., 1999; Hall, 2002; Schellart et al., 2006). The most significant collision episode is that of the Ontong Java Plateau, which collided with the Melanesian arc in the vicinity of the modern Solomon Islands, some 500–1000 km along-arc distance to the east of New Britain (Figures 3-2 and 3-3; Kroenke, 1984; Musgrave, 1990; Petterson et al., 1999). Collision of the Ontong Java Plateau with this margin has been previously suggested to have occurred in the Upper Oligocene, at approximately 26–23 Ma (Knesel et al., 2008) or 25–20 Ma (Hall, 2002; Schellart et al., 2006). Subsequently, New Britain has undergone secondary arc development as the result of subduction polarity reversal to a north-dipping Australian plate beneath the late Pliocene–Quaternary Bismarck Sea (Cooper and Taylor, 1985; 1987; Woodhead et al., 1998). This has resulted in some overprinting of the former arc, but ample exposure of the Melanesian arc remains and has only undergone gentle warping and tilting in recent times (Madsen and Lindley, 1994; Woodhead et al., 1998; Lindley, 2006).

In this paper I present a detailed study into the Eocene–Lower Miocene evolution of New Britain and the Melanesian arc, with implications for the timing of Ontong Java Plateau arrival at the Melanesian trench. I present a new high-resolution coupled U-Pb zircon geochronology and geochemical evolution of the magmatic arc from the Simuku Igneous Complex of West New Britain. The location of this study is significant in that it is well removed from the site of plateau collision, in this case by approximately 500–1000 km along arc distance, and thus not affected directly by any collision-related processes such as crustal thickening. Therefore, we can investigate the potential effects of distant collision events and subduction cessation. This has implications for the study of major collision events in both island-arc and convergent continental margins globally, particularly with regard to the imposed physical or structural processes during collision coupled with the geochemical response of arc magmatism.

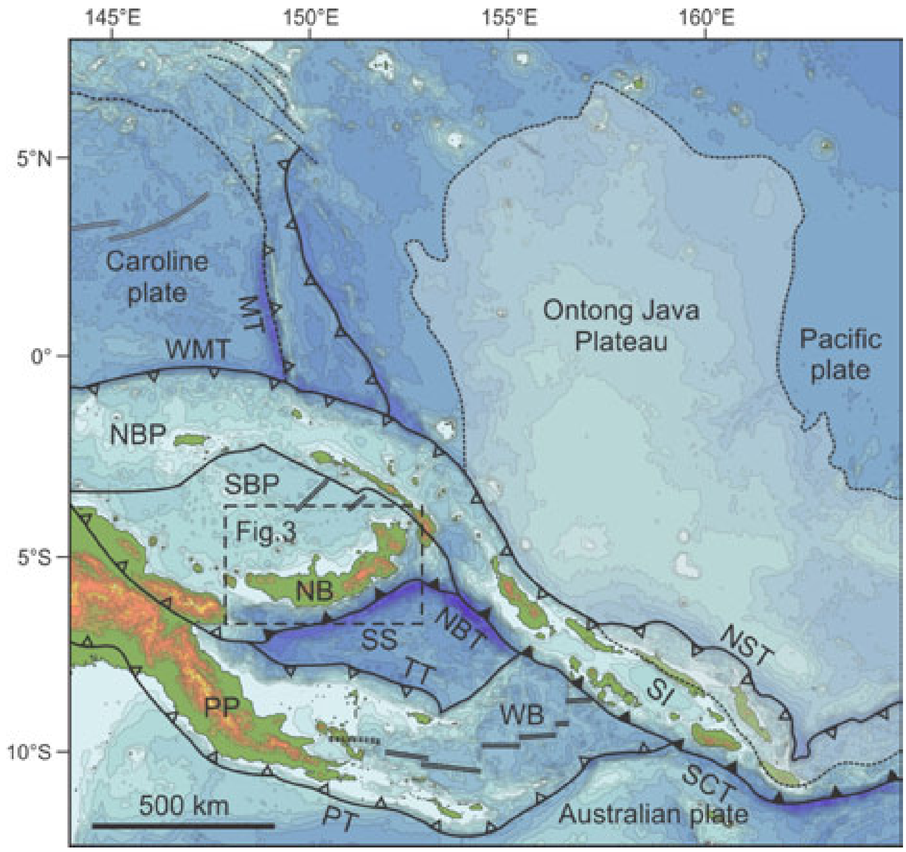

Figure 3-1. Topography, bathymetry and major tectonic elements of eastern Papua New Guinea and Solomon Islands region. Major tectonic plates are as indicated; MT: Manus trench; WMT: West Melanesian trench; NBP: North Bismarck plate; SBP: South Bismarck plate; NB: New Britain; SS: Solomon Sea plate; NBT: New Britain trench; TT: Trobriand trough; PP: Papuan Peninsula; PT: Pocklington trough; WB: Woodlark Basin; SI: Solomon Islands; SCT: San Cristobel trench; NST: North Solomon trench.

Geological Setting and Samples

Tectonic Setting: Upper Oligocene–Lower Miocene Reorganization in the Southwest Pacific

The southwest Pacific underwent a period of extensive tectonic reorganization during the Upper Oligocene and Lower Miocene. Collision of the Ontong Java Plateau with the northern Australian plate margin at the Solomon Islands between 26 and 20 Ma (Figure 3-2; Petterson et al., 1999; Hall, 2002; Schellart et al., 2006; Knesel et al., 2008) is thought to be one of the main drivers of this reorganization, being significant enough to cause temporary disruption to the Australian and Pacific plate motion circuit (Knesel et al., 2008). However, no direct structural responses to collision have conclusively been identified and directly linked to convergent processes on the plate margin at this time. It should be noted this lack of contemporaneous evidence of arc/forearc collision has led several authors to suggest a more recent Upper Miocene timing for collision (Mann and Taira, 2004; Phinney et al., 2004), although Upper Oligocene collision is widely accepted.

Tectonic reorganization of the region is reflected over the entire northwestern through to northeastern Australian plate and wider plate margin, with cessation of sea floor spreading in the Caroline Sea, Solomon Sea, Rennell trough and South Fiji Basin at or around 25 Ma (Davey, 1982; Hall, 2002; Gaina and Muller, 2007; Mortimer et al., 2012). Concomitantly we see a termination of

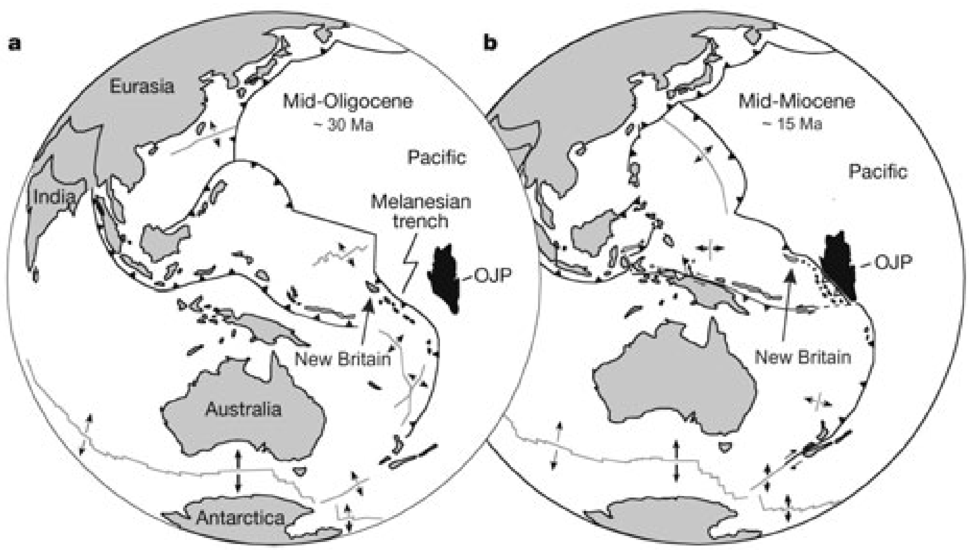

Figure 3-2. Simplified reconstructions of the western Pacific (Modified from Knesel et al., 2008; Hall, 2002). a, Mid-Oligocene epoch, ~ 30 Ma; b, Mid-Miocene epoch, ~ 15 Ma. Reconstruction illustrates the location of New Britain prior to, and after collision of the Ontong Java Plateau (OJP) with the Melanesian trench at the Solomon Islands; leading to jamming and cessation of the southwest-dipping subduction.

magmatism in at least the western Melanesian arc in the earliest Miocene (Petterson et al., 1999; Lindley, 2006), and opening of a series of intra-arc basins along the same arc from approximately the Upper Oligocene (Central Solomon Basin [Wells, 1989; Cowley et al., 2004]; New Hebrides intra-arc basins [Bradshaw, 1992]). Locally in New Britain a Lower Miocene extensional regime is apparent from north-northeasterly extensional joint sets and associated hydrothermal activity dated at 22–23 Ma (Wilcox et al., 1973; Lindley, 2006), which are part of a wider horst and graben zone straddling New Ireland and east New Britain (Lindley, 2006). This time is also a significant metallogenic epoch in the Melanesian arc with porphyry emplacement of Poha, Guadalcanal at 24.4 Ma (Chivas, 1981), Simuku-Kulu (22–28.7 Ma), Esis (25 Ma; Hine and Mason, 1978), and Plesyumi (25–24 Ma; Titley, 1978) of New Britain. Although these tectonic processes have previously been identified within their individual geological contexts, they have not yet been drawn together as part of a regional tectonic study. Taken together, the geological phenomena are indicative of a major tectonic regime shift and likely resulted from Ontong Java Plateau collision and processes related to subduction cessation.

Further afield at this time, New Caledonia is intruded by anomalous Upper Oligocene post-obduction granitoids (Cluzel et al., 2005). Further west, Hall (2002) proposed collision of the East Philippines-Halmahera-South Caroline arc with the northern margin of New Guinea at 25 Ma, and Fujiwara et al. (1995) interprets initiation of the Ayu trough at 25 Ma, contemporaneous with formation of the Yap trench and associated arc (Ohara et al., 2002). No direct links between these southwest Pacific tectonic phenomena have previously been suggested and the magnitude of tectonic reorganization makes this an extremely complex region in the Upper Oligocene to the Lower Miocene, similar to the intricacies of the present day tectonic setting. This preliminary study into the evolution of the Melanesian arc will aid in unraveling these tectonic processes and help understand the response of plate margins and interiors to large collision events, and how such events may be recognized in the geological record.

New Britain Geology

The recent tectonic history of New Britain is strongly coupled to that of the Bismarck Sea region (Figure 3-1). North-dipping subduction of the Solomon Sea plate beneath New Britain and the Bismarck Sea at the New Britain trench forms the active eastern Bismarck volcanic arc. The arc occupies the northern part of New Britain (Figure 3-3) and ranges from basalt to rhyolite in composition with typical island arc tholeiite signatures (Jakes and Gill, 1970) that are characterized by exceptional depletions in high field strength elements (Woodhead et al., 1998). On a regional-scale, docking of the Finisterre Terrane with the New Guinea mainland at 3.5 Ma initiated rupture of the New Britain back-arc creating two independent tectonic plates; the South Bismarck and North Bismarck plates (Taylor, 1979). It has generally been accepted that the history of New Britain and the adjacent Finisterre Terrane share a common origin as part of the Melanesian arc. However, Findlay (2003) provides evidence from lithostratigraphic relationships in the two terranes that clearly demonstrate that they are unrelated (Figure 3-2). The Finisterre, Sarawaget and Adelbert Mountains are part of an autochthonous plateau formed adjacent to northern New Guinea while New Britain was part of the Melanesian arc. For further details regarding the recent geological history of New Britain and development of the Bismarck Sea, readers are directed to Madsen and Lindley (1994), Woodhead et al. (1998), Wallace et al. (2004), and references therein.

While the modern tectonics of the Bismarck Sea, Bismarck arc and recent structural movements of New Britain are understood in some depth, the pre-Upper Miocene history of New Britain has been the topic of comparatively few studies. It is well understood that New Britain was previously part of the Melanesian arc where the Pacific plate subducted to the southwest beneath the Australian plate at the West Melanesian trench (Figure 3-2; Petterson et al., 1999). However, the timing for initial arc formation is poorly constrained. The main body of New Britain is composed of typical island arc magmatic rocks (Figure 3-3). Upper Eocene mafic and intermediate pillow lavas, breccias and volcaniclastics outcrop extensively throughout New Britain (e.g. Baining Volcanics), often with lenses of coralline limestone (Madsen and Lindley,

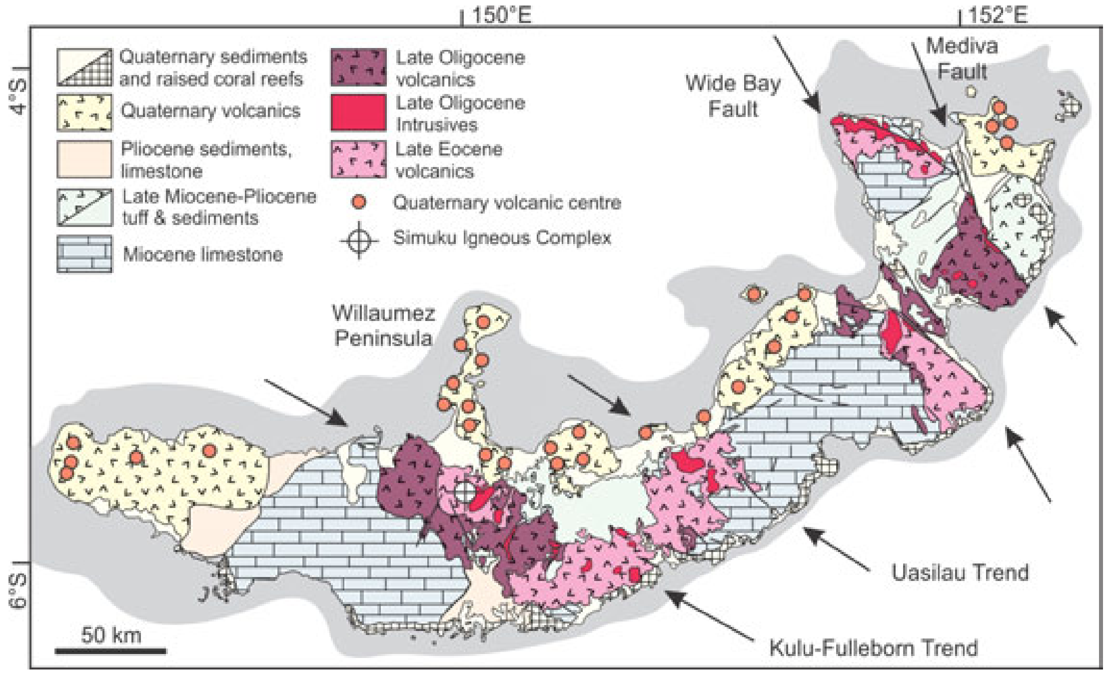

Figure 3-3. Geology and major structural lineaments of New Britain. The Simuku Igneous Complex is comprised of Upper Eocene volcanics and Upper Oligocene volcanics and intrusives as previously mapped, and lies on the Kulu-Fulleborn trend. Grey shading represents the limit of New Britain at the 1000 m bathymetric contour. After Australian Bureau of Mineral Resources (1976) and Lindley (2006).

1994; Lindley, 2006; this study). These are overlain by Upper Oligocene volcaniclastic formations (e.g. Merai Volcanics and Kapuluk Volcanics), and intruded by Upper Oligocene-Lower Miocene plutonic and hypabyssal rocks of mafic to intermediate composition (Madsen and Lindley, 1994; Christopher, 2002; Lindley, 2006; this study). The timing for termination of the Melanesian arc in the Upper Oligocene-Lower Miocene temporally coincides with, and has been attributed to, collision of the Ontong Java Plateau with the Solomon Islands (Figure 3-2; Kroenke, 1984; Musgrave, 1990; Petterson et al., 1999).

Following the change in the subduction regime during the Lower Miocene, the Melanesian arc underwent gradual subsidence and New Britain was overlain in part by the Lower and Middle Miocene Yalam and Sai Limestones (Figure 3-3; Madsen and Lindley, 1994; Woodhead et al., 1998; Christopher, 2002; Audra et al., 2011). A large proportion of these platform deposits have only undergone gentle tilting or arching and simple, regionally uniform uplift in the order of 1500-1800 m since the Upper Miocene, despite their location in tectonically active areas adjacent

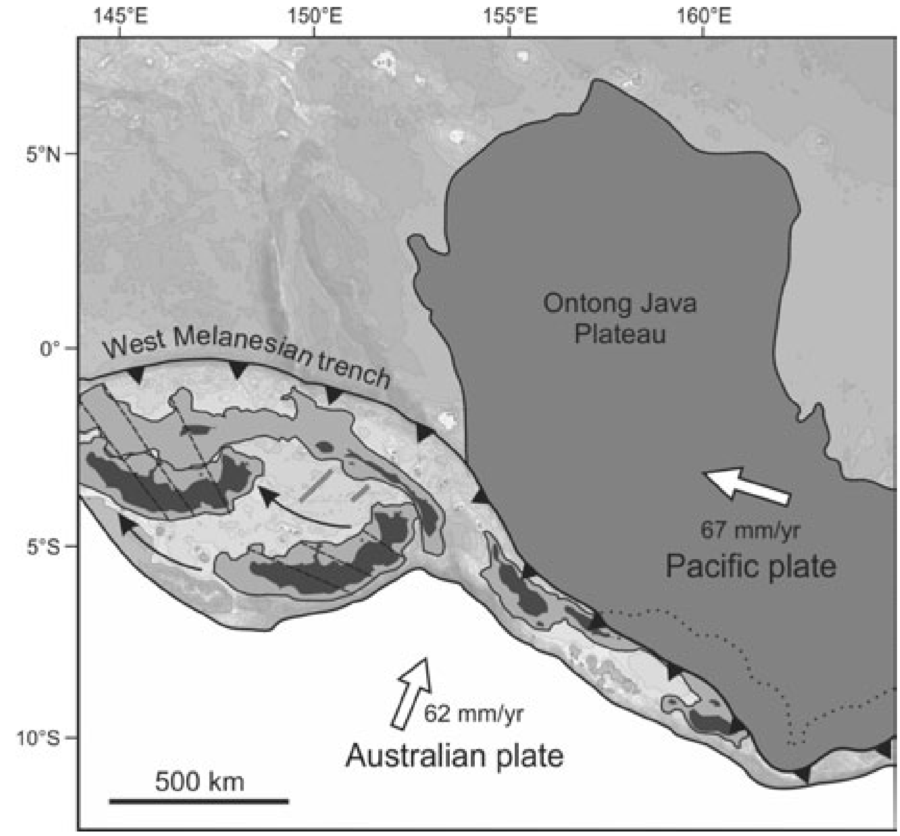

Figure 3-4. Simplified schematic reconstruction of the Melanesian arc terranes. Tectonic setting illustrates the distribution of arc basement prior to opening of the Bismarck Sea. The reconstruction highlights the location of New Britain to the west and well removed from the Ontong Java Plateau. Basement terranes are defined by the present day 1000 m bathymetric depth contour. Closure of the Bismarck Sea is reconstructed on the basis of lineament locations and orientations (dashed lines) defined from Lindley (2006). Melanesian trench is indicated from the present day plate boundary morphology. See text for discussion.

to the New Britain trench (Madsen and Lindley, 1994; Lindley, 2006). Widespread deposition of fluvial and marine volcaniclastics occurred during the Pliocene–Holocene associated with resumption of volcanism along the north coast of New Britain from the Pliocene (Figure 3-3). Raised Pleistocene–Holocene coral reefs fringe many of the islands of the region (Christopher, 2002; Lindley, 2006).

The regional structure of New Britain was poorly understood until relatively recently. Lindley (2006) documented the alignment of Tertiary intrusive bodies in fossil structural zones throughout New Britain (Figure 3-3). The structural corridors or lineaments have long activity histories, are oblique to existing major morphotectonic features, such as the New Britain trench, and have localized the emplacement of Oligocene–Pliocene copper ± gold mineralized porphyry intrusive units (Lindley, 2006). The Kulu-Fulleborn Trend (Figure 3-3) is the best understood and is represented by a northwest-southeast trending alignment or corridor of Upper Oligocene–Pliocene intrusives, volcanics and associated porphyry copper, skarn and gold mineralization (e.g. Titley, 1978; Lindley, 2006). Local structure superimposed on the prominent northwest trend control Upper Oligocene magmatic emplacement indicated by orthogonal orientation of the long axes of intrusive bodies to the primary trend (Hine and Mason, 1978; Lindley, 2006). Free air gravity and crustal depth studies of Wiebenga (1973) and Finlayson and Cull (1973) indicate the Kulu-Fulleborn Trend is a fundamental structural boundary of lithospheric-scale. An abrupt thickening of crust from 15-20 km to 40 km depth occurs from northeast to southwest across the structure (Wiebenga, 1973), with vertical movement in the order of ~1000 m apparent at the surface (Lindley, 2006). The lack of any obvious displacements of the New Britain coastline suggests the Kulu-Fulleborn structure is not presently active (Lindley, 2006).

Recent reconstructions of the region from Hall (2002), Mann and Taira. (2004), and Schellart et al. (2006) propose different times for the collision of the Ontong Java Plateau with the Melanesian arc. Nevertheless all of these studies place New Britain in excess of 500 km along-arc distance to the west of collision, and often removed by as much as 1000 km. Figure 3-4 presents a simplified schematic reconstruction of the Melanesian arc terranes at ~ 5 Ma, prior to the onset of recent tectonic complications such as rifting of the Bismarck Sea. Here New Britain is in the order of 600–800 km west of the Ontong Java Plateau. This is regarded as a minimum along-arc distance at the time of collision and assumes complete suturing between the Pacific plate and Melanesian arc with no subsequent differential motion between the two. If this assumption does not hold true it is clear from plate motions illustrated in Figure 3-4 (that more or less reflect the wider plate motions of the Pacific and Australian plates since ~45 Ma; e.g. Hall, 2002; Schellart et al., 2006), any secondary convergence between the Ontong Java Plateau and Melanesian arc since collision will reduce this along-arc distance and hence increase the distance of New Britain from the point of plateau arrival at the time of collision.

Geology of the Simuku Property

The Simuku Igneous Complex and Cu-Mo porphyry prospect in West New Britain lies on the Kulu-Fulleborn Trend (Figure 3-3). The prospect is hosted by a sequence of andesitic to dacitic volcanic and volcaniclastic rocks of the Kapuluk Volcanics, which were intruded by intermediate to felsic intrusive dykes, sills and stocks belonging to a Upper Oligocene–Lower Miocene intrusive suite (Figure 3-5; Hutchison and Swiridiuk, 2006; this study). NNE to N-trending faults and shears within a major NNE-trending "crush zone" have disrupted the volcanic sequences. These faults and shears are associated with varying degrees of intense fracturing, shearing, dislocation and brecciation and characterized by extensive areas of strong, magnetite-destructive, argillic alteration (Hutchison and Swiridiuk, 2006). Intrusive porphyritic diorite and quartz-diorite bodies observed in creeks and trenches have previously been interpreted as high-level sub-volcanic intrusives associated with the Kulu Batholith, dated at 22-28.7 Ma (Upper Oligocene; Hine and Mason, 1978). The Kulu Batholith outcrops approximately 3 km to the east of the Simuku prospect (Figure 3-5; Hutchison and Swiridiuk, 2006) and is predominantly of dioritic composition with subordinate tonalitic, monzonitic and granodioritic phases (Hine and Mason, 1978). Hutchison and Swiridiuk (2006) suggest the Simuku prospect and the regional geological environment is similar to that of several classical geological environments that host significant porphyry copper, molybdenum and related ore deposits. Recent volcanic activity of the eastern Bismarck arc (mentioned above in section "New Britain Geology"), and unrelated to Melanesian

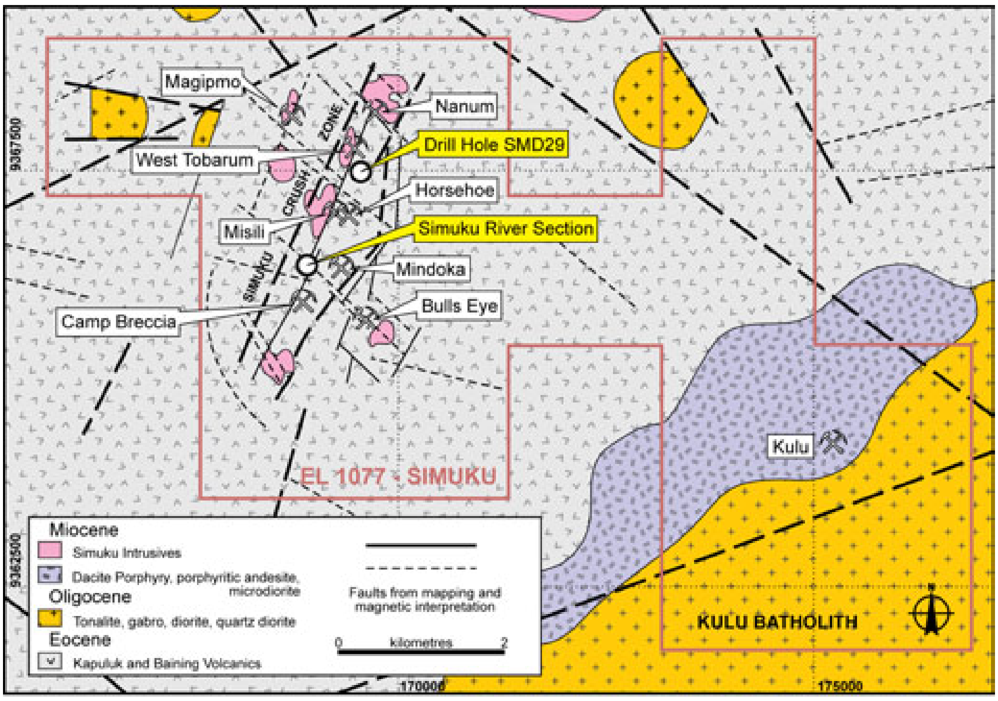

Figure 3-5. Geology of the Simuku property and locations of samples used in this study. Map is projected in UTM AGD66 Zone 56; refer to text for discussion.

arc magmatism, resulted in extensive post-mineral cover of pumice and volcanic ash over a large part of New Britain, including parts of the Simuku Property (Hutchison and Swiridiuk, 2006).

Samples

Rock samples were obtained in conjunction with Barrick Australia from the Simuku Property in West New Britain with the objective of investigating the evolution of the Simuku Igneous Complex and associated porphyry complex, and infer the history of New Britain and the Melanesian arc. Primary material was sampled from diamond drill core of drill hole SMD29; this was located adjacent to the Misili Intrusive target within the "Simuku Crush Zone" (Figure 3-5; Christopher, 2002; Lindley, 2006). Additional field samples were collected from exposures in the Simuku River. Outcrop and sample intervals were selected to include a representative sample of each logged intrusive rock unit and multiple samples of the undifferentiated host volcanic units. These sampling intervals were further scrutinized to minimize abundance of veining and effects of alteration in an effort to reflect compositions most similar to the unaltered rock. Table 3-1 provides the location and description of the rock types sampled.

The sample set can be divided in three broad categories: volcanics and porphyritic intrusives, with recognition of two porphyry rock types based on major phenocryst phases as plagioclase-hornblende ± quartz (Pl-Hbl±Qz) porphyries and plagioclase-biotite-quartz (Pl-Bt-Qz) porphyries (Table 3-1). The volcanic rocks show a wide range of compositions including basaltic trachyandesite, basaltic andesite to trachyandesite and andesite (Figure 3-8), and are highly variable in terms of texture and grain size. All volcanic rocks incorporate a fine-grained groundmass of crystal fragments with approximately half the volcanic samples containing phenocrysts of plagioclase and quartz, which are often fragmentary in nature. Plagioclase phenocrysts often exhibit oscillatory growth zoning while quartz phenocrysts demonstrate undulose extinction. Xenoliths are abundant throughout the volcanic material and represent a number of different sources of both volcanic and intrusive origin. Some samples contain both volcanic and porphyritic intrusive fragments, whereas others only contain fine-grained volcanic xenoliths.

The intrusive rocks are all porphyritic in texture with a narrow geochemical range from andesitic to dacitic compositions (Figure 3-8). Zoning of plagioclase phenocrysts and minor undulose extinction in quartz are common in the plagioclase-biotite-quartz porphyry suite. In general phenocrysts make up approximately 40–50% of sample material but can comprise as little as 20%. The matrix is typically composed of devitrified glass with common major accessory phases of apatite and spinel. Sample SMD29-261 is the notable exception with a fine–medium grained matrix primarily composed of quartz. This sample is representative of the interpreted Cu-Mo mineralizing phase of the porphyry complex.

Overprinting pervasive alteration is common in most samples with a greater apparent intensity of alteration within porphyritic sample suites. Seritization is the dominant alteration type evident in all samples, and is often coupled with chloritization. Plagioclase is commonly completely replaced by sericite with subsidiary samples exhibiting only partial alteration of plagioclase through crystal fractures. This is typical of sericitic or chlorite-sericite alteration in porphyry complexes (Sillitoe, 2010). Sulfides are found primarily as pyrite ± chalcopyrite veining with minor disseminated pyrite and chalcopyrite. Due to the nature of the Simuku Crush Zone, most lithological contacts were faulted making identification of igneous morphology and crosscutting

Table 3-1. Sample descriptions

Sample	Location (a) (b)	Phenocryts (c)	Matrix (c)	Alteration (c) (d)	Notes
Volcanics					
SMD29-229	DDH 229□255 m		Crystal frag. Spl	Int Ser	Xenolithic, no porphyritic clasts.
SMD29-268	DDH 268□282 m	Pl Qz	Crystal frag. Spl	Int Ser	Xenolithic, no porphyritic clasts.
SKB02	168894 E 9366337 N	Pl Qz	Crystal frag. Spl	Mod Ser	Zoned Pl phenocrysts, undulose extinction in Qz phenocrysts.
SKB03	168891 E 9366342 N		Crystal frag. Qz Pl Spl	Weak-Mod Ser Chl	Xenolithic, porphyritic clasts (Pl cumulate, Pl porphyry, Qz-Pl Porphyry).
SKB04	168890 E 9366343 N	Pl ± Qz	Crystal frag. Spl	Weak-Mod Ser	Xenolithic, no definative porphyritic clasts. Some Qz phenocrysts with undulose extinction.
SKB05	168888 E 9366347 N		Crystal frag. Qz Pl Spl	Weak Ser	Xenolithic, porphyritic clasts. Undulose extinction in phenocrysts within porphyries.
SKB06	168886 E 9366351 N		Crystal frag. Qz Spl	Weak-Mod Ser	Xenolithic, no porphyritic clasts. Qz exhibits undulose extinction.
SKB08	168880 E 9366361 N	Pl Qz	Crystal frag. Qz Pl Spl	Mod Ser Chl	Xenolithic, porphyritic clasts. Qz phenocrysts exhibit undulose extinction.
SKB10	168874 E 9366370 N	Pl ± Qz	Crystal frag. Spl	Mod-Int Ser Chl Bt	Xenolithic, porphyritic clasts. Phenocrysts exhibit undulose extinction.
Porphyries					
Plagioclase-Hornblende ± Quartz Porphyries					
SMD29-66	DDH 66□72 m	Pl Hbl	Dv.Glass Ap Hem Spl	Int Qtz Bt Ser	Qtz cumulates (xenoliths?) with undulose extinction. Qz + Ser replacement of Pl. 30□40% phenocrysts.
SMD29-300	DDH 300.5□336 m	Pl Hbl ± Qz	Dv.Glass Ap Spl	Mod-Int Ser Chl	40% phenocrysts.
SKB01	168896 E 9366335 N	Pl Hbl ± Qz	Dv.Glass Ap Spl	Int Qtz Ser	20% phenocrysts.
SKB07	168882 E 9366359 N	Pl Hbl Bt ± Qz	Dv.Glass Qz Spl	V. Int Ser Chl	Minor undulose extinction in Qz. 30□40% phenocrysts.
SKB09	168876 E 9366367 N	Pl Hbl Qz	Dv.Glass Ap Spl	Int Ser	Large Pl phenocrysts. 40□50% phenocrysts.
SKB11	168873 E 9366372 N	Pl Hbl Qz	Dv.Glass Ap Spl	Int Ser	Large Pl phenocrysts. 40□50% phenocrysts.
Plagioclase-Biotite-Quartz Porphyries					
SMD29-113	DDH 113□120 m	Pl Bt Qz	Dv.Glass Ap Spl	Weak-Mod Ser Chl	Pl phenocrysts show some zoning. Minor undulose extinction in Qz phenocrysts. 40□50% phenocrysts (80% Pl).
SMD29-123	DDH 123□130 m	Pl Bt Qz	Dv.Glass Ap Spl	Weak-Mod Ser Chl	Pl phenocrysts show some zoning. Minor undulose extinction in Qz phenocrysts. 40□50% phenocrysts (80% Pl).
SMD29-146	DDH 146□148 m	Pl Bt Qz	Dv.Glass Ap Spl	Weak-Mod Ser Chl	Pl phenocrysts show some zoning. Minor undulose extinction in Qz phenocrysts. 40□50% phenocrysts (80% Pl).
SMD29-203	DDH 203□206.5 m	Pl Qz ± Bt	Dv.Glass Spl	V. Int Ser	20% phenocrysts.
SMD29-261	DDH 261.2□265.7 m	Pl Bt ± Qz	Fine-Med Qz Spl	Int Ser Chl	40□50% phenocrysts. Few Qz crystals exhibit undulose extinction.

a) Diamind drill hole (DDH) SMD29 Collar location and orientation: 169573 9367454 AGD66 Zone 56; azimuth (mag): 273□; inclination: -60□

b) Field cordinates in UTM AGD66 Zone 56.

c) Mineral codes: Ap, apatitie; Bt, biotite; Chl, chlorite; Dv.Glass, devitrified glass; Hem, hematite;Hbl, hornblende; Pl, plagioclase; Qz, quartz; Ser, sericite.

d) Alteration codes; alteration intensity; V Int, very intense; Int, intense; Mod, moderate.

relationships for relative timing difficult. Where possible, inclusions were identified from adjacent units in outcrop, drill core, or thin section. For example, the presence of undisturbed, distinct mineralized veining and broken fragments of the same vein material in adjacent units, and identification of porphyritic versus non-porphyritic xenoliths in volcanic units.

Methods

Samples for geochemical analysis were selected to minimize effects of alteration. Weathering rinds were split from surface samples and edges from drill core samples were ground off with diamond implanted grinders and subsequently washed in an ultrasonic bath to minimize contamination from drilling. Rock material was then milled to a fine powder in a tungsten carbide ring mill at James Cook University (JCU). Major and trace elements analyses were done at the Advanced Analytical Centre, JCU by conventional X-ray fluorescence (XRF) using a Bruker-AXS S4 Pioneer XRF Spectrometer on fused beads and pressed powder pellets, respectively. For further trace element analyses, rock powders were mixed with 12:22 borate flux (XRF Scientific Limited, Perth, Australia) at 1:6 sample to flux ratio and fused to glass after heating to 1050 °C for 15 minutes in a F-M 4 Fusion Bead Casting Machine (Willunga, Australia). Chips of the fused glasses were mounted into a standard 2.5 cm diameter epoxy puck and analyzed for a range of trace elements using a Geolas Pro 193 nm ArF Excimer laser ablation unit (Coherent) coupled to a Bruker 820-MS Inductively Coupled Plasma Mass Spectrometer (ICP-MS) via Tygon tubing. Helium was used as the carrier gas (0.8 l/min), which was subsequently mixed with Ar via a mixing bulb between the ablation cell and the ICP-MS to smooth the ablation signal. Laser energy density was set to 6 J/cm^2, and laser spot size and repetition rate were set to 120 micrometres and 10 Hz, respectively. The ICP-MS was tuned to maximum sensitivity while retaining robust plasma conditions (U:Th sensitivity ~ 1) and low oxide production rates (ThO/Th ~ 0.5 %). NIST SRM 610 glass was used as a bracketed external standard using the standard reference values of Spandler et al. (2011). Data were quantified using Si (as previously determined by XRF) as the internal standard, and data were processed off-line using the Glitter software (Van Achterbergh et al., 2001).

14 samples were selected for U-Pb dating of zircon. These comprised 8 drill core samples and 6 field samples from the Simuku Property. Mineral separation to extract zircon crystals was carried out at JCU in a standard four-step process. Samples were crushed and milled to 500 µm, washed to remove the clay proportion, and separated by a combination of heavy liquid density separation and magnetic separation. Zircon were hand picked and mounted in epoxy with GJ1, Temora and Fish Canyon Tuff zircon standards. Epoxy mounts were polished and carbon-coated. Cathodoluminescence (CL) images of all zircon crystals were obtained using a Jeol JSM5410LV scanning electron microscope equipped with a Robinson CL detector, housed at JCU.

U-Pb dating of zircons was conducted using the laser ablation ICP-MS setup described above for bulk-rock trace element analysis. Analyses collected were ^{29}Si, ^{90}Zr, ^{202}Hg, ^{204}Pb, ^{206}Pb, ^{207}Pb, ^{208}Pb, ^{232}Th, ^{235}U, and ^{238}U. The ICP-MS was tuned to ensure approximately equal sensitivity of U, Th and Pb to minimize isotope fractionation due to matrix effects. Full details are given in Tucker et al. (2013). In order to obtain a higher sensitivity for the low Pb signal intensity expected for young zircon, the High Sensitivity mode of 820-MS was used with the sensitivity for ^{238}U of about 10,000 cps/ppm at 44 µm laser beam diameter using laser conditions of 5 Hz, 6 J/cm energy density. Remaining fractionation and mass bias was corrected by using standard bracketing techniques with every ten zircon sample measurements bracketed by two measurements of GJ1 zircon (primary calibration standard), two Temora zircon, one Fish Canyon Tuff zircon and one GJ1 zircon (secondary checking standards). For quantification of U and Th concentration in zircon samples, analysis of the NIST SRM 612 reference glass was conducted at the beginning, middle and end of every analytical session, with ^{29}Si used as the internal standard assuming perfect zircon stoichiometry. All zircons were analyzed with a beam spot diameter of 44 µm and selection of analytical sample spots was guided by CL images and targeted both cores and rims.

Data reduction was carried out using the Glitter software (Van Achterbergh et al., 2001). All time-resolved single isotope signals from standards and samples were filtered for signal spikes or perturbations related to inclusions and fractures. Subsequently, the most stable and representative isotopic ratios were selected taking into account possible mixing of different age domains and zoning. Drift in instrumental measurements was corrected following analysis of drift trends in the raw data using measured values for the GJ1 primary zircon standard. Analyses of Temora and Fish Canyon Tuff zircons were used for verification of GJ1 following drift correction (Figure 3-6). Background corrected analytical count rates, calculated isotopic ratios and 1σ uncertainties were exported for further processing and data reduction.

Initial Th/U disequilibrium during zircon crystallization is related to the exclusion of ^{230}Th due to isotope fractionation, and resulting in a deficit of measured ^{206}Pb as a ^{230}Th decay product (Schärer, 1984; Parrish, 1990). Young zircon ages (<10 Ma up to ~20 Ma) are particularly susceptible to this disequilibrium requiring an upward age correction in the order of 100 k.y. (Crowley et al., 2007), which is comparable or greater than the measured analytical uncertainty. Although final age dating for all samples returned ages >20 Ma, close to the limit of initial Th/U disequilibrium detection, this correction was applied to all samples for maximum U-Pb dating accuracy. Correction of $^{206}Pb/^{238}U$ dates for the deficit requires estimates of Th/U concentration in the zircon and Th/U concentration of the magma as the source of zircon. While Th and U concentrations of zircon were obtained as part of the analytical routine, the initial Th/U concentration of the magma is more difficult to estimate and has a larger effect on the age correction (Crowley et al., 2007). Following the procedures of Harris et al. (2004), we employ the U and Th contents determined from bulk rock analysis. Uncertainties associated with the correction were propagated into errors on the corrected ages according to Crowley et al. (2007). The effect of common Pb is taken into account by the use of Tera-Wasserburg Concordia plots (Tera and Wasserburg, 1972; Jackson et al., 2004) and weighted mean $^{206}Pb/^{238}U$ age calculations were carried out using Isoplot/Ex version 4.15 (Ludwig, 2009). Weighted averages were corrected for common Pb by utilizing the Age7Corr and AgeEr7Corr algorithms in Isoplot, and using the y-intercept and corresponding sigma errors returned from the Tera-Wasserburg plots of concordant zircon populations. All errors were propagated at 2σ level and reported at 2σ and 95% confidence for concordia and weighted averages, respectively.

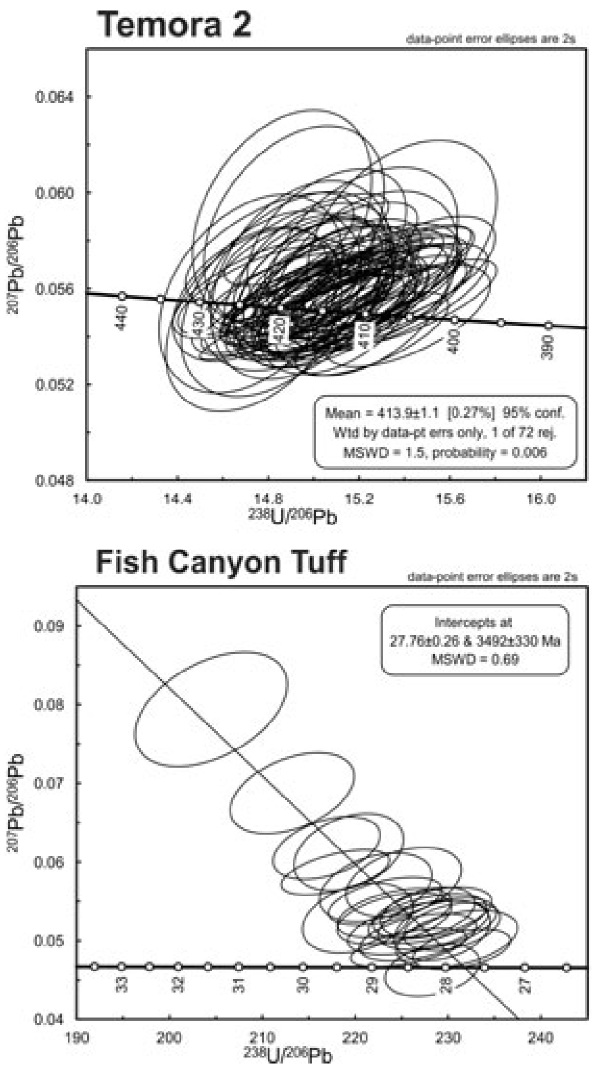

Figure 3-6. Concordia plots and weighted average (Temora 2) for U-Pb zircon geochronology standards. All data-point error ellipses and calculated errors are 2σ, and 95% confidence for associated weighted average.

Results

U-Pb Geochronology

Zircon crystals from all samples are euhedral, transparent and colorless, with the exception of minor populations of pink and yellow crystals in sample SMD29-261. Crystals are typically on the order of 100 to 200 μm in length. Aspect ratios generally range between approximately 1:2.5 and 1:2. Under CL imaging most zircon have uniform light cores with moderate oscillatory zoning in the rim. More complex zoning is uncommon with no evidence for distinct variations between core and rim zonation patterns. All zircon sampled hold CL textures consistent with a magmatic origin; that is, crystals with typically euhedral crystal shapes and oscillatory zoning (Corfu et al., 2003; Hoskin and Schaltegger, 2003). A magmatic origin for these zircons is supported by low Th/U ratios averaging 0.45 with a corresponding standard deviation of 0.25 (e.g., Heaman et al., 1990). Representative CL images are presented in the digital appendix.

U-Pb zircon ages for selected volcanic and intrusive porphyry phases from the Simuku Igneous Complex are reported in Table 3-2 and corresponding concordia and weighted average plots are shown in Figure 3-7. Ages range from the Middle–Upper Eocene (40 Ma) through to Lower Miocene (20 Ma). Details of age dating are reported by rock type as described in section “Samples”. Complete zircon isotopic data can be found in the digital appendix. Ages from both the plagioclase-hornblende ± quartz porphyries and plagioclase-biotite-quartz porphyries are within a narrow range between 24.1 ± 0.6 Ma and 20.2 ± 0.4 Ma.

Table 3-2. Resolved ages from U-Pb dating of zircon.

Sample	Weighted Average (a)	95% Confidence	MSWD	Probability of Fit	Concordia Age (b)	2σ Error	MSWD	Probability of Fit
Volcanics								
SKB02	25.19	0.35	0.56	0.57	25.20	0.40	0.95	0.33
SKB06	29.40	0.46	0.11	0.991	29.40	0.85	0.21	0.93
SKB06 [c]	37.77	0.53	0.80	0.55	37.65	0.66	1.90	0.11
SKB08	21.70	0.23	0.68	0.82	21.72	0.38	0.72	0.77
SKB08 [c]	29.60	1.30	0.21	0.93	29.60	2.60	0.57	0.63
SKB08 [c]	39.91	0.66	0.64	0.59	39.90	1.10	1.17	0.31
Pl-Hbl±Qz Porphyry								
SMD29 66	22.51	0.22	0.83	0.60	22.53	0.36	0.87	0.55
SMD29 300	20.52	0.35	0.70	0.59	20.51	0.59	1.30	0.27
SKB01	21.46	0.20	0.51	0.92	21.47	0.48	0.66	0.79
SKB07	20.21	0.18	0.76	0.73	20.23	0.35	0.74	0.74
SKB11	20.48	0.22	0.78	0.64	20.47	0.38	1.00	0.43
Pl-Bt-Qz Porphyry								
SMD29 113	22.32	0.21	0.49	0.93	22.33	0.47	0.64	0.81
SMD29 123	21.46	0.22	0.52	0.92	21.45	0.52	0.73	0.73
SMD29 146	20.68	0.27	0.54	0.90	20.66	0.68	0.81	0.64
SMD29 203	24.07	0.25	0.23	0.998	24.07	0.63	0.35	0.98
SMD29 261	21.81	0.19	0.88	0.64	21.82	0.39	0.93	0.57

a) Weighted average age corrected for initial Th disequilibrium and common-Pb.
b) Concordia age corrected for initial Th disequilibrium.
c) Inherited zircon populations with a concordant age.

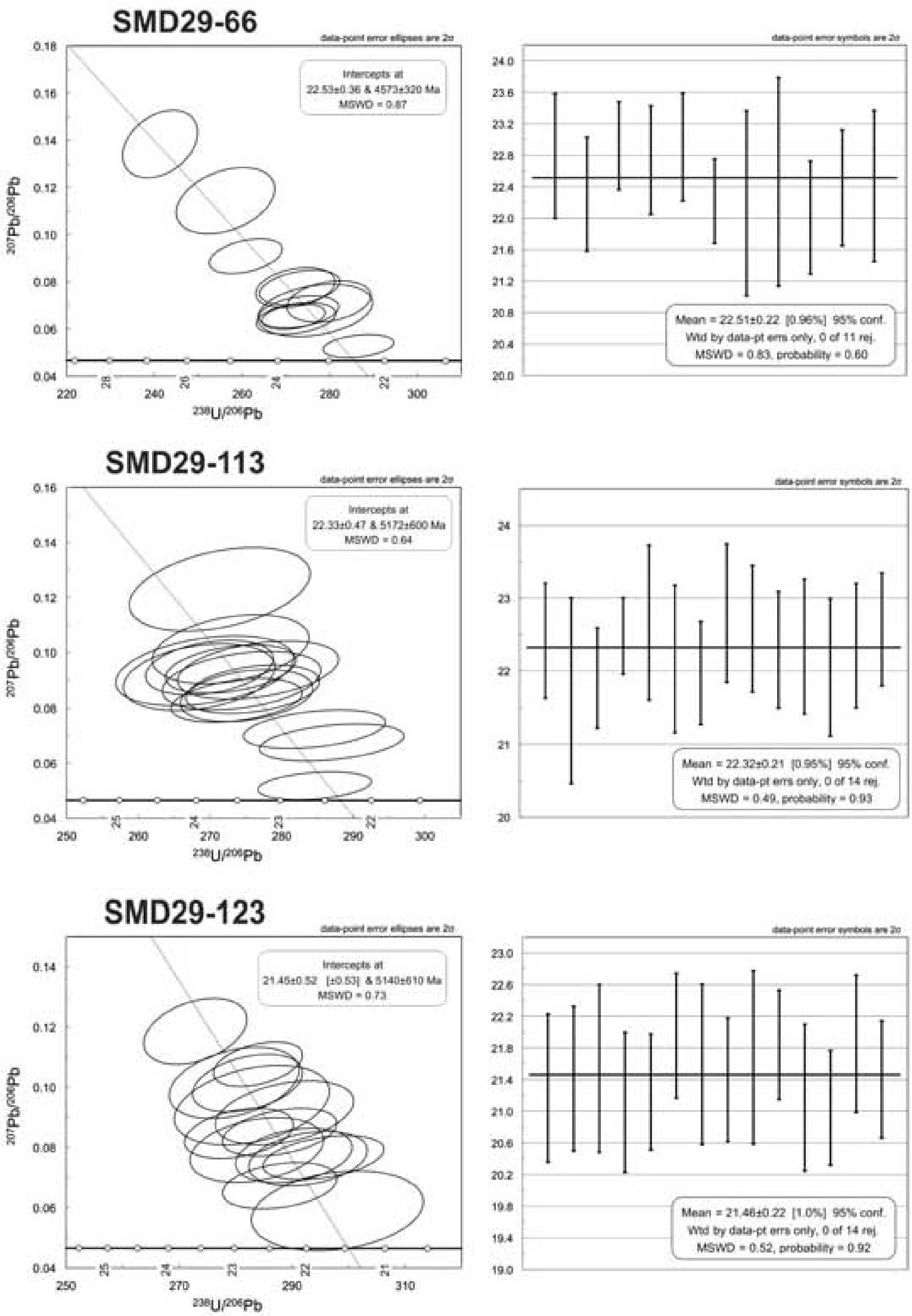
SMD29-66
data-point error ellipses are 2σ
Intercepts at
22.53±0.36 & 4573±320 Ma
MSWD = 0.87
$^{207}Pb/^{206}Pb$
$^{238}U/^{206}Pb$
data-point error symbols are 2σ
Mean = 22.51±0.22 [0.96%] 95% conf.
Wtd by data-pt errs only, 0 of 11 rej.
MSWD = 0.83, probability = 0.60
SMD29-113
data-point error ellipses are 2σ
Intercepts at
22.33±0.47 & 5172±600 Ma
MSWD = 0.64
$^{207}Pb/^{206}Pb$
$^{238}U/^{206}Pb$
data-point error symbols are 2σ
Mean = 22.32±0.21 [0.95%] 95% conf.
Wtd by data-pt errs only, 0 of 14 rej.
MSWD = 0.49, probability = 0.93
SMD29-123
data-point error ellipses are 2σ
Intercepts at
21.45±0.52 [±0.53] & 5140±610 Ma
MSWD = 0.73
$^{207}Pb/^{206}Pb$
$^{238}U/^{206}Pb$
data-point error symbols are 2σ
Mean = 21.46±0.22 [1.0%] 95% conf.
Wtd by data-pt errs only, 0 of 14 rej.
MSWD = 0.52, probability = 0.92

Figure 3-7.

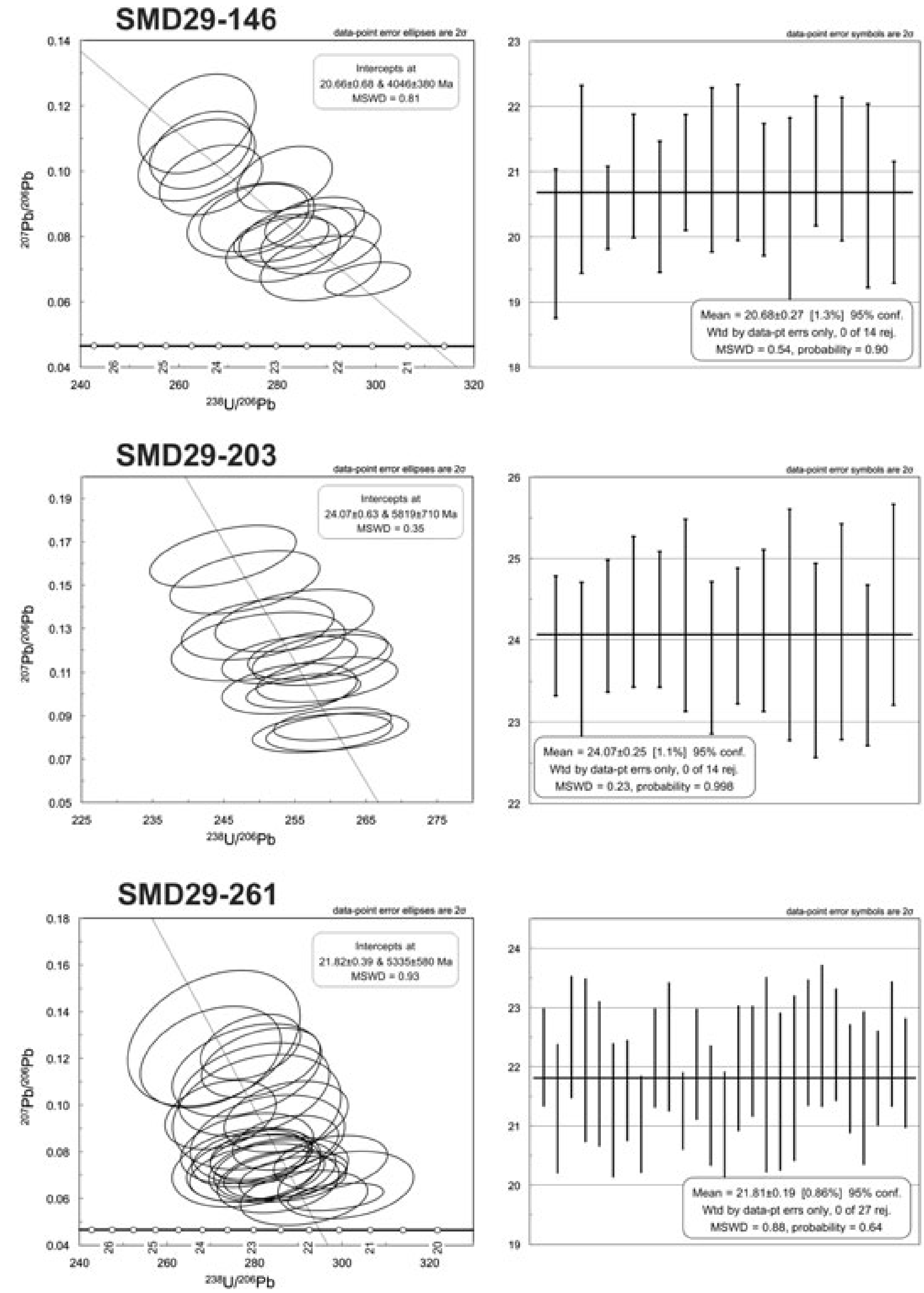

Figure 3-7 continued.

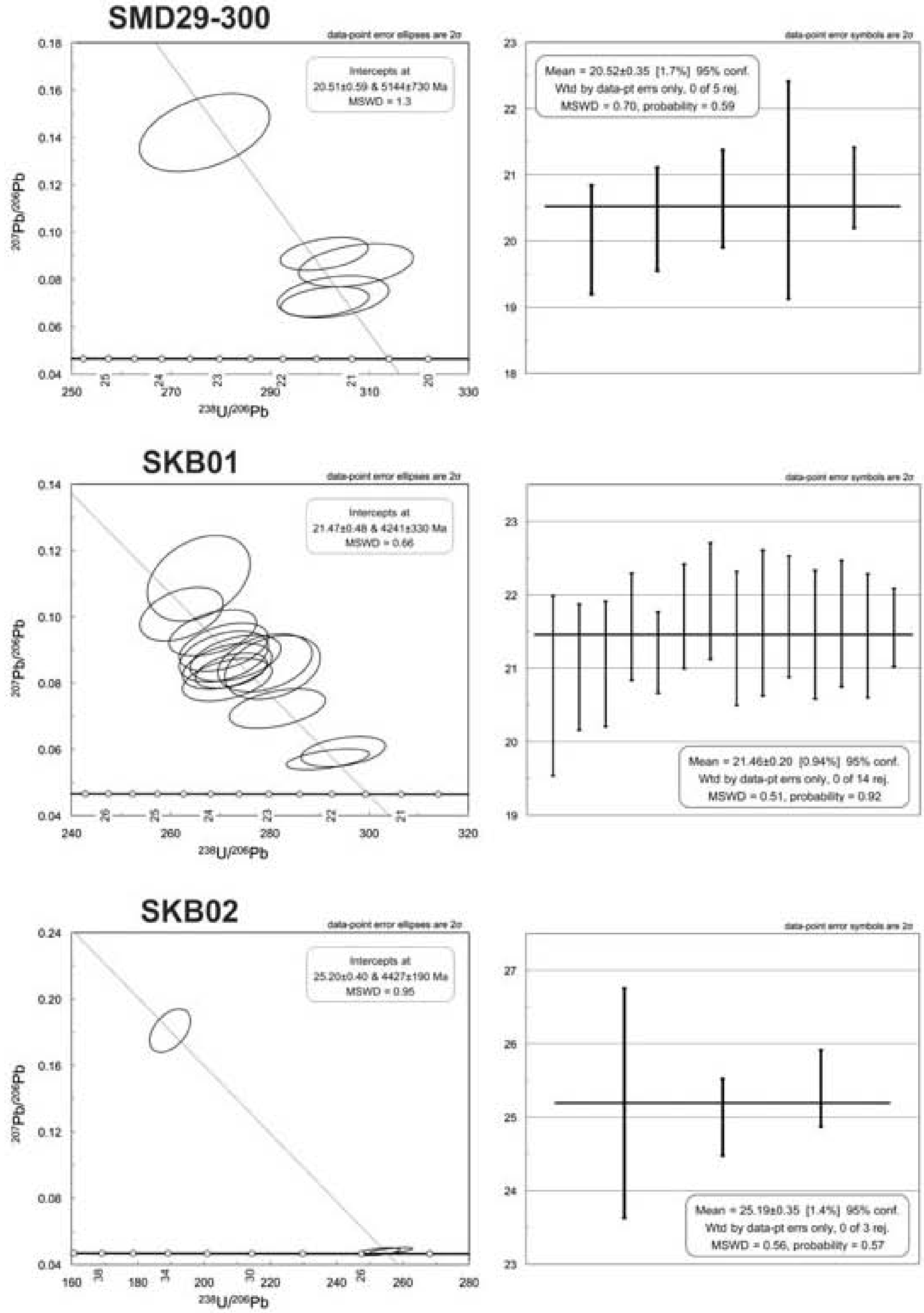

Figure 3-7 continued.

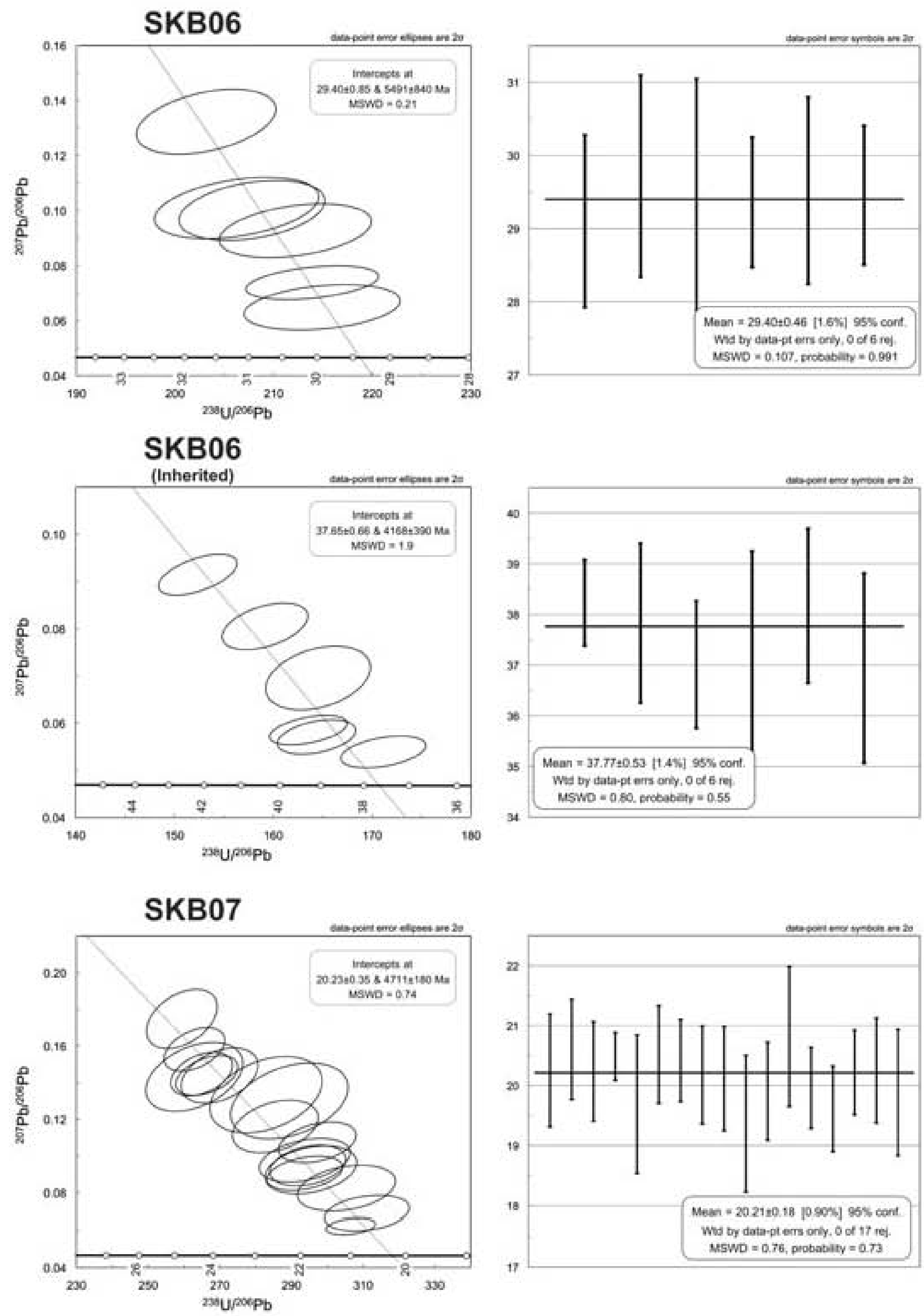

Figure 3-7 continued.

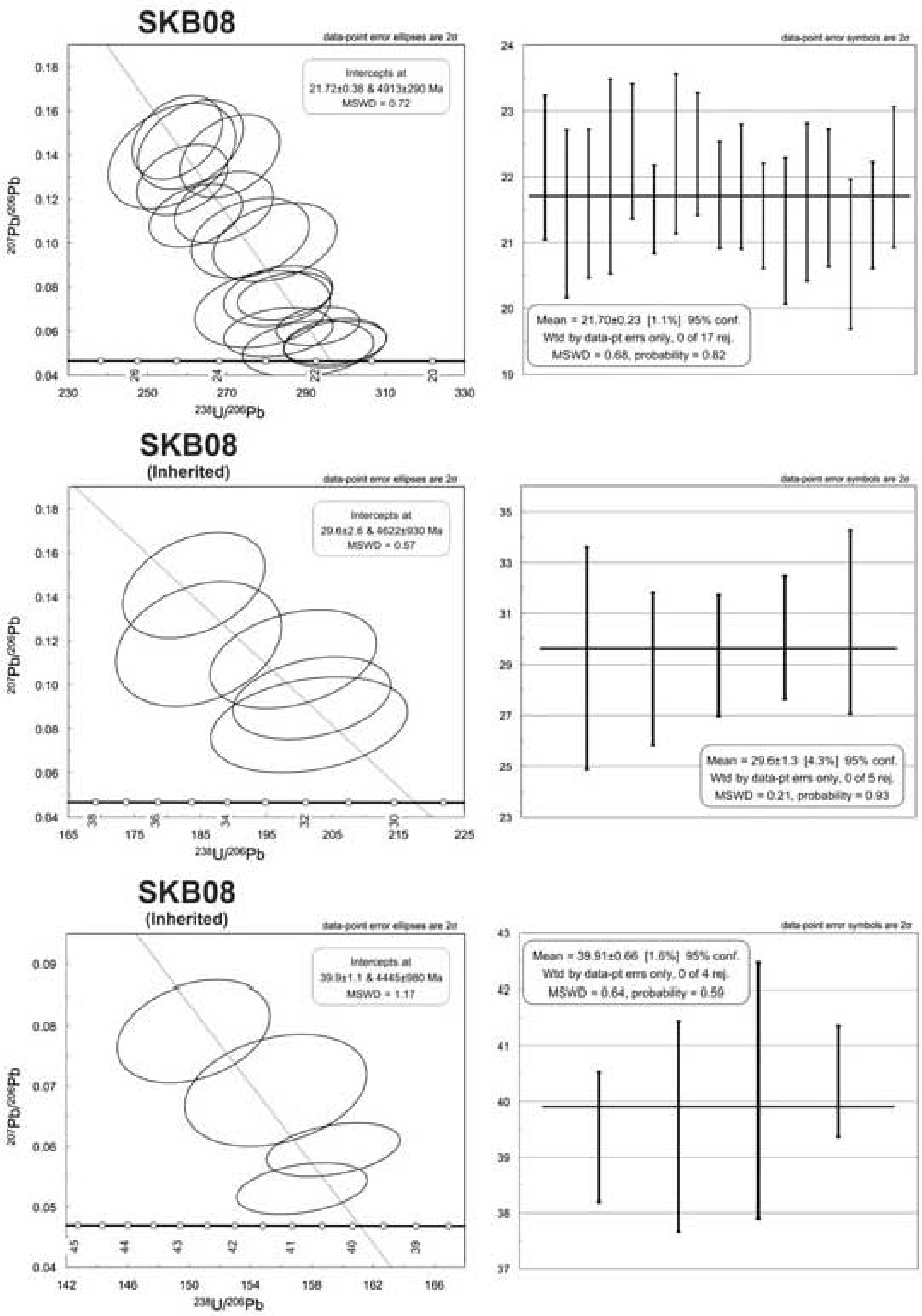

Figure 3-7 continued.

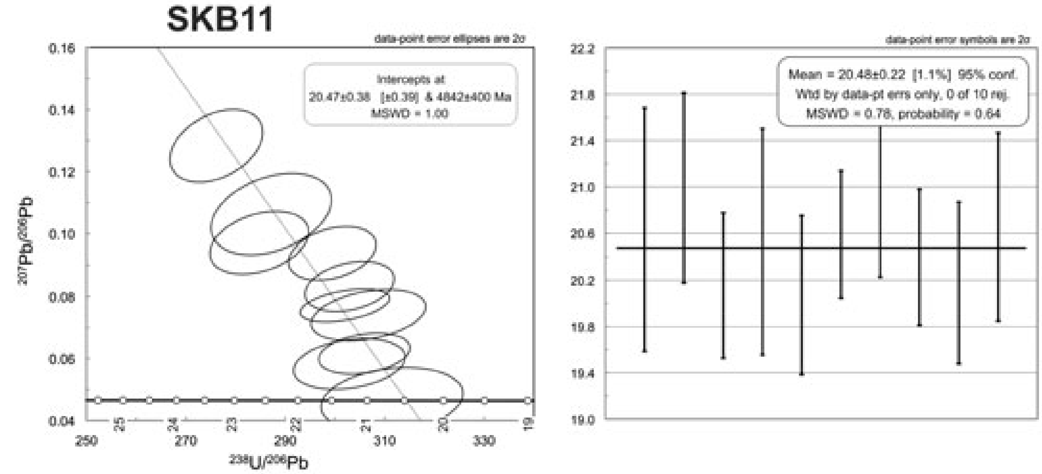

Figure 3-7. Weighted average and concordia plots for all samples. Plots are constructed from U-Pb calculated ages and isotopic compositions respectively (detailed age data in supplementary data). Tera-Wasserburg plots are corrected for initial Th disequilibrium; weighted average plots are corrected for initial Th disequilibrium and common Pb. All error bars, data-point error ellipses and calculated errors are 2σ and 95% confidence for concordia and weighted averages respectively.

The volcanic rock samples produced a much larger range of ages. These are separated into four distinct age groups. The oldest group is represented only by inherited zircon populations in samples SKB06 and SKB08, which are present as concordant isotopic populations within the analytical data and yield Middle–Upper Eocene ages of 37.7 ± 0.7 Ma and 39.9 ± 1.1 Ma respectively, similar to the previously proposed age of the Baining Volcanics. A second volcanic population of middle Oligocene age can be derived from the crystallization age of SKB06 at 29.4 ± 0.9 Ma and an inherited age of 29.6 ± 2.6 Ma from SKB08, similar to ages attributed to the Kapuluk Volcanics. Additional volcanic ages are derived from SKB02 at 25.2 ± 0.4 Ma and SKB08 at 21.7 ± 0.4 Ma. It should be noted that while the age for SKB02 is reduced from just two zircon analyses, it is a single zircon crystal that constrains this age. Two analytical spots on this zircon returned uncorrected ages of 25.4 ± 0.2 Ma and 25.1 ± 0.2 Ma with respective calculated discordance between $^{206}Pb/^{238}U$ and $^{207}Pb/^{235}U$ decay systems at 2.3% and 3.5%. Concordance of calculated ages between multiple decay systems is uncommon for zircon of such a young age; in addition, the associated isotopic ratios are unlike any other zircon from Simuku. Furthermore, concordia reveal these two analyses plot adjacent to the concordia implying no common Pb issues. When this is taken into account we conclude the resultant concordia and weighted average age represents a maximum possible deposition age and likely a true crystallization age for the volcanic event, potentially representing an important event interpreted as related to initiation of regional tectonic reorganization at 25–26 Ma. SMD29-229 was also selected for zircon dating but did not yield any zircon grains. Together with SKB02, these reflect the generally low Zr concentrations among the volcanic suite.

The oldest population of zircons found in this study, although not part of a concordant population, yielded uncorrected $^{206}Pb/^{238}U$ ages of 43.6 ± 0.5 Ma, 42.1 ± 0.4 Ma, and 41.1 ± 0.4 Ma. These zircon were all within SKB06 and pass a 15% discordance threshold between $^{206}Pb/^{238}U$ and $^{207}Pb/^{235}U$ age systems. We suggest that as these ages are similar to the ages for the Baining Volcanics they potentially represent the initial phase of igneous activity of the Melanesian arc.

Geochemistry

Major and trace elements composition of all analyzed samples are given in Table 3-3. Whole rock geochemical compositions classify both porphyry suites as peraluminous andesite–dacite. Volcanic rocks types show high variation encompassing trachyandesite, basaltic trachyandesite, basaltic andesite and andesite compositions (Figure 3-8). Harker variation diagrams have been used to show major element trends for both volcanic and porphyry rock types (Figure 3-9). Major element trends are evaluated for samples with < 5% LOI and hold more or less typical fractionation trends through both rock types. TiO_2, Al_2O_3 and Fe_2O_3 all show a well-defined linear decrease with increasing SiO_2, with the TiO_2 trend becoming more scattered at SiO_2 contents below 56 wt.%. MgO shows a similar but gradually decreasing trend with increasing SiO_2. MnO increases exponentially with increasing SiO_2. CaO appears relatively constant at around 3.5 wt.% across all SiO_2 values with some scatter in volcanic rock types. Likewise, Na_2O is relatively constant with some degree of scattering. K_2O appears highly variable between 0.5 and 2.7 wt.% SiO_2, particularly in volcanic rock types.

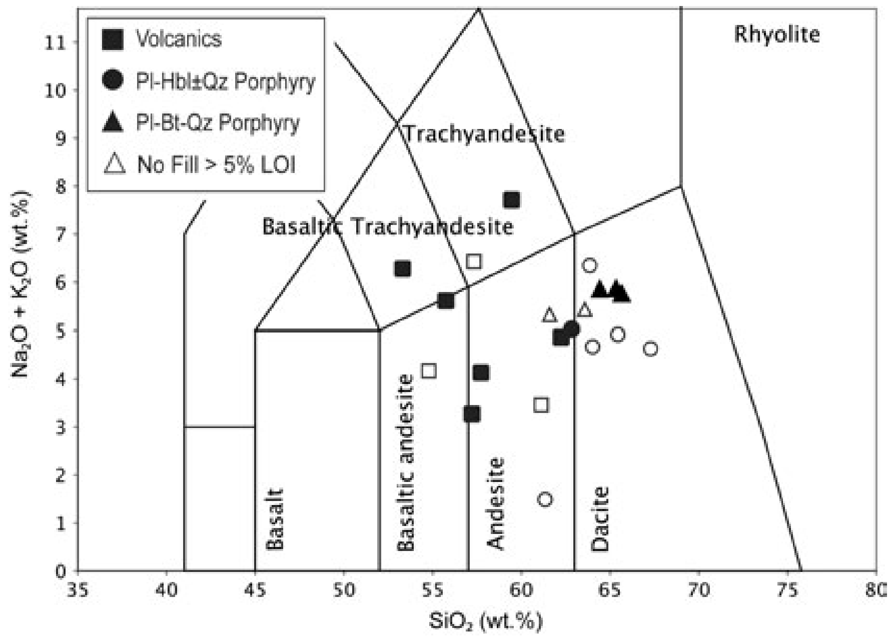

Figure 3-8. Total alkali versus silica classification diagram for the Simuku Igneous Complex (TAS - Le Maitre, 2002). Rock types are as labeled; porphyry sample suites are generally clustered about the andesite-dacite compositional boundary while volcanics are comparatively scattered, see text for discussion.

Table 3-3. Representative major and trace element data.

	Volcanics									Pl-Hbl±Qz Porphyry						Pl-Bt-Qz Porphyry				
Sample	SMD29 229	SMD29 268	SKB02	SKB03	SKB04	SKB05	SKB06	SKB08	SKB10	SMD29 66	SMD29 300	SKB01	SKB07	SKB09	SKB11	SMD29 113	SMD29 123	SMD29 146	SMD29 203	SMD29 261
SiO_2	57.32	57.21	53.30	62.23	55.75	59.44	61.12	54.78	57.72	61.34	63.85	65.44	62.83	67.28	64.02	65.65	65.33	63.57	61.59	64.42
TiO_2	1.16	1.20	1.45	0.78	0.60	0.78	0.62	0.83	0.86	0.37	0.37	0.30	0.60	0.40	0.38	0.38	0.38	0.40	0.50	0.47
Al_2O_3	20.03	15.99	20.98	17.81	21.46	21.01	15.98	18.85	19.01	15.30	16.31	15.88	17.10	17.41	16.37	16.21	16.20	16.17	16.05	16.57
Fe_2O_3*	4.53	8.79	8.87	4.99	6.10	3.66	6.39	7.67	6.69	2.30	2.30	1.99	4.82	3.44	2.37	3.37	3.43	3.85	3.51	3.34
MnO	0.05	0.04	0.03	0.03	0.04	0.06	0.08	0.82	0.04	0.17	0.07	0.03	0.09	0.02	0.11	0.15	0.11	0.10	0.06	0.11
MgO	2.00	3.46	1.66	1.87	2.80	1.66	2.46	2.60	2.55	0.96	0.83	0.60	2.03	0.45	0.99	1.26	1.39	1.33	1.63	1.44
CaO	2.50	4.26	3.71	4.70	3.72	2.54	2.79	3.02	5.82	6.59	4.17	4.02	4.07	0.97	3.83	3.74	3.17	3.01	3.77	3.48
Na_2O	2.77	2.11	3.84	4.19	3.30	5.03	1.20	1.22	3.14	0.12	4.45	3.35	4.51	2.18	1.78	4.36	4.20	3.73	3.45	4.53
K_2O	3.66	1.16	2.44	0.67	2.31	2.68	2.26	2.95	0.99	1.37	1.90	1.57	0.52	2.45	2.89	1.40	1.66	1.71	1.88	1.32
P_2O_5	0.06	0.10	0.06	0.07	0.07	0.08	0.08	0.11	0.14	0.14	0.13	0.10	0.23	0.12	0.12	0.12	0.12	0.12	0.13	0.15
SO_3	0.30	0.22	0.17	0.08	0.24	0.18	0.40	0.16	0.19	0.71	0.20	0.39	0.10	0.07	0.89	0.11	0.38	0.54	0.28	0.11
LOI	5.06	5.58	3.83	3.21	3.93	3.60	7.08	7.04	3.36	10.94	5.58	6.98	3.70	5.41	6.71	3.81	3.62	5.42	6.97	4.07
Total	99.43	100.11	100.34	100.66	100.32	100.73	100.45	100.04	100.51	100.31	100.16	100.65	100.59	100.20	100.46	100.57	99.99	99.95	99.83	100.02
Sc	35	34	33	23	20	24	19	23	22	5.5	5.8	5.5	9.9	6.6	6.3	7.3	6.9	7.0	8.7	8.4
V	212	310	270	149	110	150	116	135	138	37	36	25	106	46	48	47	49	70	72	72
Cr	18	29	36	23	29	17	19	17	15	45	20	11	22	20	9.0	22	25	23	25	12
Co	21	55	40	30	41	28	63	25	34	13	20	18	36	27	24	33	23	30	31	46
Cu	3304	610	1093	84	1382	516	869	129	405	9.1	12	4.5	29	853	340	294	1189	838	2373	1124
Zn	48	38	32	32	16	15	74	1675	30	110	69	29	172	60	101	77	69	77	16	58
Ga	17	17	17	14	15	17	14	16	15	15	17	16	17	17	17	17	16	18	12	17
As	1.4	1.6	1.8	1.3	1.5	1.5	1.4	1.4	1.2	1.6	2.1	1.1	0.6	8.7	22	0.6	1.2	1.8	1.5	1.4
Rb	57	30	49	15	49	58	66	73	29	32	40	34	12	59	73	28	34	38	28	28
Sr	179	285	304	204	315	250	85	90	296	106	860	276	934	209	176	806	671	560	442	663
Y	37	31	28	23	22	23	33	41	29	5.8	5.9	7.0	8.3	5.9	5.2	5.5	5.6	5.9	7.5	8.2
Zr	113	80	120	129	65	133	138	175	111	128	131	113	113	110	104	105	109	111	104	105
Nb	1.3	1.0	1.9	1.8	0.9	1.7	2.3	2.4	1.6	3.5	3.7	2.0	2.3	2.0	1.9	1.8	1.9	1.9	2.0	1.4
Mo	70	1.8	3.5	0.9	3.1	14	2.8	1.1	2.5	0.9	1.2	7.2	1.4	9.5	1.1	3.8	12	3.7	34	33
Cd	0.3	0.3	0.3	1.4	0.3	0.3	0.7	5.9	0.3	0.5	0.3	0.2	1.6	0.5	0.5	1.4	0.8	0.4	bd	1.1
Sn	4.0	4.5	3.6	3.0	4.2	4.4	3.4	3.5	2.7	2.0	2.3	2.3	3.3	3.8	3.0	3.5	2.7	2.9	4.4	2.9
Sb	1.0	0.8	1.2	0.7	1.0	1.3	1.2	1.1	0.8	4.3	1.1	1.2	0.8	2.4	7.0	0.6	0.9	0.9	0.9	0.9
Cs	1.1	1.5	1.3	1.2	1.4	1.1	2.6	3.6	1.9	2.6	2.3	1.9	1.2	2.6	2.5	1.2	1.1	1.4	0.7	0.7
Ba	275	42	252	48	187	294	51	76	49	38	152	166	90	182	198	144	160	145	151	124
La	14	8.0	6.3	10	6.6	9.5	6.0	5.4	5.3	14	15	12	18	12	10	9.9	11	11	10	10
Ce	37	20	16	27	16	23	16	12	13	33	34	26	41	23	23	21	22	24	23	23
Pr	5.9	3.2	2.4	3.9	2.5	3.0	2.3	1.8	2.0	4.2	4.4	3.4	5.7	3.2	3.0	2.6	2.7	2.9	3.0	3.1
Nd	29	17	12	18	12	14	11	9.0	9.7	17	17	13	24	13	12	10	11	12	13	14
Sm	7.7	4.9	3.3	4.6	3.3	3.5	3.1	2.8	2.8	2.7	2.9	2.4	4.5	2.1	2.1	1.7	1.8	2.0	2.3	2.5
Eu	1.8	1.4	1.3	1.1	1.4	1.0	0.8	1.0	0.8	0.8	0.8	0.8	1.1	0.7	0.6	0.6	0.7	0.8	0.9	0.9
Gd	7.4	5.3	4.0	4.4	3.6	3.6	4.1	4.4	3.5	1.7	1.5	1.6	3.0	1.6	1.4	1.2	1.2	1.3	1.7	1.8
Tb	1.1	0.8	0.7	0.7	0.6	0.6	0.7	0.8	0.6	0.2	0.2	0.2	0.3	0.2	0.2	0.2	0.2	0.2	0.2	0.3
Dy	7.0	5.6	4.5	4.3	4.1	4.1	5.3	5.7	4.4	1.0	1.1	1.2	1.7	1.1	1.0	0.9	1.0	1.1	1.5	1.5
Ho	1.5	1.2	1.0	0.9	0.9	0.9	1.2	1.3	1.0	0.2	0.2	0.3	0.3	0.2	0.2	0.2	0.2	0.2	0.3	0.3
Er	3.8	3.4	3.1	2.4	2.5	2.8	3.5	4.1	3.0	0.5	0.5	0.7	0.8	0.5	0.5	0.5	0.6	0.6	0.8	0.8
Tm	0.5	0.5	0.5	0.3	0.4	0.4	0.5	0.6	0.4	0.1	0.1	0.1	0.1	0.1	0.1	0.1	0.1	0.1	0.1	0.1
Yb	3.6	3.2	3.2	2.8	2.4	3.1	3.9	4.2	3.1	0.5	0.5	0.8	0.8	0.5	0.5	0.6	0.5	0.6	0.9	0.7
Lu	0.6	0.5	0.5	0.5	0.4	0.5	0.6	0.6	0.5	0.1	0.1	0.1	0.1	0.1	0.1	0.1	0.1	0.1	0.1	0.1
Hf	3.3	2.4	3.3	3.4	1.8	3.5	3.6	4.5	3.0	3.1	3.2	3.0	2.8	2.9	2.7	2.8	2.9	2.9	2.6	2.8
Tl	0.4	0.1	0.2	bd	0.3	0.4	0.5	0.6	0.1	0.3	0.2	0.2	0.1	0.4	0.4	bd	0.2	0.3	0.1	0.1
Pb	3.9	6.0	5.5	3.1	3.2	3.4	7.6	52	3.6	18	13	6.6	7.1	18	28	6.4	5.5	6.6	2.3	4.8
Bi	0.2	0.1	0.2	0.1	0.3	0.2	0.2	0.1	0.1	0.0	0.0	0.0	0.1	0.5	0.2	0.1	0.4	1.1	0.4	0.1
Th	0.5	0.4	0.8	1.0	0.6	1.0	1.3	1.3	0.9	1.7	1.7	1.8	2.1	1.5	1.5	1.4	1.6	1.4	0.8	0.9
U	0.4	0.4	0.5	0.4	0.3	0.6	0.6	0.6	0.3	0.8	0.9	1.0	0.4	1.0	1.1	0.4	0.5	1.0	0.5	0.6

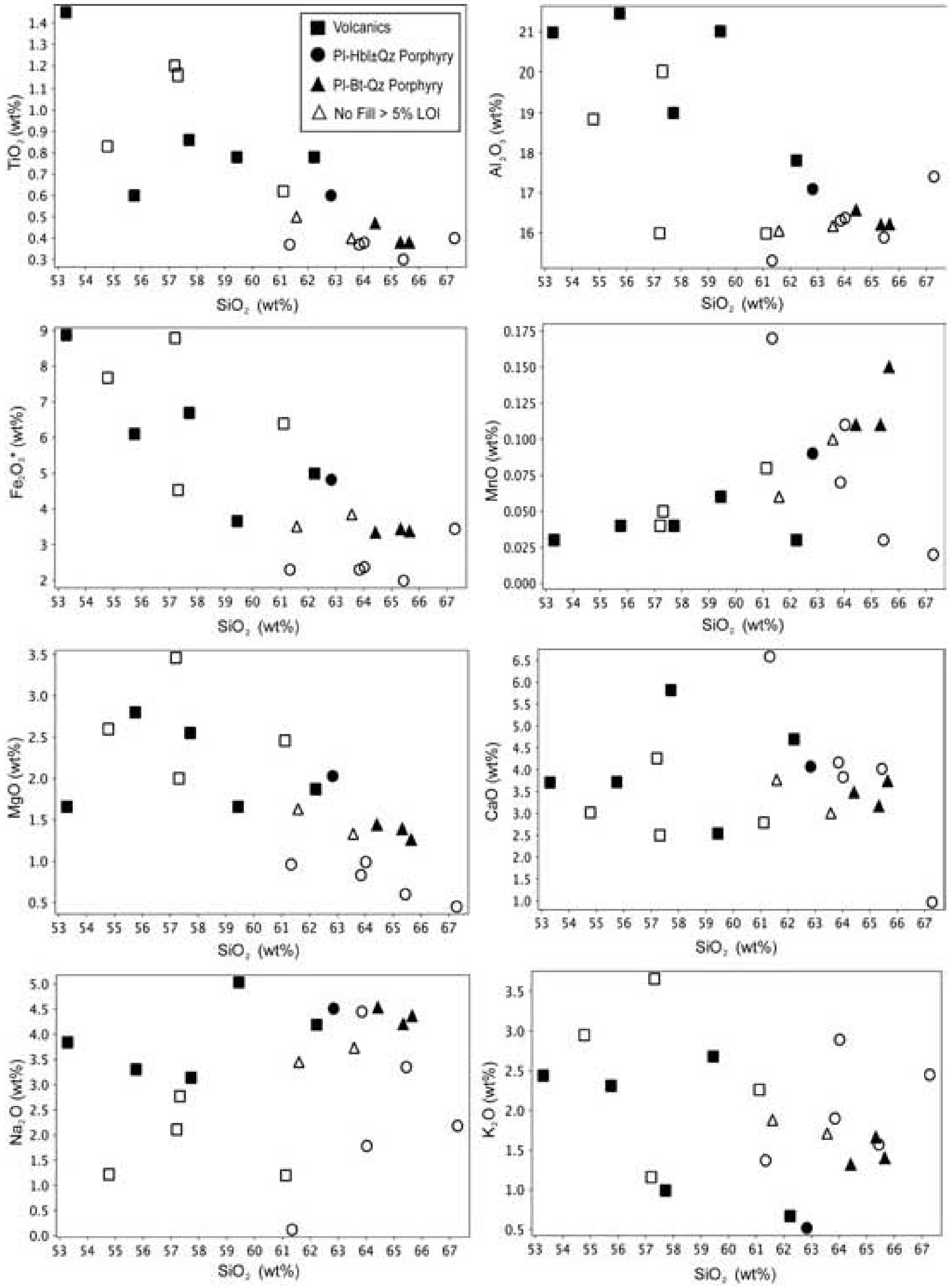

Figure 3-9. Major element variation diagrams for all samples.

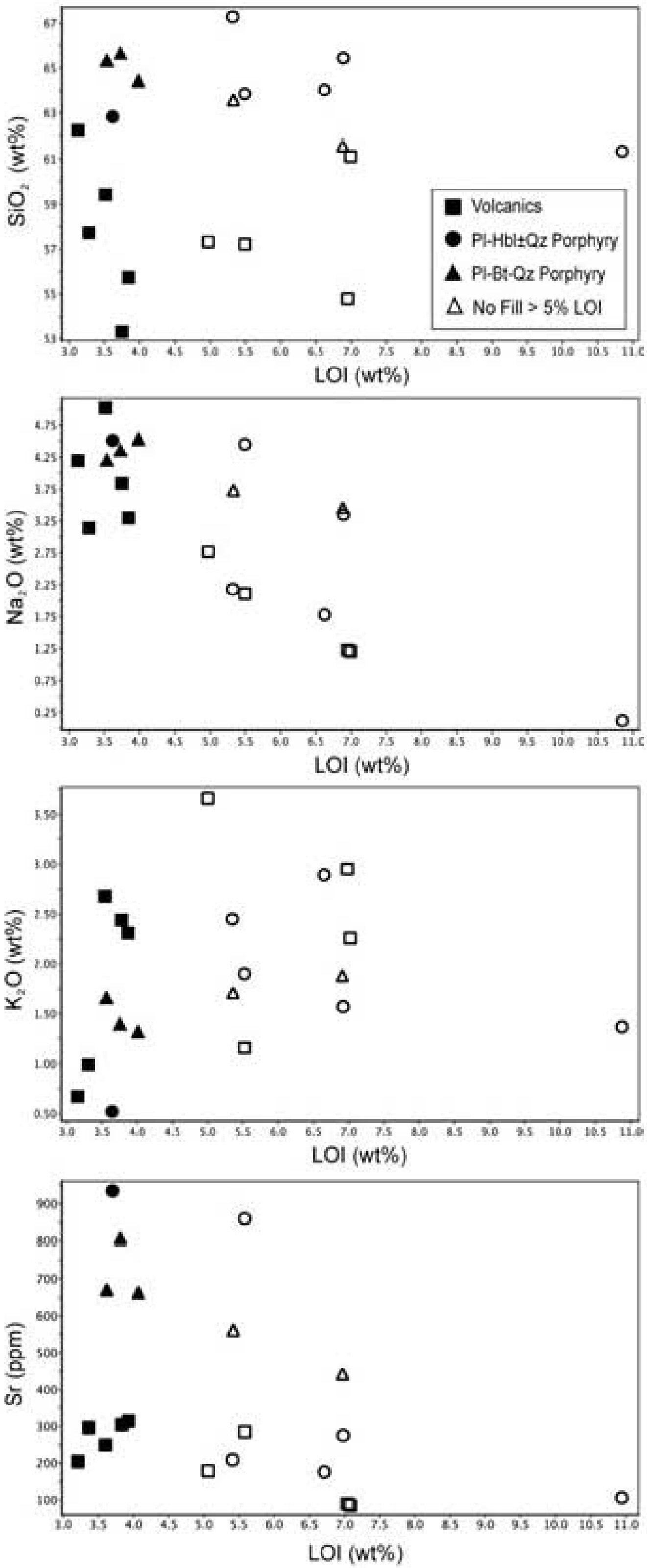

Figure 3-10. Major and trace element variation with alteration intensity (LOI) diagrams for all samples.

Alteration has significantly affected the whole rock geochemistry with noteworthy loss on ignition (LOI) percentages of over 5% in multiple samples and in excess of 10% in one sample (Figures 3-9 and 3-10). TiO_2, Fe_2O_3 and MgO appear unaffected by alteration for the most part showing negligible variation from their respective major element fractionation trends. MnO shows little variation with SiO_2 and it appears the plagioclase-hornblende ± quartz porphyry is affected by alteration. K_2O wt.% increases with increasing LOI showing enrichment by alteration, whereas Na_2O and Sr contents tend to decrease with alteration (Figure 3-10).

Given the Simuku Igneous Complex has previously been identified as a Cu-Mo mineralized porphyry prospect it is useful to assess the metal content of the different intrusive porphyry phases. Figure 3-11 displays measured Cu and Mo content of porphyritic rock types in this study. The Plagioclase-Hornblende ± Quartz porphyry suite is essentially barren and devoid of metal content with no samples exceeding 10 ppm Mo and only one sample with noteworthy Cu content which is still below 1000 ppm Cu. In contrast the Plagioclase-Biotite-Quartz porphyry appears to be a significant mineral bearing sample suite with three of five samples exceeding 1000 ppm Cu and 10 ppm Mo.

Trace element data is presented by way of a multi-element plot normalized to N-MORB (Sun and McDonough, 1989) in Figure 3-12. All samples from both the volcanic and porphyry rock suites exhibit typical subduction-related island arc geochemical affinities with negative Nb anomalies

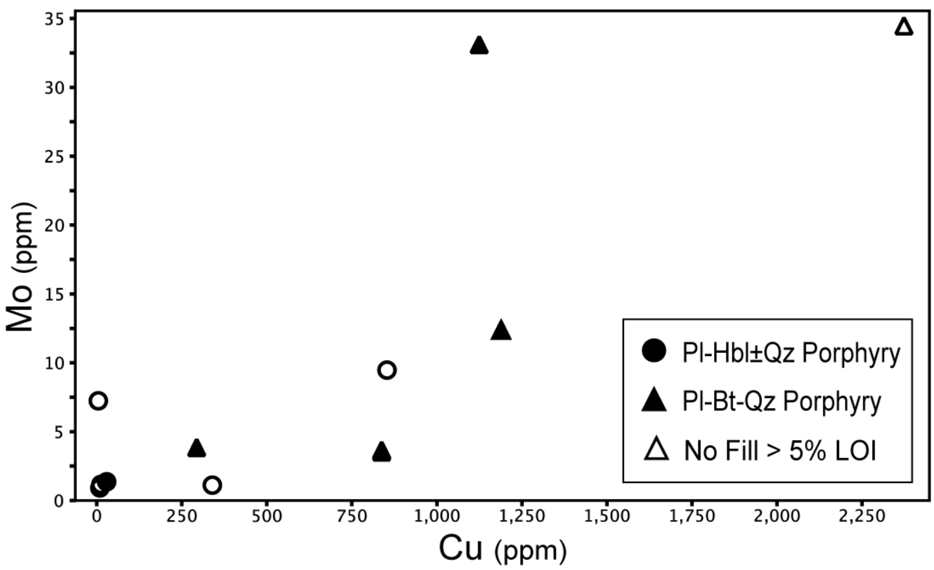

Figure 3-11. Cu-Mo content plot for porphyry samples.

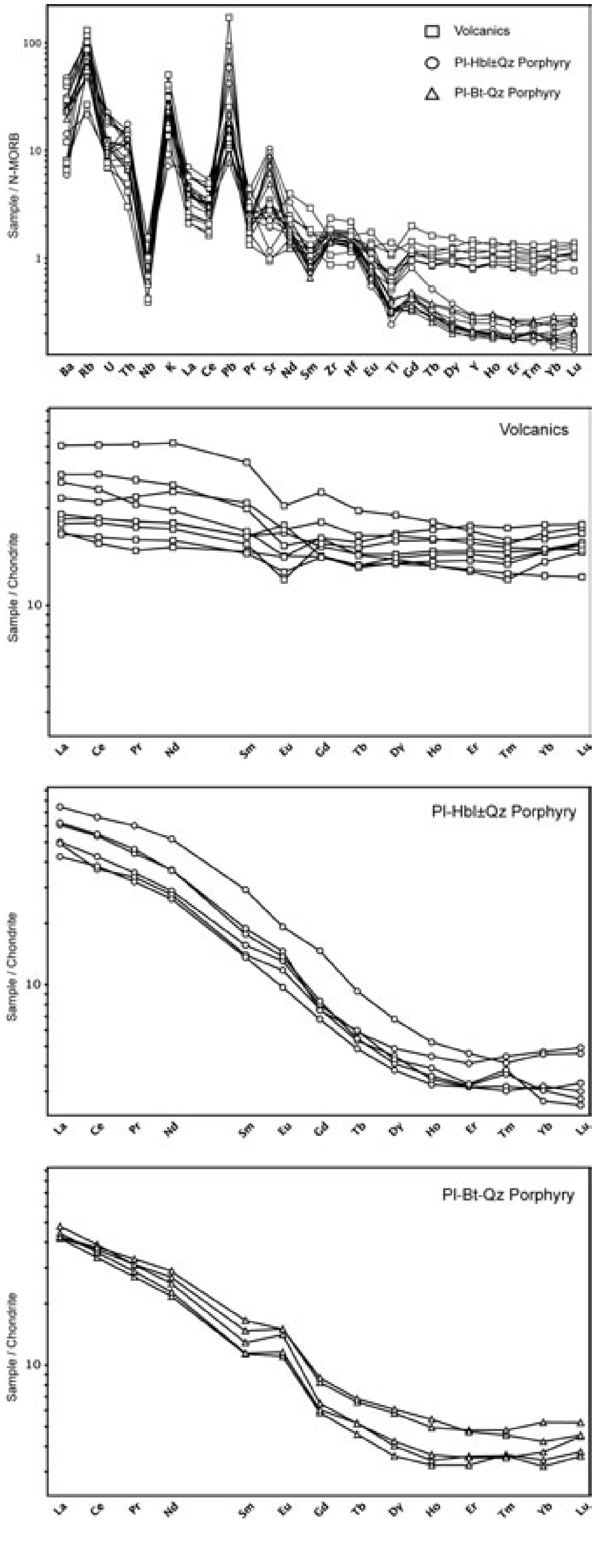

Figure 3-12. N-MORB normalized multi-element plot and C1 chondrite normalized REE plots for the Simuku Igneous Complex. All samples hold arc-like enrichment in LILE, volcanic rocks have HFSE values close to that of N-MORB while both porphyry suites are depleted in HFSE. REE trends are typically flat to moderately enriched in LREE; both porphyry suites exhibit minor LREE enrichments with high levels of HREE depletion. See text for discussion. N-MORB and C1 chondrite normalizations are from Sun and McDonough (1989).

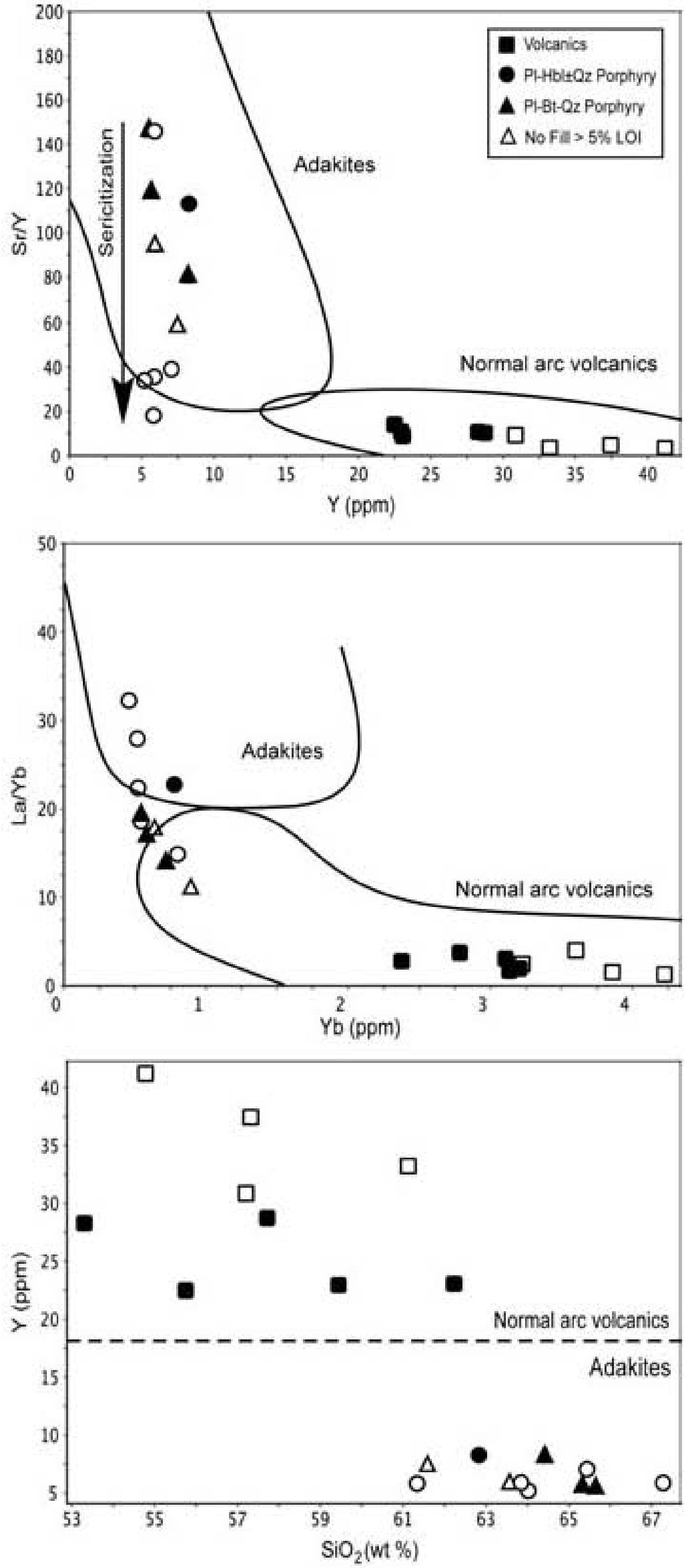

Figure 3-13. Sr/Y versus Y, La/Yb versus Yb, and Y versus SiO_2 plots for rocks of the Simuku Igneous Complex. Volcanics display geochemical behavior of normal arc rocks while both porphyry suites exhibit traits of adakite-like rocks. Sericitization of plagioclase and Sr mobility has lead to an apparent reduction in Sr/Y values. For discussion refer to text. The adakite and normal arc volcanic fields are from Castillo et al. (1999) and Richards (2007).

and relative enrichments in large-ion lithophile elements (LILE), Th, U, Pb and Sr. The volcanic rock types display a flat and relatively smooth trend from Nd through to Lu with minor depletions in Ti. Rare earth element (REE) patterns (normalized to C1 Chondrite; Sun and McDonough, 1989) highlight significant differences between the volcanic and porphyry data sets. Volcanic rock types have flat chondrite-normalized REE patterns, with most having slight negative Eu anomalies. Both of the porphyry suites are LREE enriched and are significantly depleted in HREE (Figure 3-12). The Plagioclase-Biotite-Quartz porphyries exhibit a measurable positive Eu anomaly of Eu/Eu* = 1.2–1.5 indicative of accumulation of plagioclase, while the Plagioclase-Hornblende ± Quartz porphyry suite hold just minor to negligible Eu anomalies at Eu/Eu* = 0.9–1.1 (Figure 3-12).

The porphyritic intrusives of the Simuku Igneous Complex are characterized by pronounced depletions in the heavy rare earth elements (HREE), low Y and Yb, high Sr, and high Sr/Y (Figures 3-12 and 3-13; Table 3-3) when compared to volcanic members of the igneous complex. These geochemical traits are typical of so called ‘adakite-like magmas’ (Drummond and Defant, 1990; Macpherson et al., 2006; Richards, 2011) and will be discussed below in more detail. However, it must be noted that in the context of New Britain, the adakite-like geochemical signature has been adversely affected by intense seritization of plagioclase and associated removal of Sr (Figures 3-10 and 3-13).

Discussion

Arrival of the Ontong Java Plateau at the Melanesian trench

A key premise of this study is the timing for the arrival of the Ontong Java Plateau at the Melanesian trench. As mentioned in section “Tectonic Setting”, there are two main arguments that appeal to different lines of geological evidence to constrain this timing. Firstly, termination of Melanesian arc activity in the Upper Oligocene reflects cessation of subduction due to plateau arrival (Yan and Kroenke, 1993; Petterson et al., 1999; Hall, 2002; Schellart et al., 2006; Knesel et al., 2008), or alternatively, Pliocene crustal shortening in the Solomon Islands is the result of Ontong Java Plateau collision (Cowley et al., 2004; Mann and Taira, 2004; Phinney et al., 2004). I suggest both arguments can be expressed by a tectonic evolution marked by initial Upper Oligocene “soft-docking” of the Ontong Java Plateau and a later episode of Pliocene “hard-docking”, similar to the model previously developed by Yan and Kroenke (1993) and Petterson et al. (1999). I take the approach that changes in the tectonic regime of island-arc settings are strongly coupled to changes in subduction dynamics. The relative motion of the upper and lower plates leads to either subduction hinge advance or hinge retreat, and may also influence the angle of slab subduction. These changes in slab angle are important as they impact significantly on the structural, magmatic, and geochemical evolution of the overriding plate through either compressional or extensional tectonism (Schellart, 2004; Arcay et al., 2005; Heuret and Lallemand, 2005; Lallemand et al., 2005; Schellart, 2008). Moreover, switches in subduction dynamics are often triggered by the arrival of a buoyant section of crust, such as the Ontong Java Plateau (Pubellier and Cobbold, 1996; Wallace et al., 2005; Schellart, 2008; Baes et al., 2011; Rosenbaum and Wo, 2011).

By applying these principles to the arrival of the Ontong Java Plateau at the Melanesian trench, I can assess the existing evidence to establish a scenario for the timing of collision. An Upper Oligocene arrival of the plateau at the Melanesian trench would be expected to result in subduction hinge advance, but there is no record of crustal shortening within the Solomon Islands at this time. We do, however, see an initiation of a new extensional regime in the Solomon Islands at this time, as evidenced by opening of the Central Solomon Basin (Wells, 1989; Cowley et al., 2004). This extensional phenomenon is repeated along much of the Melanesian arc (see section "Tectonic Setting") and may have been induced by slab steepening in response to large-scale reduction in the driving force on the downgoing slab (e.g. Schellart, 2004; Arcay et al., 2005; Heuret and Lallemand, 2005; Lallemand et al., 2005; Schellart, 2008). We can therefore account for changes in the upper plate consistent with a "soft docking" style of plateau arrival, but given the absence of upper plate shortening during this time we must also account for long-term redistribution of plate convergence due to termination of Pacific plate subduction. Indeed several authors have postulated that arrival of the Ontong Java Plateau resulted in the initiation of new subduction systems further to the south to accommodate regional convergence, as evidenced by the onset of arc magmatism on the Papua New Guinea mainland (e.g. Hall, 2002; Stern, 2004; Schellart et al., 2006).

An alternative model invokes Pliocene crustal shortening across the Solomon Islands as a result of "hard docking" of the Ontong Java Plateau collision from approximately 5 Ma (Cowley et al., 2004; Mann and Taira, 2004; Phinney et al., 2004). However, models from Petterson et al. (1997; 1999) and Chadwick et al. (2009) attribute shortening in the Solomon Islands as a response to increased coupling at the San Cristobal subduction zone as a result of spreading in the Woodlark Basin from 6 Ma (Weissel et al., 1982; Taylor et al., 1999). I agree with the latter models of crustal shortening and cite a strong spatial correlation between the extent of the subducted Woodlark Basin at the San Cristobal trench and zone of deformation within the Solomon Islands and adjacent North Solomon trench (Figure 3-1). Accordingly, I suggest Upper Oligocene timing for initial arrival of the Ontong Java Plateau at the Solomon Islands is a more credible argument and is the timing I adopt in this study.

Melanesian arc development and emplacement of the Simuku Porphyry Complex

The new U-Pb zircon ages presented in this study correlate well with the previously established geological history of New Britain. In addition, these new ages provide the first robust absolute dating constraint on magmatism associated with the Melanesian arc in New Britain, and the wider southwest Pacific. The Baining Volcanics represent the initiation of arc magmatism at the convergent plate boundary between the Australian and Pacific plates (Madsen and Lindley, 1994; Lindley, 2006) active between approximately 41 and 37 Ma (Figures 3-14 and 3-15). The oldest concordant inherited zircon associated with this suite is dated at 43.6 ± 0.5 Ma, possibly representing the earliest arc activity. The nature or composition of this early arc are not known as direct evidence for this activity is based on inherited zircons of younger rocks. Xenoliths of fine-grained or glassy volcanics within younger volcanic units may be representative of the Baining Volcanics, but this remains to be tested. Previous work has identified the Baining Volcanics as basic to intermediate pillow lavas, breccias and volcaniclastics (Madsen and Lindley, 1994; Lindley, 2006). Evidence of coralline limestone lenses interbedded with the volcanics suggests this activity was generally marine to shallow marine (Madsen and Lindley, 1994; Lindley, 2006). These results establish a preliminary timeframe in agreement with previous work suggesting Upper Eocene timing for initiation of the arc. The tectonic framework of this margin prior to this time remains unconstrained.

Emplacement of the Kapuluk Volcanics followed deposition of the Baining Volcanics (Figures 3-14 and 3-15). The Kapuluk Volcanics are typified by fine-grained pyroclastics with variable but limited phenocryst crystal growth of plagioclase and quartz prior to eruption. Previous geological mapping has also observed volcaniclastics, tuff, agglomerate and lavas (Madsen and Lindley, 1994; Lindley, 2006). This volcanic succession has previously been interpreted as Upper Oligocene in age. However, in light of new U-Pb zircon dating at 29.4 ± 0.9 Ma and an associated inherited age of 29.6 ± 2.6 Ma, I suggest the Kapuluk Volcanics should be assigned primarily an Lower Oligocene age, which may continue into the Upper Oligocene (Figure 3-14). Both the Baining Volcanics and Kapuluk Volcanics are “normal” subduction-related island arc volcanics with generally flat REE patterns (Figure 3-12).

There is an apparent cessation of magmatism between deposition of the Baining Volcanics and the Kapuluk Volcanics from approximately 37–32 Ma (Figure 3-14). However, it is important to note that my age constraints on the Baining Volcanics derive from inherited zircon populations in the Kapuluk Volcanics, and hence may reflect preferential sampling of zircon populations during reworking of the underlying volcanic sequences. In this case there may have been continuity of volcanism that is not completely preserved in our samples. Alternatively, the apparent volcanic hiatus may genuinely be a record of temporary arc cessation, as is observed in other long-lived arc systems (e.g. Izu-Bonin; Taylor, 1992), or may be due to erosive loss of the upper parts of the volcanic sequence prior to deposition of the overlying Kapuluk Volcanics. Volcanic textures and interbedded carbonate lenses of the Baining Volcanics (see section "New Britain Geology") indicate that the rocks are likely to be near-surface or sub-aerial deposits and hence were likely to have undergone erosional processes. By contrast The Kapuluk Volcanics, are well preserved following final arc cessation from 20 Ma due to subsidence and burial beneath regional carbonate platforms.

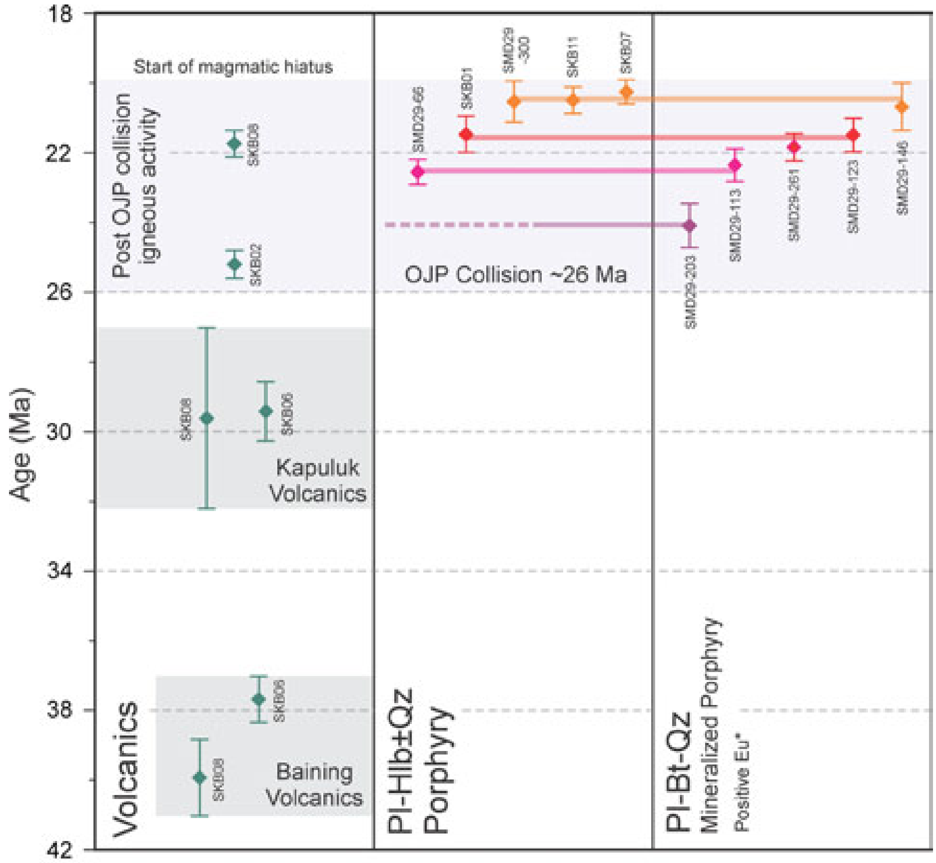

Figure 3-14. Geochronology and petrogenesis of the Simuku Igneous Complex. Correlation of U-Pb dating results across the three main rock types derived from characteristics of petrography and geochemistry. Three main divisions are suggested in the history of the Simuku Igneous Complex and Melanesian arc; the early arc growth phases of the Baining Volcanics and Kapuluk Volcanics, and a post-OJP collision igneous suite comprising normal arc volcanics and porphyry complex (adakite-like signature). We interpret individual pulses of magma intrusion within the porphyry complex at c. 1 m.y. intervals as shown. See text for further discussion. The end of the post-OJP igneous activity marks the onset of a magmatic hiatus over the majority of New Britain that is in effect until initiation of the modern New Britain arc. Points are U-Pb ages derived from concordia; error bars are 2σ.

Arrival of the Ontong Java Plateau and the associated stalling and cessation of Pacific subduction from 26 Ma resulted in a profound change in arc behavior (Figures 3-14 and 3-15). Shortly after the deposition of the SKB02 volcanics at 25.2 ± 0.4 Ma, the first intrusive pulse of the post-OJP collision porphyry complex is recorded at 24.1 ± 0.6 Ma by SMD29-203. This represents the inception of a new phase in the history of Melanesian arc magmatism shortly after (~2 m.y.) Ontong Java Plateau collision (Figure 3-14). This porphyry complex forms two distinct intrusive porphyry suites defined on mineralogical (Table 3-1), and geochemical (Figure 3-12) grounds. Both the plagioclase-hornblende ± quartz porphyry and plagioclase-biotite-quartz porphyry are dated by five new U-Pb zircon crystallization ages, which are statistically indistinguishable. However, our understanding of other porphyry complexes around the world suggests a prolonged igneous crystallization history such as we see in the Simuku porphyry complex is likely comprised of multiple intrusive pulses. Previous studies interpret the elapsed time for total activity of porphyry complexes is typically in the order of 2 to 5 m.y. with intrusion of individual igneous pulses at intervals of 0.5–1.5 m.y. (e.g. Andean deposits; Ballard et al., 2001; Maksaev et al., 2004; Padilla-Garza et al., 2004; Harris et al., 2008; Sillitoe, 2010). I interpret evolution of the Simuku porphyry complex to include four distinct individual pulses of intrusion that must have occurred at 1-2 m.y. intervals (Figure 3-14).

Sample SMD29-203 represents the first igneous pulse of the Simuku porphyry complex at c. 24 Ma, while the last intrusion was emplaced at c. 20 Ma based on samples SMD29-300, SKB11, SKB07 and SMD29-146 (Figure 3-14). Each intrusive pulse can be broken down into two different components represented by the plagioclase-hornblende ± quartz porphyry and plagioclase-biotite-quartz porphyry suites. The plagioclase-biotite-quartz porphyry was a more evolved magma that also exhibits significant positive Eu anomalies indicative of plagioclase accumulation and typical of a late crystallizing magmatic reservoir. With the exception of the Eu anomaly, the geochemical signature of the two porphyries is essentially identical indicating these intrusive phases likely have a similar source, with minor differences arising from late fractionation during high-level crustal intrusion and emplacement. Post-emplacement faulting and the lack of outcrop make interpretation of intrusive relationships speculative. However, given mineralogical and geochemical porphyry relationships I infer the plagioclase-hornblende ± quartz porphyry phases may represent volcanic stocks or dikes fed by the plagioclase-biotite-quartz porphyry from an upper crustal parental magma chamber. Higher Cu and Mo grades of the plagioclase-biotite-quartz porphyry (Figure 3-11) indicate this phase was potentially the source of metalliferous fluids and porphyry mineralization.

Post OJP arrival porphyry adakite-like signatures

The least altered porphyry suite samples are peraluminous dacites with relatively high Na_2O (4 – 5 wt.%), high Sr, high Sr/Y (Figure 3-13) and relative depletion in heavy rare earth elements (HREE) (Figure 3-12). These geochemical traits are often attributed to adakites, or adakite-like rocks (Macpherson et al., 2006; Alonso-Perez et al., 2009; Chiaradia et al., 2009; Richards, 2011). The use of the term adakite remains somewhat controversial as the initial usage had petrogenetic implications; these rock types were initially thought to have been derived from melting of eclogitized subducted oceanic crust and are observed only infrequently in subduction settings (Kay, 1978; Defant and Drummond, 1990; Yogodzinski and Kelemen, 1998; Castillo et al., 1999; Falloon et al., 2008; Hidalgo et al., 2011). It has only recently been appreciated that an array of potential tectonic environments can give rise to adakite-like geochemical signatures (Macpherson et al., 2006; Alonso-Perez et al., 2009; Chiaradia et al., 2009; Richards, 2011; Eyuboglu et al., 2012), which result from melt generation and/or fractionation within the garnet stability field. Geological scenarios that permit these conditions include garnet fractionation from mantle-derived melt at high pressure (i.e. deep crust or mantle) or melting of a garnet-bearing source, such as eclogite or garnet amphibolite of the subducting slab or thickened arc crust (Sen and Dunn, 1994; Rapp and Watson, 1995; Macpherson et al., 2006; Richards and Kerrich, 2007; Chiaradia, 2009; Chiaradia et al., 2009; Richards, 2011; Eyuboglu et al., 2012). The Simuku adakitic rocks are peraluminous with low MgO contents and so do not represent melts equilibrated with mantle rocks. Comparable melt compositions have been produced experimentally from dehydration melting of mafic rocks at high pressures (e.g. Sen and Dunn, 1994) or by high-pressure fractionation of primitive andesite (Alonso-Perez et al., 2009). However, in the absence of more definitive data for tracing petrogenesis, such as radiogenic isotopes, and potential modifications to primary geochemical signatures by intense alteration as mentioned earlier (Figure 3-13), it is currently not possible to detail the origin of the adakite-like signatures of the Melanesian arc of New Britain. I am currently working to build radiogenic isotope datasets to tackle this problem, which will form the basis for later studies. Nevertheless, here it is worthwhile to briefly discuss the potential scenarios and tectonic drivers leading to the generation of different adakite source mechanisms in the context of New Britain and the Melanesian arc during subduction cessation.

Formation of the Ontong Java Plateau is dated to approximately 122–120 Ma (Mahoney et al., 1993; Tejada et al., 2002; Hall and Riisager, 2007), so the adjacent oceanic crust of the Pacific plate subducted beneath the Melanesian arc and proto-New Britain is of similar age or older. This crust would generally be regarded to be too old and cold to undergo partial melting (and hence, adakite melt generation) during subduction (Defant and Drummond, 1990; Peacock, 1996; Arcay et al., 2007). Shallow slab subduction and slab windows have been envisaged as potential scenarios to invoke partial melting of subducted slab (Yogodzinski et al., 2001; Schuth et al., 2009; Eyuboglu et al., 2012), but there is no evidence for either of these processes in New Britain. One scenario not commonly appreciated is the result of subduction cessation on the subducting slab, Should subduction cease, the slab will either remain stranded/hanging in the upper mantle, or alternatively will break up and sink (Davies and von Blanckenburg, 1995; Gerya et al., 2004; Rosenbaum et al., 2008; Schmalholz, 2011). Previous numerical modeling by Davies and von Blanckenburg (1995) and Gerya et al. (2004) suggests the subducted slab can remained attached for 5–10 m.y. or more after subduction ceases. If this should occur, the previously cold slab is exposed to the ambient temperature of the surrounding mantle and will warm. Relatively shallow portions of this slab may be susceptible to partial melting under the conditions of an elevated geotherm to produce slab melts and the resulting adakitic geochemical signatures we see in the Simuku porphyry complex (Figure 3-15).

In recent years, several authors have proposed additional scenarios where adakite-like geochemical signatures in arc magmatism can develop in response to fractionation or equilibration of partial melts with mantle or lower crustal garnet (e.g. Garrido et al., 2006; Macpherson et al., 2006; Alonso-Perez et al., 2009). "Normal" arc behavior is the result of primary basaltic arc magmas ascending toward the surface, and typically stalling at density barriers in the mantle, or at one or more crustal levels in oceanic or continental arcs. The processes of wall-rock assimilation and fractional crystallization (AFC; DePaolo, 1981), or MASH processes (melting, assimilation, storage, and homogenization; Hildreth and Moorbath, 1988; Annen et al., 2006), result in development of intermediate composition "calc-alkaline" magmas. However, stalling or ponding of mafic magmas at deeper levels, in the mantle or at the base of the crust, can cause crystallization of ultramafic to gabbroic cumulates in which garnet is a common early fractionating or residual phase (Hamilton, 1981; Klepeis et al., 2003; Dufek and Bergantz, 2005; Garrido et al., 2006; Macpherson et al., 2006; Macpherson, 2008; Alonso-Perez et al., 2009). This leads to the formation of andesitic to dacitic differentiates with adakite-like trace element characteristics (i.e. relative HREE-depletion, high La/Yb and Sr/Y: Feeley and Davison, 1994; Kay et al., 1999; Klepeis et al., 2003). As outlined in sections "New Britain Geology" and "Geology of the Simuku Property", above, there is a clear relationship between the major crustal-scale structural lineaments cutting New Britain and emplacement of volcanic and intrusive rocks associated with the Melanesian arc (Lindley, 2006). This suggests that the lineaments acted as significant conduits allowing passage of magma to the surface. It is reasonable to propose that the activity of such arc oblique structures were maintained by stresses induced in the upper plate during subduction (e.g. Glen and Walshe, 1999; Richards et al., 2001; Sillitoe, 2010). Therefore, if subduction at New Britain ceased due to distant collision of the Ontong Java Plateau, changes in the large-scale stress regime may have caused lineament activity to lapse and the magma conduits close, preventing easy passage through the crust. Such a process would favor stalling and ponding of mantle-wedge derived melts at the base of the crust, wherein they may have undergone garnet fractionation and generation

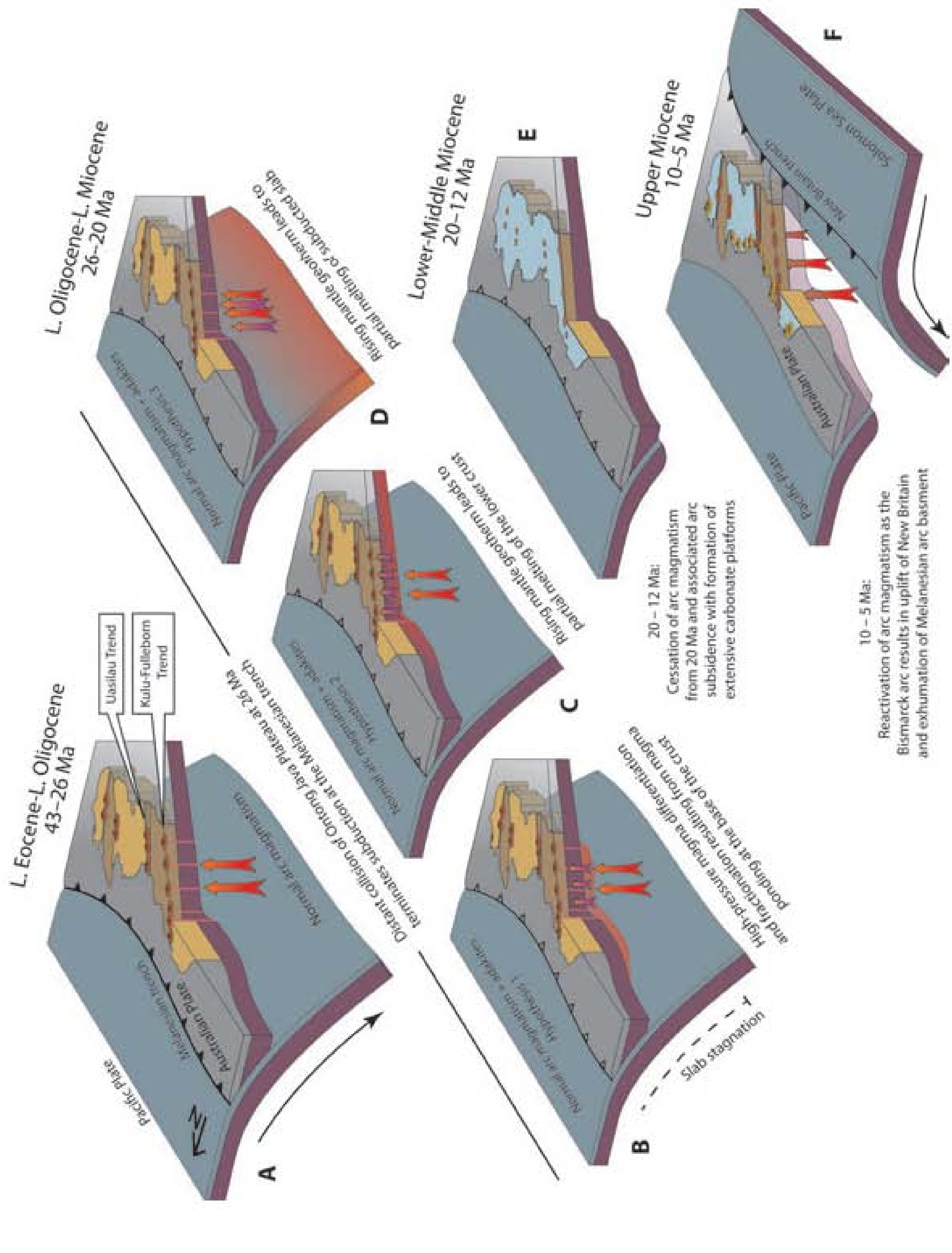

Figure 3-15. Cenozoic geodynamic evolution of New Britain and the Melanesian arc. The cartoon illustrates generalized time steps in the evolution of New Britain. New Britain is illustrated as a series of crustal blocks of different thicknesses with intervening lineaments. These lineaments act as conduits controlling the distribution of Melanesian arc magmatism (brown volcanoes). The Miocene history of New Britain is marked by accumulation of extensive carbonate platforms (light blue) and magmatism related to the Bismarck arc (yellow volcanoes).

of adakite-like magmas (Figure 3-15). Episodic tapping of these magmas to higher crustal levels may have allowed emplacement of spatially and temporally associated porphyry intrusive rocks with either adakitic or 'normal' arc magma geochemical signatures.

An additional mechanism by which adakite-like geochemical signatures are generated is the melting of subduction-modified lower crustal rocks or basaltic underplating induced by elevation of the geotherm. Partial melts derived from the lower crustal rocks or assimilated by arc magmas likely include garnet amphibolites (Hildreth and Moorbath, 1988; Rushmer, 1993; Macpherson et al., 2006). Previous studies have identified present day crustal blocks comprising New Britain to have anomalous thicknesses in the order of 40 km (as mentioned previously in section "New Britain Geology"; Wiebenga, 1973; Lindley, 2006). This crustal thickness can be attributed to normal island arc development over approximately 40 m.y., particularly where the loci of magmatism is relatively stable such as we see in New Britain. Given the tectonic setting, this thickened crust is unlikely to have a cool lithospheric root as would be typical for thickened continental crustal settings. The origin of this crustal root has not conclusively been established, but it should be noted that the undisturbed Lower Miocene reef limestones provide evidence to preclude significant crustal deformation and thickening post-OJP collision (Madsen and Lindley, 1994; Lindley, 2006) and support the suggestion of an association with early arc-building. This thickness of crust will be inherently unstable at such a dynamic plate boundary setting with large heat transfer. Any changes to this subduction regime may induce partial melting of the lower crust. For example, slowing or stagnation of subduction preventing the renewal of newly subducted cold slab material in the mantle may lead to an ambient rise in the local geotherm sufficient to heat (and partially melt) the lower crust (Figure 3-15). As this tectonic scenario is highly plausible for New Britain, lower crustal partial melting is also a possible origin of the adakite-like signature of the post-OJP collision porphyry suite.

Generation of adakitic signatures in arc rocks and collisional tectonic settings is relatively well established and has been the focus of extensive studies over recent years. Investigation of arc-systematics during subduction cessation, however, remains poorly understood and the significance of adakitic signatures in this dynamic tectonic setting even less so. Here I have proposed several mechanisms adapted from previous studies for the generation of adakite-like geochemical signatures in the context of New Britain and termination of Melanesian arc activity in response to collision of the Ontong Java Plateau. Extensive alteration of the post-OJP collision Simuku porphyry complex precludes simple identification of a single mechanism for adakite formation or a combination of multiple mechanisms. Nevertheless further studies on adakite formation at New Britain have the potential to broaden understanding of the magmatic response to complex tectonics events such as plateau collision and subduction termination, as well as inform on the role of adakites in porphyry mineralization.

Conclusions

The Simuku Igneous Complex of New Britain, Papua New Guinea is an excellent place to study the tectono-magmatic effects of major collision events on magmatic arcs. I present the first combined U-Pb geochronology and geochemical investigation into the evolution of the Melanesian arc from initiation of arc magmatism to arc termination. The Baining Volcanics represent the onset of Melanesian arc volcanism in New Britain from at least 43–37 Ma; and are succeeded by the Kapuluk Volcanics, potentially active from approximately 32 Ma until 27 Ma. Collision of the Ontong Java Plateau with the Solomon Islands at 26 Ma, and the resulting subduction cessation led to a profound response in arc behavior with initiation of the post-collision igneous suite from 25 Ma, shortly after collision, until 20 Ma with termination of Melanesian arc activity. “Normal” arc volcanism continued intermittently throughout this time, with contemporaneous formation of the Simuku porphyry complex from 24 to 20 Ma. Within the porphyry complex we recognize four distinct pulses of porphyritic magmatism, each marked by intrusive stocks and parental magma chambers represented by plagioclase-hornblende ± quartz and plagioclase-biotite-quartz porphyries respectively. The latter are marked by more evolved mineralogy and positive Eu anomalies indicating plagioclase accumulation in the parental reservoir. The main mineralizing porphyry intrusive bodies within the Simuku prospect were the more evolved plagioclase-biotite-quartz porphyry. In addition, the porphyry intrusives all exhibit adakite-like geochemical signatures, in contrast to the “normal” arc volcanics. The origins of adakite-like characteristics are unclear, but within the tectonic context of New Britain we propose the signatures arise from either melting of the stagnant subducted slab or lower crustal melting in response to a rising geotherm following subduction cessation; or high pressure magma differentiation and fractionation due to cessation of magma conduit activity and stalling of magma at the base of the crust.

Chapter 4

Petrogenesis and geodynamic evolution of the Maramuni arc, Papua New Guinea: Upper-Miocene continental collision, orogenesis and arc magmatism at the northern Australian plate boundary

Abstract

Understanding of the tectonic evolution of Papua New Guinea throughout the Miocene is hampered by a lack of robust geological evidence, leading to uncertainty in the plate tectonic and subduction framework of the region. The Maramuni arc of Papua New Guinea represents the only continuous tectonic element throughout this dynamic period marked by complex collision events and orogenesis. I present the first detailed U-Pb geochronology and geochemical investigation of the Maramuni arc utilizing a suite of intrusive rocks from the Kainantu region of the eastern Papuan Highlands. Arc magmatism related to north-dipping subduction at the Pocklington trough is punctuated by arrival of the Australian continent at approximately 12 Ma, which also coincides with initial growth of the New Guinea Orogen. Arc geochemistry from 12 Ma highlights a changing tectonic setting and arc magmatism marked by anomalous enrichments in high-field strength elements at 9 Ma. Subsequently, break-up of the subducted material and crustal delamination from approximately 7 Ma is coincident with porphyry intrusion bearing similarities to adakitic rocks. This timing is significant in that it corresponds to isotatic crustal rebound and renewed uplift of the New Guinea Orogen from 6 Ma. Although not conclusive as to revealing the fundamental controls on arc evolution, this study contributes towards the defininition of a tectonic framework and understanding of subduction dynamics in Papua New Guinea during the Miocene.

Introduction

Cenozoic tectonics in the southwest Pacific is often used as an analogue to illustrate the formation of complex tectonic terranes, and in particular the development of accretionary orogens (e.g. northern Appalachians and British Caledonides; Van Staal et al. [1998]; Central Asian Orogenic Belt and Arabian-Nubian shield; Kröner et al. [2007]; Lachlan Fold Belt; Collins and Richards, [2008]; Western Alps; Malusà and Garzanti [2012]). Tectonic complexity arises in the southwest Pacific as the result of multiple episodes of large-scale tectonic reorganization driven primarily by major collision events, such as the collision of the Ontong Java Plateau with the Melanesian arc (Petterson et al., 1999; Hall, 2002; Mann and Taira, 2004; Holm et al., 2013; Chapter 3), and collision of the Australian continent with New Guinea (Cloos et al., 2005; Hill and Hall, 2003). However, the nature and timing of these events is the subject of much dispute in the geological community, which in turn compromises understanding of even the basic regional geodynamic framework of the southwest Pacific. Papua New Guinea is critical to our understanding of southwest Pacific tectonics, as it lies within a zone of oblique convergence between the Ontong Java Plateau of the Pacific plate, and the Australian continent (Figure 4-1), and records a complex tectonic history of terrane collision and orogenesis, arc magmatism, microplate development and varying subduction dynamics. Of additional significance, the Maramuni arc of Papua New Guinea and West Papua hosts some of the world's largest subduction-related porphyry ore deposits including Ok Tedi, Frieda River, Porgera and Grasberg.

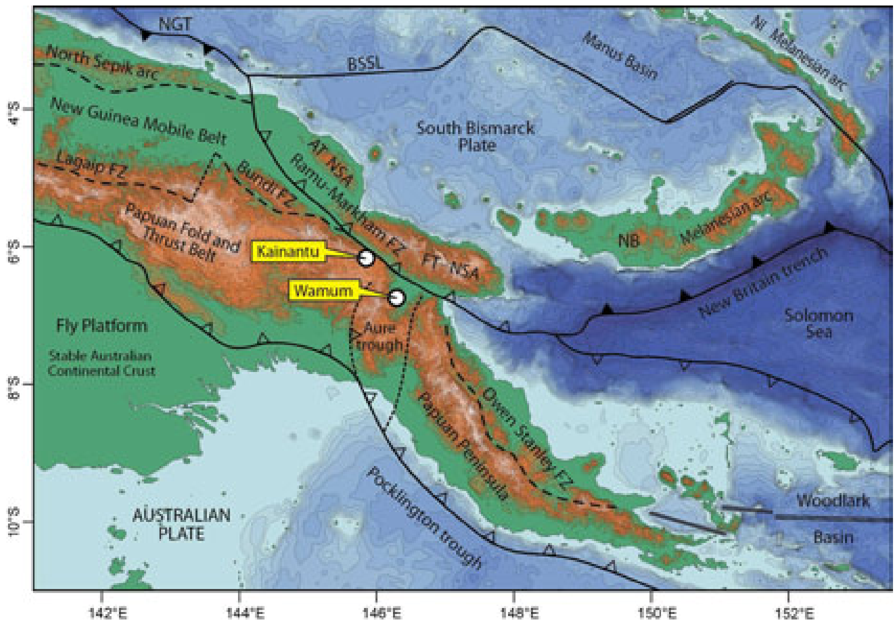

Figure 4-1. Topography, bathymetry and major tectonic elements of Papua New Guinea. Major tectonic plates and boundaries are as indicated; the North Sepik arc (NSA) is comprised of the Bewani-Toricelli-Prince Alexander, Adelbert (AT) and Finisterre Terranes (FT); the Melanesian arc comprises New Britain (NB) and New Ireland (NI); BSSL, Bismarck Sea seismic lineation; NGT, New Guinea trench; FZ, fault zone. The study locations of Kainantu and Wamum are as labeled.

Much of the tectonic framework of Papua New Guinea remains the subject of debate and controversy related to uncertainty over the timing of tectonic events, and the nature or location of events or plate boundaries. This uncertainty arises from a lack of data and evidence for specific tectonic factors that contribute to Papua New Guinea geology, as highlighted in the work of Hall (2002). This uncertainty is reflected by the often overwhelming and contrasting array of tectonic reconstructions for the region (e.g. Abbott, 1995; Hill and Raza, 1999; Hall, 2002; Hill and Hall, 2003; Cloos et al., 2005; Schellart et al., 2006; Davies, 2012). Therefore, Papua New Guinea and the Maramuni arc present an ideal setting to examine the tectonic and geodynamic processes associated with arc magmatism, subduction, orogenesis, continental growth and mineralization.

This work seeks to unravel the complex tectonic history of Papua New Guinea and the northern Australian plate boundary, and present a clear case as to the nature and development of the Maramuni arc, and provide insights into the recent tectonic development of the northern Australian plate boundary. Studies into the nature of arc magmatism through time - particularly during periods of tectonic change - can provide us with insights into subduction dynamics and crustal processes that may be difficult to resolve via other means. In this paper I present a detailed investigation into the Middle–Upper Miocene evolution of Papua New Guinea using the Maramuni arc as a proxy for the dynamic tectonic and crustal behavior during this time. To achieve this I present a new dataset of high-resolution U-Pb zircon geochronology coupled with detailed geochemistry of the Maramuni arc from the porphyry mineralization prospects of Wamum and Kokofimpa of the Kainantu region in the eastern Papuan Highlands. Considering these new data together with previous data and tectonic models of New Guinea, I put forward a new tectonic framework and geodynamic model for the evolution of New Guinea. I also emphasize the difficulty in interpreting tectonic history in a region lacking in geological data and we stress the need for further work on the tectonic, geochemical and mineralogical characteristics of this arc to further refine models of tectonic development and crustal growth.

Geological Setting and Samples

Tectonic Setting

The island of New Guinea, incorporating Papua New Guinea and West Papua, Indonesia, is geologically composed of terranes accreted to the northern Australian continental margin during the Cenozoic northward drift of the Indo-Australia plate (Hill & Hall 2003; Crowhurst et al., 2004; Davies, 2012). Current knowledge of Papua New Guinea geology and tectonics is covered in depth by the recent review articles of Baldwin et al. (2012) and Davies (2012). Geologically, the focal point of New Guinea is the New Guinea Orogen or Central Range, which runs along the east-west axis of the island and comprises the Papuan Fold and Thrust Belt and uplifted areas of the New Guinea Mobile Belt (Figures 4-1 and 4-2). The Papuan Fold and Thrust Belt is an accretionary orogen of sedimentary cover rocks developed on Australian continental basement (Hill and Gleadow, 1989; Craig and Warvakai, 2009) and buttressed against variably deformed sedimentary, metamorphic and crystalline rocks of the New Guinea Mobile Belt (Hill and Raza, 1999; Davies, 2012). The Lagaip and Bundi fault zones mark the contact zone between the two orogenic belts and comprise uplifted and exhumed Australian continental basement rocks at the rear of the Papuan Fold and Thrust Belt. Growth of the New Guinea Orogen is generally accepted to have occurred in two distinct phases of uplift and deformation, with initial uplift from 12 Ma (Hill and Raza, 1999; Cloos et al., 2005) and a secondary event from approximately 6 Ma that was responsible for development of the Papuan Fold and Thrust Belt (Hill and Gleadow, 1989; Hill and Raza, 1999; Cloos et al., 2005).

The Late Cenozoic Maramuni arc intrudes the New Guinea Orogen. Early arc magmatism was emplaced into the New Guinea Mobile Belt during the Upper Oligocene with the initiation of subduction beneath New Guinea (Figure 4-2; Davies et al., 1987; Lock et al., 1987; Hill and Raza, 1999; Cloos et al., 2005). Magmatism migrated south into the Papuan Fold and Thrust Belt during the Upper Miocene (Page, 1976; Rogerson and Williamson, 1985; Davies, 1990), while recent Pliocene and Quaternary igneous activity is almost exclusively hosted within the

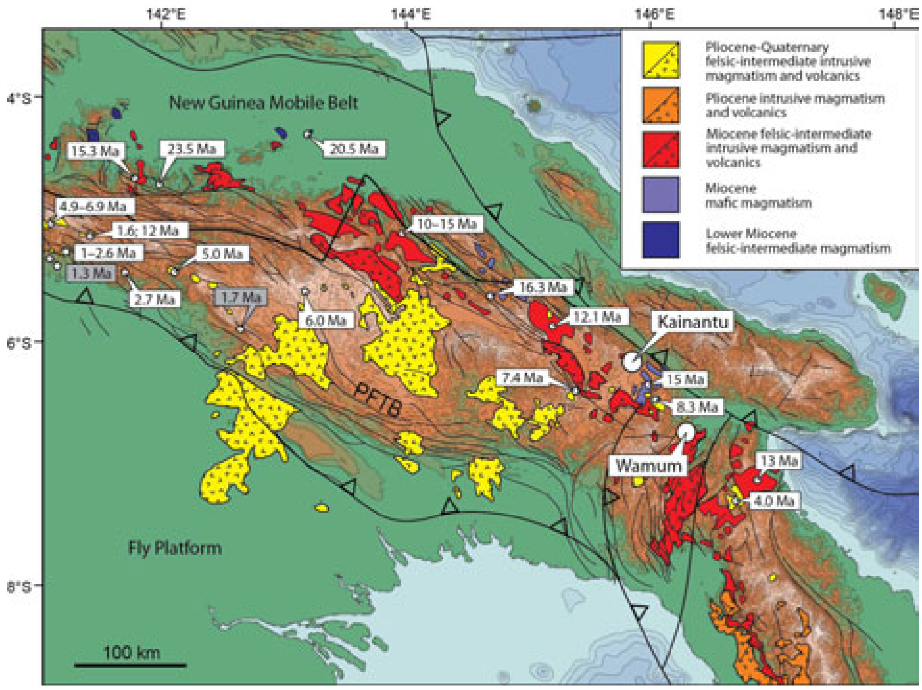

Figure 4-2. Magmatism of the Maramuni arc. Distribution of mapped magmatic occurrences (Australian Bureau of Mineral Resources, 1972) and major tectonic boundaries from Figure 4-1. K/Ar ages (white boxes) for Late Cenozoic magmatism are as indicated from Page (1976), Rogerson and Williamson (1985), Richards and McDougall (1990), Page and McDougall (1972), Whalen et al. (1982), and Grant and Nielsen (1975), and incorporating U-Pb ages (grey boxes) from van Dongen et al. (2010) and Chapter 2. Minor lines indicate mapped structure from Australian Bureau of Mineral Resources (1972).

Papuan Fold and Thrust Belt and stable Australian continental crust of the Fly Platform (Figure 4-2). It is worth noting that the source of Pliocene and Quaternary magmatism has not yet been conclusively determined; it may be associated with partial melting of the upper-mantle following arc-continent collision and crustal thickening (Johnson et al. 1978; Johnson & Jaques 1980), or alternatively, it may be due to crustal delamination and adiabatic compression of the mantle following arc-continent collision (Cloos et al., 2005).

There are two leading but contrasting theories regarding the tectonic setting for emplacement of the Maramuni arc and associated subduction geometry during this period. Much of the difficulty in establishing the subduction orientation arises from the absence of a seismically active subducted slab in the mantle (Hall and Spakman, 2002) making this one of the most intensely debated questions concerning New Guinea tectonics. The generally accepted view invokes south-dipping subduction at the Trobriand trough to the north of New Guinea (e.g. Hamilton, 1979; Ripper, 1982; Davies et al., 1984; Davies et al., 1987; Lock et al., 1987; Davies, 2012). This idea was founded on the premise of a "trench-like feature" that is spatially associated with Late Cenozoic magmatism of the Maramuni arc (Johnson et al., 1978; Hamilton, 1979). Although little subsequent work has tested this hypothesis of subduction at the Trobriand trench, the idea has become entrenched in the recent literature (e.g. Hall, 2002; Cloos et al., 2005; Schellart et al., 2006; Davies, 2012; Smith, 2013). Initiation of subduction at the Trobriand trough in the Lower Miocene is commonly attributed as a response to collision of the Ontong Java Plateau with the Melanesian arc (Hall, 2002; Hill and Hall, 2003; Schellart et al., 2006). Furthermore, arc-continent collision at the Trobriand trough is often attributed to the development of the New Guinea Orogen from approximately 12 Ma (Davies, 1990; Abbott et al., 1994; Hill and Raza, 1999).

The alternate theory appeals to a north-dipping subduction system located to the south of New Guinea, which accommodates Miocene convergence between the Australian and Pacific plates and is responsible for development of the Maramuni arc (Cloos et al., 2005). Initiation of this subduction system is also generally attributed to jamming of the Melanesian trench by arrival of the Ontong Java Plateau in the Upper Oligocene coupled with reorganization of regional convergence. Cloos et al. (2005) is one of few studies to propose northwards subduction to the south of West Papua but at the same time retains reference to southwards subduction at the Trobriand trough in Papua New Guinea creating inconsistencies between the tectonic evolution of West Papua and Papua New Guinea. This northwards subduction associated with West Papua is said to be subsequently responsible for convergence between the leading northern Australian continental margin and an outer arc terrane. Cloos et al. (2005) also propose that arrival and collision of the Australian continent with the outboard terrane is responsible for growth of the New Guinea Orogen from 12 Ma. It is important to also note that the proposed north-dipping subduction zone has also been utilized by other authors as a zone of earlier Cenozoic convergence between the Australian continent and an outboard terrane (e.g. Pigram and Symonds, 1991; Schellart et al., 2006; Davies, 2012).

The variable definitions of different tectonic domains in New Guinea are also a cause of confusion in establishing a robust geodynamic framework for the region. In particular, previous studies of Papua New Guinea have often interchanged terms givens to specific tectonic domains depending on the rock types or ages involved. For example, Paleozoic and Mesozoic Australian continental basement is generally referred to as comprising the New Guinea Mobile Belt (e.g. Hill and Raza, 1999; Crowhurst et al., 2004). However, rocks of this age are exposed as basement in both the New Guinea Mobile Belt and the Papuan Fold and Thrust Belt. For accurate communication of the different terranes and tectonic setting I will clearly define the distinct tectonic terranes of New Guinea based on their role in the tectonic evolution. I recognize the Lagaip and Bundi fault zones as equivalent but displaced crustal suture zones (Figure 4-1; Chapter 5). I define rocks to the south of the Lagaip-Bundi suture as belonging to the Papuan Fold And Thrust Belt with corresponding Australian continental basement. I regard these as distinct from Paleozoic and Mesozoic rocks to the north of the suture that comprise the New Guinea Mobile Belt. These tectonic divisions will be further developed in this study.

Samples

Rock samples were obtained in conjunction with Barrick Australia from the Wamum and Kokofimpa, Kainantu porphyry prospects in the eastern Papua New Guinea Highlands with the objective of investigating the evolution of the respective porphyry complexes, and associated history of the Maramuni arc. Rock material was sampled from diamond core of drill holes BWDD4 (Wamum) and BKDD22 (Kokofimpa). Drill core sample intervals were selected to include a representative sample of each logged rock unit. These sampling intervals were further scrutinized to minimize abundance of veining and effects of alteration in an effort to reflect compositions most similar to the unaltered rock. One additional field sample was collected from outcrop in Kora Creek, adjacent to the Kokofimpa prospect. Table 4-1 provides the location and description of the rock types sampled.

I divide the sample set into three broad categories: samples from the Wamum porphyry prospect; and samples from the Kokofimpa porphyry prospect are separated into either tonalites or porphyritic rock types. The Wamum porphyry prospect comprises two samples, BWDD4 482 and BWDD4 585, both are foliated plagioclase porphyry of andesite composition with extensive growth zonation within preferentially aligned plagioclase phenocryts that make up approximately 50% of the rock mass, set within a primarily quartz and biotite matrix. Tonalites of the Kokofimpa porphyry prospect (BKDD22 468, 472, 475, 511, 560, and 658) are generally uniform in character;

they exhibit a phaneritic texture of medium–coarse grains of quartz, plagioclase, biotite and spinel (predominantly magnetite). In contrast, porphyritic rock types of the Kokofimpa porphyry prospect are diverse in nature with three general varieties. BKDD22 299 is a plagioclase porphyry comprising 20–30% phenocrysts with a medium-grained quartz matrix and accessory spinel phases. Secondly BKDD22 546 is a plagioclase-quartz-biotite porphyry (20–30% phenocrysts) with comparatively larger plagioclase phenocryts and an associated matrix of quartz, plagioclase and spinel. BKDD22 582 and KKS01 are similar in nature to the BKDD22 546 porphyry but differ in that plagioclase and biotite make up make up an increased proportion of the matrix, and more strikingly, the plagioclase phenocrysts are characteristically highly fractured. This latter porphyry is interpreted to form part of the Elandora Batholith, a regionally significant intrusive unit within the Kainantu region. All porphyry rock types of the Kokofimpa porphyry prospect are of intermediate chemical composition.

Overprinting alteration is common in most samples from the Kokofimpa prospect with a greater apparent intensity of alteration within tonalite sample suites. Samples from the Wamum

Table 4-1. Sample descriptions

Sample	Location (a) (b)	Texture	Phenocrysts (c)	Matrix (c)	Alteration (c) (d)	Notes
Kokofimpa, Kainantu						
Tonalite						
BKDD22 468	DDH 468.2–469.5 m	Phaneritic Med–Coarse		Qz Pl Bt Spl	V. Int Ser Chl	Almost porphyritic Pl.
BKDD22 472	DDH 472.7–473.9 m	Phaneritic Med–Coarse		Qz Pl Bt Spl	V. Int Ser Chl	Almost porphyritic Pl.
BKDD22 475	DDH 475.6–476.4 m	Phaneritic Med–Coarse		Qz Pl Bt Spl	Int Ser Chl	Almost porphyritic Pl.
BKDD22 511	DDH 511–512 m	Phaneritic Coarse–Med		Qz Pl Bt Spl	V. Int Ser Chl	
BKDD22 560	DDH 560.5–562.5 m	Phaneritic Coarse–Med		Qz Pl Bt Spl	V. Int Ser Chl	
BKDD22 658	DDH 658–659.5 m	Phaneritic Med–Coarse		Qz Pl Bt Spl	Int Ser Chl	Almost porphyritic Pl.
Porphyries						
BKDD22 299	DDH 299–301 m	Porphyritic	Pl	Qz Spl	V. Int Ser	Medium-grained Qz matrix. 20–30% phenocrysts.
BKDD22 546	DDH 546.5–548.8 m	Porphyritic	Pl Qz Bt	Qz Pl Spl	Int Ser Chl	Large Pl Phenocrysts. 20–30% phenocrysts.
BKDD22 582	DDH 582–584 m	Porphyritic	Pl Qz Bt	Pl Qz Bt	Mod Ser Chl	Highly fractured Pl phenocrysts. 20–30% phenocrysts.
KKS01 (Kora Creek)	373139 E 9317942 N	Porphyritic	Pl Qz Bt	Pl Qz Bt	Mod-Int Ser Chl	Highly fractured Pl phenocrysts. 20–30% phenocrysts.
Wamum						
BWDD4 482	DDH 482.5–485 m	Foliated Porphyritic	Pl	Qz Bt	Fresh	Strong growth zoning in Pl phenocrysts. 50–60% phenocrysts.
BWDD4 585	DDH 585–588 m	Foliated Porphyritic	Pl	Qz Bt	Weak Ser Chl	Strong growth zoning in Pl phenocrysts.30–40% phenocrysts.

a) Diamind drill hole (DDH) Collar location (UTM AGD66 Zone 55) and orientations:
BKDD22: 372931E 9317014N; azimuth (mag): 300°, inclination: -50°
BWDD4: 420856E 9254093N; azimuth (mag): 330.6°, inclination: -63.2°
b) Field cordinates in UTM AGD66 Zone 55.
c) Mineral codes :Bt, biotite; Chl, chlorite; Pl, plagioclase; Qz, quartz; Ser, sericite.
d) Alteration codes; alteration intensity; V Int, very intense; Int, intense; Mod, moderate.

prospect are affected by only weak alteration. Seritization is the dominant alteration type evident in all samples, and is often coupled with chloritization. Plagioclase is commonly completely replaced by sericite with subsidiary samples exhibiting only partial alteration of plagioclase dominantly through crystal fractures. This is typical of sericitic or chlorite-sericite alteration in porphyry complexes (Sillitoe, 2010). Given the Kokofimpa and Wamum porphyry prospects have previously been identified as a Cu-Au mineralized porphyries it is worthwhile to note the metal content of the different intrusive phases, although this will not form a major component of this study. Figure 4-3 displays assay data for Cu and Au content of all intrusive rock types of the Kokofimpa Porphyry Prospect, Kaiantu (Barrick Australia, unpub. data). Copper content generally shows a good correlation with both Au and Mo content. Early tonalite intrusives (9.4 Ma) are shown to contain only low levels of mineralization while the 9.2 Ma porphyry and later 8.7 Ma tonalites generally exhibit the highest metal grades, these are therefore considered as the primary lithology for hosting mineralization. This is consistent with observed mineralogy where sulfide mineralization is found primarily as disseminated pyrite ± chalcopyrite in late tonalite samples BKDD22 511, 560 and 658. The early tonalite and late porphyry phases are essentially barren and devoid of metal content (Figure 4-3). Samples from the Wamum Porphyry Prospect are un-mineralized.

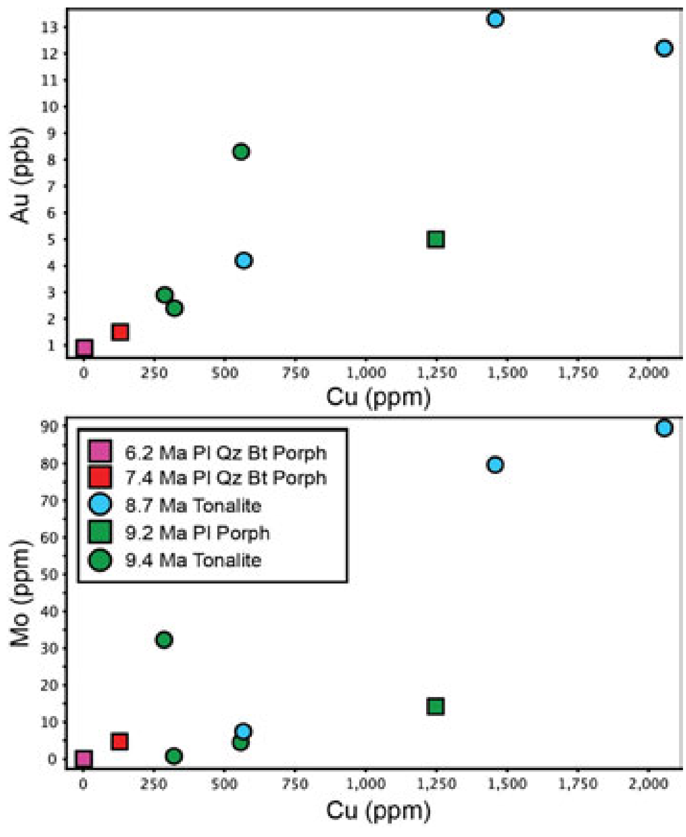

Figure 4-3. Cu-Au-Mo content for samples of the Kokofimpa porphyry prospect.

Methods

Samples for geochemical analysis were selected to minimize effects of alteration. Weathering rinds were split from surface samples and edges from drill core samples were ground off with diamond implanted grinders and subsequently washed in an ultrasonic bath to minimize contamination from drilling. Rock material was then milled to a fine powder in a tungsten carbide ring mill at James Cook University (JCU). Major and trace elements analyses were analyzed at the Advanced Analytical Centre, JCU by conventional X-ray fluorescence (XRF) and ICP-MS methods using the same techniques and set-up outlined in Holm et al. (2013; Chapter 3). NIST SRM 610 glass was used as a bracketed external standard using the standard reference values of Spandler et al. (2011). Data were quantified using Si (as previously determined by XRF) as the internal standard, and data were processed off-line using the Glitter software (Van Achterbergh et al., 2001).

Nine samples were selected for U-Pb dating of zircons. These include two samples from Wamum and seven samples from Kokofimpa; all derived from drill core with the exception of a single field sample. Mineral separation to extract zircon crystals was carried out at JCU in a standard four-step process. Samples were crushed and milled to 500 µm, washed to remove the clay proportion, and separated by a combination of heavy liquid density separation and magnetic separation. Zircon crystals were hand picked and mounted in epoxy with grains of GJ1 (Jackson et al., 2004), Temora 2 (Black et al., 2004) and Fish Canyon Tuff zircon standards (Schmitz and Bowring, 2001; Renne et al., 2010). Epoxy mounts were polished and carbon-coated. Cathodoluminescence (CL) images of all zircon crystals were obtained using a Jeol JSM5410LV scanning electron microscope equipped with a Robinson CL detector, housed at JCU.

All U-Pb dating work was completed at the Advanced Analytical Centre, JCU. U-Pb dating of zircons was conducted using the laser ablation ICP-MS using the set-up described in Tucker et al. (2013) and using the same methods as Holm et al. (2013; Chapter 3). Analytes collected were ^{29}Si, ^{90}Zr, ^{202}Hg, ^{204}Pb, ^{206}Pb, ^{207}Pb, ^{208}Pb, ^{232}Th, ^{235}U, and ^{238}U. For quantification of U and Th concentration in zircon samples, analysis of the NIST SRM 612 reference glass was conducted at the beginning, middle and end of every analytical session, with ^{29}Si used as the internal standard assuming perfect zircon stoichiometry. All zircons were analyzed with a beam spot diameter of 44 µm and selection of analytical sample spots was guided by CL images and targeted both cores and rims.

Data reduction was carried out using the Glitter software (Van Achterbergh et al., 2001). All time-resolved single isotope signals from standards and samples were filtered for signal spikes or perturbations related to inclusions and fractures. Subsequently, the most stable and representative isotopic ratios were selected taking into account possible mixing of different age domains and zoning. Drift in instrumental measurements was corrected following analysis of drift trends in the raw data using measured values for the GJ1 primary zircon standard. Analyses of Temora 2 and Fish Canyon Tuff zircons were used for verification of GJ1 following drift correction (Figure 4-4). Background corrected analytical count rates, calculated isotopic ratios and 1σ uncertainties were exported for further processing and data reduction.

Initial Th/U disequilibrium during zircon crystallization is related to the exclusion of ^{230}Th due to isotope fractionation, and resulting in a deficit of measured ^{206}Pb as a ^{230}Th decay product (Schärer, 1984; Parrish, 1990). Zircon ages of <10 m.y. are particularly susceptible to this disequilibrium with an upward age correction in the order of 100 k.y. (Crowley et al., 2007), which is comparable or greater than the measured analytical uncertainty. All samples returned ages within the limit of initial Th/U disequilibrium detection, so this correction was applied to all samples for maximum U-Pb dating accuracy following the methods outlined in Holm et al. (2013; Chapters 2 and 3). The effect of common Pb is taken into account by the use of Tera-Wasserburg Concordia plots (Tera and Wasserburg, 1972; Jackson et al., 2004) and weighted mean ^{206}Pb/^{238}U age calculations

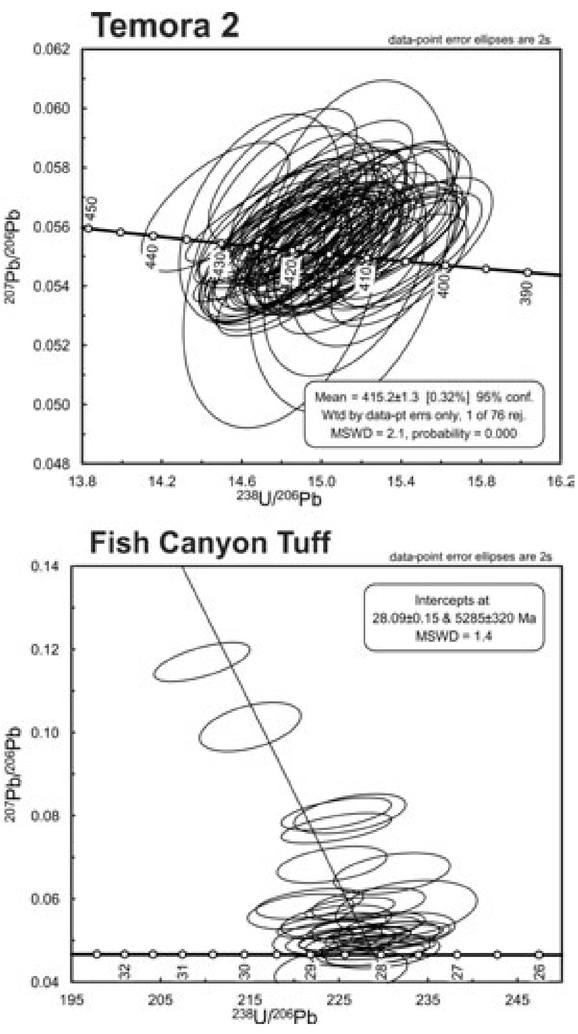

Figure 4-4. Concordia plots and weighted average (Temora 2) for U-Pb zircon geochronology standards. All data-point error ellipses and calculated errors are 2σ, and 95% confidence for associated weighted average.

were carried out using Isoplot/Ex version 4.15 (Ludwig, 2009). Weighted averages were corrected for common Pb by utilizing the Age7Corr and AgeEr7Corr algorithms in Isoplot, and using the y-intercept and corresponding sigma errors returned from the Tera-Wasserburg plots of concordant zircon populations. All errors were propagated at 2σ level and reported at 2σ and 95% confidence for concordia and weighted averages, respectively.

Results

Textures and U-Pb Geochronology of Zircon

Zircon crystals extracted from Kokofimpa tonalite samples (BKDD22 472, 511 and 560), are generally 100–200 μm long euhedral stubby to prismatic crystals that are typically characterized by bright oscillatory CL zoning with a uniform dark CL core (Figure 4-5). The porphyry samples are more variable in zircon characteristics. Zircon crystals from sample BKDD22 299 are marked by high contrast oscillatory CL zoning and either CL dark or CL light cores. Many of the crystals are euhedral and stubby to prismatic in shape, however, a substantial proportion of crystals are fragmental or broken. Sample BKDD22 546 zircon crystals are euhedral and prismatic in shape on the order of 100–150 μm in length. They generally exhibit highly luminescent crystal cores and a high contrast in CL zoning of the rim. Samples BKDD22 582 and KKS01 exhibit similar morphology of zircon crystals. The crystal populations have extremely variable crystal sizes from 100 to 1000 μm in length. Oscillatory zoning with CL bright uniform cores is typical of both zircon populations, with few crystals exhibit complex CL zoning. Crystals are typically euhedral

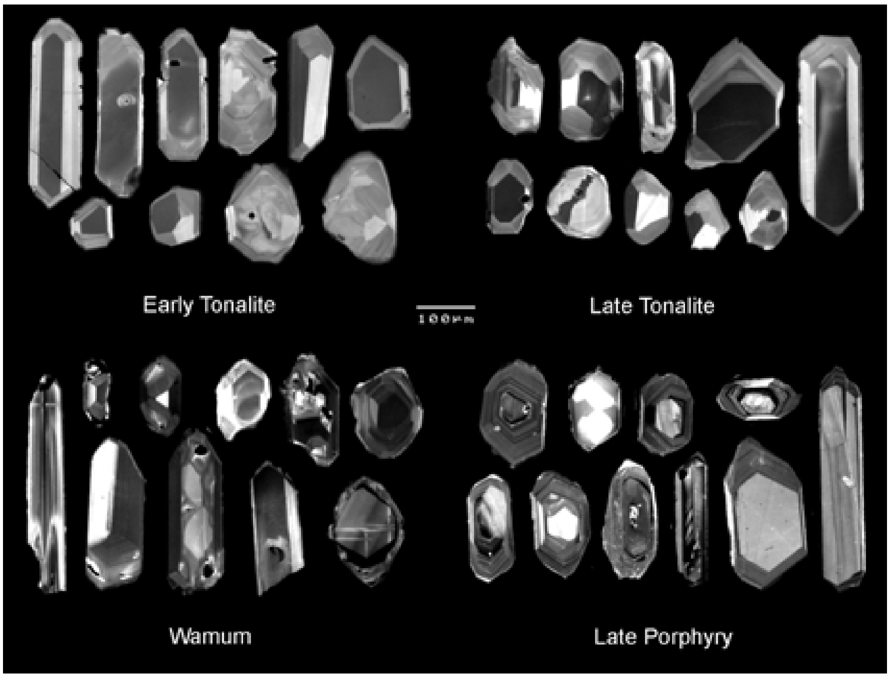

Figure 4-5. Representative cathodoluminescence images for zircon crystals of different intrusive phases of Wamum and Kokofimpa.

and prismatic with aspect ratios generally around 1:2.5. All zircon samples typically feature euhedral crystal shapes and oscillatory zoning in CL is consistent with a magmatic origin (Corfu et al., 2003; Hoskin and Schaltegger, 2003). A magmatic origin for these zircon is also supported by low Th/U , with all sample sets averaging between 0.65 and 0.98, and an overall average of 0.81± 0.27 (e.g. Ahrens et al., 1967; Heaman et al., 1990).

Zircon yields from both of the Wamum samples (BWDD4 482 and 585) were low compared with the Kokofimpa samples. The Wamum zircon crystals did not exhibit a uniform set of CL imaging characteristics, but instead are marked by complex zoning patterns with only minor oscillatory zoning (Figure 4-5). The crystals vary from stubby to elongate in shape, typically between 100 and 200 µm in length, although some larger crystals are present, and many are broken or fractured. Where cores are present they have either uniform and dark CL intensity or exhibit simple, high CL contrast zoning. Some zircon crystals preserve evidence for minor dissolution with irregular crystal boundaries. All zircon crystals sampled hold CL textures consistent with a magmatic origin comprising euhedral crystal shapes and oscillatory zoning (Corfu et al., 2003; Hoskin and Schaltegger, 2003), and a low Th/U ratio averaging 0.80 ±0.30 (e.g. Ahrens et al., 1967; Heaman et al., 1990).

U-Pb zircon ages corrected for common Pb and initial Th disequilibrium for selected tonalite and porphyry phases from both Wamum and Kokofimpa, Kainantu are reported in Table 4-2 and corresponding concordia and weighted average plots are shown in Figure 4-6. Weighted averages agree with concordia age results with a high degree of certainty, but given more conservative 2σ uncertainty measurements, the concordia ages are cited as the resolved ages. Returned ages are all constrained within the Middle–Upper Miocene (12–6 Ma), details of age dating are reported by rock type. Complete zircon isotopic data can be found in the supplementary material.

Table 4-2. Resolved ages from U-Pb dating of zircon.

Sample	Weighted Average (a)	95% Confidence	MSWD	Probability of Fit	Concordia Age (b)	2σ Error	MSWD	Probability of Fit
Kokofimpa, Kainantu								
Tonalite								
BKDD22 472	9.41	0.10	0.70	0.81	9.41	0.17	0.69	0.80
BKDD22 560	8.78	0.12	0.54	0.90	8.79	0.24	0.59	0.85
BKDD22 511	8.70	0.10	0.90	0.59	8.70	0.19	0.87	0.63
Porphyry								
BKDD22 299	9.19	0.10	0.68	0.81	9.20	0.18	0.87	0.59
BKDD22 546	7.38	0.09	0.68	0.76	7.38	0.18	0.82	0.61
BKDD22 582	6.28	0.05	0.61	0.79	6.28	0.10	0.93	0.49
KKS01	6.24	0.07	0.69	0.66	6.24	0.11	0.82	0.53
Wamum								
BWDD04 482	11.87	0.09	0.81	0.69	11.88	0.13	0.85	0.63
BWDD04 585	12.07	0.10	0.84	0.64	12.08	0.13	0.82	0.66

a) Weighted average age corrected for initial Th disequilibrium and common-Pb.
b) Concordia age corrected for initial Th disequilibrium.

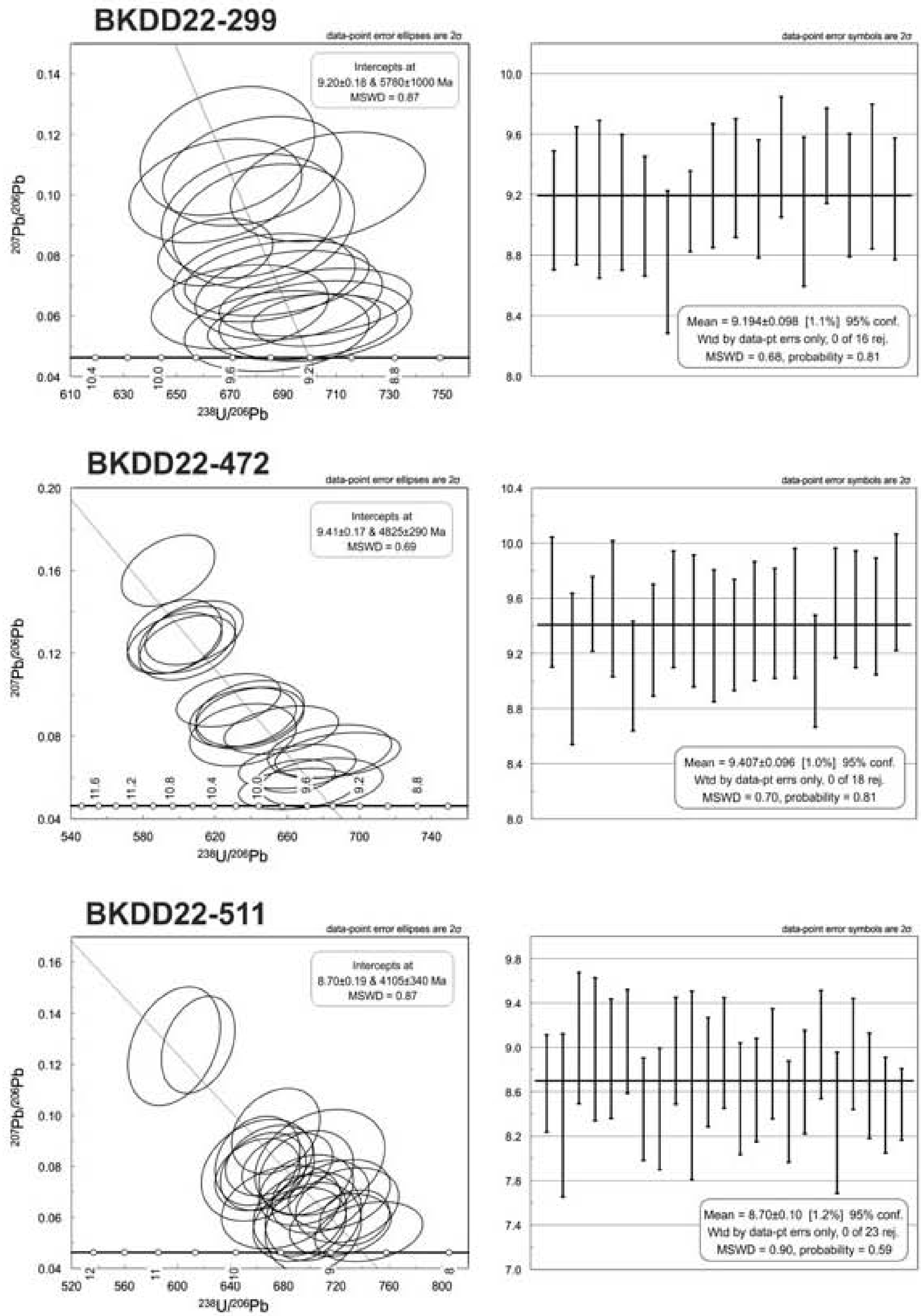

Figure 4-6. Weighted average and concordia plots for all samples. Plots are constructed from U-Pb calculated ages and isotopic compositions respectively (detailed age data in digital appendices). Tera-Wasserburg plots are corrected for initial Th disequilibrium; weighted average plots are corrected for initial Th disequilibrium and common Pb. All error bars, data-point error ellipses and calculated errors are 2σ and 95% confidence for concordia and weighted averages respectively.

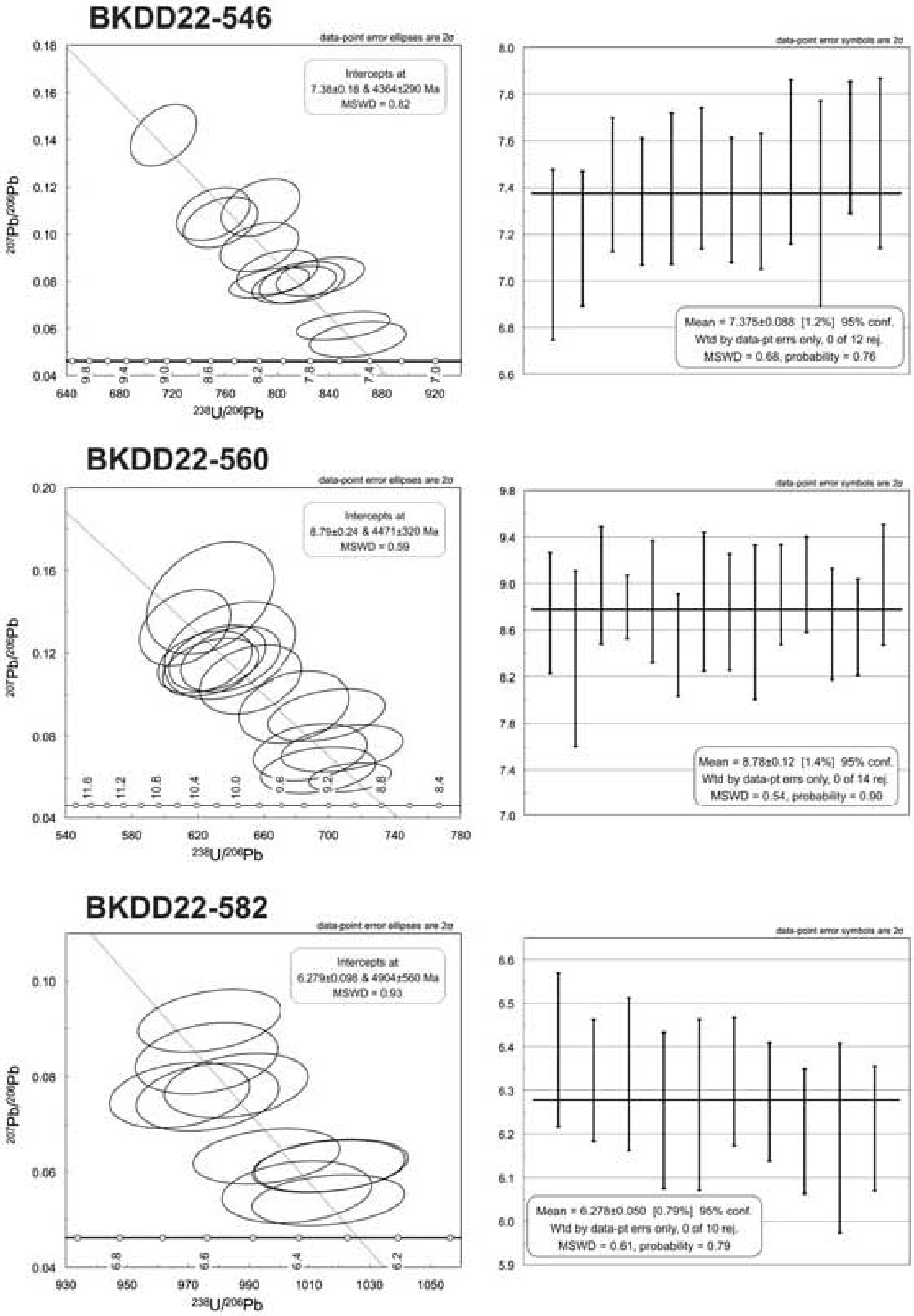

Figure 4-6 continued.

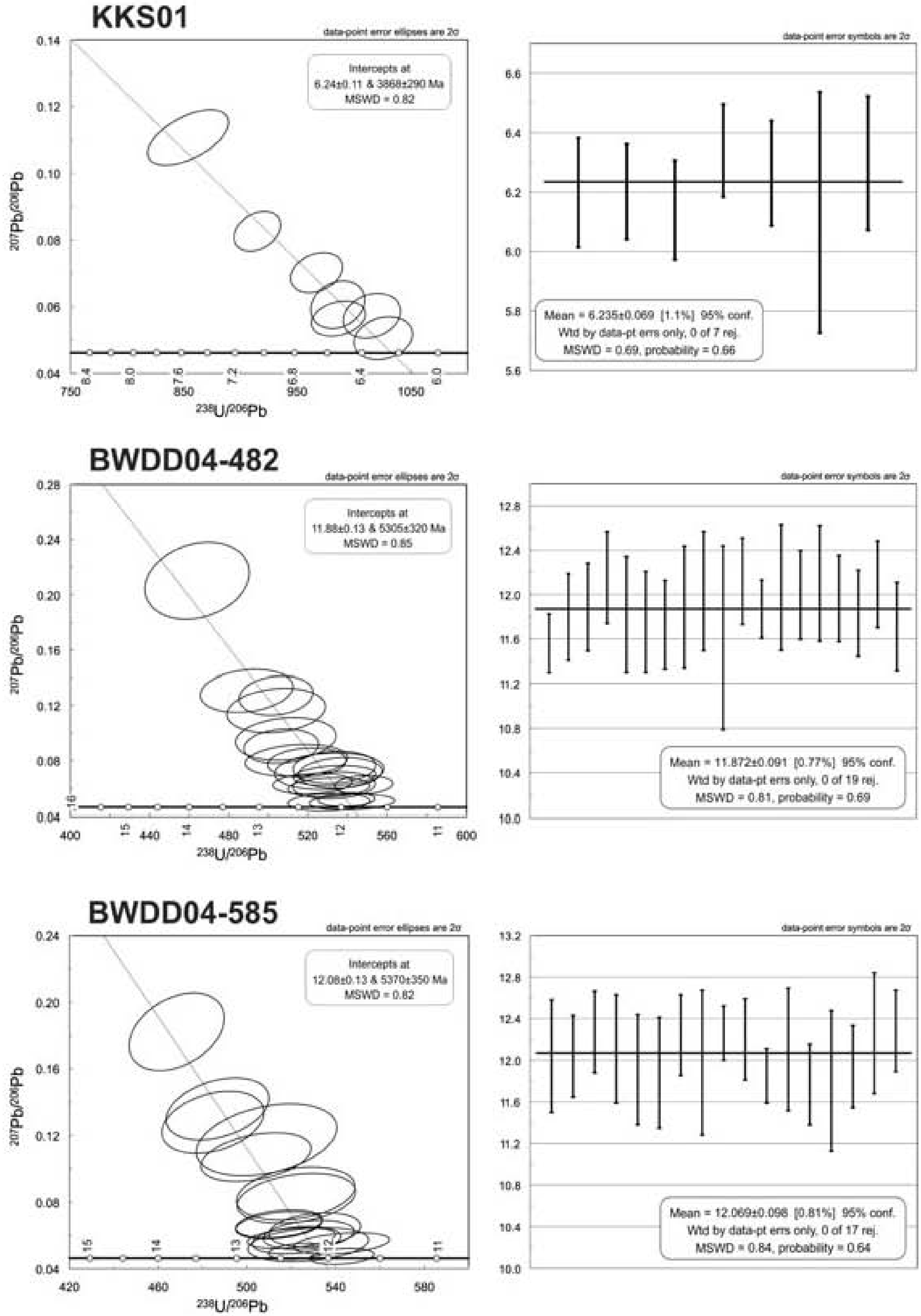

Figure 4-6 continued.

Foliated plagioclase porphyries of the Wamum porphyry prospect, BWDD4 482 and BWDD4 585 returned the oldest ages found in this study at 11.88 ± 0.13 Ma and 12.08 ± 0.13 Ma respectively. These two ages are within uncertainty of each other and, given the similar rock types, are interpreted to represent a single intrusive phase.

Rocks types of the Kokofimpa porphyry prospect yielded a greater spread in ages between 9.4 and 6.2 Ma. Of these ages, the dated tonalites were generally the older phases of the intrusive complex at 9.41 ± 0.17 Ma (BKDD22 472) and two similar ages of 8.79 ± 0.24 Ma and 8.70 ± 0.19 Ma for BKDD22 560 and BKDD22 511 respectively. The latter ages are within uncertainty of each other, and are suggested to record the same intrusive phase. Porphyritic rock types from Kokofimpa comprise the largest range of ages; there are three clearly resolvable intrusive phases. The first and oldest is BKDD22 299 at 9.20 ± 0.18 Ma overlapping with the earlier tonalite ages. Sample BKDD22 546 returned an age of 7.38 ± 0.18 Ma, while BKDD22 582 and KKS01 yielded essentially a single intrusive age with 6.28 ± 0.10 Ma and 6.24 ± 0.11 Ma respectively.

Geochemistry

Alteration has significantly affected the whole rock geochemistry with noteworthy loss on ignition (LOI) percentages of up to and over 5% in over many of the samples (Table 4-3; Figure 4-7). For the most part the alteration does not display clear trends of addition or removal of particular elements. There are however, minor trends consistent with typical alteration associated with porphyry systems, such as is removal of mobile elements such as Sr and Ba, and addition of K_2O. Major and trace element composition of all analysed samples are given in Table 4-3. Harker variation diagrams have been used to show major element trends for all rock types from both Wamum and Kokofimpa (Figure 4-8). SiO_2 generally increases from Wamum, which yielding the most primitive sample at 59 wt% SiO_2 through to ~70 wt% SiO_2 from porphyritic intrusives of the Kokofimpa Prospect. Sample BKDD22 299 is apparent as an outlier from this trend with the highest SiO2 content found in this study of 70 wt% occurring within the tonalitic intrusive sequence from the Kokofimpa prospect. Other major elements similarly follow fractionation trends with time, TiO_2, Al_2O_3, Fe_2O_3, MnO, MgO, CaO, and Na_2O, that is all major elements with the exception of K_2O, show poorly defined but linear decreases with increasing SiO_2. K_2O increases linearly with increasing SiO_2 and holds a somewhat well defined trend in contrast to the other major elements. Wamum rock types exhibit a reduced TiO_2 and MgO content relative to samples from Kokofimpa outside the observed fractionation trend.

Trace element data is presented by way of a multi-element plot normalized to N-MORB (Sun and McDonough, 1989) in Figure 4-9. Further, incompatible element abundances and ratios thereof are presented in Figures 4- 10 respectively. All samples from both the Wamum and Kokofimpa

Table 4-3. Representative major and trace element data.

	Kokofimpa, Kainantu										Wamum	
	Tonalite						Porphyry					
Sample	BKDD22 468	BKDD22 472	BKDD22 475	BKDD22 511	BKDD22 560	BKDD22 658	BKDD22 299	BKDD22 546	BKDD22 582	KKS01	BWDD04 482	BWDD04 585
SiO_2	62.29	62.38	62.06	64.34	63.17	64.61	70.45	63.72	66.37	69.35	58.98	60.69
TiO_2	0.64	0.63	0.64	0.64	0.69	0.63	0.39	0.53	0.33	0.38	0.54	0.54
Al_2O_3	16.02	15.93	16.06	16.08	16.70	15.42	15.18	16.79	15.65	16.57	18.06	17.87
Fe_2O_3*	5.56	5.93	5.63	3.26	5.35	4.99	4.24	3.58	1.87	2.22	6.32	5.24
MnO	0.05	0.09	0.12	0.05	0.07	0.03	0.01	0.07	0.06	0.04	0.15	0.04
MgO	2.48	2.48	3.51	2.46	2.80	2.32	0.41	2.76	1.04	1.17	2.46	2.21
CaO	2.70	3.66	2.35	2.31	1.64	3.38	0.07	1.89	3.43	0.37	5.15	4.44
Na_2O	1.89	3.32	1.79	1.62	2.03	3.15	0.45	1.79	2.94	1.97	3.64	4.13
K_2O	3.09	1.17	2.18	3.10	2.80	2.31	3.91	3.30	2.83	4.77	1.25	2.09
P_2O_5	0.18	0.17	0.17	0.13	0.18	0.17	0.04	0.20	0.11	0.15	0.22	0.16
SO_3	0.12	0.06	0.14	0.13	0.07	0.01	0.05	0.31	0.05	0.01	0.04	0.06
LOI	5.01	4.18	5.20	5.21	4.60	2.67	4.42	5.18	5.32	3.01	3.38	2.07
Total	100.03	100.00	99.85	99.31	100.10	99.69	99.63	100.13	100.00	100.00	100.19	99.55
Sc	13	13	13	13	14	13	8.6	7.9	5.1	6.0	11	9.8
V	108	111	110	113	120	113	63	78	36	40	135	144
Cr	26	28	25	25	25	21	25	31	25	6.0	10	4.0
Co	32	35	33	28	23	60	48	23	15	13	35	41
Cu	79	32	959	2473	345	381	127	292	7	26	166	1839
Zn	51	65	122	31	48	40	8	68	43	103	119	35
Ga	15	17	17	14	17	16	16	16	16	17	18	17
As	1.9	0.7	3.0	0.8	0.8	1.2	1.8	3.5	1.6	2.1	4.5	1.1
Rb	121	40	93	99	86	70	99	127	70	157	29	40
Sr	182	408	230	164	157	455	26	178	587	262	699	714
Y	21	19	19	19	20	21	9.5	9.0	6.6	9.0	11	13
Zr	194	184	186	191	208	194	145	116	108	116	103	122
Nb	7.2	7.2	7.3	8.0	7.5	7.2	7.1	4.7	4.1	5.4	5.2	5.3
Mo	1.6	1.5	42	640	6.0	22	13	2.0	7.5	0.7	9.0	5.5
Cd	0.4	0.5	0.6	0.4	0.6	0.4	0.6	0.4	0.4	0.3	0.5	0.7
Sn	3.2	3.0	2.7	5.1	3.3	3.5	6.9	3.1	2.0	2.1	2.0	1.8
Sb	1.7	0.9	1.6	0.8	0.9	1.0	1.0	1.0	0.8	1.2	0.9	0.8
Cs	3.0	1.9	3.3	3.7	2.9	1.3	1.1	4.3	3.5	12	1.1	0.7
Ba	330	262	323	431	368	400	187	417	563	633	479	770
La	23	17	20	22	24	21	17	17	15	16	11	10
Ce	49	38	44	46	50	45	33	34	31	33	16	20
Pr	5.9	4.6	5.2	5.5	6.0	5.4	3.5	4.2	3.5	4.1	2.0	2.5
Nd	23	19	20	21	24	21	13	16	14	16	8.5	10
Sm	4.4	3.8	4.1	3.9	4.6	4.3	2.2	2.9	2.3	2.9	1.8	2.3
Eu	0.8	1.1	0.9	1.1	1.2	1.1	0.5	0.8	0.7	0.7	0.7	0.8
Gd	3.6	3.4	3.3	3.3	3.9	3.5	1.6	2.0	1.5	2.0	1.8	2.2
Tb	0.6	0.5	0.5	0.5	0.6	0.5	0.3	0.3	0.2	0.3	0.3	0.3
Dy	3.6	3.3	3.1	3.2	3.5	3.6	1.6	1.6	1.2	1.5	1.8	2.1
Ho	0.7	0.7	0.7	0.7	0.7	0.7	0.4	0.3	0.2	0.3	0.4	0.5
Er	2.1	2.0	1.9	1.9	2.1	2.0	1.0	0.9	0.6	0.8	1.1	1.3
Tm	0.3	0.3	0.3	0.2	0.3	0.3	0.2	0.1	0.1	0.1	0.2	0.2
Yb	2.3	2.3	2.2	2.0	2.1	2.3	1.3	0.9	0.7	0.8	1.2	1.3
Lu	0.3	0.3	0.3	0.3	0.3	0.4	0.2	0.2	0.1	0.1	0.2	0.2
Hf	5.0	4.9	4.8	5.0	5.5	5.3	3.9	3.1	3.0	3.3	2.8	3.2
Tl	0.5	0.2	0.6	0.5	0.4	0.2	0.5	0.5	0.4	1.4	0.0	0.1
Pb	4.9	12	27	15	6.4	11	10	31	15	8.8	4.0	4.6
Bi	0.4	0.1	0.4	0.2	0.0	0.5	1.2	0.5	0.1	0.1	0.1	0.1
Th	11	10	10	11	10	11	14	4.9	4.0	4.8	3.1	3.8
U	2.6	2.6	3.0	2.5	2.8	4.0	2.4	2.0	1.5	1.7	0.6	0.7

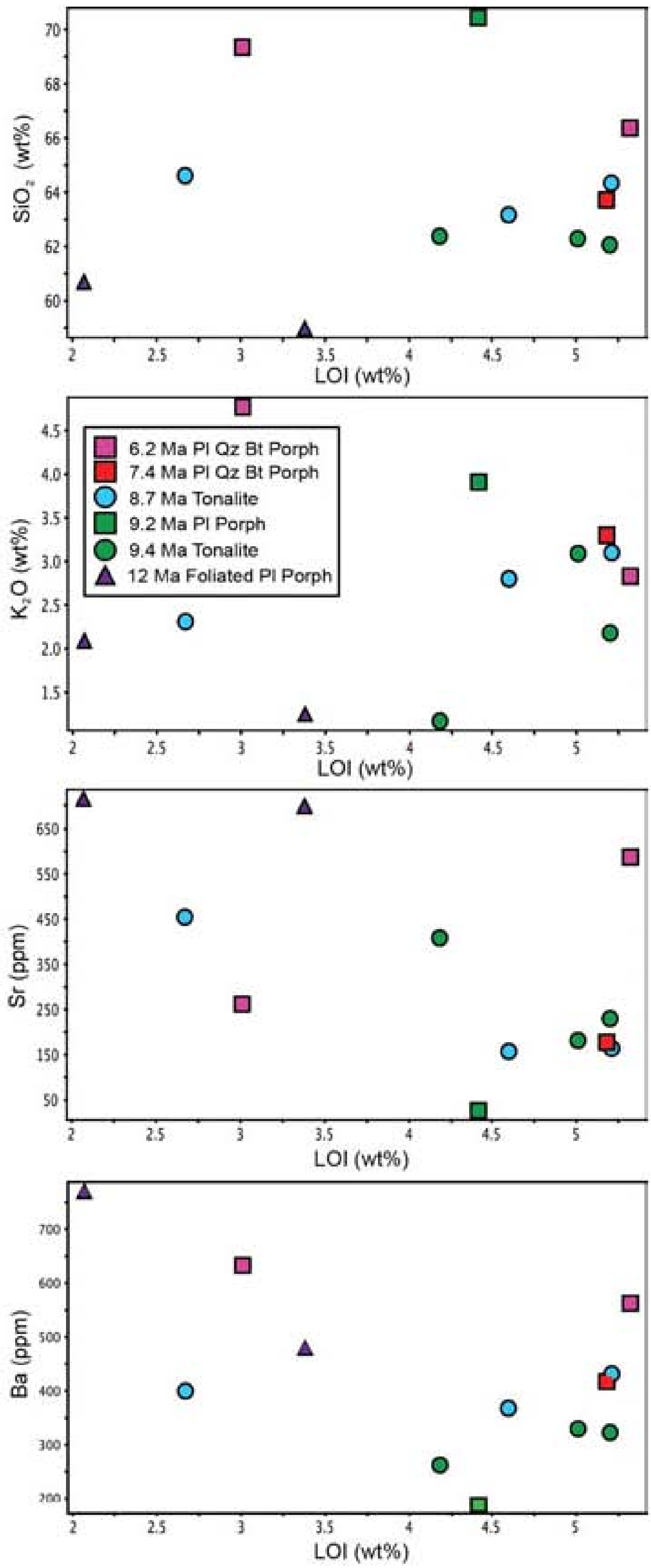

Figure 4-7. Major and trace element variation with alteration intensity (LOI) diagrams for all samples.

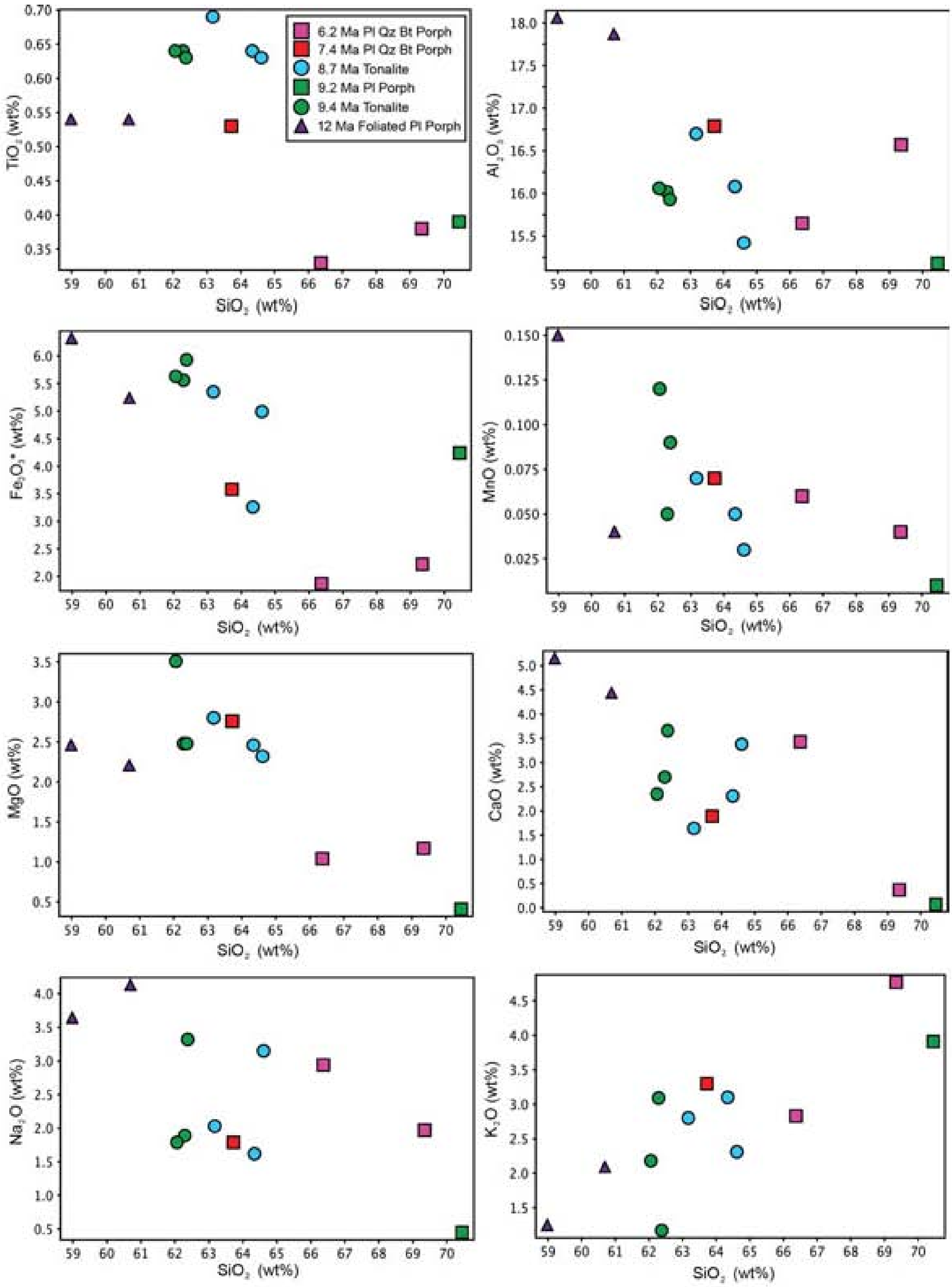

Figure 4-8. Major element variation diagrams for all samples.

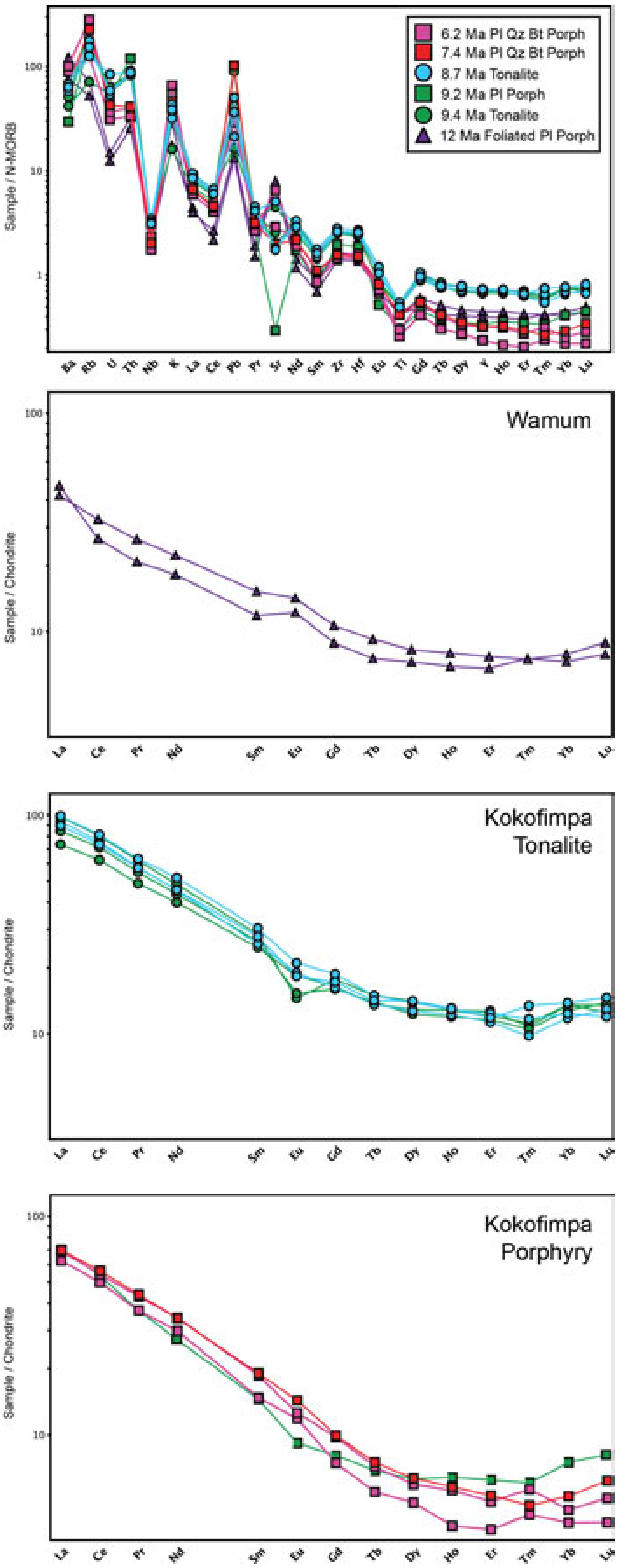

Figure 4-9. N-MORB normalized multi-element plot and C1 chondrite normalized REE plots for the Kokofimpa and Wamum porphyry prospects. N-MORB and C1 chondrite normalizations are from Sun and McDonough (1989).

porphyry prospects exhibit typical subduction-related geochemical affinities with negative Nb and Ti anomalies and relative enrichments in large-ion lithophile elements (LILE), Th, U, Pb and Sr, although the latter variably affected by alteration. Both the Wamum rock types and tonalites of Kokofimpa display what is regarded as typical rare earth element (REE) trends of high-K arc magmatism with well-developed LREE enrichment. The tonalites show a measurable higher level of REE enrichment relative to chondrite compared to Wamum samples. Two of three early tonalite phases of the Kokofimpa prospect hold minor negative Eu anomalies of Eu/Eu* = 0.63 and 0.72, both samples from Wamum hold minor positive anomalies at Eu/Eu* = 1.18 and 1.10, these are the only notable Eu anomalies within the data presented in this study. Rare earth element patterns of all porphyritic rock types of the Kokofimpa prospect hold LREE abundances consistent with the tonalite suite, but marked by a significant degree of MREE-HREE depletion.

Differences in the degree of fractionation can introduce potential problems in the comparison and interpretation of the sample suite. It is therefore constructive to also investigate incompatible elements and ratios thereof. The LILE (K, Rb, Cs, Ba) show a trend of increasing with both time and SiO_2 content (not shown), however, these are potentially mobile during alteration and further interpretation is speculative (Figure 4-7). For this reason, I will address the less fluid-mobile high field strength elements (HFSE; Ti, Zr, Hf, Nb, Th). These are variable in content and are marked by non-linear trends with regard to both time and SiO_2 content. Zirconium, Hf, Nb and Th all show pronounced enrichment within the tonalite suite relative to samples from both Wamum and the late porphyry suites of Kokofimpa, while Ti is similarly enriched in tonalites relative to the remainder of the samples, this enrichment is comparatively minor. Sample BKDD22 299 is again variable in composition and not consistent with either the contemporaneous tonalite suite or other porphyry samples.

Discussion

Geochemical evolution of the Wamum and Kokofimpa intrusive systems

This study seeks to contribute to the somewhat lacking quantitative database of Maramuni arc magmatism and use this new information to shed light on the tectonic evolution of Papua New Guinea during the dynamic Upper Miocene. I approach this through a geochronology and geochemical investigation of the Wamum and Kokofimpa intrusive systems in an effort to gain insight into the underlying geodynamic controls on arc magmatism. It is worth noting here that Wamum and Kokofimpa are different intrusive systems separated by some 100 km, potentially giving rise to differences in tectonic setting, it must therefore be appreciated that geochemical variation between the two localities may exist and will be considered. However, I also make the assumption that the Maramuni arc is a regional magmatic manifestation, and as such, major

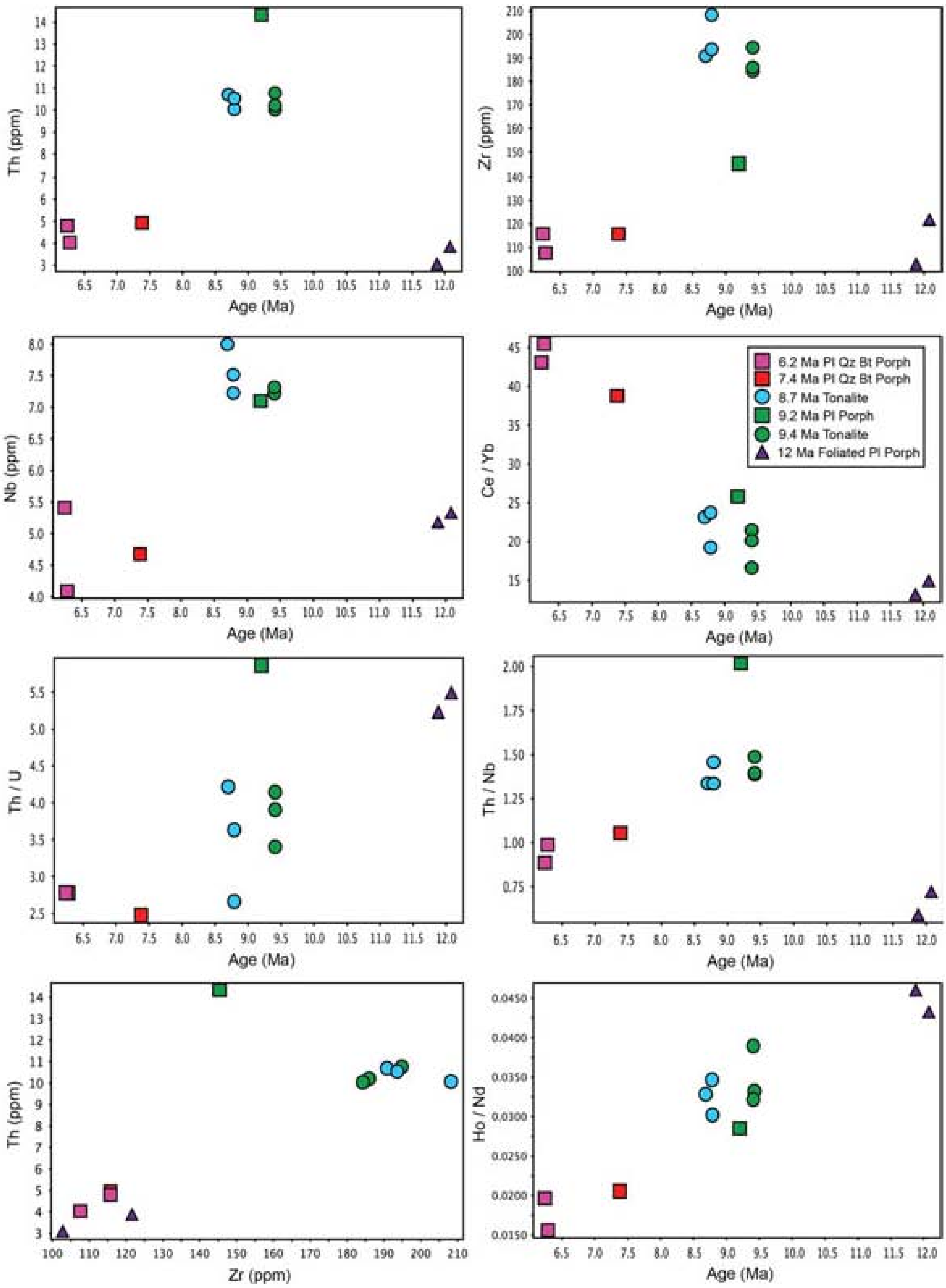

Figure 4-10. Selected incompatible element variation and ratios for all samples.

fundamental geochemical changes related to the regional tectonic setting will more or less be represented across the arc as a function of the changing nature and composition of the source, reflecting the mantle wedge, subducting plate, and the process of mass transfer between the two, but also taking into account subsequent fractionation or differentiation of the melts, and crustal assimilation during their ascent through the crust.

Firstly, I will briefly address the geochronology of the sample suite to provide a framework for further investigation. From the twelve samples utilized in this study, I recognize six different intrusive phases. The earliest intrusive event is recorded from Wamum at 12 Ma comprising the foliated plagioclase porphyry. The remainder of intrusive phases are from the Kokofimpa prospect of the Kainantu region. Early intrusive activity at Kokofimpa comprises tonalites, these are grouped into two main phases on the basis of geochronology, petrography and geochemistry, and consist of an early intrusive phase coincident with the timing of sample BKDD22 472 at 9.4 Ma and also incorporating samples BKDD22 468 and 475; and a later tonalite intrusion comprising samples BKDD22 511, 560 and 658 at 8.7 Ma. Sample BKDD22 299 is also included within the same tonalite intrusive phase with similar geochronology at 9.2 Ma but forms a highly altered plagioclase porphyry distinct from the other tonalite samples. Subsequently, two further episodes of porphyry emplacement occurred at 7.4 Ma and 6.2 Ma, both comprise plagioclase-quartz-biotite porphyries, and the latter is interpreted as part of the regionally important Elandora Porphyry intrusive on the basis of geochronology. Moreover, the U-Pb geochronology presented here spans the temporal variation of the highly dynamic Upper Miocene period in Papua New Guinea, and emplaced during growth of the New Guinea Orogen from initial orogenesis at 12 Ma up until renewal of orogenic activity at approximately 6 Ma.

Having established the temporal context for the sample suite I will now discuss the geochemistry of the Wamum and Kokofimpa intrusive systems. As a first pass observation it is evident that the porphyry intusives of Kokofimpa generally represent more evolved magma suites with higher silica contents, and major element trends consistent with typical magma fractionation and differentiation. However, samples from Wamum are often offset from these major element trends, associated with relative enrichments in Al_2O_3, CaO and Sr, and relatively low of TiO_2 and MgO. This shift in major element composition can most readily be explained by plagioclase accumulation, supported by positive Eu anomalies. This will also inherently result in minor SiO_2 depletions. Taking this into consideration, the major element compositions show no fundamental differences in the sample suite.

In an effort to gain insight into the evolution of Maramuni arc magmatism, I turn now to trace element variations. Here, I will focus on the less-mobile HFSE. It is clear from Figure 4-10 that there are distinct differences in the HFSE abundances within the sample suite that correspond to the different intrusive phases. For instance, significant enrichment of Th, Zr and Nb is observed in the tonalite suite relative to both Wamum and the late porphyry intrusives of Kokofimpa. Similar compositional domains can be observed in plots of Th/Nb and Th versus Zr (Figure 4-10). It is proposed that these compositional differences mark distinct geochemical domains associated with the different intrusive phases that cannot nominally be explained by fractionation or differentiation processes alone. Therefore this geochemical change likely represents some fundamental difference in the magma composition that in turn, reflects either changes in the sub-arc mantle composition or subduction dynamics, or alternately differences in the degree of crustal assimilation during ascent of the magma through the crust (e.g. Elliott et al., 1997; Rubatto and Hermann, 2003; Spandler and Pirard, 2013). Beyond this, we can only speculate on the roles of mantle source versus crustal assimilation for controlling this compositional change. Nonetheless, there is clearly value in the recognition that the variation in HFSE presented here is potentially linked to underlying tectonic controls.

The REE patterns likewise can tell us more about the magmatic processes beyond fractionation and alteration. From Figure 4-9 it is apparent that Wamum and the tonalites of Kokofimpa more or less hold the same trends of LREE enrichment and relatively flat MREE and HREE patterns, typical of high-K calc-alkaline magmatism. Given the similar trends, the different levels of REE - that is, elevated REE abundances in the tonalite suite relative to Wamum - are readily attributed to magma fractionation within the bounds of normal arc magmatism. The porphyry intrusives of Kokofimpa, however, hold REE trends quite different to those of Wamum and the Kokofimpa tonalites. Given the similar LREE abundances and patterns of the porphyry and tonalite suites, it is a reasonable first pass assumption that the two are potentially related, and further, the porphyries have undergone an additional fractionation process of a specific mineral phase to remove to MREE and HREE.

Previous work in the field of REE fractionation has associated diagnostic REE patterns to the fractionation of specific minerals (e.g. Guo et al., 2007; Davidson et al., 2007); for example, removal of amphibole from a melt by fractionation is represented by MREE depletion (Macpherson et al., 2006; Davidson et al., 2007). Furthermore, identification of specific mineral fractionation phases via REE pattern evaluation can be useful in inferring some characteristic of magma origin or fractionation conditions the magma has undergone during ascent (e.g. Macpherson et al., 2006; Davidson et al., 2007). This could be some pressure threshold at which the melt resided for a period of time for instance. Evaluation of the REE patterns derived from the porphyry samples therefore has the potential to reveal some aspect of the magma evolution that is different to those of Wamum and the Kokofimpa tonalite suites. Various ratios of REE abundances are used to quantitatively describe the trend or slope for particular REE patterns, for example, ratios of La/Yb or Ce/Yb describe the slope for the entire REE suite, or La/Sm is often used as an indicator for the LREE slope (e.g. Elburg et al., 2002; Woodhead et al., 2010). In this case, Ce/Yb ratios reveal a trend of increasing REE slope through time (Figure 4-10). A gradual increase from Wamum to the Kokofimpa tonalites can be related to typical magma fractionation processes, however, the significant increase in Ce/Yb ratios between the tonalite suite and late porphyries cannot be accounted for in terms of normal fractionation trends and must be investigated further.

A plot of Ho/Nd (Figure 4-10) as an analysis of MREE slope reveals that BKDD22 299, the porphyry intrusive within the tonalite suite, behaves similarly to the remainder of the tonalites, in contrast to the late porphyry suite. More specifically, REE plots for the late porphyry suites display a relative depletion in the MREE and HREE signatures that is most commonly attributed to fractionation of amphibole or garnet mineral phases respectively (Macpherson et al., 2006; Davidson et al., 2007). Differentiation between the two mineral fractionation processes is often ambiguous. Davidson et al. (2007) utilize a plot of Dy/Yb with magma differentiation to discriminate between the two potential fractionating mineral phases. Figure 4-11 illustrates a similar plot and again highlights the different nature between the tonalitic porphyry and late porphyry intrusives relative to the tonalites. From this it is possible to interpret that the tonalite porphyry is potentially derived from a common magma source shared with the tonalite suite but may have undergone amphibole fractionation represented by MREE depletion. The late porphyries, however, follow a differentiation trajectory akin to that indicated for garnet fractionation (i.e., pronounced HREE depletion). This interpretation relies on the assumption that the tonalite suite and porphyries share a common melt composition. However, it is apparent from discussion of the HFSE elements above that there is potential for a different magma source making this a possibility but also a speculative interpretation. Evaluation of garnet as a potential fractionating

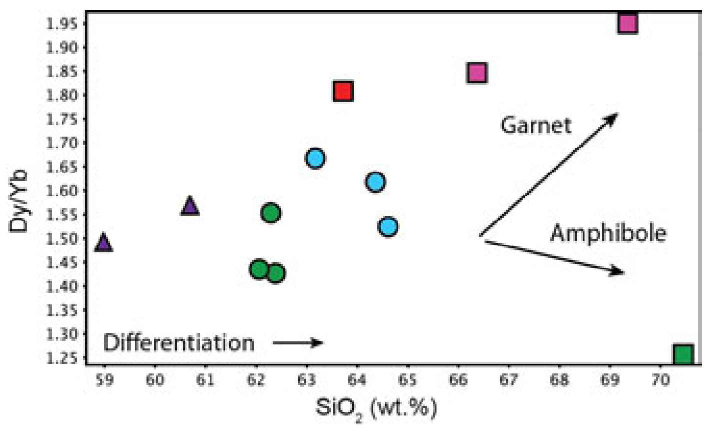

Figure 4-11. Dy/Yb vs. SiO2 for Wamum and Kokofimpa intrusives. Mineral fractionation trends are from Davidson et al., 2007. Sample BKDD22 299 can be related to the tonalite suite by amphibole fractionation while the late porphyry intrusive follow a differentiation trend typical of garnet fractionation.

mineral phase draws similarities with the adakitic rocks of Chapter 3. The implications and possible origins of this geochemical signature are covered in some detail in Chapter 3. Taking a similar approach to evaluation of adakitic rocks, it is apparent from figure 12 that the latest porphyry phase of this study does satisfy the criteria for adakite classification. However, given the relatively unconstrained nature of the regional tectonic setting for arc magmatism and limited definitive geochemical insight into arc processes in this study, it would be speculation to consider a mechanism that may give rise to adakites in this scenario.

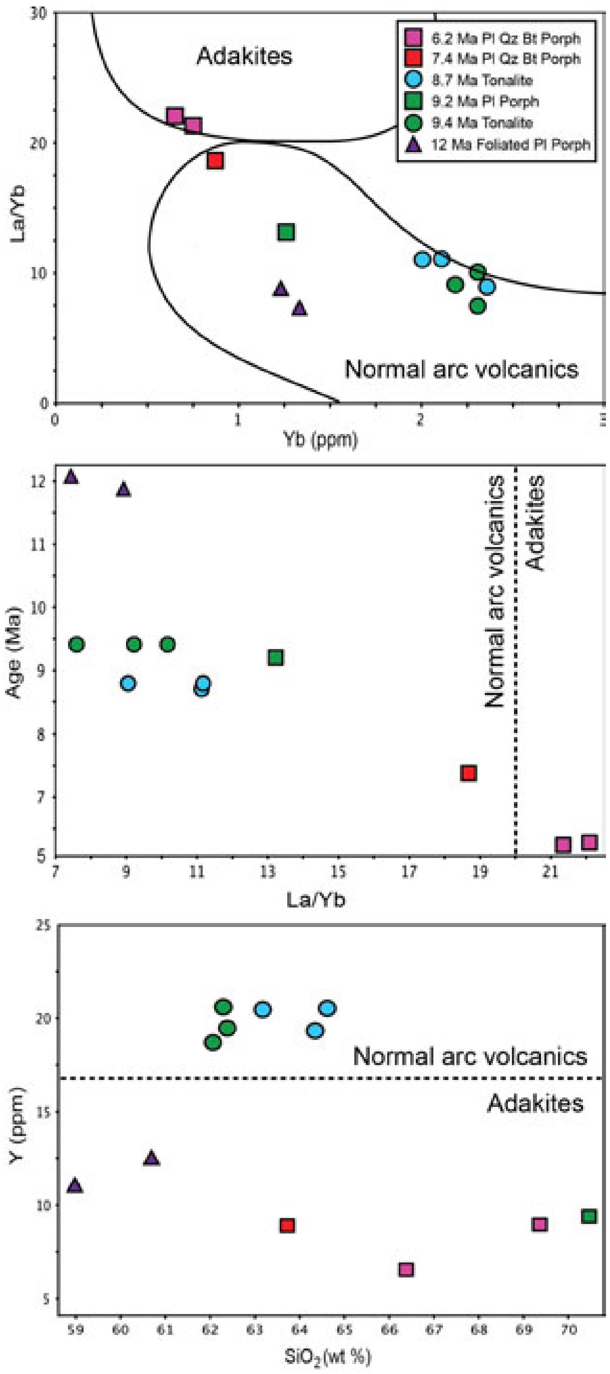

Figure 4-12. La/Yb vs Yb, Age vs La/Yb and Y vs. SiO2 plots for Wamum and Kokofimpa intrusives. Late porphyry intrusives of Kokofimpa exhibit geochemical traits associated with adakites. The adakite and normal arc volcanic fields are from Castillo et al. (1999) and Richards and Kerrich (2007).

Evaluation of the geochronology and geochemistry presented here tells a story of an evolving magmatic system in the eastern Papuan Highlands from 12 Ma through to 6 Ma, albeit a loosely constrained one. With little insight possible into the nature and definitive characteristics of specific intrusive suites, I instead take an approach that addresses changes between the different magmatic phases through time. Firstly, transitioning from intrusion of the Wamum plagioclase porphyry at 12 Ma to the tonalite intrusive sequence of Kokofimpa there is a marked increase in the relative HFSE abundance with particular enrichment in Th, Zr and Nb contents. While this is a significant change in the incompatible element composition of the magma we cannot determine if it arises from a changing source composition in the mantle, possibly related to subduction dynamics, or simply a high degree of crustal assimilation by the magma during ascent. Intrusion of a porphyry phase within the tonalite sequence can be explained through derivation from a common magma source but affected by amphibole fractionation.

From the 9 Ma tonalite suites to the late porphyry suite we see a somewhat more dramatic shift in geochemical composition. The HFSE contents transition back to values typical of Wamum samples, a significant change in itself, but is coupled with a significant shift in REE trends. Observed REE patterns marked by depletion of MREE and HREE cannot be related to the tonalite suite simply by amphibole fractionation, and are potentially indicative of garnet fractionation. Hence between 12 and 9 Ma, and between 9 and 6 Ma there are two major shifts in the nature of arc magmatism, which are tentatively identified as time periods of major tectonic transitions that fundamentally change the composition or emplacement conditions of Maramuni arc magmatism.

Geodynamic evolution of the Maramuni arc

Early Maramuni arc calc-alkaline magmatism from the Upper Oligocene through to the Middle Miocene intrudes the New Guinea Mobile Belt and comprises magmatism of felsic-intermediate to mafic composition (Figure 4-2). Evidence for the nature of this early arc activity, however, is sparsely exposed at the surface and obscured by subsequent deposition of sedimentary basins. In the north of Papua New Guinea the arc is buried beneath sediment basins in the Sepik region associated with Upper Oligocene collision of the North Sepik arc terranes (Crowhurst et al., 1996; Davies, 2012), and in northeast Papua New Guinea by underthrusting of the leading arc and continental margin beneath the Adelbert and Finisterre Terranes during Plio-Pleistocene arc-continent collision (Abbott et al., 1994; Woodhead et al., 2010; Holm and Richards, 2013). While this study offers no further insight into the nature of early Maramuni arc activity, the previous work carried out on the early arc magmatism - although limited - does provide a context for the later arc evolution.

From approximately 12 Ma and coincident with the start of the Upper Miocene period there is a profound change in the tectonics of Papua New Guinea marked by development of the New Guinea Orogen. This coincides with a distinct change in the composition of Maramuni arc magmatism coupled with a distinct southward migration of the arc from the New Guinea Mobile Belt into the Papuan Fold and Thrust Belt (Figure 4-2). An increase in the degree of magma fractionation and differentiation throughout Papua New Guinea at this time to produce abundant intermediate–felsic magmatism is most easily attributed as a response to crustal thickening of the New Guinea Orogen, and related to longer crustal residence times during magma ascent to shallow crustal levels (e.g. DePaolo, 1981; Hildreth and Moorbath, 1988; Barbarin, 1999). This pattern is expressed as common fractionation trends of major element concentrations within the sample suite, for example, increasing SiO_2 and K_2O content, but decreasing Al_2O_3, Fe_2O_3, MgO, CaO and Na_2O content from early Wamum activity through to the Kokofimpa intrusive suites (Figure 4-8). Although we can easily relate crustal thickening to increased magma fractionation in the Maramuni arc, this contributes little to our understanding of the underlying controls on arc development.

The process of orogenesis can be non-unique as to the triggering mechanism, in this scenario either an episode of arc-continent collision from the north (Trobriand trough; Davies, 1990; Abbott et al., 1994; Hill and Raza, 1999) or collision of the Australian continent from the south (Pocklington trough; Hill and Hall, 2003; Cloos et al., 2005) are plausible. However, a regional evaluation of the distribution of magmatism can be useful with regard to subduction dynamics. This requires development of two generalized subduction models that can account for the southward migration of the arc. Firstly, migration of the arc to the south increases the distance between the magmatic front and subduction at the Trobriand trough; this requires a shallowing of the subduction angle, commonly referred to as flat-slab subduction (Gutscher et al., 2000; van Hunen et al., 2002; Rosenbaum and Mo, 2011). The alternative model of north-dipping subduction at the Pocklington trough, in contrast, requires a steepening angle of subduction as the arc migrates towards the plate boundary (e.g. Schellart, 2004; Arcay et al., 2005; Heuret and Lallemand, 2005; Lallemand et al., 2005; Schellart, 2008). Both models are feasible and reflect commonly observed tectonic responses to collision events. A renewal of orogenesis at 6 Ma, however, can help us discriminate further between the models. There is no record of any further episodes of collision at either the Trobriand trough or Pocklington trough between 12 and 6 Ma pertaining to another mechanism to explain this later orogenesis. The model of Cloos et al. (2005) appeals to crustal delamination of the subducted plate at the Pocklington trough coupled with isostatic crustal rebound to explain uplift. No such model exists for the Trobriand trough and any subsequent subduction dynamics would be expected to hold implications for northern New Guinea as opposed to the more distal central and southern regions of New Guinea where deformation is most apparent. Based on these simple tectonic relationships I favour the model of Cloos et al. (2005) for north-dipping subduction at the Pocklington trough to explain the tectono-magmatic relaionship between Maramuni arc magmatism and development of the New Guinea Orogen.

The geochronology and geochemistry presented has potential to provide further insight into the geodynamic evolution of the Maramuni arc and shares several consistencies with the tectonic evolution presented by Cloos et al. (2005) for West Papua (Figure 4-13). For example, although speculative, the significant increase in HFSE at 9 Ma evident in the Kokofimpa tonalite suite can be explained by an increase in crustal contamination of the melts (Rubatto and Hermann, 2003; Woodhead et al., 2010; Spandler and Pirard, 2013) and may be associated with abundant sediments or crustal material of the Australian continent entering the subduction zone (Figure 4-13). Subsequent to this, at 7–6 Ma there is another apparent fundamental change in the nature of arc magmatism, coincident with the interpreted crustal delamination of Cloos et al. (2005). In such a scenario, breakup and detachment of the subducted plate can lead to inflow of hot asthenospheric mantle, which can result in increased heat flow to the sub-arc environment, potentially destabilizing the subducted material or lower crust (Figure 4-13). This can generate high-pressure melts of adakitic composition explaining the unusual geochemical signature of the late porphyry suite (Hildreth and Moorbath, 1988; Rushmer, 1993; Macpherson et al., 2006). Alternatively, crustal thickening associated with orogeneis interacting with crustal delamination and complex subduction dynamics may cause ponding or stalling of magma at depth at the base of the crust, again producing the adakitic signature (Garrido et al., 2006; Macpherson et al., 2006; Alonso-Perez et al., 2009). These are simply suggestions as to how the geochemistry presented here may relate to this geodynamic model, nevertheless, periods of change in the nature of arc magmatism correlate in time with the tectonic model of Cloos et al. (2005) and contribute to our understanding of the evolution of New Guinea. I stress that this is, however, still a preliminary model for the evolution of arc magmatism and tectonics in Papua New Guinea and based on a small area of the Maramuni arc. Further work is planned to measure isotope compositions in the same sample suite in an effort to provide additional evidence to support the geodynamic history presented here.

A Late Cenozoic geodynamic evolution model for Papua New Guinea

Previous work regarding the tectonic evolution of Papua New Guinea is characterized by a relative lack of robust evidence and inferred information to fill our knowledge gaps. This has resulted in an array of different geodynamic models that appeal to as many different tectonic processes and timing for events to reconstruct the geological history. Although coverage of geological data throughout Papua New Guinea remains sparse we review the published data available for Papua New Guinea and present this in a new geodynamic evolution model for Papua New Guinea supplemented by the additional geochronological and geochemical evidence presented within

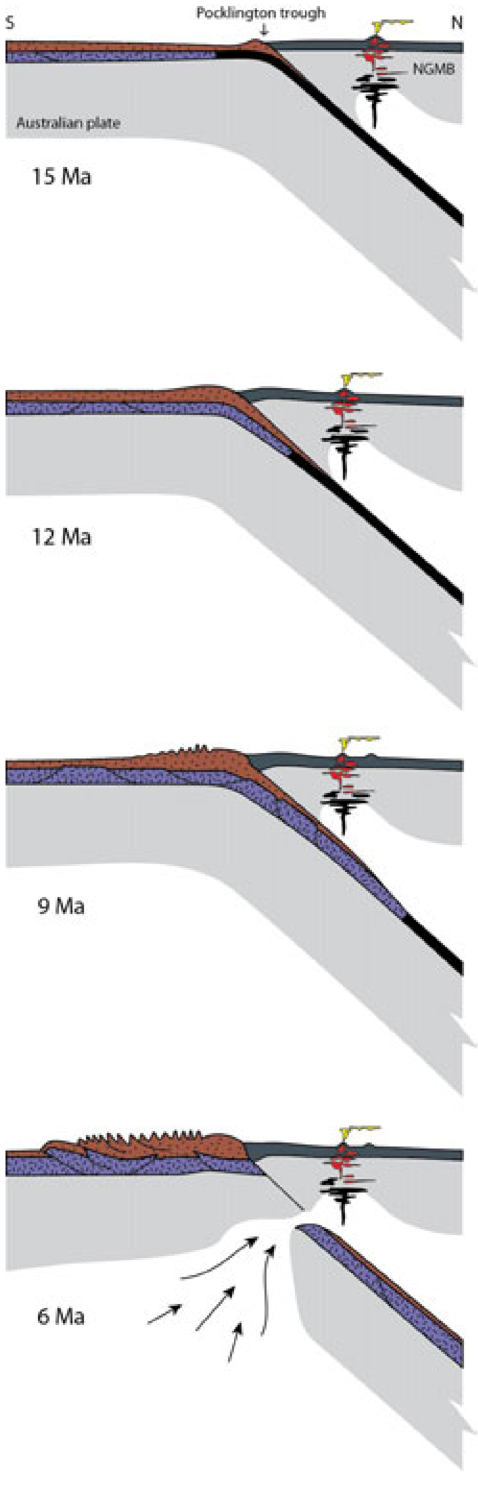

Figure 4-13. Generalized schematic geodynamic setting for Maramuni arc emplacement at Wamum and Kokofimpa (modified from Cloos et al., 2005). Time steps represent pre-continental collision at 15 Ma and each of the subsequent intrusion events at Wamum (12 Ma) and Kokofimpa (9 Ma and 6 Ma). Magmatism at 15 and 12 Ma is typified by normal slab dehydration processes derived from the north-dipping subduction of oceanic crust (black) of the Australian plate at the Pocklington trough beneath the New Guinea Mobile Belt (NGMB); underthrusing and partial subduction of the leading continental margin (purple) and passive margin sediments (brown) by 9 Ma; crustal delamination at approximately 6 Ma exposes the subducted plate and lower crust inflow of hot asthenospheric mantle.

this study. I propose a new model that is consistent with the current data and holds true to the observed tectono-magmatic relationships within the New Guinea Orogen and Maramuni arc (Figure 4-14).

The tectonic framework for development of the Maramuni arc begins at approximately 26 Ma with arrival of the Ontong Java Plateau at the Melanesian trench to the northeast of proto-New Guinea (Petterson et al., 1999; Knesel et al., 2008; Holm et al., 2013). Cessation of southwest-dipping Pacific plate subduction beneath the Melanesian arc (Petterson et al., 1999; Lindley, 2006; Holm et al., 2013) led to a dramatic reorganization of southwest Pacific plate tectonics including the redistribution of regional convergence at the Australia-Pacific plate boundary and, more importantly, intra-plate stress partitioning within the Australian plate. This period of plate reorganization is marked by accretion of the North Sepik Bewani-Toricelli-Prince Alexander arc terranes (unrelated to the Melanesian arc; Findlay, 2003) to the northern margin of the proto-New Guinea Mobile Belt by the Upper Oligocene (Figure 4-14; Pigram and Davies, 1987; Struckmeyer et al., 1993; Crowhurst et al., 1996). At this time the New Guinea Mobile Belt existed as a ribbon of continental crust overprinted by a Cretaceous volcanic arc that was rifted from the Australian continent, perhaps somewhat analogues to the modern day Lord Howe Rise or Norfolk Ridge of the Tasman Sea. During this time we also see commencement of north-dipping subduction of the Australian plate (Cloos et al., 2005) to the south of, and beneath the proto-New Guinea Mobile Belt (Figures 4-13 and 4-14). This fossil subduction zone is preserved today in Papua New Guinea as the Pocklington trough, Moresby trough and Aure trough in central and eastern Papua New Guinea (henceforth referred to as the Pocklington trough), and while the active deformation front of the Papuan Fold and Thrust Belt marks the present day plate boundary, the primary crustal suture zone is marked by the Lagaip and Bundi fault zones (Figures 4-1 and 4-2; Chapter 5), and their West Papuan equivalents. I adopt north-dipping Pocklington trough subduction model as opposed to the south-dipping Trobriand trough model and suggest that it is the only model able to fully account for the spatio-temporal tectonic relationships of the New Guinea Orogen and Maramuni arc. Cloos et al. (2005) previously developed a north-dipping subduction model for West Papua, however, here I present a new unifying tectonic model for the Late Cenozoic evolution of New Guinea; this model draws from the multitude of previous studies in both Papua New Guinea and West Papua.

Upper Oligocene accretion of the North Sepik arc terranes and initiation of north-dipping subduction at the Pocklington trough (Figure 4-14) related to far-field arrival of the Ontong Java Plateau at the Solomon Islands, feeds back into the initiation of subduction-related Maramuni arc magmatism (ca. 24–20 Ma; Page, 1976) within the New Guinea Mobile Belt to the north of, and adjacent to the Lagaip and Bundi fault zones (Figures 4-2, 4-13 and 4-14). With maturity of Pocklington trough subduction we observe a general southward migration of the Lower and

Middle Miocene intrusive activity of the Maramuni arc towards the Lagaip and Bundi fault zones (Figure 4-2). In addition, Hill and Raza (1999) identify a period of extension in the exposed Australian continental basement of the Papuan Fold and Thrust Belt at 17 Ma from fission track analysis. These findings have previously been attributed to upper plate extension in response to subduction initiation (Hill and Raza, 1999), however, the temporal relationship infers up to a 5–10 m.y. delay in upper plate processes. Instead I suggest this extension is consistent with tectonism of the Australian continental basement through crustal arching and extension in the subduction hinge on approach to the Pocklington trough (Figure 4-14; Isacks et al., 1968; Bradley and Kidd, 1991; Doglioni, 1995; Cloos et al., 2005). This is perhaps related to initial underthrusting of the leading continental margin (e.g. Cloos et al., 2005), and similar to extension observed in the Marianas trench and the Apulian foreland of the Apenninic subduction zone (Doglioni, 1995). Beyond the insight provided by Hill and Raza (1999) and age control on Maramuni arc magmatism (Page, 1976), there is very little data available on the tectonic evolution of New Guinea between Upper Oligocene (~26 Ma) and 12 Ma. We can, however, gain some understanding of regional tectonics through the sedimentary records of the Australian continental shelf edge in the Gulf of Papua from the work of Tcherepanov et al. (2010). The authors document a marked increase in depocenter thickness of Upper Oligocene–Lower Miocene sedimentary sequences associated with localized subsidence on the Australian continental platform. These observations are consistent with carbonate accumulation on the continental passive margin during northward plate motion, and acting in combination with the extensional tectonism mentioned above. Furthermore, Tcherepanov et al. (2010) identifies contemporaneous siliciclastic influx in the Aure trough (Pocklington trough), quite independent from carbonate deposition, hence complimenting the timing for initiation and expected sedimentary response to Pocklington trough subduction adjacent to the early Maramuni arc.

Just 14 million years after the prior tectonic reorganization at 26 Ma, another dramatic and sudden change in regional tectonics transpires at approximately 12 Ma. This is most pronounced in the geological record as representing the first indication of uplift in the New Guinea Orogen (Hill and Raza, 1999; Cloos et al., 2005). This timing does not correspond with any documented collision events on the Trobriand trough. The north-dipping Pocklington subduction model, however, can provide a simpler and more straightforward explain for these tectonic phenomena that is consistent with geological evidence to date. By approximately 12 Ma the Australian continent arrives at the Pocklington trough (Cloos et al., 2005) and collides with the New Guinea Mobile Belt resulting in lock up of the subduction system and represents closure of the Pocklington Sea (Figures 4-13 and 4-14). From 12 Ma we see growth of the New Guinea Orogen (Cloos et al., 2005) driven by shortening and uplift of the New Guinea Mobile Belt, particularly adjacent to the Lagaip-Bundi suture; and orogenesis of the Australian continental platform sediments forming the initial stage of an extensive accretionary complex termed the Papuan Fold and Thrust

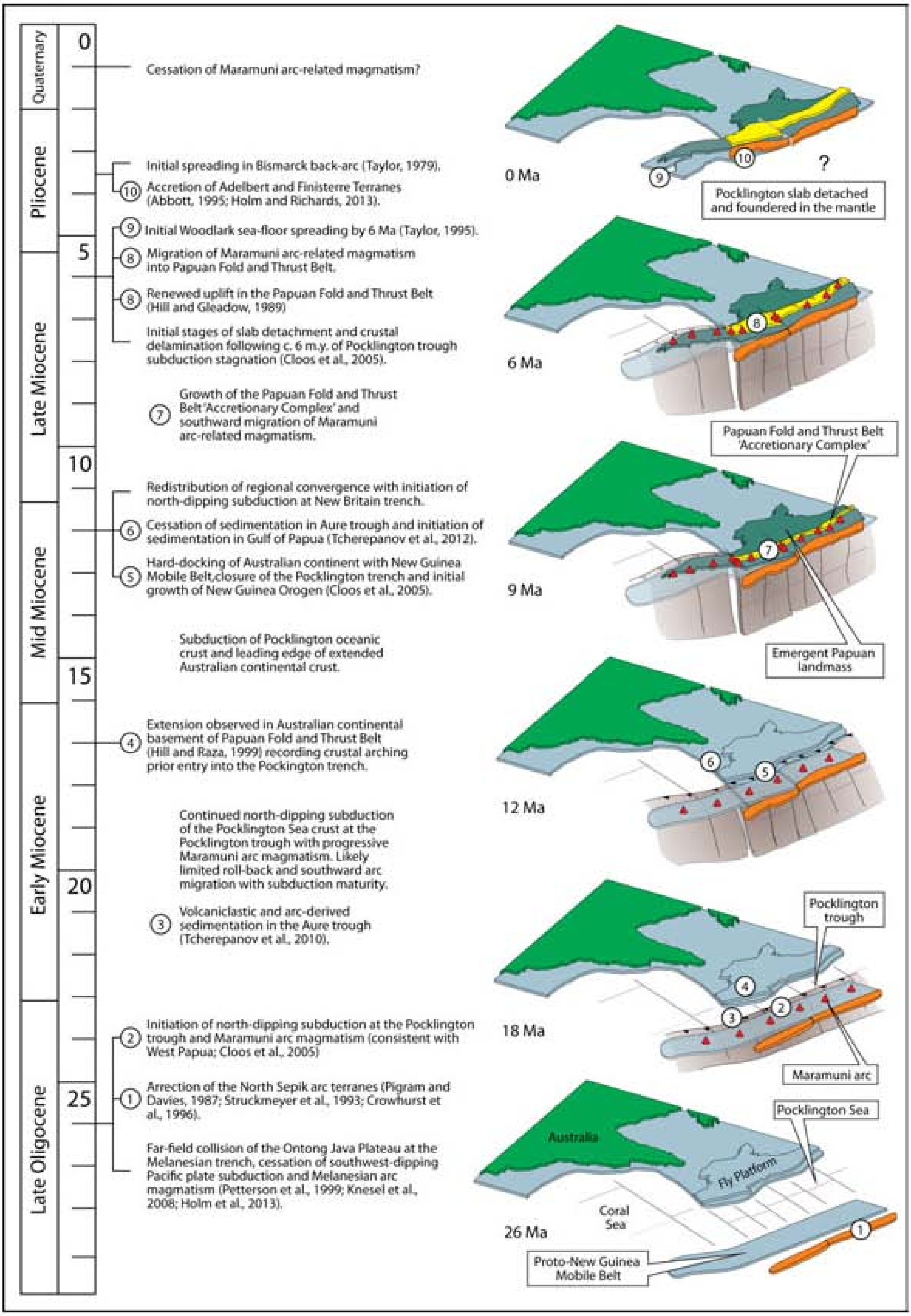

Figure 4-14. Geodynamic model for the Late Cenozoic tectonic evolution of New Guinea. Reconstruction model is looking from the northeast. See explanatory notes for details and text for further discussion.

Belt. Furthermore, it is at this time a number of regionally important geological changes occur. Upper Miocene–Lower Pliocene cessation of sedimentation in the Aure trough coupled with the initiation of siliciclastic sedimentation in the Gulf of Papua (Pigram and Symonds, 1991; Tcherepanov et al., 2010) marks closure of the Pocklington trough and the subsequent bypass of sediments over the continental Fly Platform. In addition, a redistribution of regional convergence in response to closure of the Pocklington trough results in a northward trench jump and initiation of north-dipping subduction of the Solomon Sea plate at the New Britain trench (Figure 4-1; Petterson et al., 1999). The strong temporal and spatial correlations reflect near geologically instantaneous tectonic feedbacks between continental collision, orogenesis and redistribution of regional convergence. Although the Maramuni arc also extends east-southeast into the Papuan Peninsula, indicative of active subduction at the Pocklington trough, the geology of the peninsula more than c. 100 km removed from collision of the Australian continent with New Guinea shows little structural evidence of post-Oligocene convergence and shortening. This may be a function of the lack of work carried out here, conversely, we also know that during collisional events such as this, the upper plate effects of collision can diminish relatively quickly away from the point of collision and subduction cessation, and may not result in any structural implications for the adjacent upper plate (e.g. Mason et al., 2010; Rosenbaum and Mo, 2011; Holm et al., 2013). Therefore a lack of documented evidence for post-Oligocene crustal shortening in the Papuan Peninsula does not preclude prior subduction at the Pocklington margin.

During the period 12–7 Ma, approximately the span of the Upper Miocene, initial continental collision is followed by an apparent cessation or slowing of Maramuni arc activity, presumably in response to termination of subduction at the Pocklington trough and slab stagnation, while the onset of crustal shortening begins to uplift the New Guinea Orogen (e.g. Hill and Raza, 1999; Cloos et al., 2005). There is however, very little direct evidence as to the tectonics of New Guinea during this time, limited to only apatite fission track records (Crowhurst et al., 1996; Hill and Raza, 1999) tied to K-Ar geochronology from Page (1976). The majority of this age data is from the Kainantu district and the surrounding regions. New results of the same region contained in this study reveal that while New Guinea is in a state of crustal shortening during the Upper Miocene, the Maramuni arc activity continues but is in a dynamic state of change in response to crustal thickening associated with growth of the New Guinea Orogen and underthrusting of the Australian continental margin beneath New Guinea (Figures 4-13 and 4-14). Moreover, this timing is marked by a pronounced migration of Maramuni arc magmatism from northeast to southwest (Figures 4-2 and 4-14), a trend previously recognised by Davies (1990).

From approximately 7 Ma, the New Guinea Orogen and magmatism undergo an apparent resurgence in activity (Hill and Gleadow, 1989; Closs et al., 2005). During this time there is a clear migration of magmatism to the south forming a latest Miocene–Quaternary magmatic belt that intrudes the Papuan Fold and Thrust Belt and stable Australian continental crust of the Fly Platform. However, it is not yet conclusive as to whether this later arc magmatism is a continuation and transformation of the Maramuni arc or the initiation of a new magmatic arc following termination of the Maramuni arc. Cloos et al. (2005) suggests this most recent phase of arc volcanism represents the detachment of the stagnated Pocklington slab and collisional delamination of the underthrust lithosphere by at least 6 Ma to produce adiabatic decompression of the underlying athenosphere that resulted in volumetrically minor but widespread, collision-generated magmatism along the axis of the New Guinea Orogen (McDowell et al., 1996; Cloos et al., 2005). Isostatic uplift of the New Guinea Orogen also resulted from crustal delamination; Cloos et al. (2005) interpreted that vertical isostatic uplift occurred above the zone of maximum upwelling, particularly the Papuan Fold and Thrust Belt, and that the orogenic belt rapidly rose by as much uplift as during the earlier prolonged orogenesis of the initial continental collision. By 4 Ma delamination of the Australian lithosphere is complete and asthenospheric upwelling has ended, and magma generation is in the final stages (Cloos et al., 2005) but continues to at least 1.2 Ma in Papua New Guinea (Ok Tedi; van Dongen et al., 2010; Chapter 2). This early Pliocene timing for renewed orogenesis is supported by apatite fission track studies from Hill and Gleadow (1989) who recognize renewed uplift and exhumation of the Papuan Fold and Thrust Belt from 5 Ma.

The most recent collision event involving the Papuan New Guinea mainland is the collision of the Adelbert and Finisterre Terranes, the easternmost North Sepik arc terranes (Figure 4-14; Abbott et al., 1994; Abbott, 1995; Holm and Richards, 2013; Chapter 6). Collision of the Adelbert and Finisterre Terranes with Papua New Guinea is interpreted to have been caused by closure of the Solomon Sea at the New Britain trench due to subduction-driven convergence between the Australian and South Bismarck plates (e.g. Abbott, 1995; Hill and Raza, 1999; Weiler and Coe, 2000). Abbott et al. (1994) studied clastic sequences on the southern flanks of the Finisterre Range and concluded that the collision must have initiated at ca. 3–3.7 Ma. This timing suggests collision occurred in the later stages of the Miocene–Quaternary orogenesis and magmatism in the New Guinea Orogen. Oblique collision started in the west and propagated southeastwards, producing progressive thrusting and uplift of the north-coast Adelbert and Finisterre Ranges as they overthrust the leading New Guinea Mobile Belt and underthrusting the leading edge of continental crust downwards in the mantle (Johnson and Jaques, 1980; Abbott, 1995; Weiler and Coe, 2000; Holm and Richards, 2013; Chapter 6). It is also significant that this underthrust margin is part of the New Guinea Mobile Belt and is host to the early phases of Maramuni arc volcanism (Holm and Richards, 2013; Chapter 6). At present the ongoing convergence between the Finisterre Terrane and the Australian plate is accommodated by the Ramu–Markham Thrust Fault (e.g. Cooper and Taylor, 1987; Abbott et al., 1994; Pegler et al., 1995).

Conclusions

The plate tectonic evolution of Papua New Guinea from the Miocene onwards is ambiguous with multiple and contrasting models for the geometry and timing of subduction systems and terrane-collision events. I present the first detailed U-Pb geochronology and geochemical investigation from the Maramuni arc of Papua New Guinea in an effort to provide insight into the evolving tectonic setting for arc emplacement throughout the Middle and Upper Miocene. Samples from the eastern Papuan Highlands porphyry prospects of Wamum and Kokofimpa (Kainantu region) provide evidence for at least five periods of significant intrusive events at approximately 12 Ma, 9.4 Ma, 8.7 Ma, 7.4 Ma and 6.2 Ma. The associated bulk rock major and trace element geochemistry reveals a highly dynamic magmatic setting of calc-alkaline high-K arc magmatism punctuated by terrane-collision and development of the New Guinea Orogen; crustal thickening is reflected in not only a shift to more fractionated and evolved magmatic compositions, but also a changing magmatic environment marked by distinctly different geochemical characteristics. These changes are marked at 9.4–8.7 Ma by a significant enrichment in HFSE, while from 7.4 Ma, and more significantly at 6.2 Ma, the geochemical signature of magmatism indicates a shift towards adakitic compositions with possible garnet fractionation. I interpret that this magmatic history is consistent with a tectonic model marked by north-dipping subduction of the Australian plate to the south of New Guinea. Arrival of the Australian continent at the Pocklington trough and collision at 12 Ma provides a likely mechanism for to the onset of orogenesis in Papua New Guinea. Some 6 m.y. after continental collision, break-up of the subducted plate, or crustal delamination is reflected in the upper plate by contemporaneous isostatic crustal rebound and renewed uplift in the New Guinea Orogen from approximately 6 Ma.

Chapter 5

Tracing the Tasman Line in Papua New Guinea: The geological expressions of a subducted continental suture

Abstract

Cenozoic tectonics in the southwest Pacific provide a unique insight into the processes of orogenesis, magmatism and continent accretion that can be used to infer processes that have operated throughout the Earth's crustal evolution. Papua New Guinea is a unique part of the planet in that Cenozoic orogenesis is superimposed on an earlier basement structure that has, in turn, influenced how the New Guinea Orogen has grown over time. Specifically, the underlying/underthrust Australian continental basement is characterized by a major accretionary boundary referred to as the Tasman Line. The Tasman Line separates the younger Paleozoic-Mesozoic Tasmanide orogenic belt from the Precambrian cratonic rocks to the west. Using precise age dating of inherited zircon populations from Quaternary magmatics in the overriding Cenozoic fold belt coupled with an evaluation of orogen-scale deformation and magmatic morphology I am able to show where the Tasman Line extends to the north beneath younger crust. This result is significant as it demonstrates that with the use of a well established and scientifically proven technique combined with detailed structural and tectonic assessment, deep crustal boundaries can be traced in relatively young terrains where any evidence of underthrust plate or terrane boundaries are completely obscured.

Introduction

Australia's eastern continental margin is characterized by a major suture separating the older Precambrian rocks of central Australia from the Phanerozoic rocks and north-south trending accretionary orogens of eastern Australia. This boundary, referred to as the "Tasman Line", is evident in geophysical imaging reflecting a strong contrast between the igneous, metamorphic, deformation and metalogenic history of rocks in the west from those in the east (e.g. Scheibner and Veevers, 2000; Glen, 2005). Cloos et al. (2005) suggested that the Tasman Line might have played a significant role in the recent tectonic evolution of New Guinea because it acted as a boundary between two continental domains with contrasting crustal properties. However, the exact location of the Tasman Line has only been inferred and more data has been required before its location can be more accurately determined (Figure 5-1). If the Tasman Line can be defined beneath Papua New Guinea, then its influence on the structural and magmatic evolution of the orogen can be much better defined. At the global-scale the results will provide a potential explanation and an additional tool to help unravel the complexity of accretionary orogens that exhibit markedly different structural, magmatic and even metamorphic characteristics in what appears to be a single arc or accretionary event.

I present new data that shed light on the continuation of the Tasman Line into Papua New Guinea. The age and morphology of inherited zircon populations from two magmatic occurrences unearth the location of the important terrane boundary. Comparison of inheritance ages with established links between crustal properties and deformation in the overriding New Guinea Orogen are used to support the results from zircon analysis. The methodology used here are not specific to Papua New Guinea but could be applied to orogenic belts around the world where inherited zircons can be used to map basement architecture if the technique is combined with other geological methods such as geochemistry and structural geology. The results presented here may be used to help interpret ancient magmatic arcs where major contrasts in inherited zircon patterns are recorded. Furthermore, these results can be used to gain a better understanding of ancient orogenic belts where ongoing deformation and magmatism may have masked some of the evidence for ancient fold belt subduction.

Geological Setting and Samples

The recent and ongoing tectonic evolution of Papua New Guinea allows a unique insight into a young arc-continent collision accretionary terrain. The island of New Guinea, incorporating Papua New Guinea and West Papua is geologically composed of numerous terranes accreted to the Australian continental margin during the Cenozoic northward drift of the Indo-Australia plate (Figure 5-1; Hill & Hall 2003; Crowhurst et al., 2004; Davies, 2012). The Papuan Fold and Thrust Belt forms an accretionary orogen of sedimentary cover rocks formed on Australian continental basement (Hill and Gleadow, 1989; Craig and Warvakai, 2009) but buttressed against variably deformed sedimentary, metamorphic and crystalline rocks of the New Guinea Mobile Belt (Hill and Raza, 1999; Davies, 2012), together these comprise the New Guinea Orogen. The Late Cenozoic Maramuni arc intruded into rocks of the New Guinea Orogen. Early arc magmatism is evidenced by intrusions emplaced into the New Guinea Mobile Belt during the Upper Oligocene caused by initiation of north-dipping subduction beneath New Guinea (Hill and Raza, 1999; Cloos et al., 2005), and migrated into the Papuan Fold and Thrust Belt in the Upper Miocene (Page, 1976; Rogerson and Williamson, 1985). Recent Pliocene and Quaternary igneous activity is almost exclusively hosted within the Papuan Fold and Thrust Belt and Fly Platform (Figure 5-1).

Although much of southern Papua New Guinea is composed of, or rests on stable Australian continental crust, there are only rare exposures of it. Basement windows such as these are reminiscent of exposures of high-grade crystalline rocks found along the Himalayan Orogen such as the Garhwal-Kumaun (Bhattacharya, 2008). In Papua New Guinea, inliers of Carboniferous–Jurassic rocks are limited to exposures within the Muller and Kubor Anticlines (Figure 5-1),

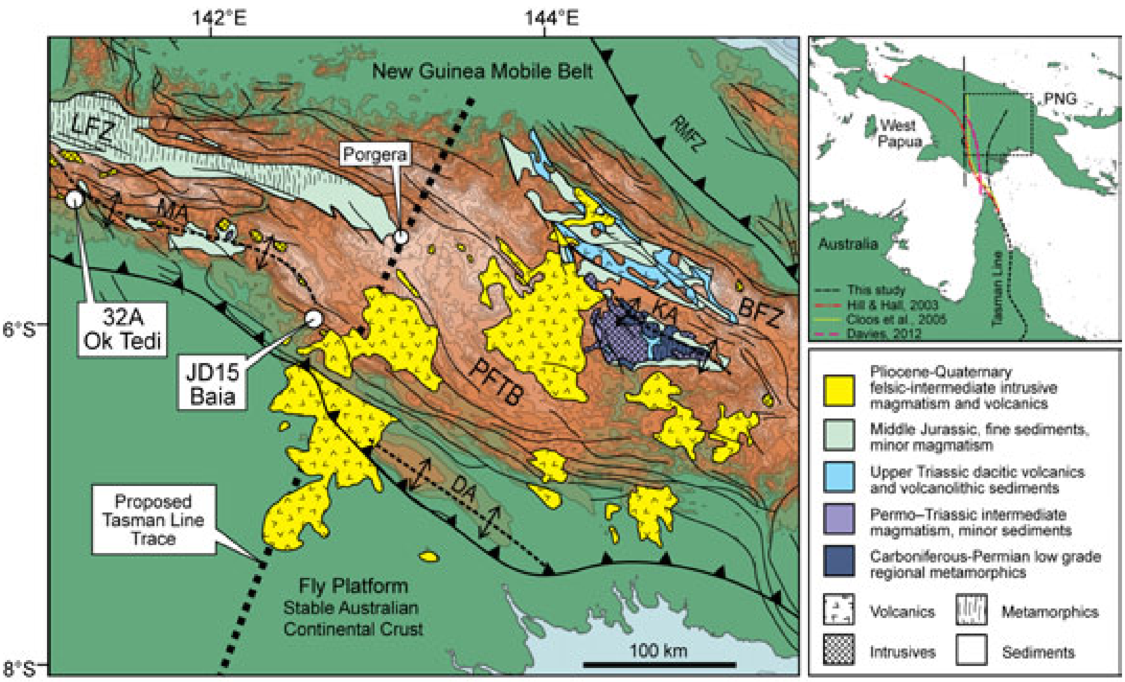

Figure 5-1. Geology of the central Papua New Guinea Highlands. Geological units relevant to this study are shown, samples 32A and JD15 (668956 9341950 AGD66 zone 54) lie within a belt of Quaternary magmatism intruding the New Guinea Mobile Belt. Geology is from Australian Bureau of Mineral Resources (1972) and shown over topography of the Papua New Guinea Highlands. Structures labeled are: DA: Darai Anticline; KA: Kubor Anticline; LFZ: Lagaip Fault Zone; MA: Muller Anticline; PFTB: Papuan Fold and Thrust Belt; RMFZ: Ramu-Markham Fault Zone; BFZ: Bundi Fault Zone. Inset indicates the Tasman Line in Australia (Glen, 2005) and previously interpreted extensions of the Tasman Line into New Guinea (see references in figure).

and exhumed belts of the same aged rocks uplifted and exposed within the Lagaip and Bundi fault zones that mark the suture zone between the Papuan Fold and Thrust Belt and New Guinea Mobile Belt (Figure 5-1). Moreover, these rocks show significant lateral variation along the orogen, with predominantly sedimentary rocks of Middle Jurassic age in the west and Permian-Triassic magmatic and metamorphic rocks in the east (Figure 5-1). These spatio-temporal relationships link the basement rocks of the eastern Papuan Highlands to the Tasmanide orogenic belt of eastern Australia (Van Wyck and Williams, 2002; Crowhurst et al., 2004).

Two Quaternary magmatic occurrences were sampled within the Papuan Fold and Thrust Belt in western Papua New Guinea (Figure 5-1). Both sample localities occupy a similar tectonic setting within the New Guinea Orogen hosted by Mesozoic shelf platform sedimentary rocks and Cenozoic sedimentary cover sequences (Australian Bureau of Mineral Resources, 1972; Hill et al., 2002). Sample 32A, from Ok Tedi, is a porphyritic phase of the Sydney Monzodiorite that comprises phenocrysts of plagioclase and mafic minerals, especially hornblende. Sample JD15 (Baia) is an andesitic volcanic, crystal-rich lapilli tuff with complexly zoned plagioclase and hornblende in a fine-grained fragmental matrix.

Methods

Samples selected for U-Pb dating of zircon were taken from the Ok Tedi Sydney Monzodiorite (sample 32A) and Baia prospect (sample JD15). Mineral separation was carried out at James Cook University (JCU) by a standard process of crushing and milling, heavy liquid density separation and magnetic separation. Zircons were hand picked and mounted in epoxy with GJ1, Temora 2 and Fish Canyon Tuff zircon standards. Epoxy mounts were polished and carbon-coated. Cathodoluminescence (CL) images of zircon grains were obtained using a Jeol JSM5410LV scanning electron microscope equipped with a Robinson CL detector, housed at JCU.

U-Pb dating of zircon was conducted using a laser ablation ICP-MS setup using the procedure described in Tucker et al. (2013) and Holm et al. (2013; Chapter 3). The majority of zircon analyses utilized a 60 μm beam diameter, however, a 24 μm diameter was used for JD15-2 analyses. The selection of analytical spots was guided by CL images with the aim of targeting both cores and rims. Data reduction was carried out using Glitter software (Van Achterbergh et al., 2001). All time-resolved single isotope signals were filtered for signal spikes or perturbations. The most stable and representative isotopic ratios were selected, taking into account possible mixing of different age domains and zoning. Drift in instrumental measurements was corrected following analysis of drift trends in raw data for the GJ1 primary zircon standard. Analyses of Temora 2 and Fish Canyon Tuff zircon were used for verification of GJ1 following drift correction (Figure 5-2). Background corrected analytical count rates, calculated isotopic ratios and ages, and 1σ uncertainties were exported for further processing and data reduction. Ages were assessed for discordance using a 10% cut-off. Further, analyses were evaluated for common Pb, where $^{206}Pb/^{238}U$ ages yielding $^{206}Pb/^{204}Pb$ analytical counts <1000 (background subtracted) were corrected using the Age7Corr algorithm of Isoplot/Ex version 4.15 (Ludwig, 2009); common Pb composition was modeled from Stacey and Kramers (1975). Ages were plotted using the cumulative probability plot and histogram function of Isoplot. Full records of zircon analytical data are included in the digital appendices.

Results

Zircon morphology provides an initial guide to population discrimination. Zircons from samples 32A and JD15 are all pink in color. Inherited zircons of 32A vary between 125 µm and 300 µm in length, and the aspect ratio ranges from 1:3 to 1:1.5. The CL appearance is characterized by high luminescence contrast and either dark or bright cores. While most grains are commonly complexly zoned, some exhibit simple oscillatory zoning (Figure 5-3). Inherited zircons occur as both independent grains and inherited cores, and generally exhibit some rounding of the grain or core. Inherited zircons from JD15 are highly variable, ranging in length from 60–350 µm with equally variable length to width ratios from 1:1 to 1:5.5. While some appear identical to magmatic zircon with euhedral crystal shapes, dull and featureless cores, and minor oscillatory zoning in the rim, most are comparatively more luminescent and exhibit complex zoning patterns. Grain shape varies from euhedral to rounded.

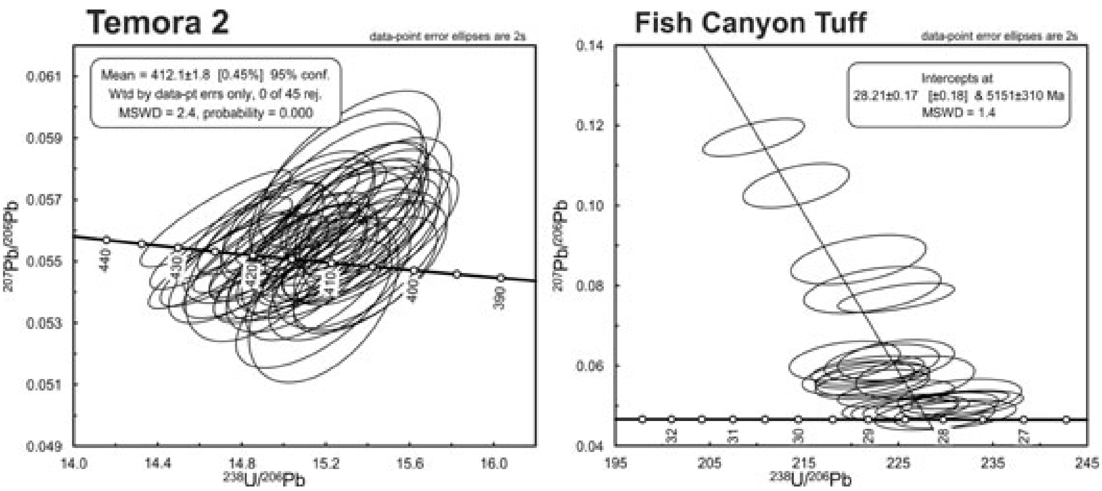

Figure 5-2. Concordia plots and weighted average (Temora 2) for U-Pb zircon geochronology standards. All data-point error ellipses and calculated errors are 2σ, and 95% confidence for associated weighted average.

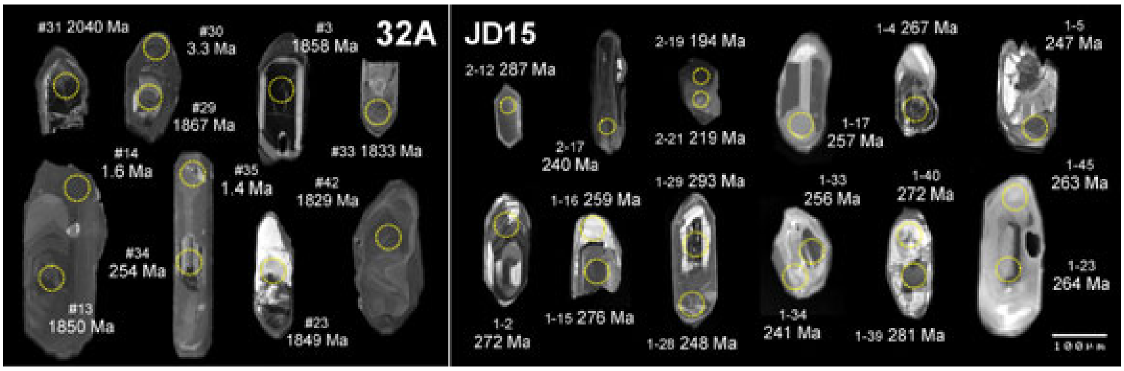

Figure 5-3. CL images of inherited zircon from 32A and JD15. Analytical spots are indicated with the associated ages calculated from $^{206}Pb/^{238}U$ (< 1 Ga) or $^{207}Pb/^{206}Pb$ (>1 Ga) analyses.

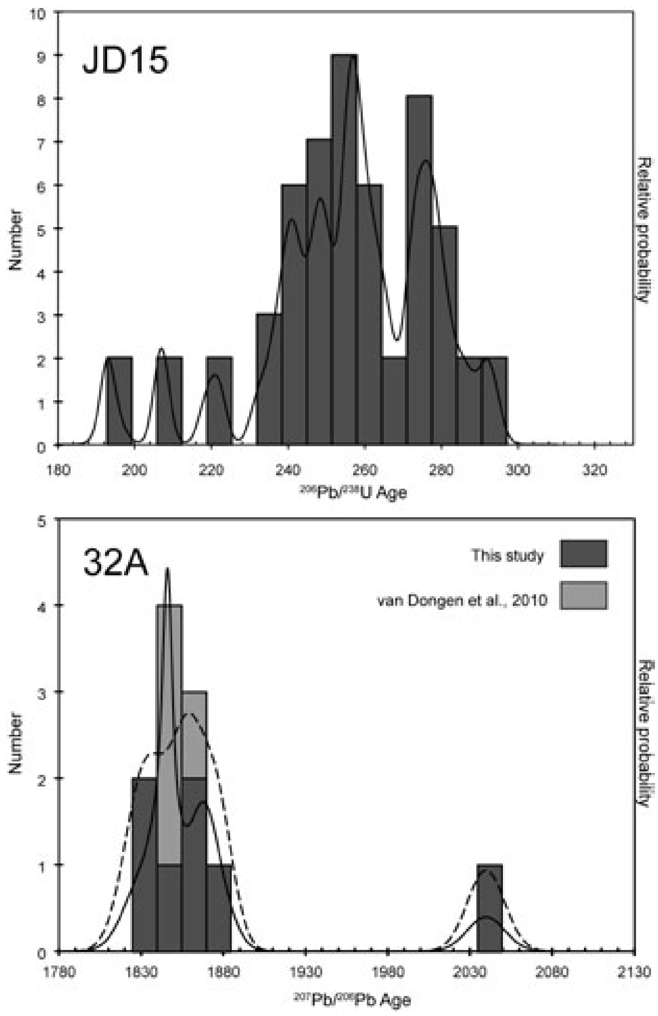

Figure 5-4. Histograms and cumulative probability plots for inherited zircon ages of JD15 and 32A. JD15 is comprised largely of Triassic and Permian ages while 32A ages from this study (dashed probability line) are Paleoproterozoic in agreement with previous data from van Dongen et al. (2010). Combined probability is indicated as a solid line.

The inherited ages differ markedly between the two samples. In sample JD15, 60 out of 89 analyses yielded inherited ages; 56 of these passed 10% discordance. These ranged between Late Paleozoic and Early Mesozoic in age at between 193 and 292 Ma (Figure 5-4) with peaks at 240–255 Ma and 275 Ma. In contrast, sample 32A only produced 12 out of 50 analyses with robust inherited ages; just seven passed discordance. These were Paleoproterozoic in age ranging from 1822 to 2040 Ma (Figure 5-4) and peaking at 1850 Ma. A single but notable $^{206}Pb/^{238}U$ age of 257 ± 6 Ma from an inherited core (Figure 5-3) fell outside the primary discordance cut-off at 15.1%. While this age cannot be regarded as precise due to the high discordance it is indicative of a provenance age close to the host sediment depositional age.

Discussion and Implications

Zircon inheritance patterns can be used as a tectono-magmatic fingerprint of a region. Specifically, inherited age patterns can be used to help match terranes and infer the source, or in this instance, a magmatic pathway for the intrusives. This method has been used around the world as support for the age and tectonic evolution of a terrain (Van Wyck and Williams, 2002; Paquette and Le Pennec, 2012). For the first time, we interpret the tectonic context of zircon inheritance patterns for the magmatic rocks that form throughout the compression-dominated evolution of the Papuan Highlands.

In what appears to be a continuous and uninterrupted magmatic arc, results of this study show that two spatially associated intrusives, Ok Tedi and Baia not only occupy comparable geological positions within deformed Triassic-Jurassic platform sedimentary rocks of the Papuan Fold and Thrust Belt (Figure 5-1) but they are also considered to be of the same Quaternary age (Chapter 2). Despite these similarities, the inherited age populations exhibited by the magmatic rocks contrast markedly. The western-most sample of the suite, sample 32A from Ok Tedi, exhibits Paleoproterozoic ages with a single Permian age. In contrast, the eastern-most of the two samples from Baia (JD15) exhibits Permian-Triassic ages (Figure 5-4). The majority of inherited zircons from both samples are also abraded (Figure 5-3) suggesting that the zircons are detrital in origin. This interpretation is also supported by an oxygen and hafnium isotope study on Ok Tedi inherited zircons (van Dongen et al. 2010).

A detrital origin for the inherited zircons rules out a direct link to crustal basement ages. However, the striking age contrast must be explained in lieu of outstanding differences in tectonic setting. This may reflect, for example, a regional tectonic setting contemporaneous with deposition of the Jurassic-Cretaceous sediments where uplift and exhumation of the Permo-Triassic Tasmanides resulted in a high rate of zircon supply in detritus to adjacent sedimentary basins (e.g. Baia), while distal continental platform depocenters in the west were comparatively starved (e.g. Ok

Tedi). Such sedimentological relationships can be interpreted as foreland basin and passive margin depositional settings respectively, in line with findings by Cawood et al. (2012) (Figure 5-5). Although limited to just two samples, the contrasting age populations resemble documented timing across the Tasman Line in eastern Australia (e.g. Glen, 2005) and justify an interpretation that supports previous suggestions that the Tasman line has been underthrust to the north beneath Papua New Guinea.

In 2005, Cloos et al. proposed that along-strike structural variation in the New Guinea Orogen was controlled or influenced by the type of basement being thrust northward under the younger fold belt rocks. Similar along-strike variations in orogen morphology are characteristic of major orogenic belts and exemplified by the Cordilleran and Himalayan orogens (Kley et al., 1999; McClelland et al., 2000; Yin, 2006; McQuarrie et al., 2008). The inherited ages presented above support this interpretation and, with this extra information at hand, a more accurate and informed

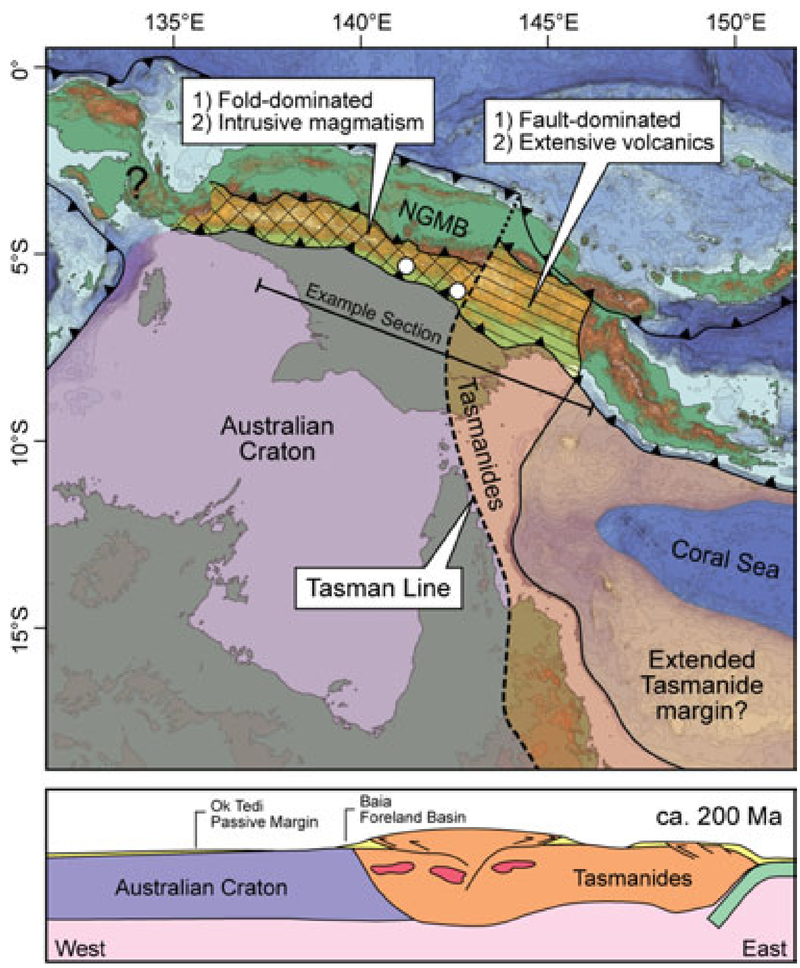

Figure 5-5. Regional-scale interpretation for the location of the Tasman Line and crustal architecture in Australia and New Guinea. NGMB: New Guinea Mobile Belt. A schematic section is illustrated below highlighting the depositional and tectonic setting of samples in this study (modified from Cawood et al., 2012).

interpretation of the controls on upper plate tectonics can be made. In the western New Guinea Orogen, deformation is dominated by en-echelon folding with subsidiary thrust faulting (Cloos et al., 2005), while both thin and thick-skinned thrust faulting with subsidiary folding control the morphology in the east (Hobson, 1986; Hill, 1991). Guided by the inherited zircon ages, I propose that a major structural transition is coincident with the change in inherited zircons, from fold-dominated to fault-dominated deformation east of Baia (Figures 5-1 and 5-5). I interpret this transition to mark the location of the Tasman Line. This transition has also impacted on the occurrence or preferential exposure of magmatic rocks in the region. Intrusive magmatic rocks are dominant in the west, while volcanism or extrusive rocks are preserved in the east (Figures 5-1 and 5-5). This partitioning may reflect variations in the degree of uplift or style of deformation through faulting and thrusting but may also suggest differences in the development of suitable conduits for magma migration from source to surface. Regardless, the transition between deformation styles and magmatism provides a compelling argument for constraining the location of the Tasman Line in New Guinea.

The recognition of the Tasman Line beneath Papua New Guinea holds applications beyond the recent morphological development of New Guinea with implications for our wider understanding of convergent margin processes. For example, intraplate alkalic basalts hosting the giant Porgera gold deposit (Richards et al., 1990) overlie the interpreted trace of the Tasman Line in the New Guinea Orogen (Figure 5-1). This geochemistry is unique within the extensive calc-alkaline Maramuni arc of Papua New Guinea, highlighting discrete geochemical domains within a continuous magmatic arc. Major crustal sutures or discontinuities entering convergent plate boundaries are prone to significant buoyancy contrasts and reactivation, particularly between a craton and bounding orogenic belt. I suggest that reactivation of the Tasman Line during subduction resulted in tearing of the lower plate allowing influx of mantle material, and resulting in the anomalous geochemistry and gold-endowment of Porgera. Therefore, major crustal discontinuities such as the Tasman Line may have a profound influence on subduction dynamics and the metal potential at convergent margins. Furthermore, constraint of the Tasman Line within New Guinea and recognition of the orogenic expressions of underlying crustal architecture during continental collision hold implications for our understanding of both active and ancient plate boundaries.

Chapter 6

A re-evaluation of arc–continent collision and along-arc variation in the Bismarck Sea region, Papua New Guinea

Published in *Australian Journal of Earth Sciences*

Abstract

The Bismarck Sea region of Papua New Guinea is marked by recent arc-continent collision giving rise to a highly dynamic tectonic environment, characterized by complex plate interactions that are yet to be fully understood. We present a new crustal and upper mantle crustal architecture model for northeastern Papua New Guinea and western New Britain that reveals complex tectonic geometries of overprinting slab subduction and partial continental subduction, resulting in a unique setting in which to investigate along-arc magmatic variation. Earthquake hypocentre databases are combined with detailed topography and seafloor structure together with geology and regional-scale gravity to unravel the sub-surface structure of northeastern Papua New Guinea. These data are used in conjunction with an updated 3-D slab map of the region to propose a new interpretation of the area whereby Australian continental crust extends as an underthrust block beneath the accreted Finisterre Terrane. The subducting continental crust combined with slab stagnation has resulted in a complex pattern of arc-related geochemical signatures from east to west along the Bismarck arc. In the east where the Solomon Sea plate is subducting beneath New Britain, the sedimentary component is low whereas in the west the arc volcanics exhibit a greater sedimentary component, consistent with subduction of Australian crustal sediments. As a result, a new plate reconstruction is provided for the region together with a forward-looking reconstruction of the Papuan peninsula, the Solomon Sea plate and New Britain that illustrates that the same process will likely be repeated in some 5–10 m.y.

Introduction

The boundary between the northern Australian plate and the Pacific plate, which includes the Bismarck Sea region of Papua New Guinea (Figure 6-1), comprises some of the youngest and most active tectonic elements of the southwest Pacific (e.g. Taylor, 1979; Abbott, 1995; Martinez and Taylor, 1996; Weiler and Coe, 2000). Northward motion of the Australian plate has led to a scenario where both continental and oceanic crust is interacting along the northern plate boundary. The complexities of present-day crustal and mantle geometries have emerged from new information and a reinterpretation of the mechanisms leading to the tectonic amalgamation of the area is required. Here we focus on just the latest 4 m.y. or so in northeastern Papua New Guinea where in this short time arc-continent collision has consumed tectonic plates and uplifted mountain ranges to more than 4000 m, neighboured by contemporary island arc magmatism, culminating in highly dynamic and striking geological landscapes. Numerous workers have sought to explain these processes of, for example, arc volcanism in the western Bismarck Sea, the source of earthquakes, or the timing and nature of arc-continent collision; however, these models lack an overarching geological model with cross-disciplinary foundations that can account for all geological phenomena.

We present a compilation and reinterpretation of an extensive catalogue of previous data, including topography/bathymetry, earthquake hypocentres, regional-scale gravity, geology and geochemistry, and models depicting the complex tectonic history of Papua New Guinea and the southwest Pacific. From this we re-evaluate and address gaps in our knowledge of the present day 3-D tectonic setting of northeast Papua New Guinea and the Bismarck Sea. Using a new and robust regional tectonic model, we assess the role of recent arc-continent collision in construction of the present-day tectonic puzzle that is Papua New Guinea.

The global importance of arc-continent collision has been addressed by several authors related to the Africa-Europe collision (e.g. Rosenbaum et al., 2002; Kley and Voigt, 2008) or the India-Asia collision (e.g. Hendrix et al., 1994; Sobel and Dumitru, 1997; Najman et al., 2010), however, the southwest Pacific offers the unique opportunity to observe the process in action. Furthermore, recognition of the subtle processes and mechanisms of collision that are not apparent at the surface, such as crustal underthrusting and associated arc magmatism, will contribute to our understanding of collision events and terrane accretion at ancient convergent margins.

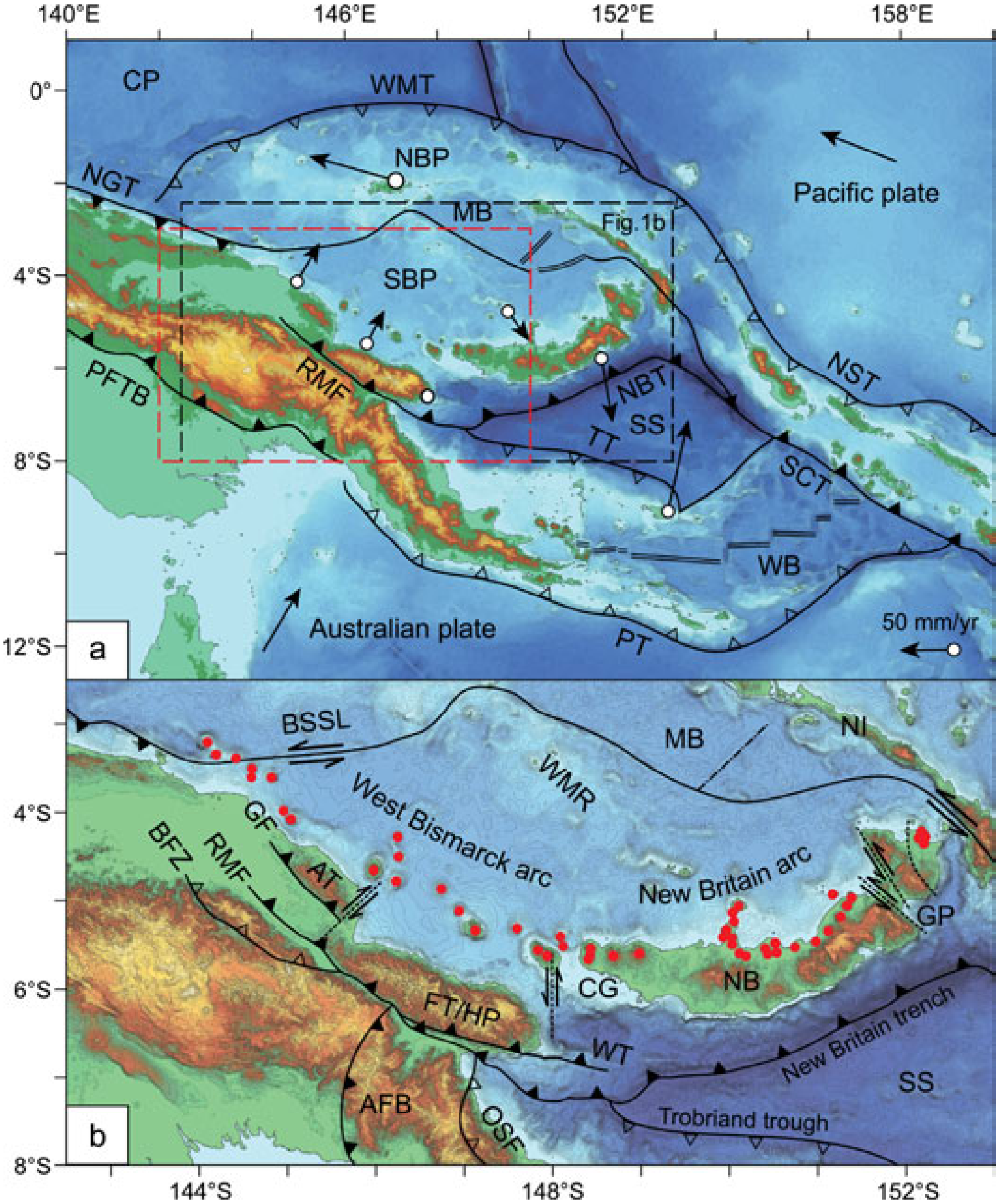

Figure 6-1 Topography, bathymetry and major tectonic elements of the Bismarck Sea region. a) Major tectonic boundaries of Papua New Guinea and the western Solomon Islands; CP, Caroline plate; MB, Manus Basin; NBP, North Bismarck plate; NBT, New Britain trench; NGT, New Guinea trench; NST, North Solomon trench; PFTB, Papuan Fold and Thrust Belt; PT, Pocklington trough; RMF, Ramu-Markham Fault; SBP, South Bismarck plate; SCT, San Cristobal trench; SS, Solomon Sea plate; TT, Trobriand trough; WB, Woodlark Basin; WMT, West Melanesian trench. Study area is indicated by rectangle; red inset rectangle highlights location for subsequent figures. Present day GPS motions of plates are indicated (from Tregoning et al., 1998, 1999; Tregoning, 2002; Wallace et al., 2004). b) Detailed topography, bathymetry and structural elements significant to the South Bismarck region (terms not in common use are referenced); AFB, Aure Fold Belt (Davies, 2012); AT, Adelbert Terrane (e.g. Wallace et al., 2004); BFZ, Bundi Fault Zone (Abbott, 1995); BSSL, Bismarck Sea Seismic Lineation; CG, Cape Gloucester; FT, Finisterre Terrane; GF, Gogol Fault (Abbott, 1995); GP, Gazelle Peninsula; HP, Huon Peninsula; MB, Manus Basin; NB, New Britain; NI, New Ireland; OSF, Owen Stanley Fault; RMF, Ramu-Markham Fault; SS, Solomon Sea; WMR, Willaumez-Manus Rise (Johnson et al., 1979); WT, Wonga Thrust (Abbott et al., 1994); minor strike-slip faults are shown adjacent to Huon Peninsula (Abers and McCaffrey, 1994) and in east New Britain, the Gazelle Peninsula (e.g. Madsen and Lindley, 1994). Red points indicate centres of Quaternary volcanism of the Bismarck arc. Filled triangles indicate active thrusting or subduction, empty triangles indicate extinct or negligible thrusting or subduction.

Tectonic Setting

Papua New Guinea and much of the southwest Pacific occupy a zone of oblique convergence between the Australian and Pacific plates (Figure 6-1). The tectonic history of the region is significantly more complex than other arcs due to the number of recognised small plates within the region. This scenario arises from the positioning of Papua New Guinea within a regional-scale collision zone between the Australian continental crust in the south (Abbott, 1995; Hall, 2002; Davies, 2012) and the Ontong Java Plateau in the northeast (Petterson et al., 1999; Hall, 2002; Mann and Taira, 2004). The relative direction of plate convergence has resulted in development of oblique spreading centres and the formation of numerous micro-plates and associated plate boundaries. The principal tectonic elements comprising this complex zone are shown on Figure 6-1 but emphasis is placed on the Australian plate, the Finisterre Terrane (described in detail below), New Britain and the North and South Bismarck plates.

Previous research has suggested that from the Upper Oligocene to the latest Neogene, northern Papua New Guinea is marked by a series of arc-continent collisions. The youngest and most significant of these collisions resulted in the accretion of the Adelbert and Finisterre Terranes, the latter of which forms a prominent topographic high known as the Finisterre Range (Figure 6-1; Abbott et al., 1994; Abbott, 1995). Abbott et al. (1994) studied clastic sequences on the southern flanks of the Finisterre Range and concluded that the collision must have initiated at ca 3.7–3.0 Ma. The Adelbert and Finisterre Terranes are largely composed of Paleogene through to earliest Neogene volcanic arc rocks overlain by Miocene to Plio-Pleistocene limestone (Jaques and Robinson, 1977; Weiler and Coe, 2000). Collision of these terranes with Papua New Guinea is interpreted to have resulted from the closure of the Solomon Sea at the New Britain trench due to subduction-driven convergence between the Australian and South Bismarck plates (e.g. Abbott, 1995; Hill and Raza, 1999; Weiler and Coe, 2000). Oblique collision started in the west and propagated southeastwards, producing progressive thrusting and uplift of the north coast Adelbert and Finisterre Ranges (Johnson and Jaques, 1980; Abbott, 1995; Weiler and Coe, 2000).

At present, the ongoing convergence between the Finisterre Terrane and the Australian plate is accommodated by activity along the Ramu-Markham Thrust Fault (e.g. Cooper and Taylor, 1987; Abbott et al., 1994; Pegler et al., 1995). All previous studies regarding this episode of arc-continent collision have focused on the Finisterre Terrane, the uplifted and exposed upper plate. The outstanding topography of the Finisterre Range, however, only arises as the Finisterre Terrane is thrust over the former northern coastward margin of Papua New Guinea. This concept, and the nature or expanse of the now underthrust Papua New Guinea margin has only been suggested in passing by previous studies, but should be regarded as an important, although missing piece of Papua New Guinea. This statement is particularly significant given the prominence of major suture zones and structures converging with the Ramu-Markham Fault and underthrust beneath the Finisterre Terrane, for example the Owen Stanley Fault and the Aure Fold Belt (Figure 6-1).

The recent collision of the Adelbert and Finisterre Terranes is reflected in the regional tectonics of the Bismarck Sea. The inferred timing of plate coupling at 3.7 Ma (Abbott et al., 1994) is coincident with the earliest breakup and opening of the New Britain back-arc, which in turn created two new microplates, the North and South Bismarck plates (Taylor, 1979). The South Bismarck plate is currently rotating clockwise at a rate of 8°/Ma relative to Australia (Tregoning et al., 1999; Weiler and Coe, 2000; Wallace et al., 2004) while the west-northwest motion of the North Bismarck plate is similar to the Pacific plate (Tregoning et al., 1998; Wallace et al., 2004) suggesting almost complete coupling between the North Bismarck and Pacific plates (Figure 6-1). In the eastern Bismarck Sea, the East Manus spreading centre separates the North and South Bismarck Sea plates (Martinez and Taylor, 1996). However, in the western Bismarck Sea, the boundary becomes the Bismarck Sea seismic lineation, defined primarily by earthquake epicentre locations and characterized by left-lateral transform faults and associated step-over rifts (Denham, 1969; Taylor, 1979). Thus, the Manus Basin accommodates the majority of extension and rotation in the eastern part of the Bismarck Sea while in the west, the Bismarck Sea seismic lineation becomes a discrete, east–west oriented strike-slip plate boundary (Figure 6-1; Cooper and Taylor, 1987; Llanes et al., 2009).

North-dipping subduction of the Solomon Sea plate beneath New Britain, in addition to the convergence responsible for terrane accretion, has resulted in the formation of the active Bismarck volcanic arc. The arc occupies the northern part of the island of New Britain and extends to the west where it is present as a series of volcanic islands off the northwest coast of New Britain and northeast coast of the Papua New Guinea mainland where it forms the West Bismarck Arc (Figure 6-1). The composition of the volcanics centred on and around the island of New Britain range from basalt to rhyolite with typical low-K, island arc tholeiite signatures (Jakes and Gill, 1970). The compositions differ markedly in the West Bismarck arc with predominantly a medium-K character (Woodhead et al., 2010). Along-arc variation, recently been investigated by Woodhead et al. (2010), is discussed below.

Data and Data Analysis Techniques

Earthquakes

The interpretations and reconstructions presented below have been resolved using a variety of datasets combined into a single 3-D tectonic map of the region using the software GOCAD. Seismic data provides a useful indicator for active tectonic structures such as faults and subducting slabs (Figure 6-2). We utilise a combination of earthquake records including the EHB hypocentre catalogue (Engdahl et al., 1998; Engdahl, 2006) and the USGS National Earthquake Information Center (NEIC) database for the period between 1973 and 2010 (Figure 6-2). In addition, Centroid-Moment-Tensor (CMT) earthquake solutions were derived from the Harvard Global CMT database (1976–2010) and plotted within ArcScene in ArcGIS using the USGS 3D Visualizations of Earthquake Focal Mechanisms extension. The NEIC earthquake database and CMT database include all earthquakes with moment magnitude values (Mw) greater than Mw 4.5; the EHB database utilises earthquakes greater than Mw 4.3.

The earthquake hypocentre data were scrutinized using a variety of software and techniques. Initially, the data was imported into the 4DEarth model (GOCAD) where slab surface models were derived. Details of the slab model are presented below. In order to estimate earthquake abundance distributions and clustering (Figure 6-2), a simple gridding function was used to derive a map highlighting the number of earthquakes within grid cells with dimensions of 0.04 × 0.04 degrees latitude and longitude. This grid cell size allowed the minimum number of cells to be chosen without biasing towards the generation of many separate but isolated clusters or points. In addition, the use of equi-dimensional cell size removed any directional bias; therefore, the trends observed in the density distribution maps represent a true cluster orientation. The results are presented as a series of density distribution maps which are plotted for depth bins of 0–40 km, 40–100 km and 100–300 km (depths of 0–20, 20–40, 40–60, 60–80, 80–100, 100–120 and 120–140 km are shown in Figure 6-3).

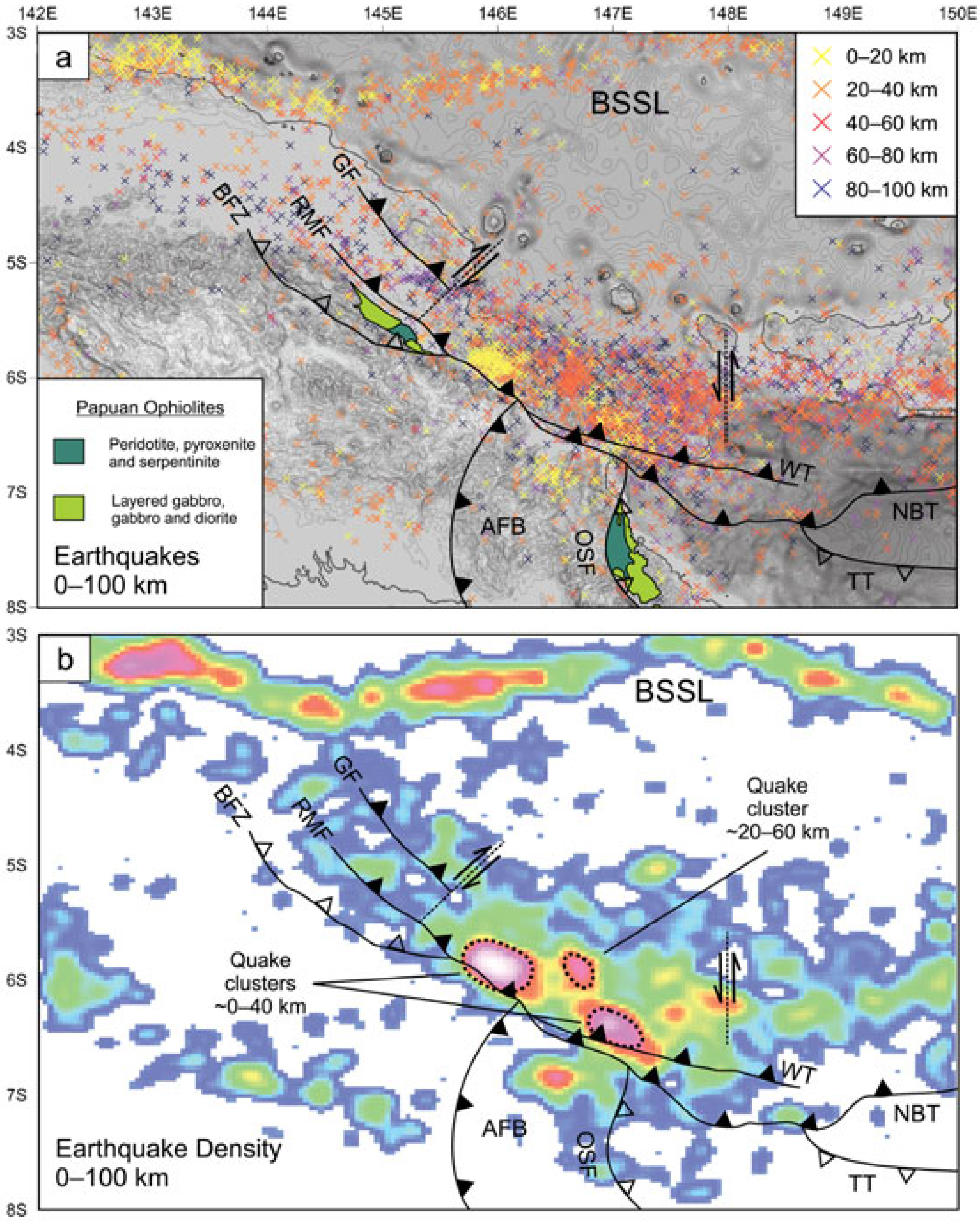

Figure 6-2 Seismicity and major structure of northwest Papua New Guinea. Earthquakes are derived from the NEIC earthquake database (1990–2010) for the 0–100 km depth bin. a) Seismicity, structure and geology of the southwest Bismarck Sea–Huon Peninsula region. Structures and labels follow Figure 6-1b; see text for discussion of geology. b) Earthquake density distribution map for the same region. Earthquake densities are contoured from high density (white) to low density (blue). We note there are high-density earthquake clusters adjacent to the point where the Bundi Fault Zone and Owen Stanley Fault intersect and underthrust the Ramu-Markham Fault.

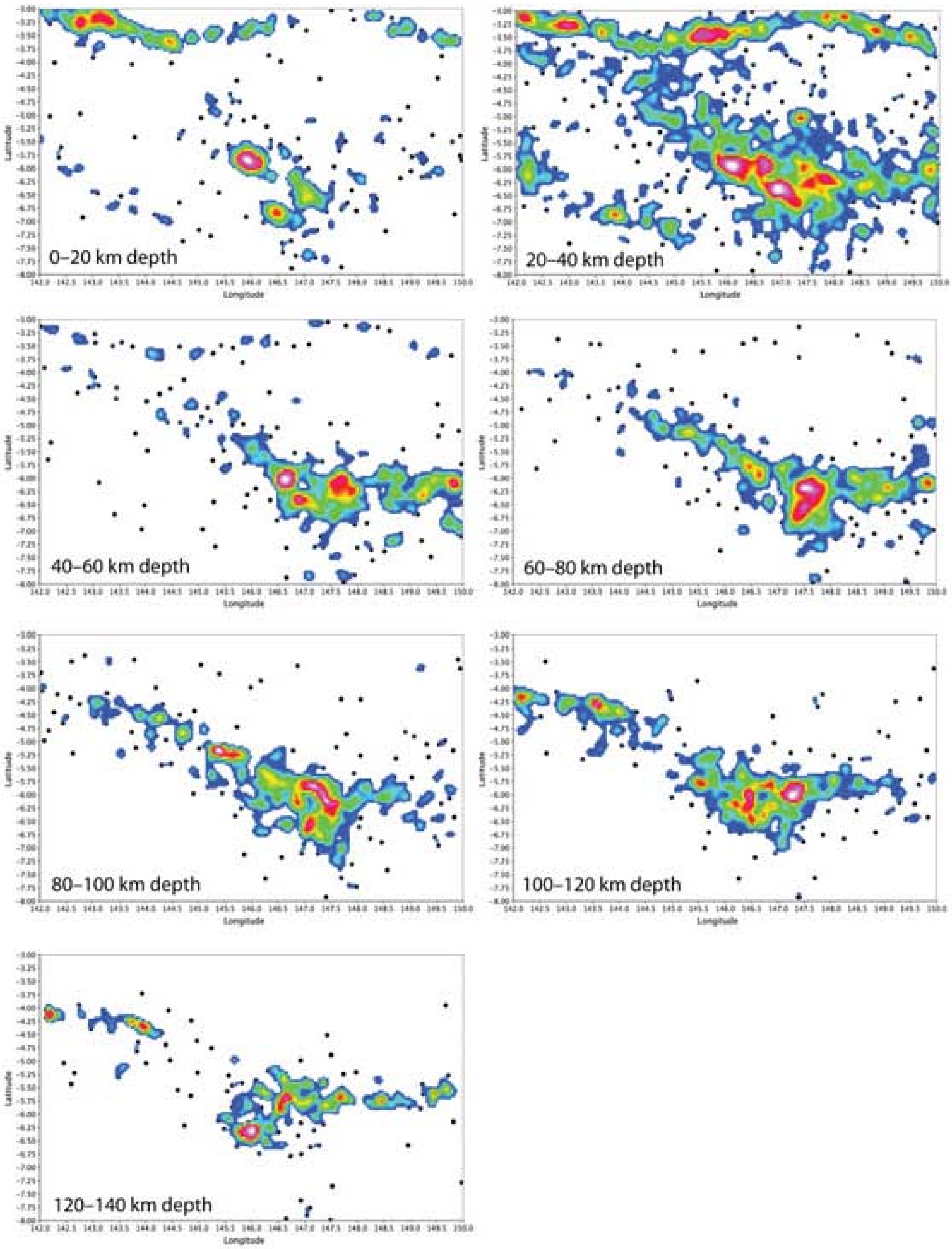

Figure 6-3. Earthquake density distribution maps for depth bins of 0–20, 20–40, 40–60, 60–80, 80–100, 100–120 and 120–140 km. Earthquake densities are contoured from high density (white) to low density (blue).

Seafloor Gravity and Topography

Seafloor gravity data for the Bismarck Sea (Figure 6-4) is sourced from the Australian Bureau of Mineral Resources (1970). The gravity model provided has been corrected for a uniform ocean thickness.

Topography and bathymetry data derived from the National Oceanic and Atmospheric Administration ETOPO1 1-minute global relief model (Amante and Eakins, 2009) provide an additional framework for correlation and interpretation.

Geochemical Data

Woodhead et al. (1998, 2010) created an extensive geochemical dataset for the New Britain and West Bismarck arcs based on new and existing geochemical data from New Britain from Johnson and Chappell (1979) and Woodhead and Johnson (1993). The majority of this geochemical data was produced for major and trace elements by X-ray fluorescence (XRF) and limited use of spark-source mass spectrography (SSMS; Johnson and Chappell, 1979; Woodhead and Johnson, 1993; and references therein). Woodhead and Johnson (1993) and Woodhead et al. (1998, 2010) used inductively coupled plasma mass spectrometry (ICPMS) and Pb, Sr, Nd and Hf isotope analyses to develop the best compilation of data for eastern Papua New Guinea. Woodhead et al. (2010) investigated along-arc geochemical changes of the Bismarck arc, and we re-evaluate this data in the context of the new tectonic model presented here.

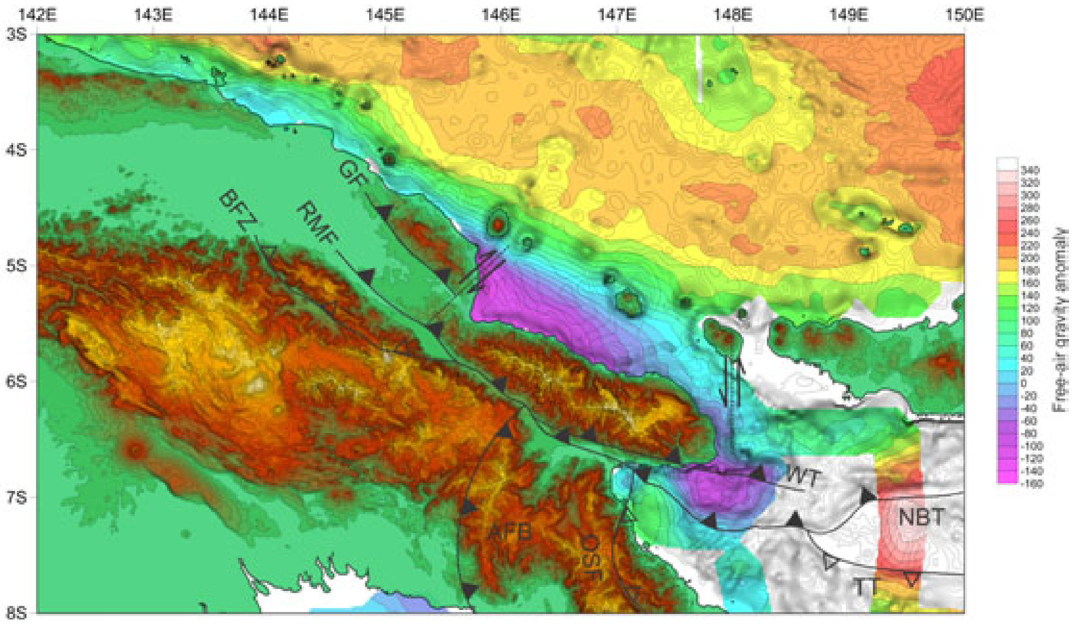

Figure 6-4 Seafloor free-air gravity anomaly map for the southwest Bismarck–Huon Peninsula region (Data from Australian Bureau of Mineral Resources, 1970).

Interpretation and Results

Subduction Zone and Slab Architecture

Previous work in the region focused on establishing an accepted plate boundary model using information such as seismicity and instantaneous GPS motions (e.g. Denham, 1969; Johnson and Molnar, 1972; Ripper, 1982; Abers and Roecker, 1991; Pegler et al., 1995; Wallace et al., 2004). It is widely accepted that multiple subduction zones have existed since the beginning of crustal amalgamation of Papua New Guinea, however the details pertaining to the geometry and type of crust subducting along the northeastern Papua New Guinea coast and western New Britain are unresolved, despite its infancy.

Construction of new 3-D subducted slab models, up to 600 km depth in the mantle, build on earlier work by O'Kane (2008). Earthquake hypocentre data (Engdahl et al., 1998; Engdahl, 2006) are primarily used to generate the 3-D models of subducted slab with all earthquakes below 100 km assumed to occur within the subducting plate (Isacks et al., 1968). The method for constructing slabs follows that outlined in Richards et al. (2007, 2011). The Global CMT database is examined in 3-D to assist in interpreting the geometry of the slab. The final interpreted slab geometry of the composite Australian plate (Solomon Sea plate, Woodlark Basin and Australian plate) subducted at the New Britain and San Cristobal trenches, and termed the Solomon slab, is presented in Figure 6-5. Miller et al. (2006) used a similar method of analysing slab geometries in conjunction with earthquake failure solutions beneath the southern Mariana Arc.

Overall, the Solomon slab exhibits a moderate dip between the surface and ~100 km depth; below this depth, the slab is steeply dipping. West of the New Britain trench-Trobriand trough triple-junction, the Solomon slab currently resides at a depth of ~100 km, and remains close to this depth until it terminates in the west beneath central Papua New Guinea. Furthermore, a north-dipping slab component is modelled in the west which extends to ~250 km depth below west New Britain and continues to the west at shallower depths (Figure 6-5), consistent with findings from Johnson and Molnar (1972), Johnson and Jaques (1980), and Abers and Roecker (1991). A restricted south-dipping slab component is also imaged but this is limited to the region adjacent to the Huon Peninsula, accounting for observations made by Ripper (1982), Cooper and Taylor (1987), Pegler et al. (1995), and Woodhead et al. (2010). The lack of a definitive modern seismic or tomographic signature for either an extensive slab at depth, or plate interface seismicity at the trench (Hall, 2002; Hall and Spakman, 2002) suggests that there is very little evidence for substantial southward subduction at the Trobriand trough (Johnson and Molnar, 1972; Johnson and Jaques, 1980; Abers and Roecker, 1991) in agreement with the slab map present here. A small tear in the slab is interpreted below the eastern margin of the Huon Peninsula; this fundamentally separates the western slab domain from the remaining Solomon slab in the east.

Adjacent to east New Britain and New Ireland, the curvature of the trench and subducted slab, and associated subduction of an originally flat oceanic crustal sheet have resulted in the development of a vertical tear in the slab (Figure 6-5); in line with findings suggested by Cooper and Taylor (1989). At present the tip of the tear terminates beneath southern New Ireland and exhibits a western and an eastern flank propagating beneath the Tabar-Lihir-Tanga-Feni arc; the western

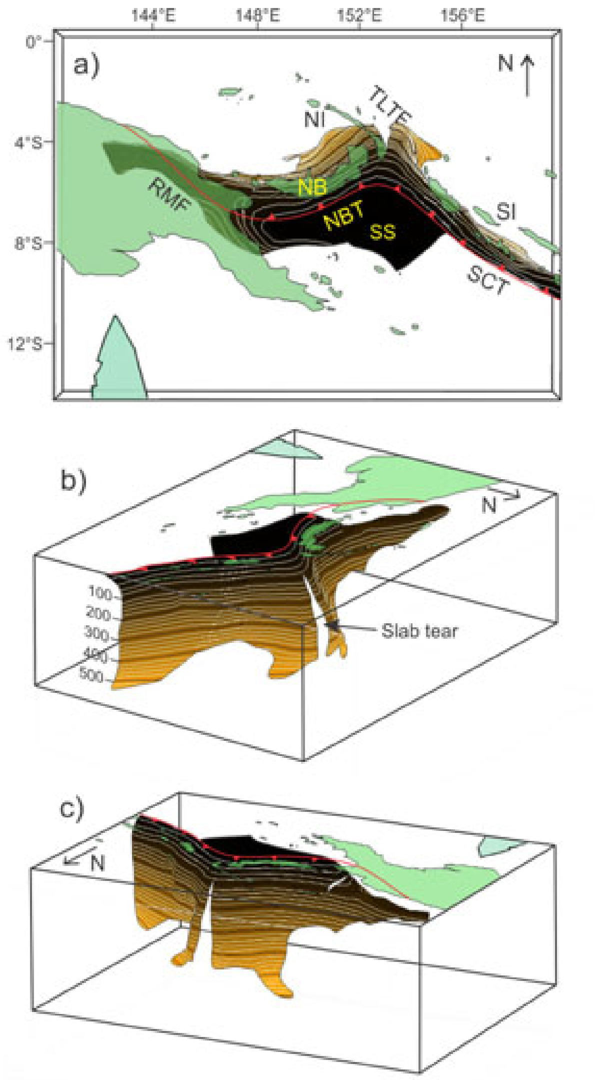

Figure 6-5 3-D model of the Solomon slab comprising the subducted Solomon Sea plate, and associated crust of the Woodlark Basin and Australian plate subducted at the New Britain and San Cristobal trenches. Depth is in kilometers; the top surface of the slab is contoured at 20 km intervals from the Earth's surface (black) to termination of slab-related seismicity at approximately 550 km depth (light brown). Red line indicates the locations of the Ramu-Markham fault (RMF)–New Britain trench (NBT)–San Cristobal trench (SCT); other major structures are removed for clarity; NB, New Britain; NI, New Ireland; SI, Solomon Islands; SS, Solomon Sea; TLTF, Tabar–Lihir–Tanga–Feni arc. See text for details.

flank propagated beneath Lihir (where the slab lies some 550 km below due to the steep dip). The tear here is significant because it provides a window where the asthenosphere can penetrate from the rear of the slab to the front. To the east, the Solomon slab is dipping beneath the Solomon Islands and reaches a maximum interpreted depth of 500 km. The subducted slab here exhibits less “structure” than the slab to the west; however, research focused on mapping the subducted extent of the Woodlark Basin rift is ongoing.

Gravity and Seismicity Correlation

At the relatively shallow sub-crustal depths (in the order of 50–100 km), upper crustal features can mask seismic tomography and earthquake distribution. We instead utilize regional seafloor gravity free-air anomaly data obtained during the 1970 Hamme Cruise (Figure 6-4; Australian Bureau of Mineral Resources, 1970) to help interpret crustal boundaries. In particular, we focus on the region adjacent to the Huon Peninsula and north coast of Papua New Guinea (Figure 6-1). Figure 6-6 presents the gravity data together with seismicity and the interpreted slab model. A large gravity-low anomaly is observed trending sub-parallel to the northern coast of Papua New Guinea defined by negative gravity values (Figure 6-4). The gravity low is particularly intense to the north of the Huon Peninsula (Davies et al., 1987; Honza et al., 1987). This anomalous gravity-low also corresponds with the location of intense seismicity beneath the Huon Peninsula at depths of between 0 and 100 km (Figure 6-6). Gravity and seismicity anomalies of the two datasets correlate extremely well suggesting a relationship between the two, to a depth of up to 100 km. This level of seismicity has been attributed to the presence of Australian lithosphere at up to 100 km depth (Pegler et al., 1995; Woodhead et al., 2010); however, this has only been explored in 2-D sections adjacent to the eastern Huon Peninsula without consideration given to the 3-D extent of the seismicity.

Figure 6-6 Gravity and seismicity correlation for the southwest Bismarck–Huon Peninsula region. All earthquakes illustrated are from the NEIC earthquake database (1990–2010) and projected on the Bismarck Sea seafloor gravity anomaly map and topography (a and c); and associated earthquake density distribution maps (b and d). a and b) gravity and seismic correlation between 40 and 100 km depth; the top surface of the slab map above 100 km depth is shown as a white shaded area (a) and area outlined in black (b). A large area of anomalously high earthquake density trending east-southeast–west-northwest and outlined by the red dashed line does not show a relationship with the defined windows for slab-related seismicity (a and b); furthermore, this anomalous seismic region correlates well with the negative (low; purple) gravity anomaly to the north of- and beneath the Huon Peninsula. We make note of the two highest density earthquake clusters; the largest in extent of the two lies at the southeast tip of the Huon Peninsula, this is a region of overlap between both the slab map and anomalous seismicity/gravity correlation implying multiple earthquake sources superimposed; the second is located at the approximate centre of the Finisterre Terrane and holds the greatest observed density, this will be discussed later. c and d) gravity and seismicity correlation between 100 and 300 km depth; the top surface of the slab below 100 km to termination is shown according to the previous description; as this surface represents the top of the slab, where the top surface is above 100 km depth, earthquakes occurring below this depth and within the slab are not atypical. Seismicity in this depth range correlates well with the outlined slab map and show little relationship with gravity anomaly trends. A zone of intense, high density seismicity is present north of the Huon Peninsula, this has previously been referred to as the “Finisterre Nest” (Abers and Roecker et al., 1991).

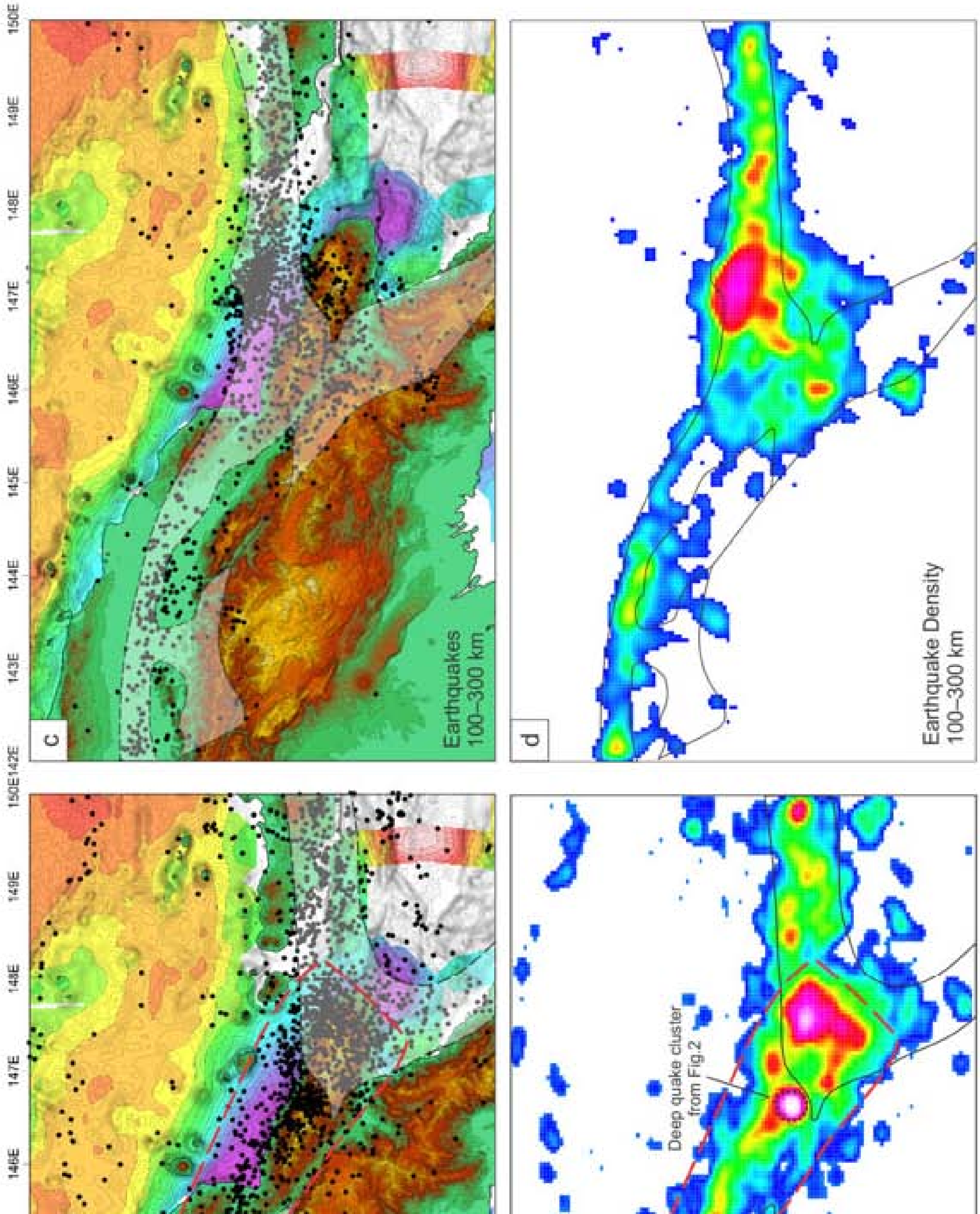
a
Earthquakes
40–100 km
b
Deep quake cluster
from Fig.2
Earthquake Density
40–100 km
c
Earthquakes
100–300 km
d
Earthquake Density
100–300 km
142E
143E
144E
145E
146E
147E
148E
149E
150E
3S
4S
5S
6S
7S
8S

An additional component of the anomalous gravity low is present to the southeast of our interpreted upper mantle crustal anomaly. This is not as seismically active as the remainder of the anomalous zone and falls within the normal bounds of slab-related seismicity for the region. This anomaly is also consistent with elevated bathymetry at the surface, and can therefore be attributed to thickened crust between the Ramu-Markham Fault–New Britain trench and the Wonga Thrust.

Previous Interpretations of Geochemistry

Woodhead et al. (2010) concluded that the West Bismarck and New Britain arcs are both "typical" subduction-related volcanic arcs, and although contiguous along strike, exhibit very different geochemical characteristics. The arc was divided into two parts, the West Bismarck arc and New Britain arc with the line separating the two drawn between the western-most volcanoes of New Britain (Cape Gloucester; Langila, Aimaga, Tangi, and Gloucester) and the remainder of New Britain in the east (Woodhead et al., 2010). In the most general terms, the distinction between New Britain and West Bismarck arcs equates to a tholeiitic–calc-alkaline transition (Jakes and Gill, 1970; Woodhead et al., 1998, 2010), and may reflect underlying differences in the nature and composition of the mantle wedge or subducting plate, or the processes of mass transfer between the two, or alternatively is a consequence of collisional processes during accretion of the Adelbert and Finisterre Terranes (Woodhead et al., 2010).

Along-arc geochemical trends of elements, ratios, and isotopic variation utilising a compilation of data from both Woodhead et al. (1998, 2010) are shown in Figure 6-7. Further characteristics of this arc will be discussed below. Woodhead et al. (2010) identified important differences between the geochemistry of the two arcs. Arc lavas from the New Britain volcanic front are derived from a mantle source highly depleted in many incompatible trace elements (Woodhead et al., 1998), while the least evolved West Bismarck arc lavas generally have higher HFSE contents than the New Britain volcanic front. Extreme element depletion in the New Britain lavas is typically attributed to prior melt extraction in the back-arc Manus Basin, however, the same process does not operate to the same extent on the mantle source of the West Bismarck lavas (Woodhead et al., 1993, 2010). The Sm/La ratios (Figure 6-7), which are higher in New Britain, suggest a depleted mantle source when compared to the West Bismarck arc lavas. Furthermore, the decrease in the Sm/La ratio to the west together with a decrease in the size of volcanic edifices and eruption rate (Johnson, 1977) suggests the degree of mantle melting falls dramatically from east to west (Woodhead et al., 2010).

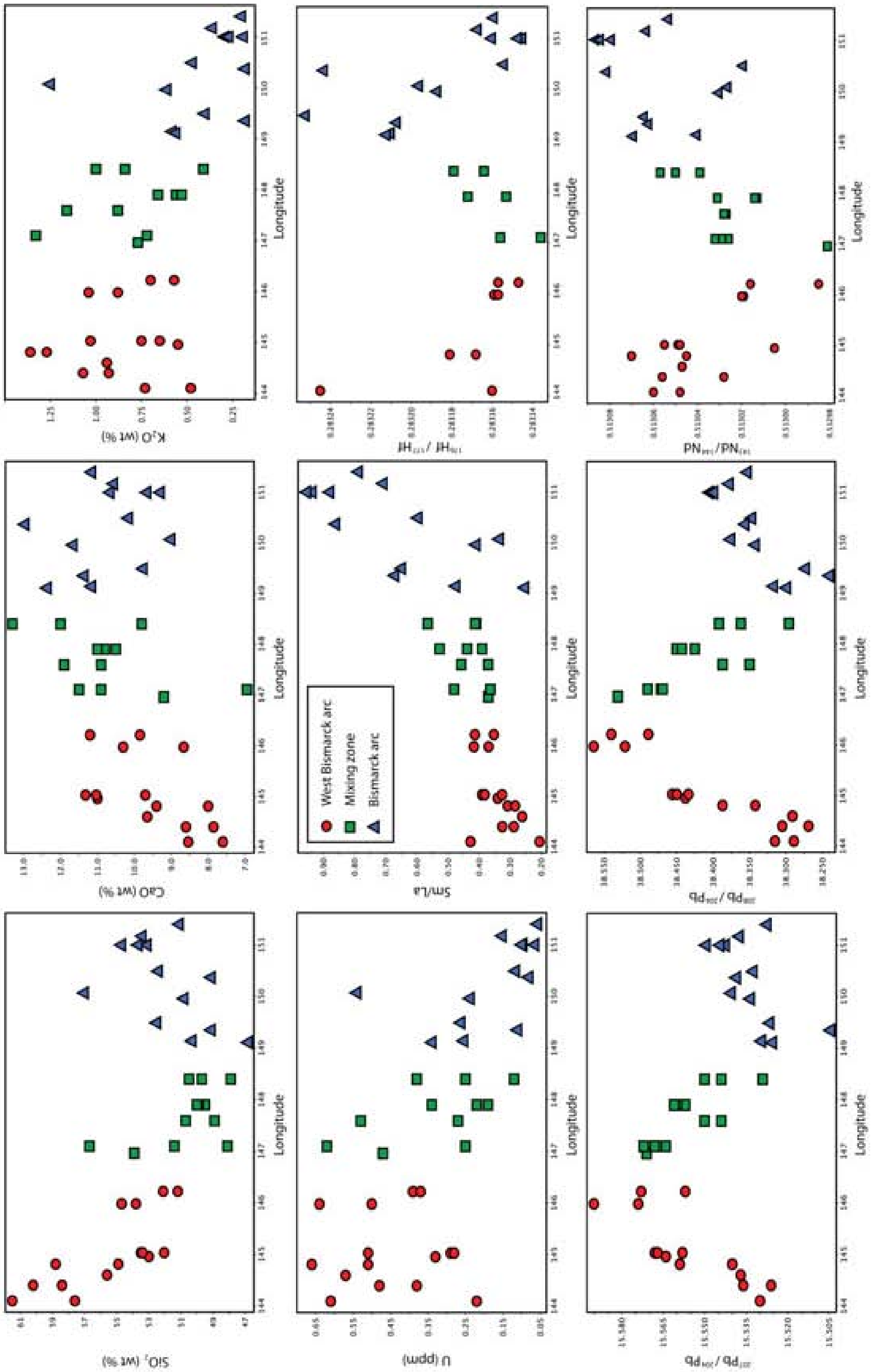

Figure 6-7 Along-arc geochemical variation in selected major and trace elements, trace element ratios, and isotopic ratios for the West Bismarck and New Britain arcs (data from Woodhead et al., 1998, 2010). See text for further discussion.

In addition, Woodhead et al. (2010) finds Th/La ratios in the West Bismarck arc are lower than that of bulk continental crust and the “average arc” (Plank, 2005) suggesting that a sedimentary component is apparent in the West Bismarck arc lavas. Woodhead et al. (2010) noted that prior to collision with the South Bismarck plate, the Australian plate likely carried high Th/La sediments derived from mainland Papua New Guinea. This is supported by the similar Th/La ratios to average sediments from the Solomon Sea (Woodhead et al., 1998), which also contain a substantial volcaniclastic input derived from the Papua New Guinea Highlands (Crook, 1987). Moreover, Pb-isotopic compositions of the West Bismarck lavas, which contain relatively radiogenic Pb compared with Manus Basin MORB (Figure 6-7), suggest a strong “crustal” signature is evident, again similar to Pb compositions found in the Solomon Sea sediments. Hafnium and Nd isotope ratios show opposite but similar trends exhibiting the highest ratio values in the New Britain arc and decreasing in the West Bismarck arc; Woodhead et al. (2010) interpreted this as a response to arc-continent collision where increased proximity to a crustal source dramatically increased the proportion of continent-derived detritus delivered to the subducting slab. These geochemical observations are important and differentiate the New Britain arc magmas, predominantly mantle derived but with a very small sedimentary component, from the West Bismarck arc where the sedimentary component is interpreted to be much greater.

Discussion

Crustal Architecture

The seismological activity or inactivity of major structures and plate boundaries should be apparent over a regional-scale, even taking into account the relatively short geological window of earthquake recording. The principal cause of seismicity in the Bismarck Sea region is subduction at the New Britain trench; this has long been recognised and accepted as the origin for shallow through to deep earthquakes. On the same regional-scale, additional earthquake trends related to major structure and plate boundary activity are those of the Bismarck Sea seismic lineation and New Guinea trench in the north and northwest, and the Papuan Fold and Thrust Belt to the southwest (Figures 6-1 and 6-2). These major tectonic structures have long been defined and are well understood. However, shallow to intermediate depth seismicity of the northeast Papua New Guinea mainland is characterized by a somewhat chaotic distribution of earthquakes (Figure 6-2). While much of the shallow seismicity has previously been correlated with upper crustal structure (Cooper and Taylor, 1987; Abers and McCaffrey, 1994; Stevens et al., 1998), it is evident that a significant proportion cannot be clearly related to any recognized structural control (Figures 6-2 and 6-6).

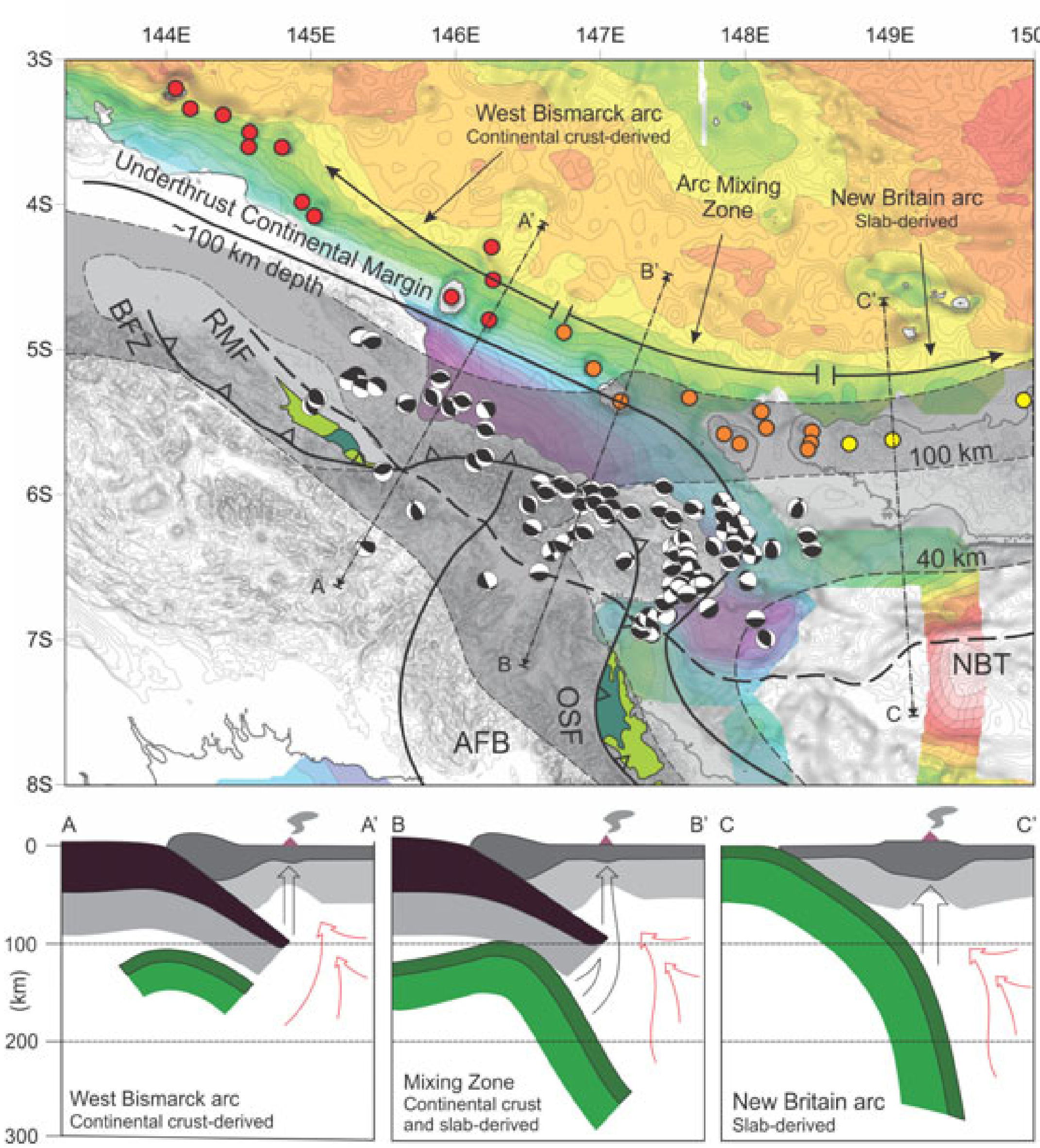

Figure 6-8 Interpretation of present day tectonic plate configuration and magmatic arc distribution in northeastern Papua New Guinea. Gravity anomaly map is provided as a base map. Bold black outlines illustrate the extent of the underthrust continental crust, formerly the leading edge of the Papua New Guinea mainland; and the associated correlation of the Bundi Fault Zone and Owen Stanley Fault in the under-thrust crust. CMT solutions are shown for the under-thrust margin between 40 and 90 km depth. Below the under-thrust margin, the distribution of subducted oceanic crust of the Solomon slab is shown for comparison, and is contoured at 40 km and 100 km until termination to the slab. The "Bismarck arc" is divided into the West Bismarck arc, New Britain arc, and mixing zone between the two; these are derived from continental crust, oceanic slab, and a combination of the two respectively. Cross sections through the plate arrangement are provided to illustrate the 3-D framework of the new plate arrangement and context of corresponding fluid sources of the equivalent magmatic arc. See text for discussion.

As presented in this study, the anomalous seismicity is focused beneath the Finisterre Terrane and immediate adjacent areas (Figures 6-2 and 6-6). This zone is defined by an uncharacteristically high abundance of earthquakes compared with “typical background” seismicity (Figure 6-6), and defines a zone extending from the surface to approximately 100 km depth beneath northeast Papua New Guinea. Furthermore, this feature correlates with a negative gravity anomaly that cannot be easily related to any near surface geological phenomena (Figure 6-4). Similar gravity lows observed adjacent to trenches are commonly interpreted as subducted low-density crust (Morales et al., 1999; Mishra et al., 2000), or alternatively, as crustal thickening and stacking of low-density crust during orogenesis (Stern, 1995; Casas et al., 1997). Both scenarios are typical of convergent margin settings much like the recent history of the Bismarck Sea region. We propose the anomalous gravity-low in combination with anomalous seismicity is the expression of a previously undefined crustal block underthrust beneath the Adelbert and Finisterre Terranes during collision with the Papua New Guinea margin. In addition, this crustal block is interpreted to be continental crust that is the underthrust and subducted leading edge of Papua New Guinea (Figure 6-8). This is significant in that the nature of the continental margin has not previously been considered in the context of the northern Papua New Guinea accreted terranes and holds implications for the dynamics of terrane collision processes. The extent of the underthrust margin is further supported by CMT solutions. These are illustrated in Figure 6-8 for between 40 and 90 km depth and highlight a regional compressional stress field orientated WNW–ESE, consistent with the trend of the underthrust margin; this regional stress distribution has previously been recognised in Australian lithosphere by Woodhead et al. (2010). At the eastern boundary of the underthrust margin we see evidence for more complex deformation occurring through translational source mechanisms and an additional dilational regime, rotated into a generally northeast–southwest orientation (Figure 6-8).

If we infer the underthrust Papua New Guinea margin is similar in extent to the margin prior to terrane accretion, we can begin to add detail to this crustal block and place it in the context of the surrounding structure and geology expressed at the surface. Within the seismic signature of the underthrust block (Figures 6-2 and 6-6) there are earthquake clusters typified by an increase in the density of seismic activity that are confined to the north side of the Ramu-Markham Fault–New Britain trench plate boundary. The regional context of these clusters, and likewise the source regions has not previously been investigated. It is clear from Figure 6-2 that these clusters are proximal to major structures; the Bundi Fault Zone, Aure Fold Belt, and Owen Stanley Fault, where the structures are currently being underthrust beneath the Finisterre Terrane at the Ramu-Markham Fault. We interpret this seismicity as possible reactivation of the former structural suture zones during their passage beneath the Finisterre Terrane. It is reasonable to assume this structure will continue to depth in the downgoing crustal block, and likewise can be defined by a similar earthquake cluster at greater depths as observed between approximately 20 and 60 km

(Figures 6-2 and 6-6). Furthermore, we propose that based on this premise, and similarities in geological context, that is, ophiolite belts of similar interpreted age adjacent to, and exhibiting analogous structural and tectonic relationships to major suture zones, that the Bundi Fault Zone and Owen Stanley Fault can be correlated as the same structural discontinuity (Figure 6-8). This provides a new context for major structures within Papua New Guinea as regionally significant suture zones rather than discrete and unrelated geological phenomena.

Along-Arc Geochemical Variation

Given the constraint provided by the new crustal architecture model presented here, we can begin to address the implications of these findings and re-evaluate current geological models of northeastern Papua New Guinea. Most significantly, we can reinterpret the geochemical signatures of the currently active New Britain and West Bismarck arcs within a robust tectonic framework. It becomes clear from the Solomon slab map that the New Britain arc is related to the Solomon slab adjacent to the island of New Britain (Figure 6-8). However, in the western Bismarck Sea, the north-dipping limb of the subducted slab is located to the south of the West Bismarck arc and beneath the accreted Finisterre and Adelbert Terranes and the Papua New Guinea mainland (Figure 6-8), spatially removed from the active West Bismarck arc. This observation immediately brings into question the relationship between the West Bismarck arc and the subducted Solomon slab proposed in previous studies. Instead, we suggest that the source of fluids and potential crustal melts is readily available in the form of the underthrust edge of Papua New Guinea crust (Figure 6-8).

The extent of the underthrust margin at depth is outlined by both gravity and seismic signatures, consistent with the interpretations of Davies et al. (1987), Honza et al. (1987) and Woodhead et al. (2010). At a depth of approximately 100 km in the mantle, the underthrust continental margin is likely to be undergoing dewatering processes and contributing fluids to the mantle wedge. Given these fluids are derived from a continental-crustal source rather than oceanic crust, this accounts for the high sediment-signature input into the magmas and comparatively reduced slab influence addressed above, in contrast to the New Britain arc in the east. This concept is further supported by the frontal edge of the underthrust margin correlating spatially with the overlying arc (Figure 6-8). Therefore, we define the New Britain and West Bismarck arc as two distinct entities with different source regions and different geochemical affinities. These two arcs are the expression of either slab-derived fluids (New Britain arc) or continental crust-derived fluids (West Bismarck arc). There is however, the added complication that the two arcs form a single, more or less morphologically continuous volcanic arc. Therefore a zone must be present where fluids derived from both subducted slab and underthrust continental crust are mixing and both contribute to arc magmatism (Figure 6-8). This model is consistent with an observed continuum in the geochemical signatures between the two arcs, transitioning from a slab signature-dominated melt in the east through to the crustal signature-dominated melt in the west (Figure 6-7). This influence of slab-derived fluids is apparent up to approximately 146.5°E at which point the slab becomes removed to the south beneath the underthrust continental margin and effectively blocked from any further contribution of fluids in the arc building process (Figure 6-8). This explains the delay in the apparent peak crustal signatures in arc geochemistry up to this point as observed by Woodhead et al. (2010).

It is also worth noting that further to the northwest along the trend of the West Bismarck arc and towards the Bismarck Sea seismic lineation we see a geochemical trend that is consistent with a return to more mantle-like signatures. We suggest the Bismarck Sea seismic lineation behaves as a leaky transform in line with findings from Llanes et al. (2009) resulting in variable continental-derived fluid contribution to arc magmatism.

Geodynamic Evolution of the Bismarck Sea

Given the regional significance of the findings outlined in this study, we propose a new plate tectonic reconstruction for the Bismarck Sea region that builds on previous reconstructions of the region (e.g. Abbott, 1995; Hill and Raza, 1999; Weiler and Coe, 2000; Hall, 2002) and incorporates the new tectonic elements introduced in this paper. Reconstructions of the Australian plate include all previously accreted terranes. GPS measurements of current, geologically instantaneous plate motions (Tregoning et al., 1998, 1999; Tregoning, 2002; Wallace et al., 2004) form the basis for this new Bismarck Sea reconstruction while the published timing for events and sea floor magnetic anomalies from Taylor (1979), Goodliffe et al. (1997), Taylor et al. (1999) and Gaina and Müller (2007) are used to infer the direction and rate of seafloor spreading. Paleomagnetic rotation data for the Finisterre Terrane from Weiler and Coe (2000) is used to further constrain reconstructions.

New reconstructions highlighting the significance of the leading Australian continental margin are shown in Figure 6-9. Between 3 and 4 Ma the Australian plate collided with the Adelbert-Finisterre Terrane, closing the western New Britain trench and forming the Ramu-Markham Fault (Abbott et al., 1994; Abbott, 1995). This is coincident with decoupling and the initial formation of the North Bismarck plate, South Bismarck plate and associated Bismarck Sea seismic lineation (Martinez and Taylor, 1996). Continued advance of the Australian plate impinging on the western South Bismarck plate resulted in the onset of clockwise rotation of the South Bismarck plate (e.g. Weiler and Coe, 2000). Furthermore, the South Bismarck plate became decoupled from the North Bismarck plate and the subducting Solomon Sea plate, allowing the South Bismarck plate to rotate freely about a pole southeast of the Finisterre Terrane (Tregoning et al., 1999). Rotation of the South Bismarck plate resulted in retreat of the New Britain trench in the east and rifting and sea-floor spreading at the Manus spreading centre from 3 Ma (Taylor, 1979; Martinez and Taylor, 1996). Fragmentation of the South Bismarck plate in response to collision with the thickened crust of the Bundi-Owen Stanley suture zone formed the independent Adelbert microplate. Right lateral offset of the Oligocene–Lower Miocene Finisterre Volcanics in the Adelbert and Finisterre Terranes is interpreted to have resulted from crustal displacement along the Adelbert microplate-South Bismarck plate boundary. Continued north-northeast motion of the Australian plate combined with clockwise rotation of the South Bismarck plate resulted in ongoing subduction of the Solomon Sea plate and initiation of rifting adjacent to the Manus spreading centre with opening the Manus microplate from ca 1 Ma (Martinez and Taylor, 1996).

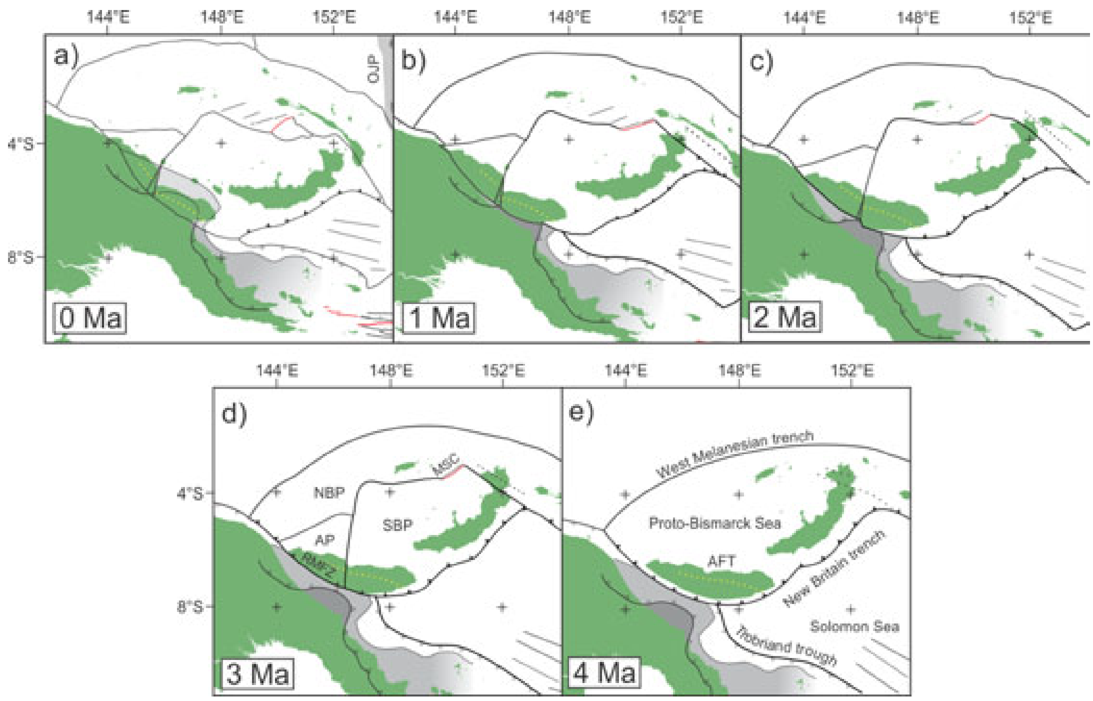

Figure 6-9 Tectonic reconstruction of the Bismarck Sea region. The inferred Papua New Guinea northeastern continental margin is shown in grey, and highlights the continuation of the Bundi–Owen Stanley suture and the seaward continental shelf; yellow dotted line represents the Finisterre Volcanics of the Adelbert and Finisterre Ranges. Magnetic isochrons and spreading centres are included for the Woodlark Basin (Taylor et al., 1999), Solomon Sea (Gaina and Müller, 2007) and Manus Basin (Taylor, 1979). Filled triangles and open triangles indicate normal and slow or extinct subduction respectively. AFT: Adelbert-Finisterre Terrane; SBP: South Bismarck Plate; NBP: North Bismarck Plate; AP: Adelbert microplate; MSC: Manus Spreading Centre; RMFZ: Ramu-Markham Fault Zone; OJP: Ontong Java Plateau. Reconstructions are presented in a fixed hot spot reference frame.

The concept of a separate Adelbert microplate, although presented here for the first time in a regional context, is not a new idea and initially arose from geological observations of the volcanic island-arc terranes in the Adelbert and Finisterre Ranges (e.g. Jaques and Robinson, 1977; Abbott et al., 1994; Wallace et al., 2004). A physical boundary between the Adelbert and Finisterre Ranges was interpreted in early mapping of cross faulting in the Finisterre Ranges (Jaques and Robinson, 1977; Abbott et al., 1994), however, dextral translational faults defined by Abers and McCaffrey (1994) (Figure 6-1) have been adopted as the Adelbert-Finisterre boundary in this study. The most apparent contrast between the Adelbert microplate and South Bismarck plate is a dramatic difference in elevation (Figure 6-1; Abbott, 1995). Abbott (1995) interpreted that the Gowop Limestone cap both the Adelbert and Finisterre Ranges and that the contrast in elevation of the Adelbert Range is due to less total uplift of the Adelbert block, and cannot be attributed to erosion in the Adelbert Range. This contrast is likely to be the result of differential plate motion with northward motion and clockwise rotation of the Adelbert microplate relative to the South Bismarck plate resulting in a lower rate of convergence with the Australian plate. Such differential motion also explains the observed offset of the Finisterre Volcanics common to both ranges (Figure 6-9; Jaques and Robinson, 1977; Abbott et al., 1994). Moreover, the nature of the continental crust underthrust beneath the Adelbert and Finisterre Terranes likely holds implications for the degree of uplift. Reconstructions show the Finisterre Terrane was forced over, and currently overlies the thickened crust of the Bundi-Owen Stanley suture zone, in contrast to the marginal continental crust beneath the Adelbert Terrane, thus resulting in reduced total uplift compared with the Finisterre Ranges. This is a new approach to explain differential uplift of the Adelbert and Finisterre Terranes where the nature and geometry of the prior continental margin, in combination with collision obliquity, controls accretion dynamics.

It is also apparent from previous reconstructions and those presented here that arc-continent collision in northeast Papua New Guinea was a consequence of oblique collision between the larger Australian and Pacific plates. This process “zipped” shut the intervening Solomon Sea between the Papua New Guinea mainland and the outboard Adelbert and Finisterre Terranes (Figure 6-9; Abbott, 1995; Hill and Raza, 1999). However, the zipping process continues to the present day along this margin, therefore, collision is considered time transgressive and will continue to migrate eastwards. Figure 6-10 presents forward-looking tectonic reconstructions where continued subduction of the Solomon Sea plate at the New Britain trench will ultimately consume the Solomon Sea leading to arc-continent collision between the Papuan Peninsula (Australian plate) and New Britain. We estimate it will take approximately 5 m.y. to consume the Solomon Sea at present plate motion rates. As in the previous instance of the Finisterre Terrane, we predict slab pull forces acting on the subducted Solomon Sea slab coupled to the Australian plate at the point of collision will lead to drawdown and underthrusting of the leading edge of continental crust. This process initiates a plate configuration where New Britain is allowed to

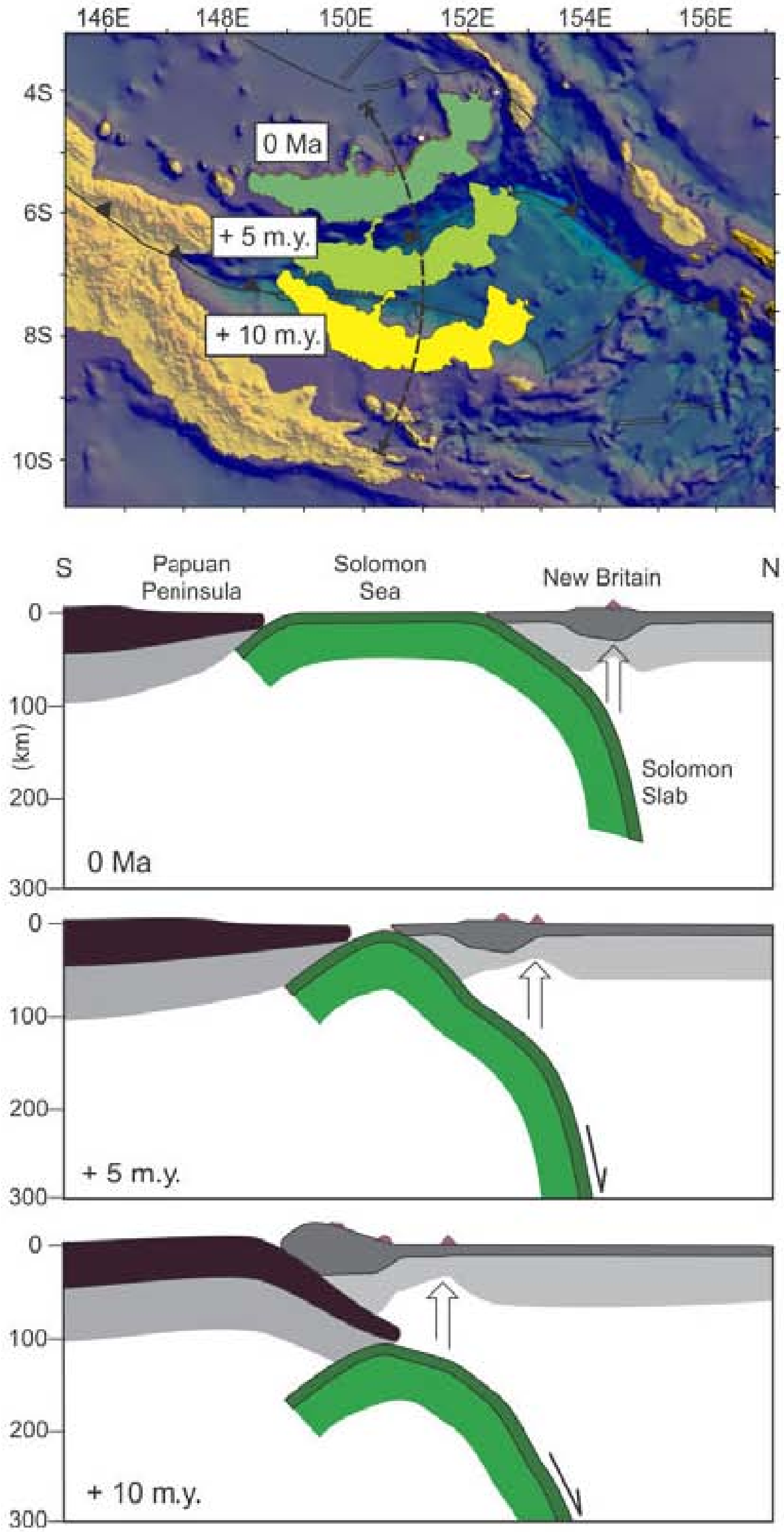

Figure 6-10 Forward tectonic reconstruction of progressive arc collision and accretion of New Britain to the Papua New Guinea margin. (a) Schematic forward reconstruction of New Britain relative to Papua New Guinea assuming continued northward motion of the Australian plate and clockwise rotation of the South Bismarck plate. (b) Cross sections illustrate a conceptual interpretation of collision between New Britain and Papua New Guinea.

overthrust the continental margin. Throughout this process we predict the apparent continual outboard migration of the associated subduction-derived magmatic arc as the accreting plate overrides the loci of slab dewatering (Figure 6-10).

The tectonic process of arc-continent accretion is not unique to the tectonic evolution of Papua New Guinea. In the geological record there are many recognised arc-continent collision episodes (e.g. Teng, 1990; Rosenbaum et al., 2002; Whattam, 2009; Najman et al., 2010), and similarly occurrences of continental crust entering a trench and failing to subduct (e.g. New Caledonia; Aitchison et al., 1995; Rawling and Lister, 2002; Spandler et al., 2005). These collision events are typically distinguished in field studies by the presence of ultra-high pressure metamorphic terranes and/or obduction of ophiolite sequences, however, these observed rock types are not present en mass in northeast Papua New Guinea, and it seems apparent that the processes of terrane accretion and partial subduction of continental crust remain active. In the distant future we can reasonably expect some exhumation of subducted continental crust will occur in line with findings in ancient arc-continent collision events. Recognizing this process in the recent geological past, and in the near future for New Britain, provides valuable insight into the dynamics and tectonic settings that give rise to such geological phenomena. Furthermore, the role of subducted continental crust as a potential source of fluids in magmatic arc generation, in this case the West Bismarck arc, is a relatively new avenue of geological research and will only occur under exceptional tectonic circumstances. Nevertheless, recognition of the expression of continental crust-derived arcs at the surface and an understanding of the tectonic events leading up to the generation of such apparent geological anomalies will be invaluable in unravelling complex tectonic regions globally.

Conclusions

We re-evaluate the tectonics of northeastern Papua New Guinea and the south Bismarck Sea region, and present a new and robust model for the 3-D architecture of the crust and upper mantle in this region. The new tectonic plate model accounts for all the observed geological phenomena including geology, geophysics, seismicity, arc geochemistry, topography, bathymetry, landscape morphology, and a newly developed slab model of crust subducted at the New Britain trench, while also drawing from studies and concepts introduced by numerous workers over decades of research. Compilation and re-evaluation of this data reveals a previously unrecognized crustal block at depth beneath the Finisterre Terrane on the northern Papua New Guinea coast, defined by anomalous seismicity and a correlative negative gravity anomaly. We interpret this as the leading edge of Australian continental crust, which has become partially subducted beneath the Adelbert and Finisterre Terranes during arc-continent collision and terrane accretion. This continental crust extends to a depth of approximately 100 km in the mantle where it is currently undergoing dewatering reactions and contributing fluids to the upper plate resulting in formation of the West Bismarck arc adjacent to the northeastern Papua New Guinea coastline. The West Bismarck arc is a distinct arc, separate from the slab-derived New Britain arc to the east, however, a mixing zone exists between the two where fluids derived from both normal subduction processes and also partially subducted continental crust are contributing to arc magmatism. In light of these findings we present a new tectonic reconstruction for the recent development of the Bismarck Sea in conjunction with a forward-looking reconstruction to highlight the role of marginal continental crust in the dynamics of arc-continent collision and accretion. Furthermore, we stress the importance of the recognition of continental crust and marginal provinces in collisional tectonic settings and their potential to contribute in arc building processes.

Chapter 7

Discussion and Summary

Late-Cenozoic geodynamic evolution of Papua New Guinea: Tectonics controlled by terrane collision and subduction trench jumps

The tectonics of Papua New Guinea and the southwest Pacific are often used as an analogue to illustrate how complex tectonic regions may have formed. However, our understanding of the geodynamic framework for much of the southwest Pacific is often insufficient to gain worthwhile insight into the relationships and feedbacks underpinning the complex plate tectonic settings, which in turn negates meaningful comparisons between the active processes in the recent geological past and those of ancient settings. Throughout this thesis I have presented multiple examples of how we can approach and unravel the complex plate tectonic settings of Papua New Guinea and the southwest Pacific through detailed studies of arc magmatism to gain further understanding of processes such as terrane collision coupled with continental subduction or underthrusting and orogenesis, and the associated subduction dynamics.

The layout of this thesis addresses the tectonic evolution of Papua New Guinea within a temporal framework from approximately 45 Ma up to the present day. Although I will not present new plate tectonic reconstructions of Papua New Guinea and the southwest Pacific as part of this thesis, this work requires that new reconstructions are considered, and remains a work in progress to be addressed in future studies. Instead, this discussion will speak to a simplified tectonic evolution of Papua New Guinea (Figure 7-1) with referral to appropriate sections within this thesis. I hope to demonstrate that formation of this part of the southwest Pacific is not the result of a series of discrete and unrelated events but is instead the consequence of several regional episodes of tectonic reorganization related to, and bounded by, major collision events resulting in a compounding chain of tectonic feedbacks. This ultimately takes place within a framework that accommodates and distributes the overall Australia-Pacific plate convergence culminating in one of the most dynamic and complex tectonic regions on Earth.

Firstly, I note that while Chapter 2 does not directly contribute to my investigation of the tectonic evolution of Papua New Guinea, it highlights developments in the methodology of dating young zircon by laser ablation ICP-MS for application in such geologically young terrains, and provides a scientific basis for the geochronological constraints utilized in the other sections.

The tectonic story begins with the initiation of convergent tectonics at the Australia-Pacific plate boundary zone from approximately 45 Ma superimposed on a tectonic setting marked by long-lived rifting and extension of the Tasman Sea that gave rise to the wider southwest Pacific. Within the Papua New Guinea region this earlier extensional regime is represented by the Coral Sea and "Pocklington Sea". With the onset of oblique convergence between the Australian and Pacific plates at 45 Ma we see the initiation of southwest-dipping subduction of the Pacific plate beneath

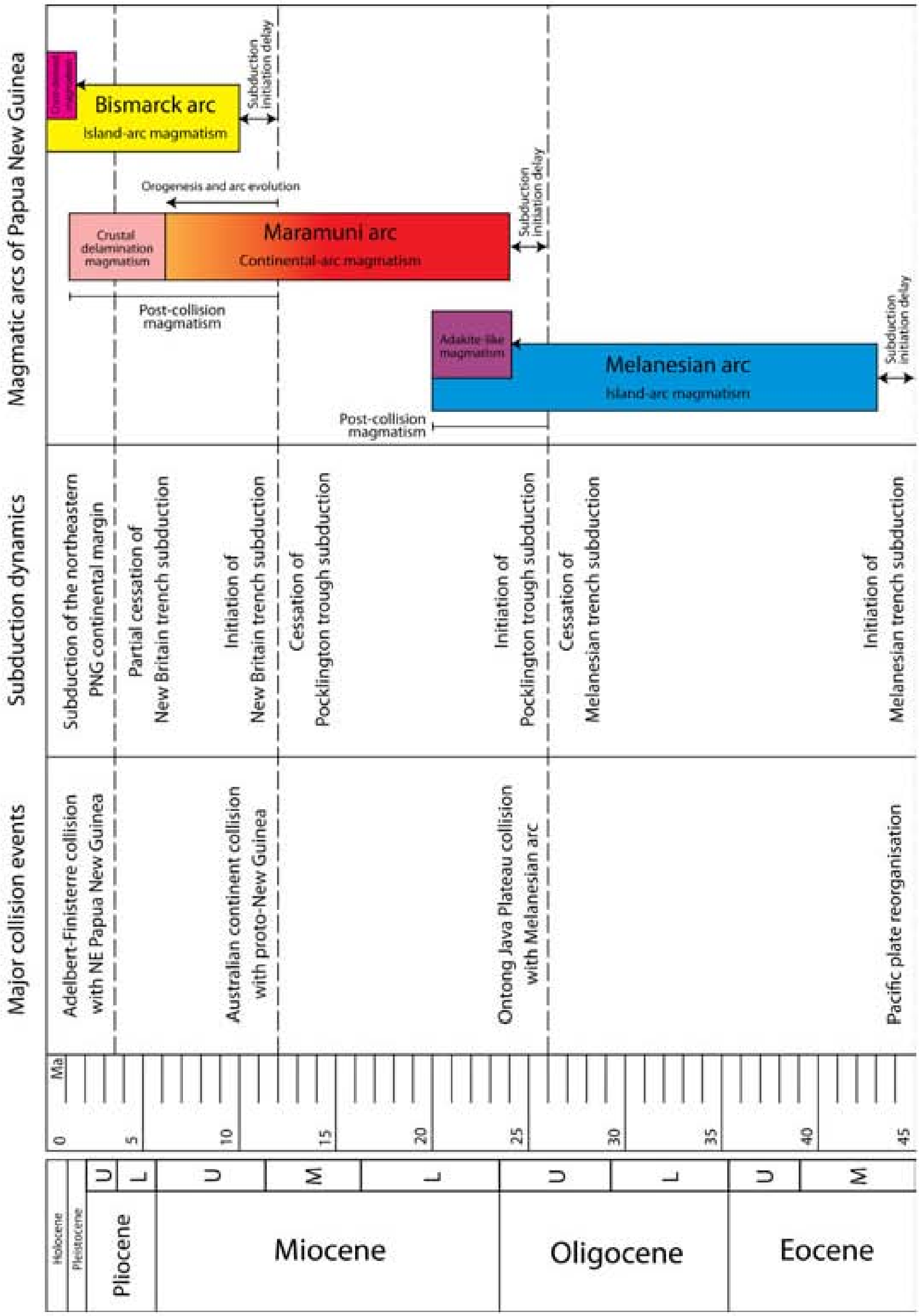

Figure 7-1. Schematic time-scale for the occurrence of major collision events, subduction dynamics and magmatism in Papua New Guinea.

the Australian plate and formation of the Melanesian trench (Figure 7-1). This period of southwest Pacific evolution is marked by convergence at the Pacific-Australia plate margin, however, with formation of the new subduction regime we see the onset of renewed extension in the southwest Pacific, likely related to slab roll-back and Melanesian trench retreat to the north and northeast. This period is marked by spreading in the Caroline Sea and Solomon Sea in the vicinity of Papua New Guinea from 45 Ma. Furthermore, with the onset of Pacific plate subduction we see the development of the Melanesian arc on the overriding Australian plate. Chapter 3 covers the dynamics and magmatism of the Melanesian arc from initiation by least 43 Ma until termination of arc activity at 20 Ma in response to arrival of the Ontong Java Plateau at the Melanesian trench and associated cessation of the subduction regime from 26 Ma.

With termination of subduction at the Melanesian trench convergence between the Pacific and Australian plates must be accommodated elsewhere. Hence we see transfer of the active plate boundary zone to the south with initiation of the Pocklington trough from approximately 26 Ma (Figure 7-1). This effectively breaks up the Australian plate into the present day Australian plate and a relict plate I will term the “Melanesian plate” to the north, encompassing a proto-New Guinea (New Guinea Mobile Belt) and the Melanesian arc terranes together with the intervening Caroline and Solomon Seas. This marks the time of an overhaul in the regional tectonic framework and ultimately constrains the wider plate boundary zone to the Melanesian plate, between the Ontong Java Plateau of the Pacific plate and the approaching Australian continent from the south. Regionally, this period reflects a shift from the mainly extensional regimes to one of convergence, highlighted by cessation of spreading in the Caroline and Solomon Seas, initiation of Australian plate subduction at the Pocklington trough, and also accretion of the North Sepik arc terranes to the northern margin of New Guinea.

Subduction at the Pocklington trough from 26 Ma gives rise to magmatism of the Maramuni arc throughout Papua New Guinea. Unlike the Melanesian arc, which essentially forms a typical island arc chain of volcanism, the Maramuni arc intrudes the New Guinea Mobile Belt, a continental ribbon that was rifted from Australia during formation of the Pocklington Sea. Activity of the Maramuni arc continues essentially undisturbed up until arrival of the Australian continent at the Pocklington trough at approximately 12 Ma. Similar to the scenario of subduction cessation at the Melanesian trench in response to arrival of the Ontong Java Plateau, we see cessation of subduction at the Pocklington trench, however, the contrasting setting of continental collision versus plateau collision results in diverse tectonic responses. This is reflected in Chapter 4 through dynamic evolution in the nature of Maramuni arc magmatism, possibly related to underthrusting of the leading Australian continental margin beneath the New Guinea Mobile Belt together with the onset of crustal shortening forming the New Guinea Orogen. The structure and morphology of the growing New Guinea Orogen is controlled by the nature of the underthrusting Australian continent and pre-existing crustal architecture as highlighted in Chapter 5. Regionally, we do see further similarities between Ontong Java collision and Australian continental collision. Once the corresponding subduction zone becomes locked, the regional convergence shifts to become accommodated elsewhere. At approximately 12 Ma the Melanesian plate is broken in two by initiation of north-dipping subduction of the Solomon Sea beneath the Melanesian arc terranes at the New Britain and San Cristobel trenches (Figure 7-1), and leading to renewed magmatism overprinting the Melanesian arc basement. Shortly after the onset of subduction at the New Britain trench, rifting and sea floor spreading is initiated in the Woodlark Basin. It is difficult to constrain the nature and timing of initial basin formation as this evidence has been removed by subduction at the San Cristobel trench; however, I consider the most likely mechanism for opening of the Woodlark Basin is a response to the new subduction regime. To further complicate this scenario, to the north of New Guinea the north-dipping New Britain subduction regime switches to south-dipping subduction at the New Guinea trench. The nature and timing of this subduction system, however, requires further constraint.

From approximately 6 million years after arrival of the Australian continent at the Pocklington trough and collision with the New Guinea Mobile Belt, we see the final expression of the Pocklington subduction system. As illustrated by Cloos et al. (2005) and further developed in Chapter 4, the subduction and underthrust segments of the Australian plate begin to break-up leading to crustal delamination beneath New Guinea at approximately 6 Ma. This is expressed at the surface by renewal of orogenesis and formation of the Papuan Fold and Thrust Belt, and also a new phase in the evolution of the Maramuni arc. At the present day there is no recorded magmatic activity in New Guinea that can be related to the Maramuni arc with the last activity associated with formation of some of the giant Papuan porphyry deposits including Grasberg at 3 Ma and Ok Tedi at 1.2 Ma.

The tectonic story of Papua New Guinea, however, does not finish with termination of the Maramuni arc. At approximately 3.5 Ma, subduction at the New Britain trench results in closure of the Solomon Sea adjacent to the north coast of the Papua New Guinea resulting in accretion of the remaining North Sepik arc terranes - the Adelbert and Finisterre Terranes - and underthrusting of the leading crustal margin of Papua New Guinea (Figure 7-1). This dynamic tectonic setting is covered in Chapter 6 and results in a unique setting of stacked subduction of both continental and oceanic crust in the mantle. At the present day the underthrust continental margin resides at approximately 100 km depth in the mantle and is undergoing dehydration reactions resulting in formation of the West Bismarck arc, distinct from the New Britain arc. Concomitant with collision of the Adelbert and Finisterre Terranes with Papua New Guinea with see another redistribution of regional tectonics, albeit on a smaller scale. Rather than the more typical relocation of suduction to accommodate the oblique convergence between the wider Australia and Pacific plates, the New Britain back-arc ruptures following lock-up of New Britain subduction creating the two distinct North Bismarck and South Bismrack plates, and the intervening Manus Basin.

Throughout the Late Cenozoic tectonic evolution of Papua New Guinea and indeed the southwest Pacific, a truly regional tectonic setting transforms into one of the most intricate and dynamic tectonic regions on Earth. From 45 Ma to the present day we see a tectonic regime that is controlled by the initiation and continuation of an overarching backdrop of oblique convergence between the Australian and Pacific plates. From an early stage we see formation of a regional tectonic setting with development of Pacific subduction coupled with formation of a regional sea-floor spreading network encompassing the Caroline Sea, Solomon Sea, Rennell trough, and South Fiji Basin. This appears quasi-stable until 26 Ma with arrival of the Ontong Java Plateau resulting in termination and disruption of the entire southwest Pacific. Subsequently, the regional tectonic setting becomes compartmentalized with termination of the spreading systems and segmentation of newly developing subduction systems. This becomes particularly evident from 12 Ma with formation of distinct tectonic domains such as the Caroline Sea-New Guinea region, the northeast Papua New Guinea-Solomon Islands domain, and the North Fiji Basin (Figure 1-1). Overall this reflects a region controlled by compounding major collision events resulting in increasing levels of tectonic complexity acting on decreasing spatial-scales. This thesis presents an insight into a relatively small area of the southwest Pacific but significantly contributes to our understanding of the dynamic Australia-Pacific plate boundary zone, and also provides new tools that we can use to unravel complex tectonic scenarios at both the present day and at ancient plate boundary settings.

References

Abbott, L.D., 1995. Neogene tectonic reconstruction of the Adelbert-Finisterre-New Britain collision, northern Papua New Guinea. Journal of Southeast Asian Earth Sciences, 11, 33–51.

Abbott, L.D., Silver, E.A., Galewsky, J., 1994. Structural evolution of a modern arc–continent collision in Papua New Guinea. Tectonics, 13, 1007–1034.

Abers, G.A., McCaffrey, R., 1994. Active arc–continent collision: Earthquakes, gravity anomalies, and fault kinematics in the Huon–Finisterre collision zone, Papua New Guinea. Tectonics, 13, 227–245.

Abers, G.A., Roecker, S.W., 1991. Deep structure of an arc–continent collision: Earthquake relocation and inversion for upper mantle P and S wave velocities beneath Papua New Guinea. Journal of Geophysical Research, 96, 6379–6401.

Aitchison, J.C., Clarke, G.L., Meffre, S., Cluzel, D., 1995. Eocene arc–continent collision in New Caledonia and implications for regional southwest Pacific tectonic evolution. Geology, 23, 161–164.

Allen, C.M., Campbell, I.H., 2012. Identification and elimination of a matrix-induced systematic error in LA-ICP-MS 206Pb/238U dating of zircon. Chemical Geology, 332–333, 157–165.

Alonso-Perez, R., Müntener, O., Ulmer, P., 2009. Igneous garnet and amphibole fractionation in the roots of island arcs: experimental constraints on andesitic liquids. Contributions to Mineralogy and Petrology, 157, 541–558.

Amante, C., Eakins, B.W., 2009. ETOPO1 1 Arc-Minute Global Relief Model: Procedures, Data Sources and Analysis. NOAA Technical Memorandum NESDIS NGDC-24.

Annen, C., Blundy, J.D., Sparks, R.S.J., 2006. The genesis of intermediate and silicic magmas in deep crustal hot zones. Journal of Petrology, 47, 505–539.

Arcay, D., Tric, E., Doin, M.-P., 2005. Numerical simulations of subduction zones: Effect of slab dehydration on the mantle wedge dynamics. Physics of the Earth and Planterary Interiors, 149, 133–153.

Arcay, D., Tric, E., Doin, M.-P., 2007. Slab surface temperature in subduction zones: Influence of the interplate decoupling depth and upper plate thinning processes. Earth and Planetary Science Letters, 255, 324–338.

Audra, P., Lauritzen, S.E., Rochette, P., 2011. Speleogenesis in the hyperkarst of the Nakanai Mountains (New Britain, Papua New Guinea). Evolution model of a juvenile system (Muruk Cave) inferred from U/Th and paleomagnetic dating. Speleogenesis and Evolution of Karst Aquifers, 10, 25–30.

Australian Bureau of Mineral Resources, 1970. Geophysical survey in Gulf of Papua; Bismarck Sea, cruise id: HAMME70, BMR survey 5.

Australian Bureau of Mineral Resources, 1972. Geology of Papua New Guinea, 1:1,000,000 map.

Australian Bureau of Mineral Resources.

Australian Bureau of Mineral Resources, 1976. Geology of Papua New Guinea, 1:2500000 scale geological map and 1:250000 geological map series, complied by: D'Addario, G.W., Dow, D.B., Swoboda, R.. Bureau of Mineral Resources, Canberra.

Australian Bureau of Mineral Resources, 1986. Geologic Map of Irian Jaya, Indonesia, 1:1,000,000 map, Australian Bureau of Mineral Resources.

Baes, M., Grovers, R., Wortel, R., 2011. Switching between alternative responses of the lithosphere to continental collision. Geophysical Journal International, 187, 1151–1174.

Baldwin, S.L., Fitzgerald, P.G., Webb, L.E., 2012. Tectonics of the New Guinea Region. Annual Review of Earth and Planetary Sciences, 40, 495–520.

Ballard, J.R., Palin, J.M., Williams, I.S., Campbell, I.H., and Faunes, A., 2001. Two ages of porphyry intrusion resolved for the super-giant Chuquicamata copper deposit of northern Chile by ELA-ICP-MS and SHRIMP. Geology, 29, 383−386.

Barbarin, B., 1999. A review of the relationships between granitoid types, their origins and their geodynamic environments. Lithos, 46, 605−626.

Barling, J., Weis, D., 2008. Influence of non-spectral matrix effects on the accuracy of Pb isotope ratio measurement by MC-ICP-MS: Implications for the external normalization method of instrumental mass bias correction. Journal of Analytical Atomic Spectrometry, 23, 1017–1025.

Bhattacharya, A.R., 2008. Basement rocks of the Kumaun-Garhwal Himalaya: Implications for Himalayan tectonics. e-Journal Earth Science India, 1, 1–10.

Bignold, S.M., Treloar, P.J., 2003. Northward subduction of the Indian Plate beneath the Kohistan island arc, Pakistan Himalaya: new evidence from isotopic data. Journal of the Geological Society, 160, 377–384.

Black, L.P., Kamo, S.L., Allen, C.M., Davis, D.W., Aleinkoff, J.N., Valley, J.W., Mudil, R., Campbell, I.H., Korsch, R.J., Williams, I.S., Foudoulis, C., 2004. Improved 206Pb/238U microprobe geochronology by the monitoring of trace-element-related matrix effect; SHRIMP, ID-TIMS, ELA-ICP-MS and oxygen isotope documentation for a series of zircon standards. Chemical Geology, 205, 115–140.

Bradley, D.C., Kidd, W.S.F., 1991. Flexual extension of the upper continental crust in collisional foredeeps. Geological Society of America Bulletin, 103, 1416–1438.

Bradshaw, M., 1992. South West Pacific Data Package, BMR-APIRA Phanerozoic History of Australia Project. Record 1992/41, Palaeogeography 43. Bureau of Mineral Resources, Geology and Geophysics, and the Petroleum Division of the Australian Mineral Industry Research Association.

Casas, A., Kearey, P., Rivero, L., Adam, C.R. 1997. Gravity anomaly map of the Pyrenean region and a comparison of the deep geological structure of the western and eastern Pyrenees.

Earth and Planetary Sciences Letters, 150, 65–78.

Castillo, P.R., Janney, P.E., Solidum, R.U., 1999. Petrology and geochemistry of Camiguin Island, southern Philippines: insights to the source of adakites and other lavas in a complex arc setting. Contributions to Mineralogy and Petrology, 134, 33–51.

Cawood, P.A., Hawkesworth, C.J., Dhuime, B., 2012. Detrital zircon record and tectonic setting. Geology, 40, 875–878.

Chadwick, J., Perfit, M., McInnes, B., Kamenov, G., Plank, T., Jonasson, I., Chadwick, C., 2009. Arc lavas on both sides of a trench: Slab window effects at the Solomon Islands triple junction, SW Pacific. Earth and Planetary Science Letters, 279, 293–302.

Chiaradia, M., 2009. Adakite-like magmas from fractional crystallization and melting-assimilation of mafic lower crust (Eocene Macuchi arc, Western Cordillera, Ecuador). Chemical Geology, 265, 468–487.

Chiaradia, M., Müntener, O., Beate, B., Fontignie, D., 2009. Adakite-like volcanism of Ecuador: Lower crust magmatic evolution and recycling. Contributions to Mineralogy and Petrology, 158, 563–588.

Chivas, A.R., 1981. Geochemical evidence for magmatic fluids in porphyry copper mineralization, Part 1. Mafic silicates from the Koloula Igneous Complex. Contributions to Mineralogy and Petrology 78, 389–403.

Christopher, P.A., 2002. Technical report on the Mt Nakru, Simuku, Sinivit, Normanby and Feni Properties, Papua New Guinea. Technical report prepared for New Guinea Gold Corporation.

Chung, S.-L., Chu, M.-F., Zhang, Y., Xie, Y., Lo, C.-H., Lee, T.-Y., Lan, C.-Y., Li, X., Zhang, Q., Wang, Y., 2005. Tibetan tectonic evolution inferred from spatial and temporal variations in post-collisional magmatism. Earth-Science Reviews, 68, 173–196.

Cloos, M., Sapiie, B., van Ufford, A.Q., Weiland, R.J., Warren, P.Q., McMahon, T.P., 2005. Collisional delamination in New Guinea: The geotectonics of subducting slab breakoff. Geological Society of America, Special Paper 400.

Cluzel, D., Bosch, D., Paquette, J., Lemennicier, Y., Montjoie, P., Ménot, R., 2005. Late Oligocene post-obduction granitoids of New Caledonia: A case for reactivated subduction and slab break-off. The Island Arc, 14, 254–271.

Collins, W.J., Richards, S.W., 2008. Geodynamic significance of S-type granites in circum-Pacific orogens. Geology, 36, 559–562.

Cooper, P.A., Taylor, B., 1985. Polarity reversal in the Solomon Islands arc. Nature, 314, 428–430.

Cooper, P., Taylor, B., 1987. Seismotectonics of New Guinea: a model for arc reversal following arc-continent collision, Tectonics, 6, 53–67.

Cooper, P., Taylor, B., 1989. Seismicity and focal mechanisms at the New Britain trench related to deformation of the lithosphere. Tectonophysics, 164, 25–40.

Corfu, F., Hanchar, J.M., Hoskin, P.W.O., Kinny P., 2003. Atlas of zircon textures, in: Hanchar, J.M., Hoskin, P.W.O. (Eds.), Reviews in Mineralogy & Geochemistry 53: Zircon. Mineralogical Society of America.

Cowley, S., Mann, P., Coffin, M.F., Shipley, T.H., 2004. Oligocene to Recent tectonic history of the Central Solomon intra-arc basin as determined from marine seismic reflection data and compilation of onland geology. Tectonophysics, 389, 267–307.

Craig, M.S., Warvakai, K., 2009. Structure of an active foreland fold and thrust belt, Papua New Guinea. Australian Journal of Earth Sciences, 56, 719–738.

Crook, K.A., 1987. Petrology and mineral chemistry of sedimentary rocks from the western Solomon Sea. Geo-Marine Letters, 6, 203–209.

Crowhurst, P.V., Hill, K.C., Foster, D.A., Bennett, A.P., Thermochronological and geochemical constraints on the tectonic evolution of northern Papua New Guinea. Geological Society, London, Special Publications, 106, 525–537.

Crowhurst, P.V., Maas, R., Hill, K.C., Foster, D.A., Fanning, C.M., 2004. Isotopic constraints on crustal architecture and Permo-Triassic tectonics in New Guinea: possible links with eastern Australia. Australian Journal of Earth Sciences, 51, 107–122.

Crowley, J.L., Schoene, B., Bowring, S.A., 2007. U-Pb dating of zircon in the Bishop Tuff at the millennial scale. Geology, 35, 1123–1126.

Davey, F.J., 1982. The structure of the South Fiji Basin. Tectonophysics, 87, 185–241.

Davidson, J., Turner, S., Handley, H., Macpherson, C., Dosseto, A., 2007. Amphibole "sponge" in arc crust? Geology, 35, 787–790.

Davies, H.L., 1990. Structure and evolution of the border region of New Guinea. In: Carman, G.J., Carman, Z. (Eds.), Petroleum Exploration in Papua New Guinea. Proceedings of the First PNG Petroleum Convention, PNG Chamber of Mines and Petroleum, Port Moresby, 245–269.

Davies, H.L., 2012. The geology of New Guinea – the cordilleran margin of the Australian continent. Episodes, 35, 87–102.

Davies, H.L., Lock, J., Tiffin, D.L., Honza, E., Okuda, Y., Murakami, F., Kisimoto, K. 1987. Convergent tectonics in the Huon Peninsula region, Papua New Guinea. Geo-Marine Letters, 7, 143–152.

Davies, H.L., Symmonds, P.A., Ripper, I.D., 1984. Structure and evolution of the southern Solomon Sea region. BMR Journal of Australian Geology and Geophysics, 9, 49–68.

Davies, J.H., von Blanckenburg, F., 1995. Slab breakoff: A model of lithosphere detachment and its test in the magmatism and deformation of collisional orogens. Earth and Planetary Science Letters, 129, 85–102.

DeBari, S.M., Sleep, N.H., 1991. High-Mg, low-Al bulk composition of the Talkeetna island arc, Alaska: Implications for primary magmas and the nature of arc crust. Geological Society of America Bulletin, 103, 37–47.

de Boer, J.Z., Drummond, M.S., Bordelon, M.J., Defant, M.J., Bellon, H., Maury, R.C., 1995. Cenozoic magmatic phases of the Costa Rican island arc (Cordillera de Talamanca). In: Mann, P. ed. Geologic and tectonic development of the Caribbean plate boundary in southern Central America. Geological Society of America Special Paper 295, Pp. 35–55.

Defant, M.J., Drummond, M.S., 1990. Derivation of some modern arc magmas by melting of young subducted lithosphere. Nature, 347, 662–665.

Denham, D., 1969. Distribution of Earthquakes in the New Guinea–Solomon Islands region. Journal of Geophysical Research, 74, 4290–4299.

DePaolo, D.J., 1981. Trace element and isotopic effects of combined wallrock assimilation and fractional crystallization. Earth and Planetary Science Letters, 53, 189–202.

Doglioni, C., 1995. Geological remarks on the relationships between extension and convergent geodynamic settings. Tectonophysics, 252, 253–267.

Drummond, M.S., Defant, M.J., 1990. A model for trondhjemite-tonalite-dacite genesis and crustal growth via slab melting; Archean to modern comparisons. Journal of Geophysical Research, 95, 21503–21521.

Dufek, J., Bergantz, G.W., 2005. Lower crustal magma genesis and preservation: A stochastic framework for the evaluation of basalt-crust interaction. Journal of Petrology, 46, 2167–2195.

Elburg, M.A., van Bergen, M., Hoogewerff, J., Foden, J., Vroon, P., Zulkarnain, I., Nasution, A., 2002. Geochemical trends across an arc-continent collision zone: magma sources and slab-wedge transfer processes below the Pantar Strait volcanoes, Indonesia. Geochimica et Cosmochimica Acta, 66, 2771–2789.

Elliott, T., Plank, T., Zindler, A., White, W., Bourdon, B., 1997. Element transport from slab to volcanic front at the Mariana arc. Journal of Geophysical Research, 102, 14991–15019.

Engdahl, E.R., 2006. Application of an improved algorithm to high precision relocation of ISC test events. Physics of the Earth and Planetary Interiors, 158, 14–18.

Engdahl, E.R., van der Hilst, R., Buland, R., 1998. Global teleseismic earthquake relocation with improved travel times and procedures for depth determination. Bulletin of the Seismological Society of America, 88, 722.

Eyuboglu, Y., Santosh, M., Yi, K., Bektaş, O., Kwon, S., 2012. Discovery of Miocene adakitic dacite from the Eastern Pontides Belt (NE Turkey) and a revised geodynamic model for the late Cenozoic evolution of the Eastern Mediterranean region. Lithos, 146-147, 218–232.

Falloon, T.J., Danyushevsky, L.V., Crawford, A.J., Meffre, S., Woodhead, J.D., Bloomer, S.H., 2008. Boninites and adakites from the northern termination of the Tonga trench: implications for adakite petrogenesis. Journal of Petrology, 49, 697–715.

Feeley, T.C., Davidson, J.P., 1994. Petrology of calc-alkaline lavas at Volcán Ollagüe and the origin of compositional diversity at Central Andean stratovolcanoes. Journal of Petrology, 35, 1295–1340.

Finch, R.J., Hanchar, J.M., Hoskin, P.W.O., Burns, P.C., 2001. Rare-earth elements in synthetic zircon: Part 2. A single-crystal X-ray study of xenotime substitution. American Mineralogist, 86, 681–689.

Findlay, R.H., 2003. Collision tectonics of northern Papua New Guinea: key field relationships demand a new model. In: Hillis, R. R., Müller, R. D. (Eds.), Evolution and Dynamics of the Australian Plate. Geological Society of Australia Special Publication 22 and Geological Society of America Special Paper 372. Pp. 291–308.

Finlayson, D.M., Cull, J.P., 1973. Structural profiles in the New Britain/New Ireland region. Journal of the Geological Society of Australia, 20, 37–48.

Fujiwara, T., Tamaki, K., Fujimoto, H., Ishii, T., Seama, N., Toh, H., Koizumi, K., Igarashi, C., Segawa, J., Kobayashi, K., Kido, M., Seno, T., Kinoshita, H., 1995. Morphological studies of the Ayu Trough, Philippine Sea – Caroline Plate boundary. Geophysical Research Letters, 22, 109–112.

Gaina, C., Müller, D., 2007. Cenozoic tectonic and depth/age evolution of the Indonesian gateway and associated back-arc basins, Earth-Science Reviews, 83, 177–203.

Garrido, C.J., Bodinier, J.-L., Burg, J.-P., Zeilinger, G., Hussain, S.S., Dawood, H., Chaudhry, M.N., Gervilla, F., 2006. Petrogenesis of mafic garnet granulite in the lower crust of the Kohistan paleo-arc complex (northern Pakistan): Implications for intra-crustal differentiation of island arcs and generation of continental crust. Journal of Petrology, 47, 1873–1914.

Gerya, T.V., Yuen, D.A., Maresch, W.V., 2004. Thermomechanical modeling of slab detachment. Earth and Planetary Science Letters, 226, 101–116.

Glen, R.A., 2005. The Tasmanides of eastern Australia. In: Vaughan, A.P.M., Leat, P.T., Pankhurst, R.J. (Eds.), Terrane Processes at the Margins of Gondwana. Geological Society, London, Special Publications 246, 23–96.

Glen, R.A., Walshe, J.L., 1999. Cross-structures of the Lachlan orogen: the Lachlan transverse zone example. Australian Journal of Earth Sciences, 46, 641–658.

Goodliffe, A.M., Taylor, B., Martinez, F., Hey, R., Maeda, K., Ohno, K. 1997. Synchronous reorientation of the Woodlark Basin Spreading Center. Earth and Planetary Science Letters, 146, 233–242.

Grant, J.N., Nielsen, R.L., 1975. Geology and geochronology of the Yandera Porphyry Copper Deposit, Papua New Guinea. Economic Geology, 70, 1157–1174.

Guillong, M., Horn, I., Günther, D., 2003. A comparison of 266 nm, 213 nm and 193 nm produced from a single solid state Nd:YAG laser for laser ablation ICP-MS. Journal of Analytical Atomic Spectrometry, 18, 1224-1230.

Guo, Z., Wilson, M., Liu, J., 2007. Post-collisional adakites in south Tibet: Products of partial melting of subduction-modified lower crust. Lithos, 96, 205–224.

Gutscher, M.,-A., Spakman, W., Bijwaard, H., Engdahl, E.R., 2000. Geodynamics of flat subduction: Seismicity and tomographic constraints from the Andean margin. Tectonics, 19, 814–833.

Hall, R., 2002. Cenozoic geological and plate tectonic evolution of SE Asia and the SW Pacific: computer-based reconstructions, model and animations, Journal of Asian Earth Sciences, 20, 353–431.

Hall, R., Spakman, W., 2002. Subducted slabs beneath the eastern Indonesia–Tonga region: insights from tomography. Earth and Planetary Science Letters, 201, 321–336.

Hall, S., Riisager, P., 2007. Palaeomagnetic palaeolatitudes of the Ontong Java Plateau from 120 to 55 Ma: Implications for the apparent polar wander path of the Pacific Plate. Geophysical Journal International, 169, 455–470.

Hamilton, W., 1979. Tectonics of the Indonesian Region. United States Geological Survey Professional Paper, 1078, 293–304.

Hamilton, W.B., 1981. Crustal evolution by arc magmatism. Philosophical Transactions, Royal Society of London, A 301, 279–291.

Harris, A.C., Allen, C.M., Bryan, S.E., Campbell, I.H., Holcombe, R.J., Palin, J.M., 2004. ELA-ICP-MS U-Pb zircon geochronology of regional volcanism hosting the Bajo de la Alumbrera Cu-Au deposit: implications for porphyry related mineralization. Mineralium Deposita, 39, 46–67, doi:10.1007/s00126-003-0381-0.

Harris, A.C., Dunlap, W.J., Reiners, P.W., Allen, C.M., Cooke, D.R., White, N.C., Campbell, I.H., Golding, S.D., 2008. Multimillion year thermal history of a porphyry copper deposit: Application of U-Pb, 40Ar/39Ar and (U-Th)/He chronometers, Bajo de la Alumbrera copper-gold deposit, Argentina. Mineralium Deposita, 43, 295–314.

Heaman, L.M., Bowins, R., Crocket, J., 1990. The chemical composition of igneous zircon suites: Implications for geochemical tracer studies. Geochimica et Cosmochimica Acta, 54, 1597–1607.

Hendrix, M.S., Dumitru, T.A., Graham, S.A., 1994. Late Oligocene–early Miocene unroofing in the Chinese Tian Shan: An early effect of the India–Asia collision. Geology, 22, 487–490.

Heuret, A., Lallemand, S., 2005. Plate motions, slab dynamics and back-arc deformation. Physics of the Earth and Planetary Interiors, 149, 31–51.

Hidalgo, P.J., Vogel, T.A., Rooney, T.O., Currier, R.M., Layer, P.W., 2011. Origin of silicic volcanism in the Panamanian arc: evidence for a two-stage fractionation process at El Valle volcano. Contributions to Mineralogy and Petrology, 162, 1115–1138.

Hildreth, W., Moorbath, S., 1988. Crustal contributions to arc magmatism in the Andes of central Chile. Contributions to Mineralogy and Petrology, 98, 455–489.

Hill, K.C., 1991. Structure of the Papuan fold belt, Papua New Guinea. American Association Petroleum Geologists Bulletin, 75, 857–872.

Hill, K.C., Gleadow, A.J.W., 1989. Uplift and thermal history of the Papuan Fold Belt, Papua New

Guinea: Apatite fission track analysis. Australian Journal of Earth Sciences, 36, 515–539.

Hill, K.C., Hall, R., 2003. Mesozoic-Cenozoic evolution of Australia's New Guinea margin in a west Pacific context. In: Hillis R.R., Müller, R.D. (Eds.) Evolution and Dynamics of the Australian Plate: Geological Society of Australia Special Publication 22, and Geological Society of America Special Paper, 372, 265–290.

Hill, K.C., Kendrick, R.D., Crowhurst, P.V., Gow, P.A., 2002. Copper-gold mineralisation in New Guinea: tectonics, lineaments, thermochronology and structure. Australian Journal of Earth Sciences, 49, 737–752.

Hill, K.C., Raza, A., 1999. Arc–continent collision in Papua Guinea: Constraints from fission track thermochronology. Tectonics, 18, 950–966.

Hine, R., Mason, D.R., 1978. Intrusive rocks associated with porphyry copper mineralization, New Britain, Papua New Guinea. Economic Geology, 73, 749–760.

Hobson, D.M., 1986. A thin-skinned model for the Papuan thrust belt and some implications for hydrocarbon exploration. Australian Petroleum Production and Exploration Association Journal, 26, 214–224.

Holm, R.J., Richards, S.W., 2013. A re-evaluation of arc-continent collision and along-arc variation in the Bismarck Sea region, Papua New Guinea. Australian Journal of Earth Sciences, Accepted.

Holm, R.J., Spandler, C., Richards, S.W., 2013. Melanesian arc far-field response to collision of the Ontong Java Plateau: Geochronology and pertrogenesis of the Simuku Igneous Complex, New Britain, Papua New Guinea. Tectonophysics, In Press.

Honza, E., Davies, H.L., Keene, J.B., Tiffin, D.L., 1987. Plate boundaries and evolution of the Solomon Sea region. Geo-Marine Letters, 7, 161–168.

Horn, I., Rudnick, R.L., McDonough, W.F., 2000. Precise elemental and isotope ratio measurement by simultaneous solution nebulisation and laser ablation-ICP-MS: Application to U-Pb geochronology. Chemical Geology, 164, 281–301.

Hoskin, P.W.O., Schaltegger, U., 2003. The composition of zircon and igneous and metamorphic petrogenesis, in: Hanchar, J.M., Hoskin, P.W.O. (Eds.), Reviews in Mineralogy & Geochemistry 53: Zircon. Mineralogical Society of America.

Hou, Z., Tian, S., Yuan, Z., Xie, Y., Yin, S., Yi, L., Fei, H., Yang, Z., 2006. The Himalayan collision zone carbonatites in western Sichuan, SW China: Petrogenesis, mantle source and tectonic implication. Earth and Planetary Science Letters, 244, 234–250.

Hutchinson, D., Swiridiuk, P., 2006. Simuku Property: West New Britain Province, Papua New Guinea. Technical Report to New Guinea Gold Corporation.

Isacks, B., Oliver, J., Sykes, L.R., 1968. Seismology and the new global tectonics. Journal of Geophysical Research, 73, 5855–5899.

Jackson, S.E., Pearson, N.J., Griffin, W.L., Belousova, E.E., 2004. The application of laser ablation-inductively coupled plasma-mass spectrometry to in situ U-Pb zircon geochronology. Chemical Geology 211, 47–69.

Jaffey, A.H., Flynn, K.F., Glendenin, L.E., Bentley, W.C., Essling, A.M., 1971. Precision measurement of half-lives and specific activities of 235U and 238U. Physical Review C, 4, 1889–1906.

Jakes, P., Gill, J., 1970. Rare earth elements and the island arc tholeiitic series. Earth and Planetary Science Letters, 9, 17–28.

Jakes, P., White, A.J.R., 1969. Structure of the Melanesian arcs and correlation with distribution of magma types. Tectonophysics, 8, 223.

Jaques, A.L., Robinson, G.P., 1977. The continent–island arc collision in northern Papua New Guinea. BMR Journal of Australian Geology and Geophysics, 2, 289–303.

Johnson, R.W., 1977. Distribution and major element chemistry of late Cenozoic volcanoes at the southern margin of the Bismarck Sea, Papua New guinea. Australian Bureau of Mineral Resources Report, vol. 188.

Johnson, R.W., Chappell, B.W., 1979. Chemical analyses of rocks from the late Cenozoic volcanoes of north-central New Britain and the Witu Islands, Papua New Guinea. Australian Bureau of Mineral Resources Report, vol. 209.

Johnson, R.W., Jaques, A.L., 1980. Continent–arc collision and reversal of arc polarity: new interpretations from a critical area. Tectonophysics, 63, 111–124.

Johnson, R.W., Mackenzie, D.E., Smith, I.E.M., 1978. Delayed partial melting of subduction-modified mantle in Papua New Guinea. Tectonophysics, 46, 197–216.

Johnson, R.W., Mutter, J.C., Arculus, R.J., 1979. Origin of the Willaumez-Manus Rise, Papua New Guinea. Earth and Planetary Science Letters, 44, 247–260.

Johnson, T., Molnar, P., 1972. Focal mechanisms and plate tectonics of the southwest Pacific. Journal of Geophysical Research, 77, 5000–5032.

Kay, R.W., 1978. Aleutian magnesian andesites: Melts from subducted Pacific ocean crust. Journal of Volcanology and Geothermal Research, 4, 117–132.

Kay, S.M., Godoy, E., Kurtz, A., 2005. Episodic arc migration, crustal thickening, subduction erosion, and magmatism in the south-central Andes. GSA Bulletin, 117, 67–88.

Kay, S.M., Mpodozis, C., Coira, B., 1999. Neogene magmatism, tectonism, and mineral deposits of the Central Andes (22° to 33°S latitude). Society of Economic Geologists, Special Publication 7, 27–59.

Klepeis, K.A., Clarke, G.L., Rushmer, T., 2003. Magma transport and coupling between deformation and magmatism in the continental lithosphere: GSA Today, 13, 4–11.

Kley, J., Monaldi, C.R., Salfity, J.A., 1999. Along-strike segmentation of the Andean foreland: causes and consequences. Tectonophysics, 301, 75–94.

Kley, J., Voigt, T., 2008. Late Cretaceous intraplate thrusting in central Europe: Effect of Africa–

Iberia–Europe convergence, not Alpine collision. Geology, 36, 839–842.

Klötzli, U., Klötzli, E., Günes, Z., Koštler, J., 2009. Accuracy of laser ablation U–Pb zircon dating: results from a test using five different reference zircons. Geostandards Geoanalytical Research, 33, 5–15.

Knesel, K.M., Cohen, B.E., Vasconcelos, P.M., Thiede, D.S., 2008. Rapid change in drift of the Australian plate records collision with Ontong Java plateau. Nature, 454, 754–757.

Košler, J., Fonneland, H., Sylvester, P., Tubrett, M., Pedersen, R.-B., 2002. U-Pb dating of detrital zircons for sediment provenance studies – a comparison of laser ablation ICP-MS and SIMS techniques. Chemical Geology, 182, 605–618.

Kroenke, L.W., 1984. Cenozoic tectonic development of the southwest Pacific. U.N. ESCAP, CCOP/SOPAC Tech. Bull. 6.

Kröner, A., Windley, B.F., Badarch, G., Tomurtogoo, O., Hegner, E., Jahn, B.M., Gruschka, S., Khain, E.V., Demoux, A., Wingate, M.T.D., 2007. Accretionary growth and crust-formation in the Central Asian Orogenic Belt and comparison with the Arabian-Nubian shield. In: Hatcher, R.D., Jr., Carlson, M.P., McBride, J.H., and Martinez Catalán, J.R. (eds), 4-D Framework of Continental Crust: Geological Society of America Memoir 200, 181–209.

Lallemand, S., Heuret, A., Boutelier, D., 2005. On the relationships between slab dip, back-arc stress, upper plate absolute motion, and crustal nature in subduction zones. Geochemistry, Geophysics, Geosystems, 6, Q09006.

Le Maitre, R.W. (Ed.), 2002. Igneous Rocks: A Classification and Glossary of Terms, 2nd ed. Cambridge Univ. Press, Cambridge, UK, 236 pp.

Lindley, I.D., 2006. Extensional and vertical tectonics in the New Guinea islands: implications for island arc evolution. Supplement to Scalera, G., Lavecchia, G., 2006. Frontiers in sciences: new ideas and interpretation. Annals of Geophysics, 49, 1, 2006.

Llanes, P., Silver, E., Day, S., Hoffman, G., 2009. Interactions between a transform fault and arc volcanism in the Bismarck Sea, Papua New Guinea. Geochemistry, Geophysics, Geosystems, 10, Q06013.

Lock, J., Davies, H.L., Tiffin, D.L., Murakami, F., Kisimoto, K., 1987. The Trobriand subduction system in the western Solomon Sea. Geo-Marine Letters, 7, 129–134.

Ludwig, K.R., 2009. User's Manual for Isoplot 3.70: A Geochronological Toolkit for Microsoft Excel. Berkeley Geochronology Center Special Publication No. 4.

Macpherson, C.G., 2008. Lithosphere erosion and crustal growth in subduction zones: Insights from initiation of the nascent East Philippine Arc. Geology, 36, 311–314.

Macpherson, C.G., Dreher, S.T., Thirlwall, M.F., 2006. Adakites without slab melting: High pressure differentiation of island arc magma, Mindanao, the Philippines: Earth and Planetary Science Letters, 243, 581–593.

Madsen, J.A., Lindley, I.D., 1994. Large-scale structures on Gazelle Peninsula, New Britain:

Implications for the evolution of the New Britain Arc. Australian Journal of Earth Sciences, 41, 561–569.

Mahoney, J.J., Storey, M., Duncan, R.A., Spencer, K.J., Pringle, M.S., 1993. Geochemistry and age of the Ontong Java Plateau. In: Pringle, M.S., Sager, W.W., Sliter, W., Stein, S., (Eds.), The Mesozoic Pacific. Geology, Tectonics, and Volcanism, Geophys. Monogra. 77, AGU, Washington, DC, Pp. 233–261.

Maksaev, V., Munizaga, F., McWilliams, M., Fanning, M., Mathur, R., Ruiz, J., and Zentilli, M., 2004. New chronology for El Teniente, Chilean Andes, from U-Pb, 40Ar/39Ar, Re-Os, and fission track dating: Implications for the evolution of a supergiant porphyry Cu-Mo deposit. Society of Economic Geologists Special Publication 11, Pp. 15−54.

Malusà, M.G., Garzanti, E., 2012. Actualistic snapshot of the early Oligocene Alps: the Alps-Apennines knot disentangled. Terra Nova, 24, 1–6.

Mann, P., Taira, A., 2004. Global tectonic significance of the Solomon Islands and Ontong Java Plateau convergent zone. Tectonophysics, 389, 137–190.

Martinez, F., Taylor, B., 1996. Backarc spreading, rifting, and microplate rotation, between transform faults in the Manus Basin. Marine Geophysical Research, 18, 203–224.

Mason, W.G., Moresi, L., Betts, P.G., Miller, M.S., 2010. Three-dimensional numerical models of the influence of a buoyant oceanic plateau on subduction zones. Tectonophysics, 483, 71–79.

Mattinson, J.M., 2005. Zircon U-Pb chemical abrasion ("CA-TIMS") method: combined annealing and multi-step partial dissolution analysis for improved precision and accuracy of zircon ages. Chemical Geology, 220, 47–66.

McClelland, W.C., Tikoff, B., Manduca, C.A., 2000. Two-phase evolution of accretionary margins: examples from the North American Cordillera. Tectonophysics, 326, 37–55.

McDowell, F.W., McMahon, T.P., Warren, P.Q., Cloos, M., 1996. Pliocene Cu-Au-bearing igneous intrusions of the Gunung Bijih (Ertsberg) District, Irian Jaya, Indonesia: K-Ar geochronology. The Journal of Geology, 104, 327–340.

McQuarrie, N., Robinson, D., Long, S., Tobgay, T., Grujic, D., Gehrels, G., Ducea, M., 2008. Preliminary stratigraphic and structural architecture of Bhutan: Implications for the along strike architecture of the Himalayan system. Earth and Planetary Science Letters, 272, 105–117.

Miller, M.S., Gorbatov, A., Kennett, B.L.N., 2006. Three-dimensional visualization of a near vertical slab tear beneath the southern Mariana Arc. Geochemistry, Geophysics, Geosystems, 7, Q06012.

Mishra, D.C., Singh, B., Tiwari, V.M., Gupta, S.B., Rao, M.B.S.V., 2000. Two cases of continental collisions and related tectonics during the Proterozoic period in India – insights from gravity modeling constrained by seismic and magnetotelluric studies. Precambrian Research, 99, 149–169.

Morales, J., Serrano, I., Jabaloy, A., Galindo-Zaldívar, J., Zhao, D., Torcal, F., Vidal, F., González Lodeiro, F., 1999. Active continental subduction beneath the Betic Cordillera and the Alborán Sea. Geology, 27, 735–738.

Mortimer, N., Gans, P., Herzer, R., Palin, M., Pelletier, B., Chaproniere, G., Monzier, M., 2012. Eocene-Oligocene ages of abyssal crust from the Rennell Basin, South Rennell Trough, D'Entrecasteaux Ridge and North Loyalty Basin. Proceedings of the 34th International Geological Congress: Unearthing our Past and Future – Resourcing Tomorrow, Brisbane.

Musgrave, R., 1990. Paleomagnetism and tectonics of Malaita, Solomon Islands. Tectonics, 9, 735–759.

Najman, Y., Appel, E., Boudagher-Fadel, M., Bown, P., Carter, A., Garzanti, E., Godin, L., Han, J., Liebke, U., Oliver, G., Parrish, R., Vezzoli, G., 2010. Timing of India–Asia collision: Geological, biostratigraphic, and palaeomagnetic constraints. Journal of Geophysical Research, 115, B12416.

Ohara, Y., Fujioka, K., Ishizuka, O., Ishii, T., 2002. Peridotites and volcanics from the Yap arc system: implications for tectonics of the southern Philippine Sea Plate. Chemical Geology, 189, 35–53.

O'Kane, T., 2008. 3-D structure and tectonic evolution of the Papua New Guinea and Solomon Islands region and its relationship to Cu–Au mineralization. Unpublished Honours thesis, Research School of Earth Sciences, The Australian National University.

Padilla-Garza, R.A., Titley, S.R., Eastoe, C.J., 2004. Hypogene evolution of the Escondida porphyry copper deposit, Chile. Society of Economic Geologists Special Publication 11, Pp. 141–165.

Page, R.W., 1976. Geochronology of igneous and metamorphic rocks in the New Guinea Highlands. Bureau of Mineral Resources, Geology and Geophysics Bulletin 162, Australian Government Publishing Service, Canberra.

Page, R.W., McDougall, I., 1972. Ages of mineralisation of gold and porphyry copper deposits in the New Guinea Highlands. Economic Geology, 67, 1034–1048.

Paquette, J.-L., Le Pennec, J.-L., 2012. 3.8 Ga zircons sampled by Neogene ignimbrite eruptions in Central Anatolia. Geology, 40, 239–242.

Parrish, R.R., 1990. U-Pb dating of monazite and its application to geological problems. Canadian Journal of Earth Sciences, 27, 1431–1450.

Peacock, S.M., 1996. Thermal and petrologic structure of subduction zones. In: Bebout, G.E., Scholl, D.W., Kirby, S.H., Platt, J.P. (Eds.), Subduction: Top to Bottom. Washington, DC, American Geophysical Union, Geophysical Monograph 96, Pp. 119–133.

Pegler, G., Das, S., Woodhouse, J.H., 1995. A seismological study of the eastern New Guinea and the western Solomon Sea regions and its tectonic implications. Geophysical Journal International, 122, 961–981.

Petterson, M.G., Babbs, T., Neal, C.R., Mahoney, J.J., Saunders, A.D., Duncan, R.A., Tolia, D., Magu, R., Qopoto, C., Mahoa, H., Natogga, D., 1999. Geological-tectonic framework of Solomon Islands, SW Pacific: crustal accretion and growth with an intra-oceanic setting. Tectonophysics, 301, 35–60.

Petterson, M.G., Neal, C.R., Mahoney, J.J., Kroenke, L.W., Saunders, A.D., Babbs, T.L., Duncan, R.A., Tolia, D., McGrail, B., 1997. Structure and deformation of north and central Malaita, Solomon Islands: tectonic implications for the Ontong Java Plateau-Solomon arc collision, and for the fate of oceanic plateaus. Tectonophysics, 283, 1–33.

Phinney, E.J., Mann, P., Coffin, M.F., Shipley, T.H., 2004. Sequence stratigraphy, structural style, and age of deformation of the Malaita accretionary prism (Solomon arc-Ontong Java Plateau convergent zone). Tectonophysics, 389, 221–246.

Pigram, C.J., Symonds, P.A., 1991. A review of the timing of the major tectonic events in the New Guinea Orogen. Journal of Southeast Asian Earth Sciences, 6, 307–318.

Plank, T., 2005. Constraints from thorium/lanthanum on sediment recycling at subduction zones and the evolution of the continents. Journal of Petrology, 46, 921–944.

Pubellier, M., Cobbold, P.R., 1996. Analogue models for the transpressional docking of volcanic arcs in the Western Pacific. Tectonophysics, 253, 33–52.

Rapp, R.P., Watson, E.B., 1995. Dehydration melting of metabasalt at 8–32 kbar: Implications for continental growth and crust-mantle recycling. Journal of Petrology, 36, 891–931.

Rawling, T.J., Lister, G.S., 2002. Large-scale structure of the eclogite-blueschist belt of New Caledonia. Journal of Structural Geology, 24, 1239–1258.

Renne, P.R., Mundil, R., Balco, G., Min, K., Ludwig, K.R., 2010. Joint determination of 40K decay constants and 40Ar*/40K for the Fish Canyon sanidine standard, and improved accuracy for 40Ar/39Ar geochronology. Geochimica et Cosmochimica Acta 74, 5349–5367.

Richards, J.P., 2011. High Sr/Y arc magmas and porphyry Cu ± Mo ± Au deposits: Just add water. Economic Geology, 106, 1075–1081.

Richards, J.P., Boyce, A.J., Pringle, M.S., 2001. Geologic evolution of the Escondida area, northern Chile: A model for spatial and temporal localization of porphyry Cu mineralization. Economic Geology, 96, 271–305.

Richards, J.P., Chappell, B.W., McCulloch, M.T., 1990. Intraplate-type magmatism in a continent-island-arc collision zone: Porgera intrusive complex, Papua New Guinea. Geology, 18, 958–961.

Richards, J.P., Kerrich, R., 2007. Adakite-like rocks: Their diverse origins and questionable role in metallogenesis. Economic Geology, 102, 537–576.

Richards, J.P., McDougall, I., 1990. Geochronology of the Porgera gold deposit, Papua New Guinea: Resolving the effects of excess argon on K-Ar and 40Ar/39Ar age estimates for magmatism and mineralization. Geochimica et Cosmochimica Acta, 54, 1397–1415.

Richards, S., Holm, R., Barber, G., 2011. When slab collide: A tectonic assessment of deep earthquakes in the Tonga–Vanuatu region. Geology, 39, 787–790.

Richards, S., Lister, G., Kennett, B., 2007. A slab in depth: Three-dimensional geometry and evolution of the Indo-Australian plate. Geochemistry Geophysics Geosystems, 8, Q12003.

Rioux, M., Hacker, B., Mattinson, J., Kelemen, P., Blusztajn, J., Gehrels, G., 2007. Magmatic development of an intra-oceanic arc: High-precision U-Pb zircon and whole-rock isotopic analyses from the accreted Talkeetna arc, south-central Alaska. GSA Bulletin, 119, 1168–1184.

Ripper, I.D., 1982. Seismicity of the Indo-Australian/Solomon Sea plate boundary in the southeast Papua region. Tectonophysics, 87, 355–369.

Rogerson, R., Williamson, A., 1985. Age, petrology and mineralization associated with the two Neogene intrusive types in the Eastern Highlands of Papua New Guinea. Geological Survey of Papua New Guinea Open File Report, 85.

Rosenbaum, G., Gasparon, M., Lucente, F.P., Peccerillo, A., Miller, M.S., 2008. Kinematics of slab tear faults during subduction segmentation and implications for Italian magmatism. Tectonics, 27, TC2008.

Rosenbaum, G., Giles, D., Saxon, M., Betts, P.G., Weinberg, R.F., Duboz, C., 2005. Subduction of the Nazca Ridge and the Inca Plateau: Insights into the formation of the ore deposits in Peru. Earth and Planetary Science Letters, 239, 18–32.

Rosenbaum, G., Lister, G.S., Duboz, C., 2002. Relative motions of Africa, Iberia and Europe during Alpine orogeny. Tectonopysics, 359, 117–129.

Rosenbaum, G., Mo, W., 2011; Tectonic and magmatic responses to the subduction of high bathymetric relief. Gondwana Research, 19, 571–582.

Rubatto, D., Hermann, J., 2003. Zircon formation during fluid circulation in eclogites (Monviso, Western Alps): implications for Zr and Hf budget in subduction zones. Geochimica et Cosmochimica Acta, 67, 2173–2187.

Rushmer, T., 1993. Experimental high-pressure granulites: Some applications to natural mafic xenolith suites and Archean granulite terranes. Geology, 21, 411–414.

Schärer, U., 1984. The effect of initial 230Th disequilibrium on young U-Pb ages: the Makalu case, Himalaya. Earth and Planetary Science Letters, 67, 191–204.

Scheibner, E., Veevers, J.J., 2000. Tasman Fold Belt System. Billion-year earth history of Australia and neighbors in Gondwanaland. In: Veevers, J.J. (Ed.), Billion-year earth history of Australia and neighbors in Gondwanaland. GEMOC Press, Sydney, 154–234.

Schellart, W.P., 2004. Quantifying the net slab pull force as a driving mechanism for plate tectonics. Geophysical Research Letters, 31, L07611.

Schellart, W.P., 2008. Overriding plate shortening and extension above subduction zones: A parametric study to explain formation of the Andes Mountains. GSA Bulletin, 120, 1441–

1454.

Schellart, W.P., Lister, G.S., Toy, V.G., 2006. A Late Cretaceous and Cenozoic reconstruction of the Southwest Pacific region: Tectonics controlled by subduction and slab rollback processes. Earth-Science Reviews, 76, 191–233.

Schmalholz, S.M., 2011. A simple analytical solution for slab detachment. Earth and Planetary Science Letters, 304, 45–54.

Schmitz, M.D., Bowring, S.A., 2001. U-Pb zircon and titanite systematics of the Fish Canyon Tuff: an assessment of high-precision U-Pb geochronology and its application to young volcanic rocks. Geochimica et Cosmochimica Acta, 65, 2571–2587.

Schmitz, M.D., Schoene, B., 2007. Derivation of isotope ratios, errors and error correlations for U-Pb geochronology using 205Pb-235U-(233U)-spiked isotope dilution thermal ionization mass spectrometric data. Geochemistry, Geophysics, Geosystems (G3), 8, Q08006.

Schuth, S., Münker, C., König, S., Qopoto, C., Basi, S., Garbe-Schönberg, D., Ballhaus, C., 2009. Petrogenesis of lavas along the Solomon Island arc, SW Pacific: Coupling of compositional variations and subduction zone geometry. Journal of Petrology, 50, 781–811.

Searle, M.P., Simpson, R.L., Law, R.D., Parrish, R.R., Waters, D.J., 2003. The structural geometry, metamorphic and magmatic evolution of the Everest massif, High Himalaya of Nepal-South Tibet. Journal of the Geological Society, 160, 345–366.

Sen, C., Dunn, T., 1994. Dehydration melting of a basaltic composition amphibolite at 1.5 and 2.0 GPa: Implications for the origin of adakites. Contributions to Mineralogy and Petrology, 117, 394–409.

Sillitoe, R.H., 2010. Porphyry copper systems. Economic Geology, 105, 3–41.

Smith, I.E.M., 2013. The chemical characterization and tectonic significance of ophiolite terrains in southeastern Papuan New Guinea. Tectonics, 32, 1–12.

Sobel, E.R., Dumitru, T.A., 1997. Thrusting and exhumation around the margins of the western Tarim basin during the India–Asia collision. Journal of Geophysical Research, 102, B3, 5043.

Spandler, C., Pettke, T., Rubatto, D., 2011. Internal and external fluid sources for eclogite-facies veins in the Monviso meta-ophiolite, Western Alps: Implications for fluid flow in subduction zones. Journal of Petrology, 52, 1207–1236.

Spandler, C., Pirard, C., 2013. Element recycling from subducting slabs to arc crust: A review. Lithos, 170–171, 208–223.

Spandler, C., Rubatto, D., Hermann, J., 2005. Late Cretaceous–Tertiary tectonics of the southwest Pacific: Insights from U–Pb sensitive, high resolution ion microprobe (SHRIMP) dating of eclogite facies rocks from New Caledonia. Tectonics, 24, TC3003.

Stacey, J.S., Kramers, J.D., 1975. Approximation of terrestrial lead isotope evolution by a two-stage model. Earth and Planetary Science Letters, 26, 207–221.

Stern, R.A., Amelin, Y., 2003. Assessment of errors in SIMS zircon U–Pb geochronology using a natural zircon standard and NIST SRM 610 glass. Chemical Geology, 197, 111–142.

Stern, R.J., 2004. Subduction initiation: spontaneous and induced. Earth and Planetary Science Letters, 226, 275–292.

Stern, T.A., 1995. Gravity anomalies and crustal loading at and adjacent to the Alpine Fault, New Zealand. New Zealand Journal of Geology and Geophysics, 38, 593–600.

Stevens, C., McCaffrey, R., Silver, E.A., Sombo, Z., English, P., van der Kevie, J., 1998. Mid-crustal detachment and ramp faulting in the Markham Valley, Papua New Guinea. Geology, 26, 847–850.

Struckmeyer, H.I.M., Yeung, M., Pigram, C.J., 1993. Mesozoic to Cainozoic plate tectonic palaeographic evolution of the New Guinea region. In: Carman, G.J., Carman, Z. (eds), Petroleum Exploration in Papua New Guinea. Proceedings of the Second PNG Petroleum Convention, Port Moresby, 261–290.

Sun, S., McDonough, W.F., 1989. Chemical and isotopic systematics of oceanic basalts: implications for mantle composition and processes. Geological Society, London, Special Publications 42, 313–345.

Taylor, B., 1979. Bismarck Sea: Evolution of a back-arc basin, Geology, 7, 171–174

Taylor, B., 1992. Rifting and the volcanic-tectonic evolution of the Izu-Bonin-Mariana Arc. in: Taylor, B., Fujioka, K. et al. (eds.). Proceeding of the Ocean Drilling Program, Scientific Results, 12, 627-651.

Taylor, B., Goodliffe, A.M., Martinez, F., 1999. How continents break up: Insights from Papua New Guinea. Journal of Geophysical Research, 104, 7497–7512.

Tcherepanov, E.N., Droxler, A.W., Lapointe, P., Mohn, K., Larsen, O.A., 2010. Siliciclastic influx and burial of the Cenozoic carbonate system in the Gulf of Papua. Marine and Petroleum Geology, 27, 533–554.

Tejada, M.L.G., Mahoney, J.J., Neal, C.R., Duncan, R.A., Petterson, M.G., 2002. Basement geochemistry and geochronology of Central Malaita, Solomon Islands, with implications for the origin and evolution of the Ontong Java Plateau. Journal of Petrology, 43, 449–484.

Teng, L.S., 1990. Geotectonic evolution of Late Cenozoic arc–continent collision in Taiwan. Tectonophysics, 183, 57–76.

Tera, F., Wasserburg, G.J., 1972. U-Th-Pb systematics in three Apollo 14 basalts and the problem of initial Pb in lunar rocks. Earth and Planetary Science Letters, 14, 281–304.

Tiepolo, M., 2003. In situ Pb geochronology of zircon with laser ablation-inductively coupled plasma-sector field mass spectrometry. Chemical Geology, 199, 159–177.

Tiepolo, M., Botazzi, P., Palenzona, M., Vanucci, R., 2003. A laser probe coupled with ICP-double focusing sector field mass spectrometer for in situ analysis of trace elements in geological samples and U-Pb dating of zircons. Canadian Mineralogist, 41, 259-272.

Titley, S.R., 1978. Geologic, history, hypogene features, and processes of secondary sulfide enrichment at the Plesyumi copper prospect, New Britain, Papua New Guinea. Economic Geology, 73, 768–784.

Tregoning, P., 2002. Plate kinematics in the western Pacific derived from geodetic observations. Journal of Geophysical Research, 107, B1 2020.

Tregoning, P., Jackson, R.J., McQueen, H., Lambeck, K., Stevens, C., Little, R.P., Curley, R., Rosa, R., 1999. Motion of the South Bismarck Plate, Papua New Guinea. Geophysical Research Letters, 26, 3517–3520.

Tregoning, P., Lambeck, K., Stoltz, A., Morgan, P., McClusky, S.C., van der Beek, P., McQueen, H., Jackson, R.J., Little, R.P., Laing, A., Murphy, B., 1998. Estimation of current plate motions in Papua New Guinea from Global Positioning System observations. Journal of Geophysical Research B: Solid Earth, 103, 12181–12203.

Tucker, R.T., Roberts, E.M., Hu, Y., Kemp, A.I.S., Salisbury, S.W., 2013. Detrital zircon age constraints for the Winton Formation, Queensland: Contextualizing Australia's Late Cretaceous dinosaur faunas. Gondwana Research, In Press.

Van Achterbergh, E., Ryan, C.G., Jackson, S.E., Griffin, W.L., 2001. Appendix, in: P J. Sylvester (Ed.), Laser Ablation-ICP-Mass Spectrometry in the Earth Sciences: Principle and Applications. Mineralog. Assoc. Can. (MAC) Short Course Series, Ottawa, Ontario, Canada, 29, 239.

van Dongen, M., Weinberg, R.F., Tomkins, A.G., Armstrong, R.A., Woodhead, J.D., 2010. Recycling of Proterozoic crust in Pleistocene juvenile magma and rapid formation of the Ok Tedi porphyry Cu-Au deposit, Papua New Guinea. Lithos, 114, 282–292.

von Huene, R., Corvalàn, J., Flueh, E.R., Hinz, K., Korstgard, J., Ranero, C.R., Weinrebe, W., CONDOR Scientists, 1997. Tectonic control of the subducting Juan Fernández Ridge on the Andean margin near Valparaiso, Chile. Tectonics, 16, 474–488.

von Quadt, A., Erni, M., Martinek, K., Moll, M., Peytcheva, I., Heinrich, C.A., 2011. Zircon crystallization and the lifetimes of ore-forming magmatic-hydrothermal systems. Geology, 39, 731–734.

Van Staal, C.R, Dewey, J.F., Mac Niocaill, C., McKerrow, W.S., 1998. The Cambrian-Silurian tectonic evolution of the northern Appalachians and British Caledonides: history of a complex, west and southwest Pacific-type segment of Iapetis. In: Blundell, D.J, Scott, A.C. (eds), Lyell: the Past is the Key to the Present. Geological Society, London, Special Publications, 143, 199–242.

Van Wyck, N., Williams, I.S., 2002. Age and provenance of basement metasediments from the Kubor and Bena Bena Blocks, central Highlands, Papua New Guinea: constrainst on the tectonic evolution of the northern Australian cratonic margin. Australian Journal of Earth Sciences, 49, 565–577.

Wallace, L.M., McCaffrey, R., Beavan, J., Ellis, S., 2005. Rapid microplate rotations and backarc rifting at the transition between collision and subduction. Geology, 33, 857–860.

Wallace, L.M., Stevens, C., Silver, E., McCaffrey, R., Loratung, W., Hasiata, S., Stanaway, R., Curley, R., Rosa, R., Taugaloidi, J., 2004. GPS and seismological constraints on active tectonics and arc-continent collision in Papua New Guinea: Implications for mechanics of microplate rotations in a plate boundary zone. Journal of Geophysical Research, 19, B05404, doi:10.1029/2003JB002481.

Weiler, P.D., Coe, R.S., 2000. Rotations in the actively colliding Finisterre Arc Terrane: paleomagnetic constraints on Plio–Pleistocene evolution of the South Bismarck microplate, northeastern Papua New Guinea. Tectonophysics, 316, 297–325.

Weissel, J.K., Taylor, B., Karner, G.D., 1982. The opening of the Woodlark Basin, subduction of the Woodlark spreading system, and the evolution of northern Melanesia since mid-Pliocene time. Tectonophysics, 87, 253–277.

Wells, R.E., 1989. Origin of the oceanic basalt basement of the Solomon Islands arc and its relationship to the Ontong Java Plateau – insights from Cenozoic plate motion models, Tectonophysics, 165, 219–235.

Whalen, R.E., Britten, R.M., McDougall, I., 1982. Geochronology and geochemistry of the Frieda River Prospect Area, Papua New Guinea. Economic Geology, 77, 592–616.

Whattam, S.A., 2009. Arc–continent collisional orogenesis in the SW Pacific and the nature, source and correlation of emplaced ophiolitic nappe components. Lithos, 113, 88–114.

Wiebenga, W.A., 1973. Crustal structure of the New Britain-New Ireland region. In: Coleman, P.J. (Eds.), The Western Pacific: Island Arcs, Marginal Seas, Geochemistry. University of Western Australia Press, Nedlands, 163–177.

Wilcox, R.E., Harding, T.P., Seely, D.R., 1973. Basic wrench tectonics. American Association of Petroleum Geologists, 57, 74–96.

Williams, I.S., Hergt, J.M., 2000. U-Pb dating of Tasmanian dolerites: a cautionary tale of SHRIMP analysis of high-U zircon. In: Woodhead, J.D., Hergt, J.M., Noble, W.P. (Eds.), Beyond 2000: New Frontiers in Isotope Geoscience, Lorne, 2000, Abstracts and Proceedings, 185–188, University of Melbourne, Australia.

Wingate, M.T.D., Compston, W., 2000. Crystal orientation effects during ion microprobe U–Pb analysis of baddeleyite. Chemical Geology, 168, 75–97.

Woodhead, J.D., Eggins, S.M., Gamble, J.G., 1993. High field strength and transition element systematics in coupled arc–back arc settings: evidence for multi-phase melt extraction and a depleted mantle wedge. Earth and Planetary Science Letters, 114, 491–504.

Woodhead, J.D., Eggins, S.M., Johnson, R.W., 1998. Magma genesis in the New Britain island arc: Further insights into melting and mass transfer processes. Journal of Petrology, 39, 1641–1668.

Woodhead, J., Hergt, J., Sandiford, M., Johnson, W., 2010. The big crunch: Physical and chemical expressions of arc/continent collision in the Western Bismarck arc. Journal of Volcanology and Geothermal Research, 190, 11–24.

Woodhead, J.D., Johnson, R.W., 1993. Isotopic and trace element profiles across the New Britain island arc, Papua New Guinea. Contributions to Mineralogy and Petrology, 113, 479–491.

Yan, C., Kroenke, L., 1993. A plate tectonic reconstruction of the SW Pacific, 0–100 Ma. In: Berger, T., Kroenke, L., Mayer, L., et al. (Eds.), Proceedings of the Ocean Drilling Program. Scientific Results, 130, 697–709.

Yin, A., 2006. Cenozoic tectonic evolution of the Himalayan orogen as constrained by along-strike variation of structural geometry, exhumation history, and foreland sedimentation. Earth-Science Reviews, 76, 1–131.

Yogodzinski, G.M., Kelemen, P.B., 1998. Slab melting in the Aleutians: implications of an ion probe study of clinopyroxene in primitive adakite and basalt. Earth and Planetary Science Letters, 158, 53–65.

Yogodzinski, G.M., Lees, J.M., Churikova, T.G., Dorendorf, F., Wöerner, G., Volynets, O.N., 2001. Geochemical evidence for the melting of subducting oceanic lithosphere at plate edges. Nature, 409, 500–504.

Appendix One

Richards, S., Holm, R., & Barber, G., 2011. When slabs collide: A tectonic assessment of deep earthquakes in the Tonga-Vanuatu region. *Geology*, 39, 787–790.

Appendix Two

Holm, R.J., Spandler, C. & Richards, S.W., 2013. Melanesian arc far-field response to collision of the Ontong Java Plateau: Geochronology and pertrogenesis of the Simuku Igneous Complex, New Britain, Papua New Guinea. *Tectonophysics*, 603, 189–212.

Appendix Three

Holm, R.J., & Richards, S.W., 2013. A re-evaluation of arc-continent collision and along-arc variation in the Bismarck Sea region, Papua New Guinea. *Australian Journal of Earth Sciences*, 60, 605–619.